

A Survey of Relaxations and Approximations of the Power Flow Equations

Daniel K. Molzahn¹ and Ian A. Hiskens²

¹*Georgia Institute of Technology; molzahn@gatech.edu*

²*University of Michigan; hiskens@umich.edu*

ABSTRACT

The power flow equations relate the power injections and voltages in an electric power system and are therefore key to many power system optimization and control problems. Research efforts have developed a wide variety of relaxations and approximations of the power flow equations with a range of capabilities and characteristics. This monograph surveys relaxations and approximations of the power flow equations, with a particular emphasis on recently proposed formulations.

1

Introduction

The power flow equations model the relationship between voltage phasors and power injections at nodes (buses) in an electric power system. These equations are fundamental in the analysis and operation of power systems. Accordingly, they form the key constraints in many optimization and control problems relevant to electric power systems, including optimal power flow (OPF), unit commitment, state estimation, contingency evaluation, voltage stability assessment, and dynamic stability analysis. The power flow equations are nonlinear and result in non-convex optimization problems. Moreover, at least some optimization problems containing the power flow equations (e.g., OPF problems) are generally NP-Hard [1], even for systems with radial network topologies [2], and may have multiple local solutions [3]. This inherent complexity is immediately apparent in the simple examples presented at the end of Chapter 2.

There exists a voluminous literature regarding the power flow equations. The intent of this monograph is to review various representations of the power flow equations, with a particular focus on those proposed in the last decade.

The power flow representations in this monograph are primarily presented in the context of optimization problems. However, note that while optimization plays an important role in many problems relevant to the design and operation of power systems (e.g., OPF, state estimation, unit commitment, transmission switching, expansion planning, etc. [4, 5]), various power flow representations are relevant to other important problems (stability analyses, dynamic simulations, analysis of control strategies such as volt/var control and automatic generation control, etc. [6, 7]). Moreover, while much of the literature develops power flow representations in the context of certain applications, this monograph focuses on the power flow representations themselves rather than specific problems. The reader interested in a specific problem or solution algorithm is referred to the surveys and tutorials that exist for power flow [8, 9], different formulations of optimal power flow [10–21] (and various extensions to consider, e.g., security constraints [22–25] and transient-stability constraints [26, 27]), unit commitment [28–31], state estimation [32–35], transmission switching [36], infrastructure planning [19], voltage stability analysis [37–40], cascading failure [41], distributed optimization and control methods [42–45], complex network theory [46], and more general power system stability concepts [6]. Several recent references of particular relevance are the surveys in [47] and [48] as well as the video lectures in [49], all of which review some of the topics covered in this monograph. Also note that reference implementations for several of the power flow representations presented in this monograph are provided in the software packages MATPOWER [50] and PowerModels.jl [51].

The power flow representations surveyed in this monograph are categorized as either *relaxations* or *approximations*. Figure 1.1 shows conceptual examples of a relaxation and an approximation of a non-convex feasible space. Relaxations enclose the non-convex feasible spaces associated with the power flow equations in a larger space. The larger space is typically chosen to be convex to enable the application of theory and algorithms developed for convex optimization problems.

Approximations use assumptions regarding certain quantities to simplify the power flow equations. Power flow approximations are capable of closely representing system behavior when the associated assumptions

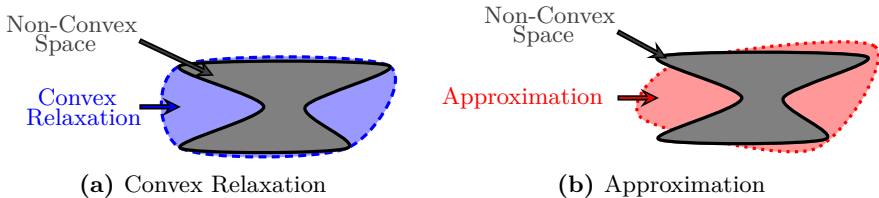


Figure 1.1: Conceptual illustrations showing a convex relaxation (blue region on the left) and an approximation (red region on the right) for the gray non-convex space.

are valid. Many power flow approximations are reasonably accurate for “typical” operating conditions.

In general, solutions to optimization problems that use power flow relaxations and approximations do not exactly satisfy the actual power flow equations. Rather, relaxations and approximations are typically employed in attempts to obtain tractable formulations which adequately represent the actual power flow physics. Optimization problems that use convex relaxations additionally provide bounds on the optimal objective value for the original non-convex problem as well as sufficient conditions for certifying problem infeasibility. Some convex relaxations also have associated sufficient conditions which guarantee their ability to provide global optima for certain limited classes of power system optimization problems. Some of these sufficient conditions can be evaluated prior to solving the relaxation based solely on the problem parameters and network topology, while other conditions are checked after solving a relaxation. In contrast, note that approximations do not provide any of the aforementioned theoretical guarantees provided by relaxations.

Solutions to relaxations and approximations may not exactly satisfy the power flow equations. This may be unacceptable for some applications, necessitating the deployment of algorithms that return a feasible power flow solution, possibly at the cost of increased computational difficulty or the lack of theoretical guarantees. A wide variety of nonlinear programming techniques have been applied to power system optimization problems. Starting from specified initializations, these techniques typically seek *local optima* for power system optimization problems, which are feasible points with objective values that are superior to all

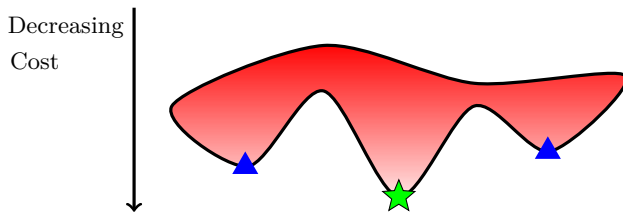


Figure 1.2: Conceptual illustration showing local optima (blue triangles) and the global optimum (green star).

nearby points but potentially inferior to the global optimum. Figure 1.2 provides a conceptual example showing the distinction between local and global optima. While surveying the power system optimization literature regarding local solution techniques is largely beyond the scope of this monograph, a brief summary of traditional nonlinear programming techniques is presented in §6. The interested reader is directed to other reviews of traditional local solution techniques, such as [13–17] for further details. Additionally, some of the power flow representations considered in this monograph form the basis of recently developed algorithms for computing local optima or “nearly globally optimal” feasible points. This monograph also reviews several such algorithms in §6.

The capabilities of various power flow relaxations and approximations are, in many ways, complementary rather than competitive with the capabilities of local solution algorithms. Local solution algorithms can benefit from the outputs resulting from power flow relaxations and approximations (e.g., using the decision variable values and the set of binding constraints to initialize certain local solution algorithms). Moreover, optimization problems may combine various power flow representations in order to balance accuracy and computational tractability. For instance, an optimization problem may have a “base case” that uses a detailed model of the power flow physics and multiple “scenarios” that use simplified power flow representations for the sake of computational tractability. As another example, an algorithm could decompose the solution of a complicated mixed-integer nonlinear program into two steps: first solve a mixed-integer problem with a simplified power flow model to select values for the discrete variables, and then apply a local

solution algorithm to the continuous optimization problem that results from fixing the discrete variables and employing a higher-fidelity power flow model.

The theoretical guarantees provided by relaxations also complement the capabilities of local solution algorithms. Infeasibility of a relaxation certifies that the original optimization problem is infeasible, but feasibility of a relaxation is not sufficient to guarantee feasibility of the original problem. Conversely, a local solution algorithm can show that a problem is feasible, but failure of a local algorithm to converge to a feasible point does not guarantee that the original problem is infeasible. Thus, relaxations and local solution algorithms have complementary capabilities with respect to the question of problem feasibility. Furthermore, many global solution algorithms compute an *optimality gap* by comparing the objective value bound from a relaxation with the achievable objective value from a feasible point obtained via a local solution algorithm. In order to provably obtain a global optimum, these algorithms then use a variety of techniques to shrink the optimality gap. Also note that the objective value bounds can be directly useful, for instance, in algorithms that aim to achieve robustness with respect to a set of possible uncertainty realizations, compute bounds on voltage stability margins, etc. The references at the end of §7.2 provide examples of these and other synergistic uses of various power flow representations.

The remainder of this monograph is organized as follows. Chapter 2 describes the power flow equations. Chapter 3 overviews the optimization tools which form the basis for the power flow representations. Chapters 4 and 5 review the literature of power flow relaxations and approximations, respectively. Chapter 6 overviews various techniques for obtaining a feasible point, focusing on recent developments. Chapter 7 concludes the monograph and discusses open research topics.

2

Overview of the Power Flow Equations

This chapter first presents the power flow equations in a variety of representations and then summarizes typical applications including solving the power flow problem for specified parameter values and embedding the power flow equations within optimization problems. Various test cases are used to illustrate the feasible spaces associated with the power flow equations.

The remainder of the monograph uses the following notation. Consider an n -bus electric power system, where $\mathcal{N} = \{1, \dots, n\}$ denotes the set of buses and (i, k) denotes the line from bus i to bus k , with the set of all lines denoted by \mathcal{L} . Each line $(i, k) \in \mathcal{L}$ is modeled with a Π circuit that has a series impedance of $R_{ik} + jX_{ik}$ and a total shunt susceptance of $b_{c,ik}$, where $j = \sqrt{-1}$. The corresponding mutual admittance is $g_{ik} + jb_{ik} = 1/(R_{ik} + jX_{ik})$. Some power flow representations are presented for the more general line model used by MATPOWER [50] that incorporates an ideal transformer with a voltage tap ratio τ_{ik} and phase shift $\theta_{shift,ik}$. (See Figure 2.1.) Also, let $g_{sh,i} + jb_{sh,i}$ denote the shunt admittance at bus $i \in \mathcal{N}$.

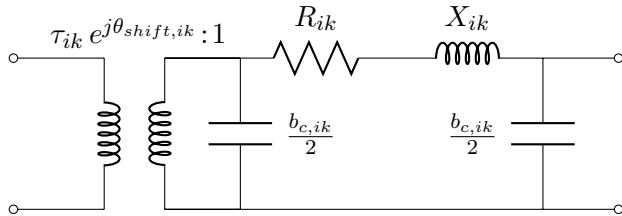


Figure 2.1: Pi-circuit line model with an ideal transformer. This is the line model used by MATPOWER [50].

This monograph presents some power flow representations using admittance matrix formulations that implicitly model the circuit elements for each line. The $n \times n$ complex network admittance matrix \mathbf{Y} is denoted in rectangular coordinates as $\mathbf{Y} = \mathbf{G} + \mathbf{B}$ and polar coordinates as $\mathbf{Y} = |\mathbf{Y}| e^{j\psi} \equiv |\mathbf{Y}| \angle \psi$, where \angle denotes the angle of a complex quantity. The admittance matrix describes the linear relationship between the bus voltage phasors and bus current injection phasors. This matrix is constructed using the electrical parameters and network topology:

$$\mathbf{Y}_{ik} = \begin{cases} g_{sh,i} + jb_{sh,i} + \sum_{m:(i,m) \in \mathcal{L}} \left(g_{im} + j \left(b_{im} + \frac{b_{c,im}}{2} \right) \right) / \tau_{im}^2 \\ \quad + \sum_{m:(m,i) \in \mathcal{L}} \left(g_{mi} + j \left(b_{mi} + \frac{b_{c,mi}}{2} \right) \right), & i = k, \\ -(g_{ik} + jb_{ik}) / (\tau_{ik} e^{-j\theta_{shift,ik}}), & (i, k) \in \mathcal{L}, \\ -(g_{ik} + jb_{ik}) / (\tau_{ik} e^{j\theta_{shift,ik}}), & (k, i) \in \mathcal{L}, \\ 0, & \text{otherwise,} \end{cases} \quad (2.1)$$

where the notation \mathbf{Y}_{ik} indicates the (i, k) element of the matrix \mathbf{Y} . Each line $(i, k) \in \mathcal{L}$ contributes terms to the diagonal entries \mathbf{Y}_{ii} and \mathbf{Y}_{kk} as well as the off-diagonal entries \mathbf{Y}_{ik} and \mathbf{Y}_{ki} . Accordingly, \mathbf{Y} inherits the sparsity pattern of the power system network. Typical large-scale power system networks are very sparse, often having less than 0.5% of the possible connections between buses. Asymmetries in \mathbf{Y} are due to the presence of phase-shifting transformers ($\theta_{shift,ik} \neq 0$ for some $(i, k) \in \mathcal{L}$). If $\theta_{shift,ik} = 0$ for all lines $(i, k) \in \mathcal{L}$, then \mathbf{Y} is symmetric, i.e., $\mathbf{Y} = \mathbf{Y}^\top$, where $(\cdot)^\top$ is the transpose operator.

2.1. Power Flow Representations

9

For notational convenience and to match the development of many of the relaxations and approximations that are reviewed in this monograph, the power flow equations are presented using a balanced single-phase equivalent network representation. More generally, and particularly for distribution networks, an unbalanced three-phase representation is most appropriate. In this latter case, each variable has an associated *phase* (i.e., ‘a’, ‘b’, and ‘c’ for a three-phase system). Where available, this monograph provides references to unbalanced three-phase representations of the surveyed power flow relaxations and approximations.

2.1 Power Flow Representations

The chapter begins by discussing typical representations of the power flow equations: bus injection models in various coordinate systems and the DistFlow equations for radial systems.

Note that developing novel representations of the power flow equations is an active research topic. Recent work has proposed a variety of new power flow representations, such as an elliptical power flow representation that is used to compute multiple power flow solutions in [52] and multiple local solutions for optimal power flow problems in [53]. As another example, the power divider formulation in [54] (with extensions proposed in [55]) relates the bus power injections to the power flows on each line in order to study network allocation, loss allocation, and active power flow satisfaction problems. Additionally, references [56, 57] use a power flow formulation that emphasizes Laplacian structural characteristics in order to identify patterns in the Lagrange multipliers of power system optimization problems.

2.1.1 Bus Injection Models

Bus injection models of the power flow equations relate the electrical quantities at each bus. After introducing notation, this section first discusses the I–V power flow formulation that relates the voltages, current injections, and power injection variables. This section then presents bus injection models that are posed solely in terms of the voltage phasors and complex power injections.

Notation

For a balanced, single-phase equivalent network representation, each bus has several associated complex values: a voltage phasor, a current injection phasor, and a complex power injection. The complex voltage phasors $V \in \mathbb{C}^n$ can be represented in polar coordinates $V = |V| e^{j\theta} \equiv |V| \angle \theta$, where $|V| > 0 \in \mathbb{R}^n$ and $\theta \in (-\pi, \pi]^n$ radians,¹ or in rectangular coordinates $V = V_d + jV_q$, with $V_d, V_q \in \mathbb{R}^n$. Similarly, the current injection phasors $I \in \mathbb{C}^n$ can be represented in polar coordinates $I = |I| e^{j\phi} \equiv |I| \angle \phi$, where $|I| > 0 \in \mathbb{R}^n$ and $\phi \in (-\pi, \pi]^n$ radians, or in rectangular coordinates $I = I_d + jI_q$, with $I_d, I_q \in \mathbb{R}^n$. Each bus $i \in \mathcal{N}$ also has complex power injections $S_i = P_i + jQ_i$, where $P, Q \in \mathbb{R}^n$ denote the active and reactive power injections, respectively. Let $\overline{(\cdot)}$ denote the complex conjugate.

Note that regardless of the particular mathematical formulation, there is a rotational degeneracy in the power flow equations associated with invariantness to the addition of a constant offset to all angles. This degeneracy is typically addressed by choosing a *reference bus* and defining the angle of its voltage phasor to be 0° . Without loss of generality, let bus 1 provide the angle reference so that $\angle V_1 = \theta_1 = 0$. Equivalently, an angle reference can be set in rectangular coordinates by specifying $V_{q1} = 0$.

The I–V Formulation

The I–V formulation of the power flow equations is based on two fundamental characteristics of AC power systems: 1) the linear relationship between the voltage phasors and current injection phasors and 2) the definition of complex power. Mathematically stating these characteristics for each bus $i \in \mathcal{N}$ yields the I–V power flow formulation:

$$I_i = \sum_{k=1}^n \mathbf{Y}_{ik} V_k, \quad (2.2a)$$

$$P_i + jQ_i = V_i \overline{I}_i. \quad (2.2b)$$

¹Even though the exponential form $e^{j\theta}$ is only strictly valid for θ expressed in radians, it is common practice for θ to be stated in degrees.

A variety of reformulations are obtained using different choices for converting the complex quantities in (2.2) to real quantities.

The I–V formulation of the power flow equations has characteristics that can be advantageous in various contexts. For instance, observe that the nonlinearities in the I–V formulation are isolated to the bilinear products in (2.2b). Moreover, each bilinear term consists solely of quantities associated with a single bus. As will be shown later in this section, this contrasts with other power flow formulations that have nonlinearities which couple variables associated with different buses. Additionally, note that modifications to the I–V formulation facilitate the straightforward representations of devices whose current flows cannot be expressed solely as functions of their terminal voltages, such as ideal transformers and ideal circuit breakers [58]. Such devices are more complicated to explicitly model in other power flow representations. Several recent publications [58–65] exploit features of the I–V formulation. On the other hand, maintaining both voltage and current variables results in the I–V formulation having more variables than other power flow representations, which can have computational implications.

Voltage-Based Formulations

Substituting the current injection equation (2.2a) into the power injection equation (2.2b) yields a system of polynomial equations in terms of the complex voltage phasors and their conjugates, V and \bar{V} :

$$P_i + jQ_i = V_i \sum_{k=1}^n \bar{\mathbf{Y}}_{ik} \bar{V}_k. \quad (2.3a)$$

Squared voltage magnitudes are

$$|V_i|^2 = V_i \bar{V}_i. \quad (2.3b)$$

Formulating the power flow equations in complex variables can be useful for various forms of analysis, such as holomorphic embedding methods [66], computing bounds on the number of power flow solutions [67], and, as will be discussed in detail in §4.1.2, constructing certain power flow relaxations.

Table 2.1: Typical formulations of the power flow equations in the bus injection model.

Representations of \mathbf{Y} and V	Power Flow Equations
$\mathbf{Y} = \mathbf{G} + j\mathbf{B}$, $V = V_d + jV_q$	$P_i = \sum_{k=1}^n V_{di} (\mathbf{G}_{ik} V_{dk} - \mathbf{B}_{ik} V_{qk}) + V_{qi} (\mathbf{B}_{ik} V_{dk} + \mathbf{G}_{ik} V_{qk}), \quad (2.4a)$ $Q_i = \sum_{k=1}^n V_{di} (-\mathbf{B}_{ik} V_{dk} - \mathbf{G}_{ik} V_{qk}) + V_{qi} (\mathbf{G}_{ik} V_{dk} - \mathbf{B}_{ik} V_{qk}), \quad (2.4b)$ $ V_i ^2 = V_{di}^2 + V_{qi}^2. \quad (2.4c)$
$\mathbf{Y} = \mathbf{G} + j\mathbf{B}$, $V = V e^{j\theta}$	$P_i = V_i \sum_{k=1}^n V_k (\mathbf{G}_{ik} \cos(\theta_i - \theta_k) + \mathbf{B}_{ik} \sin(\theta_i - \theta_k)), \quad (2.5a)$ $Q_i = V_i \sum_{k=1}^n V_k (\mathbf{G}_{ik} \sin(\theta_i - \theta_k) - \mathbf{B}_{ik} \cos(\theta_i - \theta_k)). \quad (2.5b)$
$\mathbf{Y} = \mathbf{Y} e^{j\psi}$, $V = V e^{j\theta}$	$P_i = V_i \sum_{k=1}^n V_k \mathbf{Y}_{ik} \cos(\theta_i - \theta_k - \psi_{ik}), \quad (2.6a)$ $Q_i = V_i \sum_{k=1}^n V_k \mathbf{Y}_{ik} \sin(\theta_i - \theta_k - \psi_{ik}). \quad (2.6b)$

A variety of power flow formulations are derived by converting (2.3) to real-valued quantities using different representations of the complex-valued admittance matrix, voltage phasors, and power injections. Table 2.1 presents several typical formulations. Observe that these formulations are equivalent yet exhibit significantly different mathematical representations. For instance, using rectangular coordinates for both the voltage phasors and the admittance matrix yields a system of quadratic polynomials in (2.4), while using polar coordinates for the voltage phasors results in a system of coupled trigonometric functions in (2.5) and (2.6). As will be discussed in later chapters, many of the distinctions among the power flow relaxations and approximations described

in this monograph are related to various mechanisms for exploiting these different mathematical features.

The power flow equations in rectangular voltage coordinates (2.4) have several interesting characteristics due to their quadratic nature [68]. Let (2.4) be rewritten in the generic form $f(x) = y + h(x) = 0$, where $x = [V_d^\top \ V_q^\top]^\top \in \mathbb{R}^{2n}$ and $y \in \mathbb{R}^{2n}$ is a vector of parameters formed from power injections $P_i + jQ_i$ and voltage set-points $|V_i|$ at specified buses. Solution properties include:

- Variation of x along a straight line through a pair of distinct solutions of the problem $f(x) = 0$, for fixed y , results in the mismatch vector $f(x)$ always lying on a straight line.
- Consider a straight line connecting a pair of distinct solutions denoted by x_1 and x_2 . The Jacobian $J = \frac{\partial f}{\partial x}$ is singular at the midpoint of that line. Furthermore, that line coincides with the right eigenvector of J corresponding to the zero eigenvalue.
- The maximum number of solutions of $f(x) = 0$ on any straight line in x -space is two.

These and other properties are derived in [68].

2.1.2 The DistFlow Equations

In two seminal papers [69, 70], Baran and Wu proposed a power flow representation named the “DistFlow” equations that is valid for radial systems. Baran and Wu also referred to this representation as the “branch flow equations”. In contrast to the bus injection model’s formulation in terms of the quantities at each bus, the DistFlow equations focus on the quantities flowing on the lines.

Let \mathcal{L} denote the set of branches, with $i \rightarrow k$ representing a branch connecting buses i and k where bus k is located “downstream” (further from the substation in a radial distribution system) from bus i . For the line from bus i to bus k , define real variables P_{ik} and Q_{ik} for the sending-end active and reactive power flows. Let ℓ_{ik} denote the squared magnitude of the current flow from bus i to bus k . With lines modeled as series impedances $R_{ik} + jX_{ik}$ (see Figure 2.2), the DistFlow equations

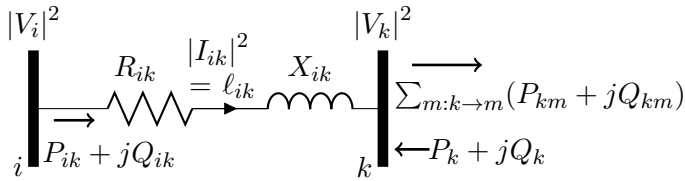


Figure 2.2: Explanation of the variables in the DistFlow equations for line $(i, k) \in \mathcal{L}$.

are defined for each line $(i, k) \in \mathcal{L}$ as

$$P_{ik} = R_{ik}\ell_{ik} - P_k + \sum_{m : k \rightarrow m} P_{km}, \quad (2.7a)$$

$$Q_{ik} = X_{ik}\ell_{ik} - Q_k + \sum_{m : k \rightarrow m} Q_{km}, \quad (2.7b)$$

$$|V_k|^2 = |V_i|^2 - 2(R_{ik}P_{ik} + X_{ik}Q_{ik}) + (R_{ik}^2 + X_{ik}^2)\ell_{ik}, \quad (2.7c)$$

$$\ell_{ik}|V_i|^2 = P_{ik}^2 + Q_{ik}^2. \quad (2.7d)$$

Note that (2.7a)–(2.7c) are linear in the squared voltage magnitudes $|V_i|^2$, $\forall i \in \mathcal{N}$. Some presentations of the DistFlow equations rewrite (2.7) by introducing new variables, $v_i = |V_i|^2$, to emphasize this linearity. This monograph refrains from using this notation in order to ease comparison among different power flow formulations.

Also note that more general line models can be incorporated in both the bus injection model and the DistFlow equations (e.g., the line model employed in MATPOWER [50], which allows for shunt susceptances, non-unity transformer voltage ratios, and non-zero transformer phase shifts). Extension of the DistFlow equations to this line model is presented in [71].

The DistFlow equations (2.7) fully represent the power flows for a balanced, single-phase equivalent model of a radial network. For mesh networks, one could assign an arbitrary orientation to each branch and apply (2.7). However, such an approach does not enforce consistency in the angle summations around cycles in the network (i.e., the summation of the angles around a cycle must be a multiple of 2π radians for true solutions). Thus, applying (2.7) to mesh networks results in a relaxation of the power flow equations. Note that this relaxation is *non-convex* due to (2.7d).

2.2. Applications of the Power Flow Equations

15

One obtains a set of equations that fully represents the power flows in mesh networks by augmenting the DistFlow equations (2.7) with constraints which ensure that there exist phase angles which, 1) are consistent with the squared voltage magnitudes, $|V_i|^2$, and power flows, P_{ik} and Q_{ik} , and 2) sum to a multiple of 2π radians around every cycle [72–75]. Ensuring consistency in the angles around all cycles can be accomplished using a “cycle basis” for the network, i.e., a set of cycles such that any other cycle in the network can be constructed via an appropriate combination of the cycles in the basis [76, 77]. As one way to construct a cycle basis, select any spanning tree of the network graph. A cycle basis is formed from the cycles which share all but one of their edges with the spanning tree. Let \mathcal{C} denote the cycle basis associated with an arbitrary spanning tree. Enforcing the constraint $\sum_{(i,k) \in C_i} \angle \left(|V_i|^2 - (R_{ik} - jX_{ik}) (P_{ik} + jQ_{ik}) \right) = 0 \bmod 2\pi$ for all cycles $C_i \in \mathcal{C}$ ensures the existence of a consistent set of angles for all cycles in the DistFlow model [74].

2.2 Applications of the Power Flow Equations

The power flow equations are at the heart of many power system analysis and control problems. This section reviews two common applications of the power flow equations: 1) solving the equations for unknown voltage phasors given certain specified power injections and voltage magnitude set-points, and 2) embedding the equations within optimization problems.

2.2.1 Solving the Power Flow Equations

A typical application of the power flow equations is to specify certain voltage magnitude set-points and power injections and solve the resulting non-linear system of equations to obtain a corresponding set of voltages, currents, and power flows. As expected for systems of non-linear equations, there may exist multiple power flow solutions. A “high-voltage/small-angle-difference” solution is typically of greatest

interest as it corresponds to a desirable operating point. Other “low-voltage/large-angle-difference” solutions are of interest for certain applications, such as stability analysis. Upper bounds on the number of power flow solutions grow exponentially with the size of the system [67, 78, 79], and there exist example systems for which these bounds are achievable asymptotically with increasing network size [80]. However, the number of power flow solutions for typical operating conditions appears to be significantly smaller than these bounds [52, 81–83].

To represent typical equipment behavior, each bus is traditionally classified as PQ, PV, or slack.² PQ buses, which typically correspond to loads, treat P_i and Q_i as specified quantities and enforce the active and reactive power equations. PV buses, which typically correspond to generators, enforce the active power and squared voltage magnitude equations with specified P_i and $|V_i|$. Finally, a single slack bus is selected with specified V_i (typically chosen such that the reference angle $\angle V_i = 0^\circ$, i.e., $V_{qi} = 0$). The active power P_i and reactive power Q_i at the slack bus are determined from the active and reactive power equations, respectively; network-wide conservation of complex power is thereby satisfied. Thus, solving the power flow equations means determining:

- Voltage phasors $V_i, \forall i \in \mathcal{N}$, for the bus injection model, or
- Squared current magnitudes and power flows ℓ_{ik}, P_{ik} , and Q_{ik} , $\forall (i, k) \in \mathcal{L}$, and squared voltage magnitudes $|V_i|^2, \forall i \in \mathcal{N}$, for the branch flow model,

such that the enforced equations are satisfied at every bus. A variety of non-linear solution algorithms are applicable to the power flow equations [8, 9].

Rather than selecting a single generator bus to serve as the slack bus, a “distributed slack” variant of the power flow problem proportionally allocates the role of balancing the active power injections among all of the generators. This is accomplished by modeling the power injections

²This traditional classification of buses is convenient but not necessary. For example, it is possible to define a QV bus with specified reactive power injection Q_i and voltage magnitude $|V_i|$. The important requirement is that the number of equations must equal the number of variables.

2.2. Applications of the Power Flow Equations

17

at each generator bus i as $P_i = P_i^\bullet + \alpha_i \delta_P$, where α is a specified “participation factor” vector with non-negative entries that sum to unity, P_i^\bullet is the specified nominal active power injection at bus i , and δ_P is a new variable that is shared among all of the active power injection equations. In the distributed slack formulation, note that the phase angle reference $\theta_i = 0^\circ$ is enforced at a single reference bus i and all generator buses have specified voltage magnitudes. Also note that the distributed slack formulation simplifies to the slack bus formulation discussed above by choosing $\alpha_i = 1$ for a single generator bus i and $\alpha_k = 0$ for all other generator buses k .

Power flow applications often involve regulating transformers that vary their tap ratio τ_{ik} and/or phase shift $\theta_{shift,ik}$ to meet specified set-point requirements. For example, a transformer may vary its tap ratio to ensure its controlled-bus voltage equals the set-point, or the phase shift may vary to ensure the active power flow at a specified location equals its set-point. A power flow solution requires that each transformer variable must be associated with a corresponding set-point constraint.

2.2.2 Embedding within Optimization Problems

The power flow equations are often embedded in optimization problems where the power injections and voltage magnitude set-points are allowed to vary in order to optimize some objective function while satisfying engineering constraints. These constraints are often equalities (e.g., $P_i = -P_{Di}$ for a specified demand P_{Di}) or box constraints (e.g., $P_i^{min} \leq P_i \leq P_i^{max}$ for specified upper and lower bounds P_i^{max} and P_i^{min}). More complicated constraints that couple P_i , Q_i , and $|V_i|$ are appropriate for representing generator capability curves and voltage-dependent loads [84–86]. Some device models may impose discrete constraints on these quantities (e.g., $Q_i = z_i b_{sh,i} |V_i|^2$ for a switched capacitor with shunt susceptance $b_{sh,i}$ and associated binary variable $z_i \in \{0, 1\}$; or $z_i P_i^{min} \leq P_i \leq z_i P_i^{max}$ modeling the ability to shut down a generator in a unit commitment problem, where $z_i \in \{0, 1\}$ represents the generator’s on/off status).

Optimal power flow (OPF) is a particularly relevant power system optimization problem which forms the basis for many applications. The OPF problem minimizes a specified cost function subject to both the power flow equations and engineering limits.

The OPF problem has a long history. An abridged presentation follows, with further details of the early history of the OPF problem provided in the surveys [10, 13]. For systems with negligible losses and no network constraints, it was recognized in the early 1930s that the least-cost operating point is achieved when all the generators have equal marginal costs [87, 88]. The 1940s and 1950s saw significant progress on loss factors that were incorporated into economic dispatch formulations [89]. Growing computational capabilities in the 1950s and 1960s facilitated the digital solution of power flow problems [90–93], which would eventually replace the “network analyzers” previously used to model power systems with analog circuits [94]. In 1960, [95] proposed an optimization formulation that minimized generation costs while accounting for losses using an AC power flow model. However, this formulation did not consider bounds on the variables. Shortly thereafter in 1962, [96] proposed what is generally considered the first OPF formulation by augmenting an AC power flow model and a generation-cost-minimizing objective function with engineering limits. In the several decades since, a wide variety of optimization algorithms have been applied to OPF problems [10–25].

This section next formally defines a prototypical formulation of the OPF problem. Let \mathcal{G} denote the set of generators. Define P_{Gi} and Q_{Gi} , respectively, as the active and reactive power outputs of the generator at bus i such that $P_{Gi} = P_i + P_{Di}$ and $Q_{Gi} = Q_i + Q_{Di}$ where $P_{Di} + jQ_{Di}$ is the complex power demand at bus i . Consider a typical OPF problem where each generator i has a cost function for active power generation denoted as $f_{Ci}(P_{Gi})$. Define upper and lower limits on active and reactive power generation, P^{max} , P^{min} , Q^{max} , and Q^{min} , which are all equal to zero at buses without generators. Specified limits on voltage magnitudes and phase angle differences are denoted as V^{min} , V^{max} and

2.2. Applications of the Power Flow Equations

19

θ^{min} , θ^{max} , respectively. The OPF problem is

$$\min \sum_{i \in \mathcal{G}} f_{Ci}(P_{Gi}) \quad (2.8a)$$

subject to

$$P_{Gi}^{min} \leq P_{Gi} \leq P_{Gi}^{max}, \quad \forall i \in \mathcal{N}, \quad (2.8b)$$

$$Q_{Gi}^{min} \leq Q_{Gi} \leq Q_{Gi}^{max}, \quad \forall i \in \mathcal{N}, \quad (2.8c)$$

$$(V_i^{min})^2 \leq |V_i|^2 \leq (V_i^{max})^2, \quad \forall i \in \mathcal{N}, \quad (2.8d)$$

$$\theta_{ik}^{min} \leq \angle V_i - \angle V_k \leq \theta_{ik}^{max}, \quad \forall (i, k) \in \mathcal{L}, \quad (2.8e)$$

$$\angle V_1 = 0, \quad (2.8f)$$

$$\text{A representation of the power flow equations,} \quad (2.8g)$$

$$\text{Limits on line flows.} \quad (2.8h)$$

At each bus $i \in \mathcal{N}$, constraints (2.8b) and (2.8c) limit the active and reactive power generation and constraint (2.8d) limits the voltage magnitude. Constraint (2.8e) limits the angle difference across each line. Angle difference limits are occasionally used as proxy constraints for transient stability requirements. Certain convex relaxations also rely on specified voltage angle limits, in which case the bounds θ^{max} and θ^{min} in (2.8e) should be large enough so that they do not restrict the OPF problem's feasible space. Constraint (2.8f) sets the reference bus angle to zero. The power flow equations in (2.8g) may take a variety of forms, as described earlier in this chapter. Moreover, any of the power flow relaxations and approximations surveyed in the remainder of this monograph may be applied to obtain a relaxation or approximation of the OPF problem.

The limits on line flows in (2.8h) are typically specified either in terms of apparent power flows or current flows, with active power flow serving as a surrogate for approximate models that do not incorporate reactive power (e.g., the DC power flow discussed in §5.2.3). The expressions for the apparent power and current flow constraints depend on the choice of power flow model, with e.g., [97, 98] providing various line flow expressions. Also, note that more general OPF formulations may include other types of constraints, such as contingency constraints, stability

constraints, and generator capability characteristics, as discussed in e.g., [18, 22–24, 50, 99].

More detailed descriptions of OPF and other power system optimization problems are presented in, e.g., [4, 5, 7, 19]. While the particulars of power system optimization problems and their associated constraints are very important for specific applications, this monograph focuses on the power flow representation itself rather than its embedding in a particular optimization problem. Therefore, the remainder of this monograph omits formulation-specific details except where they are necessary to illustrate certain representations of the power flow equations.

2.3 Examples of Power Flow Feasible Spaces

The *feasible space* for a system of equations refers to the set of points which satisfy those equations. For specified power injection and voltage magnitude set-point parameter values, as described in §2.2.1, the feasible space for the power flow equations generically consists of a finite set of isolated points corresponding to the power flow solutions. Power system optimization problems where power injection and voltage set-point parameters are allowed to vary, as described in §2.2.2, generally give rise to higher-dimensional feasible spaces. An optimization problem seeks a point in that feasible space which has least cost according to a specified objective function.

The feasible spaces defined by the power flow equations are generically non-convex. Certain optimization problems that incorporate the power flow equations, including OPF problems, may have multiple local optima [3] and are generally NP-Hard [1, 2], even for networks with radial topologies [2]. Many publications have studied the characteristics of the feasible spaces of power flow and optimal power flow problems, e.g., [3, 98, 100–114].

Many optimization solvers benefit from constraint qualification conditions that ensure strong duality (i.e., zero gap between the optimal objective values of the primal and dual problems). In order to ensure satisfaction of Slater’s constraint qualification condition [115], recent work [116] derives sufficient conditions for the existence of an interior point in the feasible spaces of power system optimization problems with

radial network topologies. Other recent work in [117] uses tools from differential topology to show that OPF problems used in various contexts almost surely satisfy the Linear Independence Constraint Quantification (LICQ) condition [118]. Thus, there generically exist unique sets of multipliers that satisfy the Karush–Kuhn–Tucker (KKT) conditions for all local optimizers to these problems. Additional related work in [119] studies critical cases of OPF problems where small parameter changes result in sharp discontinuities in the solution.

This section provides five illustrative examples of non-convex power flow feasible spaces. The one-line diagrams for all test cases in this section give values for the line impedances and shunt susceptances, power injections, and voltage magnitude set-points in per unit representation.³ A 100 MVA base power is used throughout this monograph. Note that other useful visualizations provided in [120] show the active and reactive power flows through a line as functions of various parameters.

Figure 2.3a shows the one-line diagram for the three-bus system studied in [100]. The voltage magnitudes are all fixed at 1.05 per unit and the active and reactive power injections are unconstrained. A cut through the corresponding feasible space is presented in Figure 2.3b. (Half of the surface is removed to reveal the inner folds.) This feasible space was constructed using the continuation method proposed in [100]. Observe that this feasible space is connected but non-convex as evidenced by the hole through the space seen in the projection of active and reactive power injection at bus 2 (i.e., the P_{G2} – Q_{G2} plane at the rear of the figure).

The next example corresponds to the three-bus system in [121, 122]. Figure 2.4a shows the one-line diagram for this system. Figure 2.4b provides the feasible space for this system constructed using the continuation approach in [100]. The feasible space is non-convex, with a

³Test case descriptions are available at <http://bettergrids.org>:

- Figure 2.3a: <http://item.bettergrids.org/handle/1001/418>
- Figure 2.4a: <http://item.bettergrids.org/handle/1001/419>
- Figure 2.5a: <http://item.bettergrids.org/handle/1001/420>
- Figure 2.6a: <http://item.bettergrids.org/handle/1001/422>
- Figure 2.7a: <http://item.bettergrids.org/handle/1001/421>

Table 2.2: Generation cost functions for the nine-bus system “case9mod” from [3].

Bus	c_{2i} [\$/per unit-hr] ²]	c_{1i} [\$/per unit-hr]	c_{0i} [\$/hr]
1	1100.0	500	150
2	85.0	120	600
3	122.5	100	335

hole through the space seen via a projection of active power injections P_{G1} , P_{G2} , and P_{G3} .

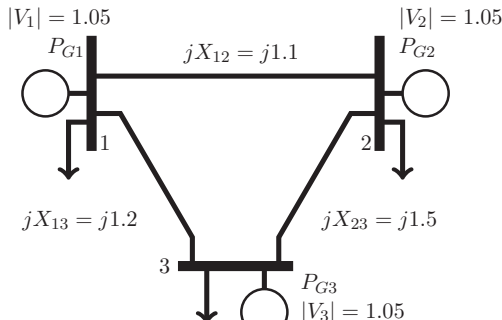
The third example corresponds to the five-bus system in [101]. Figure 2.5a shows the one-line diagram for the system and Figure 2.5b illustrates a projection of the feasible space in terms of active power injections. This example demonstrates, through the projection, that the feasible space of a lossless system may be non-convex.

The final two examples correspond to the five-bus system “WB5” and the nine-bus system “case9mod” in [3]. The feasible spaces for these examples were constructed using the algorithm proposed in [107]. This algorithm is guaranteed to yield a discretization of the entire feasible space to within a specified discretization tolerance. For these two examples, the feasible spaces are disconnected and have multiple local optima.

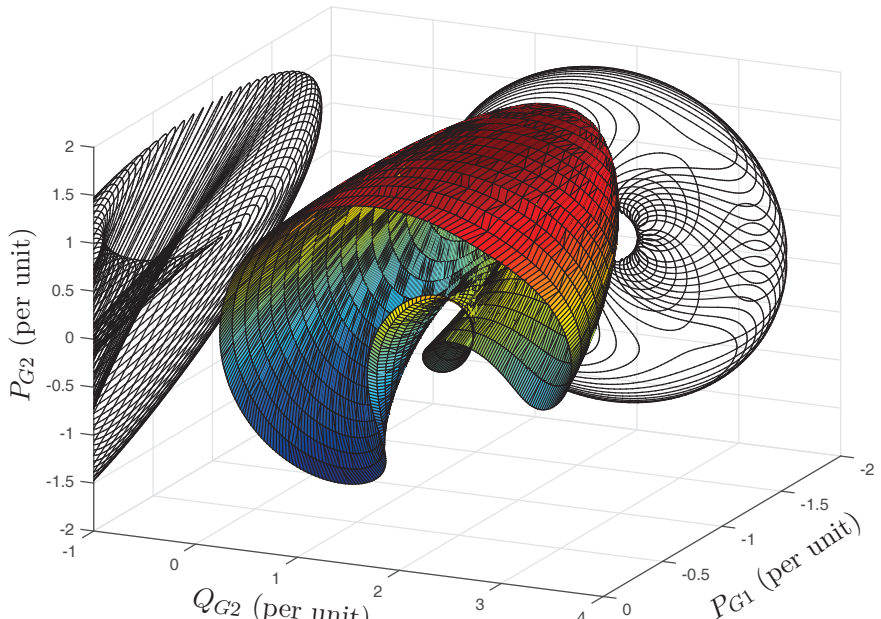
Figures 2.6a and 2.7a show the one-line diagrams for the WB5 and case9mod systems, respectively. The voltage magnitudes in WB5 are constrained to the range $|V_i| \in [0.95, 1.05]$ per unit and there are no line flow limits. The voltage magnitudes in case9mod are constrained to the range $|V_i| \in [0.90, 1.10]$ per unit and limits on the apparent power line flows are 250 MVA for all lines except for (5, 6) and (6, 7), which are limited to 150 MVA, and (3, 6), which is limited to 300 MVA. In order to better illustrate certain characteristics of the relaxations and approximations, the cost function for WB5 is modified to $10000P_{G1}^2 - 43000P_{G1} + 10000P_{G5}^2 - 36000P_{G5} + 78625\$/hr$ (for power generation values in per unit), which has an unconstrained minimizer at the point $(P_{G1}, P_{G5}) = (2.15, 1.80)$ per unit. For case9mod, the coefficients of the quadratic functions $c_{2i}P_{Gi}^2 + c_{1i}P_{Gi} + c_{0i}$ assigned to each generator $i = 1, 2, 3$ are given in Table 2.2.

2.3. Examples of Power Flow Feasible Spaces

23



(a) One-line diagram



(b) Feasible space

Figure 2.3: The three-bus system from [100]. The voltage magnitudes are all fixed to 1.05 per unit. The active and reactive power injections at each bus are unconstrained. The feasible space was constructed using the continuation approach in [100]. Half of the feasible space's surface is removed to reveal the inner folds. The feasible space is connected but non-convex.

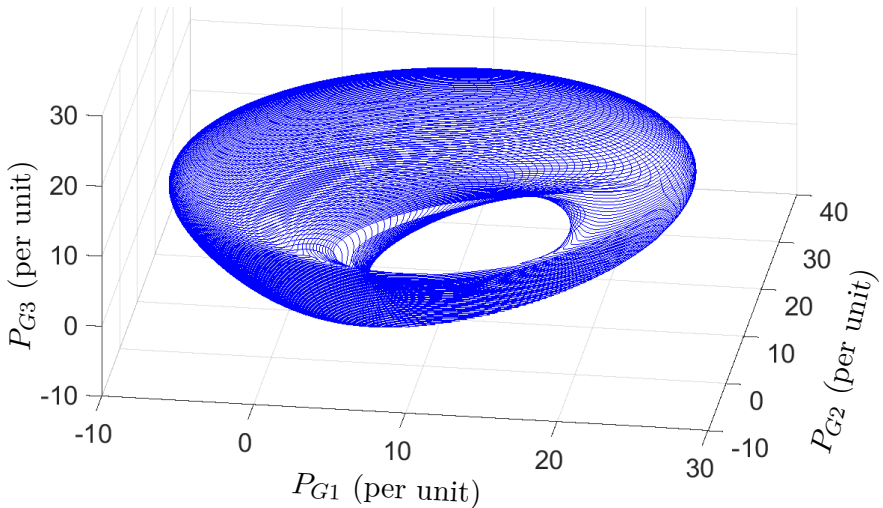
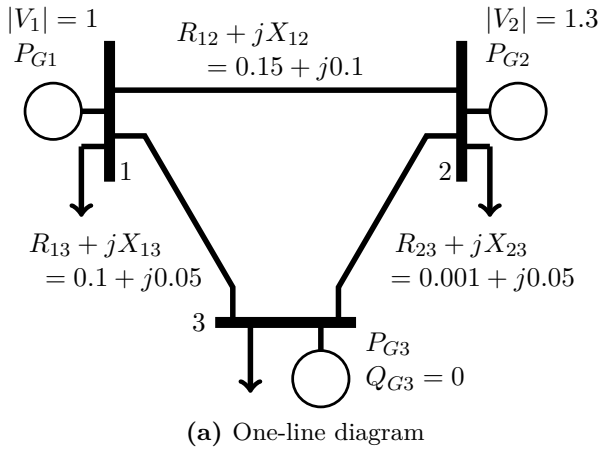


Figure 2.4: The three-bus system from [121, 122]. The voltage magnitudes at buses 1 and 2 are fixed at 1.0 and 1.3 per unit, respectively, while the voltage magnitude at bus 3 is unconstrained. The active power injections at each bus and the reactive power injections at buses 1 and 2 are unconstrained, while the reactive power injection at bus 3 is fixed to zero. The feasible space, which was constructed using the continuation approach in [100], is connected but non-convex.

2.3. Examples of Power Flow Feasible Spaces

25

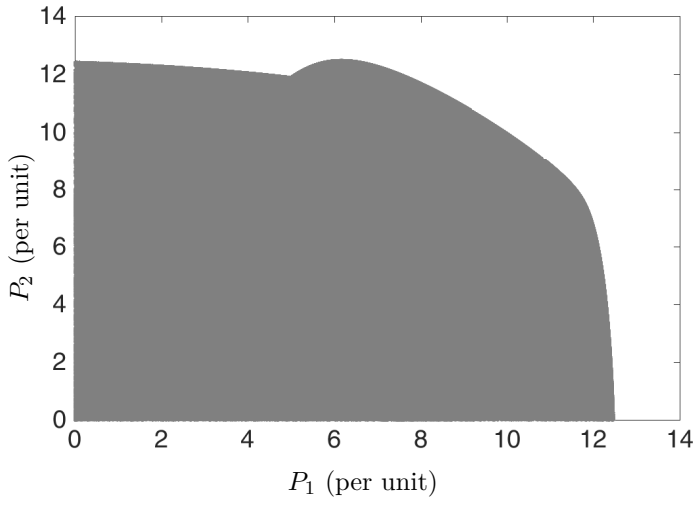
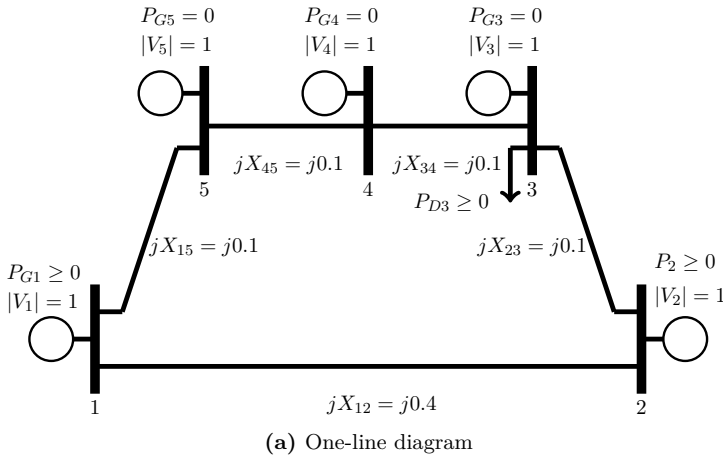
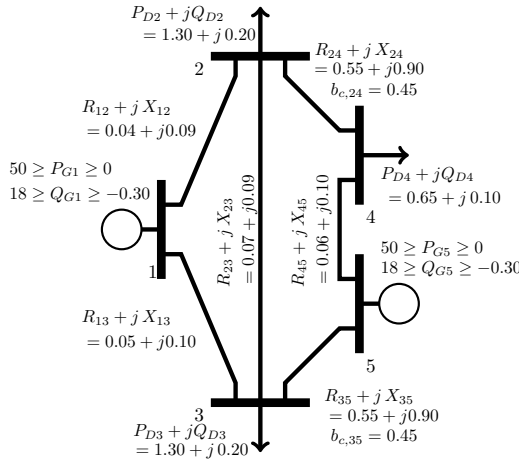
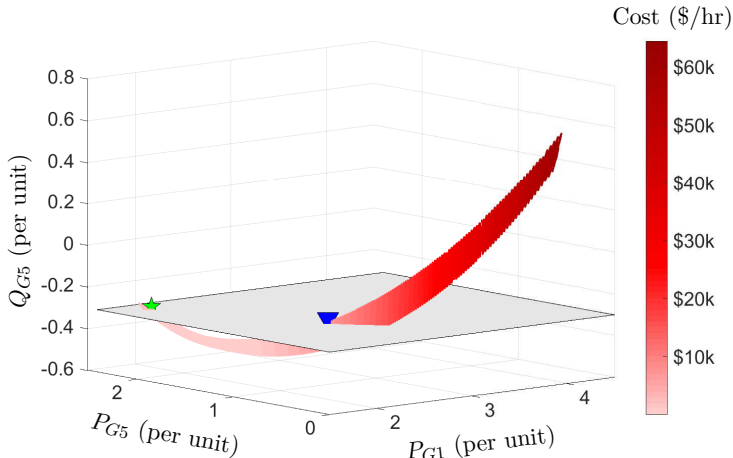


Figure 2.5: The five-bus system from [101]. The voltage magnitudes at each bus are fixed to 1.0 per unit. The active power injections at buses 1 and 2 are non-negative, the active power injection at bus 3 is non-positive, and the active power injections at buses 4 and 5 are zero. The reactive power injections at each bus are unconstrained. The particular symmetry in the parameters results in an analytical expression for the feasible space [101]. This analytical expression was exploited to create the figure. This test case demonstrates, through a projection of active power injections, that the feasible spaces of lossless systems may be non-convex.



(a) One-line diagram



(b) Feasible space

Figure 2.6: The five-bus system from [3]. The feasible space was constructed using the approach in [107]. The colors represent the generation cost. The gray plane shows the lower reactive power limit $Q_{G5} \geq -0.30$ per unit. This limit splits the feasible space into the two disconnected components which are above the gray plane. The green star shows the global solution and the blue triangle indicates a local optimum. This test case demonstrates that OPF problems with reasonable parameter values may have feasible spaces with multiple disconnected components.

2.3. Examples of Power Flow Feasible Spaces

27

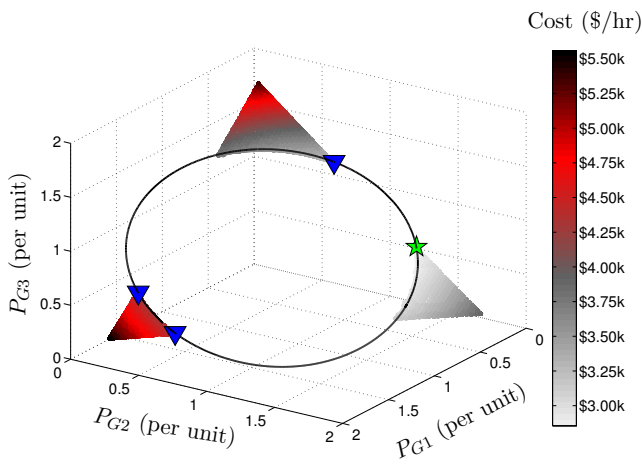
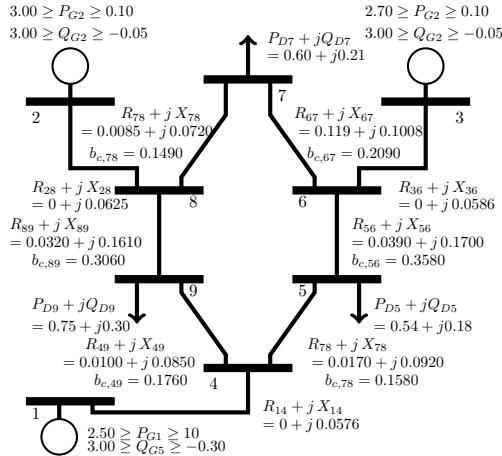


Figure 2.7: The nine-bus system “case9mod” from [3]. The feasible space was constructed using the approach in [107]. The colors represent the generation cost. The feasible space is split into three disconnected components by the black line, which signifies the set of points for which the limits $Q_{G1} \geq -0.05$, $Q_{G2} \geq -0.05$, $Q_{G3} \geq -0.05$, and $|V_9| \geq 0.9$ per unit are simultaneously binding. The green star shows the global solution and the blue triangles indicate local optima. This test case demonstrates that OPF problems with reasonable parameter values may have feasible spaces with multiple disconnected components.

The WB5 system in Figure 2.6 will be used at various points throughout the remainder of the monograph to illustrate certain salient characteristics of power flow relaxations and approximations.

3

Optimization Tools

As discussed in §2.3, the feasible spaces associated with the power flow equations can be non-convex, resulting in power system optimization problems that may have multiple local optima [3] and are generally NP-Hard [1, 2]. To circumvent the computational challenges involved with solving such optimization problems, a variety of power flow relaxations and approximations have been developed. These relaxations and approximations typically employ tools from convex optimization.

This chapter overviews four commonly used convex optimization tools relevant to both relaxations and approximations of the power flow equations: linear programming (LP), quadratic programming (QP), second-order cone programming (SOCP), and semidefinite programming (SDP) [123, 124]. This section presents these tools in their primal forms; their dual forms can be found in, e.g., [123].

3.1 Linear and Quadratic Programming

Linear programming is the most mature but least general optimization tool. Let $x \in \mathbb{R}^m$ denote the vector of decision variables. Linear programs enforce non-negativity of the decision variables: $x \geq 0$. Further linear constraints $\mathbf{A}x = b$ can be imposed, where \mathbf{A} is a specified matrix

with m columns and b is a specified vector. LPs have a linear objective function $c^\top x$. The canonical form of an LP is

$$\min_{x \in \mathbb{R}^m} c^\top x \quad (3.1a)$$

subject to

$$\mathbf{A}x = b, \quad (3.1b)$$

$$x \geq 0. \quad (3.1c)$$

Note that inequality constraints can be formulated by introducing non-negative slack variables, i.e., $\tilde{A}x \geq \tilde{b}$ is equivalently represented as the constraints $\tilde{A}x + y = \tilde{b}$ and $y \geq 0$.

A particularly relevant set of linear inequality constraints known as McCormick envelopes [125] are used in a variety of the power flow relaxations. McCormick envelopes, denoted as $\langle x y \rangle^M$, form the convex hulls of bilinear products $x y$, where x and y are generic variables with bounds x^{\min}, x^{\max} and y^{\min}, y^{\max} . These envelopes are:

$$\langle x y \rangle^M = \left\{ t : \begin{cases} t \geq x^{\min} y + y^{\min} x - x^{\min} y^{\min}, \\ t \geq x^{\max} y + y^{\max} x - x^{\max} y^{\max}, \\ t \leq x^{\min} y + y^{\max} x - x^{\min} y^{\max}, \\ t \leq x^{\max} y + y^{\min} x - x^{\max} y^{\min}. \end{cases} \right\}. \quad (3.2)$$

Figure 3.1 visualizes the lower bounding planes defined by the first two linear inequalities of (3.2). The upper bounding planes defined by the last two linear inequalities of (3.2) are similar.

A generalization of linear programming known as *quadratic programming* allows for a quadratic objective function:

$$\min_{x \in \mathbb{R}^m} x^\top \mathbf{C}x + c^\top x \quad (3.3a)$$

subject to

$$\mathbf{A}x = b, \quad (3.3b)$$

$$x \geq 0, \quad (3.3c)$$

where \mathbf{C} is a $m \times m$ matrix. If \mathbf{C} is positive semidefinite, then (3.3) is a *convex* quadratic program.

3.2. Second-Order Cone Programming

31

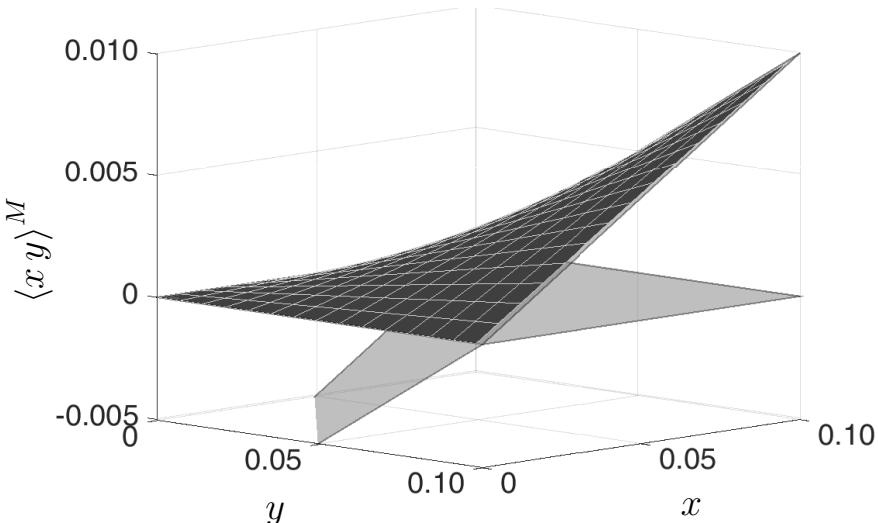


Figure 3.1: Visualization of the lower bounds for the McCormick envelopes defined in (3.2). The black region is the bilinear product xy which is lower bounded by the gray planes corresponding to the McCormick envelope. The upper bounding planes from the McCormick envelope (not shown) are similar.

A major advantage of linear and quadratic programming formulations is the existence of mature solvers, such as CPLEX, Gurobi, and MOSEK. These solvers also allow the modeling of mixed-integer linear programs (MILP) and mixed-integer quadratic programs (MIQP), which augment (3.1) and (3.3), respectively, with discrete variables that linearly enter the constraints and the objective function.

3.2 Second-Order Cone Programming

Second-order cone programs generalize linear programs. In addition to allowing linear constraints, $\mathbf{Ax} = b$, an SOCP has second-order cone constraints of the form $\|\mathbf{E}_i x + b_i\|_2 \leq g_i^\top x + d_i$, where $\|\cdot\|_2$ denotes the two-norm of a vector argument, \mathbf{E}_i is a matrix, g_i and b_i are vectors,

and d_i is a scalar. The canonical form of an SOCP is

$$\min_{x \in \mathbb{R}^m} c^\top x \quad (3.4a)$$

subject to

$$\|\mathbf{E}_i x + b_i\|_2 \leq g_i^\top x + d_i, \quad i = 1, \dots, r, \quad (3.4b)$$

$$\mathbf{A}x = b, \quad (3.4c)$$

$$x \geq 0, \quad (3.4d)$$

where r is the number of SOCP constraints. Various applications of second-order cone programming are described in [126, 127], including robust linear programming and certain operations on norms.

Observe that linear programming (3.1) is a special case of second-order cone programming (3.4). More generally, convex quadratic constraints can be represented as SOCP constraints. Consider the convex quadratic constraint

$$x^\top \mathbf{D}x + e^\top x + f \leq 0, \quad (3.5)$$

where \mathbf{D} is a positive semidefinite symmetric matrix and therefore has a Cholesky factorization $\mathbf{D} = \hat{\mathbf{D}}^\top \hat{\mathbf{D}}$, e is a vector, and f is a scalar. An equivalent representation of (3.5) takes the form of an SOCP constraint:

$$\left\| \begin{bmatrix} (1 + e^\top x + f) / 2 \\ \hat{\mathbf{D}}x \end{bmatrix} \right\|_2 \leq (1 - e^\top x - f) / 2. \quad (3.6)$$

Note that while (3.4) specifies a linear objective function, a convex quadratic objective function (3.3a) can be formulated by minimizing an auxiliary variable α and augmenting (3.4) with the constraint $\alpha \geq x^\top \mathbf{C}x + c^\top x$. Applying (3.6) yields an equivalent representation in canonical form:

$$\left\| \begin{bmatrix} (1 + c^\top x - \alpha) / 2 \\ \hat{\mathbf{C}}x \end{bmatrix} \right\|_2 \leq (1 - c^\top x + \alpha) / 2, \quad (3.7)$$

where $\hat{\mathbf{C}}$ is the Cholesky factorization of \mathbf{C} , i.e., $\mathbf{C} = \hat{\mathbf{C}}^\top \hat{\mathbf{C}}$. Convex quadratic programming (i.e., (3.3) with a positive semidefinite matrix \mathbf{C}) is therefore a special case of second-order cone programming.

In addition to convex quadratic constraints, “rotated SOCP constraints” are also particularly useful SOCP representations. A rotated SOCP constraint couples non-negative scalar variables $x \geq 0$ and $y \geq 0$ and the vector variable z :

$$x \cdot y \geq \|z\|_2^2, \quad (3.8a)$$

$$x \geq 0, \quad y \geq 0. \quad (3.8b)$$

Rotated SOCP constraints can be written in canonical form (3.4) as¹

$$\left\| \begin{bmatrix} (x - y)/2 \\ z \end{bmatrix} \right\|_2 \leq (x + y)/2, \quad (3.9a)$$

$$x \geq 0, \quad y \geq 0. \quad (3.9b)$$

While x and y in a rotated SOCP constraint must be real-valued, complex-valued vectors z are admissible. To obtain an equivalent real-valued formulation for a rotated SOCP constraint with a complex-valued

vector z , substitute (3.8a) with $x \cdot y \geq \left\| \begin{bmatrix} \operatorname{Re}(z) \\ \operatorname{Im}(z) \end{bmatrix} \right\|_2^2$.

Several commercial solvers are capable of solving SOCPs, including CPLEX, Gurobi, and MOSEK. These solvers are also applicable to SOCP problems augmented with discrete variables; however, the commercialization of solvers for *mixed-integer SOCP* problems is fairly recent compared to MILP solvers.

3.3 Semidefinite Programming

Semidefinite programs generalize second-order cone programs. In contrast to LPs and SOCPs, which have decision variables organized as a vector x , the decision variables in a semidefinite program take the form of a symmetric matrix \mathbf{X} . Let $\mathbf{X} \succeq 0$ indicate positive semidefiniteness

¹To see this equivalence, observe that (3.9) implies that $\frac{(x-y)^2}{4} + \|z\|_2^2 \leq \frac{(x+y)^2}{4}$. Expanding both sides yields $\frac{x^2 - 2xy + y^2}{4} + \|z\|_2^2 \leq \frac{x^2 + 2xy + y^2}{4}$, which simplifies to $\|z\|_2^2 - xy \leq 0$. Adding xy to both sides yields (3.8).

of the matrix \mathbf{X} . The canonical form of a semidefinite program is

$$\min_{\mathbf{X}} \text{tr}(\mathbf{C}\mathbf{X}) \quad (3.10a)$$

subject to

$$\text{tr}(\mathbf{A}_i \mathbf{X}) = b_i, \quad i = 1, \dots, r, \quad (3.10b)$$

$$\mathbf{X} \succeq 0, \quad (3.10c)$$

where $\text{tr}(\cdot)$ denotes the trace operator, \mathbf{A}_i and \mathbf{C} are specified square, symmetric matrices, and b_i are specified scalars. Since $\text{tr}(\mathbf{AB}) = \sum_i \sum_k \mathbf{A}_{ik} \mathbf{B}_{ki}$, the constraints (3.10b) are linear in the entries of the matrix variable \mathbf{X} . Various applications of semidefinite programming (e.g., certain operations on eigenvalues, singular values, and determinants) are discussed in [127].

Recall that positive semidefiniteness of a matrix implies non-negativity of all its diagonal entries [128]. Thus, scalar inequality constraints can be formulated in a semidefinite program by augmenting the positive semidefinite matrix \mathbf{X} with a 1×1 diagonal block to serve as a non-negative slack variable (i.e., the constraints $\text{tr}(\tilde{\mathbf{A}}_i \mathbf{X}) \geq \tilde{b}$ and $\mathbf{X} \succeq 0$ can be written as $\text{tr}(\tilde{\mathbf{A}}_i \mathbf{X}) + x = \tilde{b}$ and $\begin{bmatrix} \mathbf{X} & 0 \\ 0 & x \end{bmatrix} \succeq 0$ where x is a scalar slack variable). This implies that semidefinite programming generalizes linear programming.

Moreover, SOCP constraints (3.4b) can be formulated as SDP constraints, and semidefinite programming thus generalizes second-order cone programming. Specifically, (3.4b) is equivalent to

$$\begin{bmatrix} (g_i^\top x + d_i) \mathbf{I} & (\mathbf{E}_i x + b_i) \\ (\mathbf{E}_i x + b_i)^\top & (g_i^\top x + d_i) \end{bmatrix} \succeq 0, \quad (3.11)$$

where \mathbf{I} is an appropriately sized identity matrix (i.e., dimension equal to the number of rows of \mathbf{E}) [126].

Typical SDP solvers allow a mix of SDP, SOCP and LP constraints. Since linear and SOCP constraints generally result in performance that is superior to SDP constraints, it is best to formulate constraints in the simplest possible representation, i.e., only formulate a constraint as an SDP if it is not possible to formulate it as an SOCP or linear constraint.

Similarly, only formulate a constraint as an SOCP if it is not possible to write it as a linear constraint.

Complex variables are particularly relevant to the power flow equations due to the phasor representations of voltages. Although all currently available SDP solvers use real-valued operations in their internal computations, there can be both theoretical and practical advantages in complex-valued SDP formulations. (Further details can be found in §4.1.2 and [129, 130].)

Let $(\cdot)^H$ denote the complex conjugate transpose operator. Consider a positive semidefinite Hermitian matrix $\mathbf{Z} \succeq 0$. (Recall that the eigenvalues of a Hermitian matrix are real-valued, so positive semidefiniteness is well-defined.) The complex analogue of (3.10) is

$$\min_{\mathbf{Z}} \operatorname{tr}(\check{\mathbf{C}}\mathbf{Z}) \quad (3.12a)$$

subject to

$$\operatorname{tr}(\check{\mathbf{A}}_i \mathbf{Z}) = \check{b}_i, \quad i = 1, \dots, r, \quad (3.12b)$$

$$\mathbf{Z} \succeq 0, \quad (3.12c)$$

where \check{b}_i is a real scalar and $\check{\mathbf{A}}_i$ and $\check{\mathbf{C}}$ are specified Hermitian matrices, which results in $\operatorname{tr}(\check{\mathbf{A}}_i \mathbf{Z})$ and $\operatorname{tr}(\check{\mathbf{C}}\mathbf{Z})$ being real-valued quantities.

To convert (3.12) to real-valued canonical form (3.10), use the following equivalence: the Hermitian matrix $\mathbf{Z} \in \mathbb{C}^{n \times n}$ is positive semidefinite if and only if the matrix $\begin{bmatrix} \operatorname{Re}(\mathbf{Z}) & -\operatorname{Im}(\mathbf{Z}) \\ \operatorname{Im}(\mathbf{Z}) & \operatorname{Re}(\mathbf{Z}) \end{bmatrix} \in \mathbb{R}^{2n \times 2n}$ is positive semidefinite [123, 127]. Creating real-valued matrix variables representing the real and imaginary parts of \mathbf{Z} and using this equivalence on the positive semidefinite constraint (3.12c) allows the reformulation from (3.12) in terms of a $n \times n$ Hermitian matrix variable to an equivalent representation in the form of (3.10) with a $2n \times 2n$ real-valued symmetric matrix variable. Note that this conversion is done automatically in modeling languages such as YALMIP [131] and CVX [132].

While SDP solvers are generally less mature than LP and SOCP solvers, there are several commercial packages available, including MOSEK [133] and PENSDP [134], as well as a variety of academic packages (e.g., SeDuMi [135], SDPT3 [136], SDPA [137], CSDP [138],

etc.).² There are also a small number of packages capable of handling mixed-integer SDP problems, including YALMIP [131], SCIP-SDP [139], and Pajarito [140].

²A list of convex optimization solvers is available at <https://yalmip.github.io/allsolvers/>.

4

Convex Relaxations of the Power Flow Equations

This chapter overviews convex relaxations of the power flow equations. The first three sections of this chapter are organized based on the associated optimization tool (SDP, SOCP, or QP/LP). The final section reviews a variety of techniques for tightening the relaxations.

Convex relaxations enclose, within a convex space, the non-convex feasible space associated with the power flow equations. The solution to the resulting convex problem bounds the optimal objective value of the original non-convex problem. Specifically, a relaxation provides a lower bound for a minimization problem and an upper bound for a maximization problem. Furthermore, relaxations can certify problem infeasibility since infeasibility of a convex relaxation guarantees that no feasible points exist for the original non-convex optimization problem. This is a sufficient but not necessary condition: a relaxation may be feasible when the original non-convex problem is infeasible.

Some power flow relaxations are *exact* for certain power system optimization problems. An exact relaxation provides a bound that is equal to the globally optimal objective value (i.e., there is no *relaxation gap* between the objective value of the global solution to the non-convex problem and the objective value of an exact relaxation). An exact

relaxation may or may not provide globally optimal decision variables (i.e., decision variables for which the original non-convex optimization problem achieves the globally optimal objective value).¹

For many cases where relaxations do not provide the globally optimal voltage phasors, the power injections and line flows resulting from the relaxations may be close to those of the true global solution. However, there are no known guarantees that this will be the case. Empirical and analytical investigations regarding the quality of solutions provided by relaxations is an active area of research.

The convex relaxations in this monograph address the non-convexity resulting from the power flow equations. Other sources of non-convexity (e.g., on/off generator statuses in unit commitment problems and binary variables associated with switched capacitors) may result in a non-convex optimization problem even after applying a convex relaxation of the power flow equations. Regardless, a formulation that eliminates the non-convexity associated with the power flow equations often has theoretical and computational advantages. For instance, a linear relaxation of the power flow equations may result in a mixed-integer linear program, for which there exist efficient commercial solvers capable of obtaining a globally optimal solution to the relaxed problem.

In addition to the power flow equations, the ability to represent certain convex non-linear constraints in SDP and SOCP formulations facilitates the modeling of many other features relevant to power system optimization problems, such as limits on the squared magnitudes of current and apparent power flows as well as maximum phase angle differences across lines [71, 98, 141–143]. Further, steady-state induction machine models [144], approximations of ZIP load models (i.e., loads with constant-power, constant-current, and constant-impedance components) [145, 146], an approximation of Unified Power Flow Controller

¹The solution set for a relaxation may be a connected subset of the relaxation's feasible space for which all points share the same objective value. If the relaxation is exact, the objective value shared across this subset is the globally optimal objective value of the original non-convex problem, and one or more points in this subset correspond to decision variables that are feasible in the original non-convex optimization problem. Such points are global optima for the original non-convex problem. As one trivial example, all feasible points for an optimization problem with a constant objective (i.e., $\min 0$) are globally optimal.

(UPFC) devices [147], High-Voltage DC (HVDC) lines [148–151], devices modeled with discrete decision variables such as on/off loads and switchable transmission lines [152–156], and both voltage magnitude and phase shift regulating transformers [146, 147, 150, 152, 156–161] can be incorporated or approximated in many of the relaxations discussed in this chapter.

4.1 Semidefinite Programming Relaxations of the Power Flow Equations

When expressed in rectangular coordinates (2.4), the power flow equations are quadratic polynomials in the voltage components V_d and V_q . This enables the application of polynomial optimization theory, including the Shor relaxation and hierarchies of moment/sum-of-squares relaxations. Related relaxations can also be formulated using the power flow equations with complex voltage phasors (2.3).

4.1.1 The Shor Relaxation

In 1987, [162] proposed an SDP relaxation of non-convex quadratically constrained quadratic programs (QCQPs), a class of optimization problems that is highly relevant to the power flow equations. The first application of SDP to electric power systems was in [163], which presents a relaxation of the OPF problem. The work in [164] (with the core ideas initially presented in [165]) popularized the approach of using SDPs to solve OPF problems by showing that a related SDP relaxation provides both an exact bound on the optimal objective value and the globally optimal decision variables for many of the IEEE OPF test cases [166].

This section presents the mathematical formulation for the SDP relaxation of [164] and related variants, discusses the exactness of the relaxation, and summarizes computational developments.

Mathematical Formulation

The approach in [164] develops a Shor relaxation by first writing a formulation of the power flow equations where all non-convexity is contained within a rank constraint. An SDP relaxation is then constructed by not enforcing the rank constraint.

Let e_k denote the k^{th} standard basis vector in \mathbb{R}^n . For each bus $i \in \mathcal{N}$, define the matrices $\mathbf{L}_{P,k}$, $\mathbf{L}_{Q,k}$, \mathbf{M}_k , and \mathbf{N}_k :

$$\mathbf{L}_{P,k} = \frac{1}{2} \begin{bmatrix} \operatorname{Re}(\mathbf{Y}^\top e_k e_k^\top + e_k e_k^\top \mathbf{Y}) & \operatorname{Im}(\mathbf{Y}^\top e_k e_k^\top - e_k e_k^\top \mathbf{Y}) \\ \operatorname{Im}(e_k e_k^\top \mathbf{Y} - \mathbf{Y}^\top e_k e_k^\top) & \operatorname{Re}(\mathbf{Y}^\top e_k e_k^\top + e_k e_k^\top \mathbf{Y}) \end{bmatrix}, \quad (4.1a)$$

$$\mathbf{L}_{Q,k} = -\frac{1}{2} \begin{bmatrix} \operatorname{Im}(\mathbf{Y}^\top e_k e_k^\top + e_k e_k^\top \mathbf{Y}) & \operatorname{Re}(e_k e_k^\top \mathbf{Y} - \mathbf{Y}^\top e_k e_k^\top) \\ \operatorname{Re}(\mathbf{Y}^\top e_k e_k^\top - e_k e_k^\top \mathbf{Y}) & \operatorname{Im}(\mathbf{Y}^\top e_k e_k^\top + e_k e_k^\top \mathbf{Y}) \end{bmatrix}, \quad (4.1b)$$

$$\mathbf{M}_k = \begin{bmatrix} e_k e_k^\top & \mathbf{0} \\ \mathbf{0} & e_k e_k^\top \end{bmatrix}, \quad (4.1c)$$

$$\mathbf{N}_k = \begin{bmatrix} \mathbf{0} & \mathbf{0} \\ \mathbf{0} & e_k e_k^\top \end{bmatrix}. \quad (4.1d)$$

The power flow equations can then be equivalently represented as

$$P_i = \operatorname{tr}(\mathbf{L}_{P,k} \mathbf{W}), \quad (4.2a)$$

$$Q_i = \operatorname{tr}(\mathbf{L}_{Q,k} \mathbf{W}), \quad (4.2b)$$

$$|V_i|^2 = \operatorname{tr}(\mathbf{M}_k \mathbf{W}), \quad (4.2c)$$

$$0 = \operatorname{tr}(\mathbf{N}_k \mathbf{W}), \quad (4.2d)$$

$$\mathbf{W} = xx^\top, \quad (4.2e)$$

where $x = [V_{d1} \dots V_{dn} \ V_{q1} \dots V_{qn}]^\top$. Observe that (4.2d) sets the angle at the reference bus to zero. One can alternatively enforce the angle reference by deleting V_{q1} from x as well as the $(n+1)$ -th row and column from the \mathbf{W} matrix, with corresponding modifications to the matrices in (4.1a)–(4.1c) and elimination of (4.2d). This improves computational tractability by reducing the size of the semidefinite optimization problem.

The Shor relaxation is applicable to optimization problems with objective functions that are quadratic in x , or, equivalently, linear in the entries of \mathbf{W} . This includes linear functions of active and reactive power injections as well as squared voltage magnitudes. More general objectives, such as convex quadratic functions of active power injections, can also be formulated using a lifted variable in combination with an SOCP constraint as described in §3.2.

4.1. Semidefinite Programming Relaxations

41

To form an SDP relaxation, the approach in [164] replaces the rank constraint (4.2e) with the less stringent constraint

$$\mathbf{W} \succeq 0. \quad (4.3)$$

If the solution \mathbf{W}^* to the SDP relaxation satisfies the rank condition

$$\text{rank}(\mathbf{W}^*) = 1, \quad (4.4)$$

then the SDP relaxation is exact and globally optimal decision variables can be recovered. Let λ be the non-zero eigenvalue of the solution \mathbf{W}^* with associated unit-length eigenvector ν . Denote ν_d and ν_q as the vectors consisting of the entries of ν from ν_1 to ν_n and from ν_{n+1} to ν_{2n} , respectively. The globally optimal voltage phasors are

$$V^* = \sqrt{\lambda} (\nu_d + j\nu_q). \quad (4.5)$$

A complex-valued Shor relaxation is formulated using the Hermitian matrices

$$\mathbf{H}_{P,k} = \frac{\mathbf{Y}^H e_k e_k^\top + e_k e_k^\top \mathbf{Y}}{2}, \quad (4.6a)$$

$$\mathbf{H}_{Q,k} = \frac{\mathbf{Y}^H e_k e_k^\top - e_k e_k^\top \mathbf{Y}}{2j}. \quad (4.6b)$$

The corresponding power flow formulation is

$$P_i = \text{tr}(\mathbf{H}_{P,k} \mathbf{Z}), \quad (4.7a)$$

$$Q_i = \text{tr}(\mathbf{H}_{Q,k} \mathbf{Z}), \quad (4.7b)$$

$$|V_i|^2 = \text{tr}(e_k e_k^\top \mathbf{Z}), \quad (4.7c)$$

$$\mathbf{Z} = z z^H, \quad (4.7d)$$

where $z = [v_1 \dots v_n]^\top$ contains the complex voltage phasors. As will be discussed later in this section, rather than explicitly enforcing the angle reference constraint, the complex Shor relaxation sets the angle reference by rotating the voltage vector corresponding to a rank-one solution.

The SDP relaxation is formed by replacing the rank constraint (4.7d) with a positive semidefinite constraint on the $n \times n$ Hermitian matrix \mathbf{Z} :

$$\mathbf{Z} \succeq 0. \quad (4.8)$$

Recall that §3.3 discusses the mechanism for converting from a positive semidefinite constraint on a complex-valued Hermitian matrix to a real-valued symmetric positive semidefinite matrix constraint appropriate for input to typical SDP solvers.

If the solution \mathbf{Z}^* satisfies the rank condition

$$\text{rank}(\mathbf{Z}^*) = 1, \quad (4.9)$$

then the globally optimal voltage phasors are

$$V^* = \sqrt{\lambda} \nu, \quad (4.10)$$

where λ is the non-zero eigenvalue of \mathbf{Z}^* with corresponding unit-length eigenvector ν , rotated such that $\angle \nu_1 = 0^\circ$.

The real and complex Shor relaxations, (4.2a)–(4.2d), (4.3) and (4.7a)–(4.7a), (4.8), are “equivalent” in the sense that 1) both relaxations provide the same optimal objective value and 2) an optimal solution to each relaxation can easily be constructed from the optimal solution to the other relaxation [129, Appendices B and C].

Note that the Shor relaxations presented here assume a balanced single-phase equivalent network model. These relaxations can be extended to unbalanced three-phase network models [146, 159, 167–169].

Exactness

The Shor relaxation satisfies (4.4) and is therefore exact for many of the OPF problems corresponding to the IEEE test cases [164] and several large-scale models of European electric grids [129, 141].² (Test case descriptions are provided in [50, 166].)

Despite being exact for some OPF test cases, there exist OPF problems for which the Shor relaxation proposed in [164] is not exact. This was first demonstrated using the three-bus OPF test case in [170]. A variety of other test cases for which the Shor relaxation fails to be exact are explored for optimal power flow problems in [3, 103, 107, 121, 171–174] and state estimation problems in [175]. Developing further insights

²Exactness is obtained for a slight modification of these systems which enforces a small minimum series resistance (e.g., 1×10^{-4} per unit) on each line. Note that this modification’s success seems to be related to the test cases’ objectives, which minimize increasing functions of active power generation.

regarding the tightness of the Shor relaxation is largely an empirical task. Most of the related literature has focused on characterizing the exactness (or lack therefore) of the Shor relaxation with respect to OPF problems; less is known regarding exactness for other power system optimization problems. Many existing empirical studies regarding exactness of the Shor relaxation, e.g., [176, 177], have relied on the limited set of publicly available power system test cases, such as the NESTA [178] and PGLib [179] test case archives. More rigorous empirical statements will require experimentation with additional test systems, potentially leveraging forthcoming OPF benchmark problems [180]. Notable recent work in this direction is presented in [174], which finds that an optimal power flow problem for a 706-bus system used by the French Transmission Operator RTE can exhibit large optimality gaps (both for the Shor relaxation and the QC relaxation discussed in §4.2.1). Moreover, this problem undergoes “phase transitions” between large and small optimality gaps as the loading varies.

Exactness of the Shor relaxation is influenced by the choice of objective function, with objectives that minimize increasing functions of active power generation (e.g., generation cost, losses) tending to more often result in an exact relaxation [104]. Note that there are practical power system optimization problems whose objectives are not increasing functions of active power generation, such as tracking an active power setpoint, achieving a specified voltage profile, minimizing load shedding, and optimizing volt/var setpoints [181–183]. The problem’s constraints also play an important role, with constraint formulations that are similar in the non-convex problem possibly exhibiting significantly different characteristics in the relaxations (e.g., line-flow limits based on angle differences, apparent power flows, and active power flows can perform very differently in the Shor relaxation [98]).

Notice that the rank conditions (4.4) and (4.9) can only be checked after solving the relaxation. There have been efforts to find sufficient conditions for which the Shor relaxation is a priori guaranteed to be exact. Many of the resulting a priori sufficient conditions follow from conditions for a (generally weaker) SOCP relaxation. These conditions will be discussed in §4.2 and are reviewed in [75]. There are also several known a priori sufficient conditions that are specific to the Shor

relaxation. These conditions are stated with the help of two definitions related to the network topology. A “length- k loop network” consists of a single cycle with length k . A “weakly cyclic network” (also referred to as a “cactus network”) is a network where every line belongs to at most one cycle. Using these definitions, the known exactness conditions for Shor relaxations of OPF problems are:

- Weakly-cyclic meshed networks where each cycle has length equal to three, with line-flow limits specified in terms of the magnitudes of the differences in the terminal voltage phasors and a “load oversatisfaction” assumption [98].³
- Lossless networks that are cycles with at most one chord (or potentially multiple such cycles that are connected by a tree topology) and the only inequality constraints are voltage magnitude limits [184].
- Length-3 loop networks where all lines have equal resistance-to-reactance ratios, there are no lower bounds on active and reactive power injections, and line-flow limits are specified in terms of the magnitudes of the differences in the terminal voltage phasors [185].
- Lossless, length-4 loop networks without upper or lower limits on reactive power injections and no line-flow limits [185].
- Lossless, arbitrary-length loop networks without upper or lower limits on active power injection, without lower limits on reactive power injections, and line-flow limits specified in terms of the magnitudes of the differences in the terminal voltage phasors [185].
- Lossless networks without lower limits on reactive power generation, limits on active power injections at every bus that include

³Rather than fixed power injections modeled with equality constraints, the “load oversatisfaction” assumption results in load models that are inequality constraints with upper limits on the active and reactive power injections equal to the specified load demands and no lower limits (i.e., power consumption can arbitrarily increase beyond the specified demands). See §4.2.3 for further discussion on the load oversatisfaction assumption.

zero, and an objective that is an increasing function of reactive power generation [185].

Note that there exist bounds on the rank of the solution matrix based on a characteristic of the network topology called the *treewidth* [186]. The treewidth of a network is relevant to the computational aspects of SDPs and will be further discussed in the following section on computational developments. Other bounds regarding the rank of the solution matrix are derived in [185] for optimization problems which have weakly cyclic network topologies and do not enforce certain limits on active and reactive power injections.

The fact that the Shor relaxation is exact for many problems which do not satisfy any known sufficient conditions suggests the potential for developing more broadly applicable sufficient conditions. One natural speculation is that such sufficient conditions may be related to physical aspects of the power flow equations (e.g., proximity to voltage collapse). However, a small test case in [122] dampens enthusiasm for this avenue of research. The test case in [122] has two mathematically equivalent formulations. The Shor relaxation is exact for one formulation, but is not exact for the other. Thus, strictly physically based sufficient conditions cannot predict the relaxation’s success or failure to be exact for all problems. Developing more general sufficient conditions is an open problem.

There have also been approaches that seek to modify the non-convex optimization problem such that the resulting Shor relaxation is exact for the modified problem (e.g., the penalization approaches in [98, 187] and the Laplacian objective approach in [188]). These modified formulations are *not relaxations* of the original non-convex problem. These approaches are therefore discussed in §6, which focuses on methods for finding feasible points for the power flow equations.

When the Shor relaxation is not exact, it can generally be tightened via augmentation with certain convex inequalities as well as constraints from relaxations that are not dominated by the Shor relaxation. See §4.4 for further discussion on such approaches. Other tightening approaches include the “moment/sum-of-squares” relaxations presented in §4.1.2, which generalize the Shor relaxation.

It may also be the case that a solution to the Shor relaxation does not satisfy the rank constraint (4.4) but the objective value from the relaxation is, in fact, the global optimum of the original non-convex problem. This situation occurs when the global solution for the non-convex problem is contained within a larger set of solutions to the relaxation (i.e., there exists a rank-one solution within a set of solutions to the relaxation, some of which have higher rank). The iterative approach in [189] searches for such “hidden” rank-one solutions when the rank condition (4.4) is not satisfied.

Computational Developments

Significant efforts have addressed the computational challenges associated with solving the Shor relaxation. The computational challenges result from the positive semidefinite constraint on the $2n \times 2n$ real-valued matrix in (4.3) (or the $n \times n$ Hermitian matrix in (4.8)). The number of variables in the positive-semidefinite-constrained matrix grows as $\mathcal{O}(n^2)$. Directly implementing the positive semidefinite constraint on the $2n \times 2n$ matrix typically results in computational intractability for systems with more than a few hundred buses.

Fortunately, a method exists for exploiting the *chordal sparsity* of the network which enables the solution of problems with thousands of buses. The positive semidefinite matrix completion theorem of [190] provides a necessary and sufficient condition for positive semidefiniteness of a matrix where the relevant entries are defined with respect to an underlying graph (i.e., the graph corresponding to the power system network).⁴ Several graph theoretic definitions are needed to state this matrix completion theorem. In particular, a *clique* is a completely connected subgraph (i.e., a set of nodes which are all adjacent to each other). A *maximal clique* is a clique which is not a subset of another clique. A *maximum clique* is a clique which has the largest size among all cliques in the graph. A *chord* is an edge connecting two non-adjacent nodes in a cycle. A *chordal graph* has the property that all cycles with more than three nodes have a chord. A *chordal*

⁴Theorem 10.1 in [191] uses arguments based on linear algebra to provide a simplified proof of the positive semidefinite matrix completion theorem.

extension of a graph is a supergraph (i.e., a graph that includes all of the original edges plus some additional edges) that is chordal. A chordal extension can be constructed using the sparsity pattern of the Cholesky factorization of the network's adjacency matrix [141]. A minimum degree ordering [192] assists in obtaining a sparse chordal extension (i.e., reducing the number of additional edges in the chordal supergraph). Note that the maximal cliques of a chordal graph can be obtained in linear time [193]. Figure 4.1a illustrates these definitions with a small test case.

Using these definitions, the matrix completion theorem of [190] states that the \mathbf{W} matrix in (4.3) is positive semidefinite if and only if all submatrices associated with the maximal cliques of a chordal extension of the network graph are positive semidefinite. Figure 4.1b illustrates this theorem for the small test case in Figure 4.1a.

Since typical power systems have a small *treenwidth*, which is a scalar defined as one less than the size of the smallest maximum clique among all possible chordal extensions of the network graph, the largest submatrix is usually much smaller than the full matrix. Thus, the matrix completion theorem [190] allows for the decomposition of the constraint $\mathbf{W} \succeq 0$ into positive semidefinite constraints on many smaller submatrices. Figure 4.2 shows an illustration of the relative matrix sizes for the original and decomposed matrices for the IEEE 300-bus system [166]. Even though exploiting sparsity results in many more positive semidefinite matrix constraints, the decomposed matrices are significantly smaller than the original $2n \times 2n$ matrix in (4.3), resulting in substantial computational advantages.

Note that for systems modeled with balanced single-phase equivalent networks that have radial topologies, exploiting chordal sparsity for the Shor relaxation in complex voltage phasors (i.e., (4.7a)–(4.7c) and (4.8)) yields Jabr's SOCP relaxation [194], which will be described in §4.2.1. For Shor relaxations of problems with meshed networks, note that the positive semidefinite constraints on the submatrices associated with size-two maximal cliques can be formulated using SOCP constraints rather than more computationally expensive SDP constraints.

Since a completion theorem similar to that in [190] holds for the rank of a positive semidefinite matrix defined over a graph [195], the

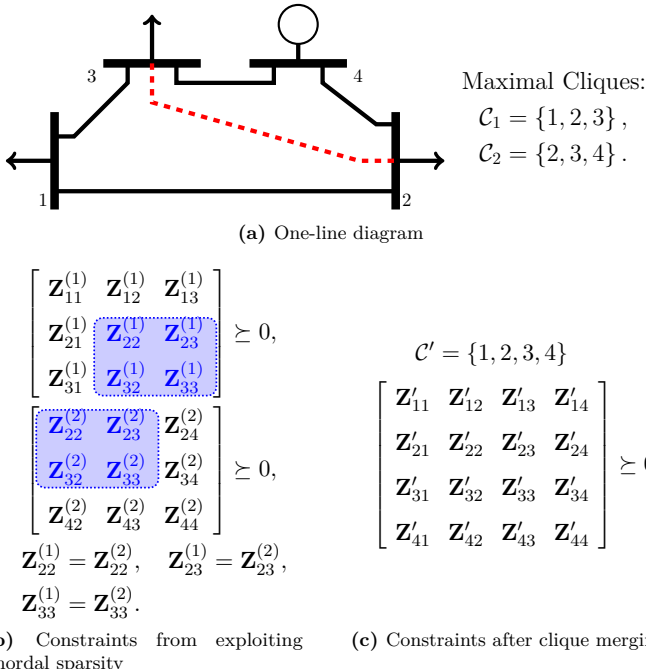
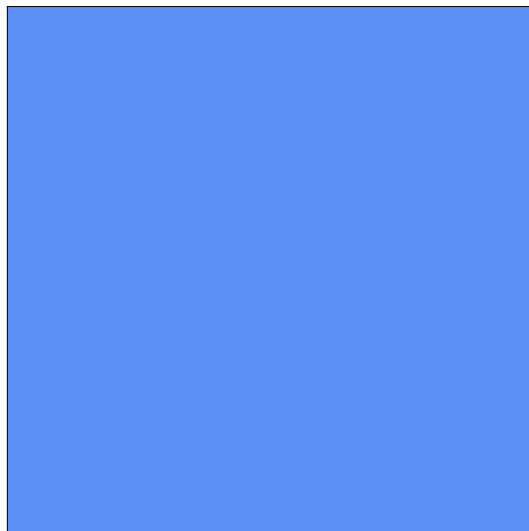
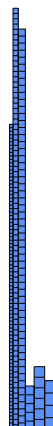


Figure 4.1: Exploitation of chordal sparsity for a four-bus system. The network in Figure 4.1a shown by the black lines is not chordal since the cycle $\{1, 2, 3, 4\}$ does not have a chord. The red dashed line in Figure 4.1a is a chord for this cycle since it connects buses 2 and 3, which are in the cycle but not adjacent. Addition of the red dashed line thus yields a chordal extension of the network topology. This chordal extension has the two maximal cliques denoted \mathcal{C}_1 and \mathcal{C}_2 . Figure 4.1b shows the decomposition of the positive semidefinite constraint (4.8) in a chordal-sparsity exploiting Shor relaxation. Superscripts $(\cdot)^{(1)}$ and $(\cdot)^{(2)}$ refer to the clique number. The highlighted blue matrix entries indicate terms which correspond to the same term in the original \mathbf{Z} matrix and therefore require equality constraints as shown in the figure. Note that the Hermitian structure enforces $\mathbf{Z}_{32}^{(1)} = \mathbf{Z}_{32}^{(2)}$ by construction.

Figure 4.1c demonstrates the possible computational advantages of merging maximal cliques. Merging cliques \mathcal{C}_1 and \mathcal{C}_2 (i.e., constructing a supergraph that has an additional connection between buses 1 and 4) yields the constraint shown in Figure 4.1c, with the prime superscript $(\cdot)'$ indicating terms in the merged clique. Observe that merging the maximal cliques eliminates the equality constraints. Moreover, merging the maximal cliques results in a single positive semidefinite matrix constraint on a 4×4 matrix rather than positive semidefinite constraints on two 3×3 matrices, reducing the total number of matrix entries from $3 \times 3 + 3 \times 3 = 18$ to $4 \times 4 = 16$. (Note that while applying clique merging to this example results in a formulation that is equivalent to the Shor relaxation without exploiting sparsity, this is not the case in general.) Further details can be found in [141].



Size of the matrix
without decomposition.



Sizes of the submatrices resulting from
the matrix completion decomposition.

Figure 4.2: Relative sizes of the matrix for the original Shor relaxation (top) and the submatrices resulting from the matrix completion decomposition (bottom) for the IEEE 300-bus system [166]. Observe that even though exploiting sparsity results in many more positive semidefinite matrix constraints, the decomposed matrices are significantly smaller than the original $2n \times 2n$ matrix in (4.3).

rank condition (4.4) (or (4.9) for the Hermitian matrix representation) can be evaluated using analogous conditions on the submatrices. An approach related to (4.5) (and (4.10) for the complex representation) can extract globally optimal solutions when each submatrix satisfies rank conditions analogous to (4.4) or (4.9) [141].

Detailed presentations on exploiting chordal sparsity in general semidefinite programs are provided in [191, 196]. Exploiting chordal sparsity was first proposed for SDP relaxations of OPF problems with balanced single-phase equivalent networks in [197] and for unbalanced three-phase radial networks in [168]. Additional computational improvements were demonstrated in [141] (and further analyzed in [198]) by merging selected maximal cliques. Merging maximal cliques of a chordal extension results in another, denser chordal extension.⁵ This can be computationally advantageous in some instances. Firstly, certain merges can reduce the total number of entries in the positive-semidefinite-constrained matrices. Furthermore, it eliminates the need to enforce equality constraints between terms in the submatrices corresponding to the merged maximal cliques which refer to the same term in the full matrix. An illustrative example is provided in Figure 4.1c. A detailed computational complexity analysis of chordal-sparsity-exploiting interior point solvers is presented in [199]. Reference[199] also proposes variants that use the dualization approach of [200] and auxiliary variables to speed solution times. Other recent work in [177] compares various formulations of the sparsity-exploiting Shor relaxations of OPF problems.

Computational improvements can be achieved at the cost of tightness by further relaxing the sparsity-exploiting Shor relaxation. The approach in [142] further relaxes the decomposed problem by not enforcing equality constraints between all terms in the submatrices that refer to the same term in the full matrix. The approach in [201] forms a further relaxation of the chordal-sparsity-based constraints by only

⁵Merging two maximal cliques can be accomplished by forming a chordal supergraph which connects all buses in the merged cliques.

enforcing positive semidefinite constraints on submatrices corresponding to a cycle basis of the graph.⁶ Reference [202] enforces positive semidefinite constraints on the 3×3 submatrices of \mathbf{Z} in (4.8) whose rows and columns correspond to the reference bus, bus i , and bus k , for all $(i, k) \in \mathcal{L}$. The further-relaxed approaches in [142, 201, 202] can speed computations of the relaxations. However, there exist cases for which the Shor relaxation is exact, but the approaches in [142, 201, 202] result in a non-zero relaxation gap.

Another approach for further relaxing the Shor relaxation is presented in [203]. Specifically, this approach exploits the fact that non-negativity of a matrix's principal minors (i.e., non-negative determinants of certain submatrices) is a necessary condition for positive semidefiniteness. Corresponding necessary conditions are enforced for the 2×2 and 3×3 submatrices of the matrix \mathbf{W} in (4.3). When considered individually, non-negativity of the determinant of 3×3 (or larger) matrices yields non-convex polynomial constraints; however, the resulting optimization problem is convex as long as non-negativity constraints for the determinants of all smaller submatrices are enforced [204, 205]. Using this approach, [203] demonstrates the potential for significantly faster solution times (more than an order-of-magnitude faster than the solution times obtained using the SDP solver SDPT3 [136]) with minimal degradation in tightness relative to the Shor relaxation.

Knowledge of the dual variable values from a local solution can also help improve the tractability of the Shor relaxation. The approach in [206] fixes certain dual variables to their values from a local solution in order to improve the computational speed of the Shor relaxation at the expense of a weaker objective value bound. The fixed dual variables are chosen via a heuristic based on the eigenvalues of submatrices from the matrix completion decomposition, evaluated using the dual variable values from a local solution.

Typical SDP solvers (e.g., MOSEK [133], SeDuMi [135], and SDPT3 [136]) use interior point algorithms which require information on second derivatives (i.e., these solvers use *second-order* algorithms, in contrast

⁶A “cycle basis” for a network is a set of cycles such that any other cycle in the network can be constructed via an appropriate combination of the cycles in the basis [77].

to *first-order* algorithms that only use information on first derivatives). (Note that “order” in this context is unrelated to the order of the moment/sum-of-squares relaxations that will be discussed in §4.1.2.) Other research efforts regarding computational improvements consider solving semidefinite programs using modified interior point algorithms. Relevant research includes parallelizing interior point methods to develop SDP solvers that can run on high-performance computing infrastructures [207], which has the potential to significantly improve the tractability of the Shor relaxation. Additionally, in contrast to existing solvers which solely operate on real-valued quantities, recent research in [130] prototypes a solver that performs interior point computations in complex variables to exploit the structure of complex-valued SDP problems such as those resulting from the power flow equations. Preliminary results suggest the potential for up to a factor-of-four speed improvement over real-valued interior point solvers.

Other research efforts aim to improve the computational tractability of the Shor relaxation through the use of alternate solution algorithms besides interior point methods. These include [208], which applies a first-order coordinate descent algorithm, and [209], which proposes a hybrid method that switches between first- and second-order algorithms. Distributed solution algorithms have also been developed, many of which are based on the Alternating Direction Method of Multipliers (ADMM), for both balanced single-phase equivalent networks [210–213] and unbalanced three-phase networks [167, 214]. (Discussion of an ADMM-based solution algorithm for an SOCP formulation is provided in §4.2.4 and [215].) These approaches allow for distributed computation techniques which can be performed in parallel. Reference [45] surveys the power systems literature regarding distributed optimization and control algorithms.

For large problems with meshed networks, none of these methods have yet demonstrated computational competitiveness in comparison to MOSEK with a chordal-sparsity exploiting formulation. Extrapolations that calculate the best possible parallel speed suggest that implementations of these methods have the potential to significantly surpass interior point methods in the future. However, it remains to be seen whether these parallel methods can achieve such speeds for large problems in

practice due to factors such as communication overhead between the computing nodes. For instance, [208] reports a solver time of 90 seconds when the proposed coordinate descent algorithm (implemented in C with OpenMP) is applied to the IEEE 300-bus system [166]. In comparison, the solver time required for MOSEK with a chordal-sparsity exploiting relaxation [129] is approximately two seconds. Similarly, while an implementation of the ADMM-based method in [213] requires 18 minutes to achieve a moderately accurate solution to the 9241-bus PEGASE system [216], the solver time required for MOSEK with a chordal-sparsity exploiting relaxation [129] is approximately 4 minutes. Note that computational speed is not the only relevant consideration; the distributed nature of certain solution algorithms can be advantageous for some applications, even when a centralized algorithm is computationally faster.

To be computationally competitive with existing non-linear programming solvers that seek a local optimum, significant effort is required to improve SDP solvers and relaxation formulations. This applies to both computational speed and numerical convergence, which can be the limiting factor in SDP relaxations of OPF problems. Recent research in [217] explores the numerical convergence challenges associated with chordal-sparsity-exploiting algorithms. The need for equality constraints between duplicated variables which appear in multiple submatrices can lead to poor numeric conditioning. So-called “facial reduction” techniques can help address these numerical conditioning issues [218]. Another approach to improving numerical convergence characteristics is presented in [219], where low-impedance lines are eliminated in order to reduce the differences in the magnitudes of the coefficient values in the resulting SDP relaxations.

An approach that sidesteps the computational challenges with current SDP solvers is proposed in [220]. Specifically, this approach tests whether a candidate solution from a primal/dual local solution algorithm satisfies the KKT conditions which are necessary and sufficient for global optimality of a solution to the Shor relaxation.⁷ Satisfaction

⁷A locally optimal candidate solution satisfies the KKT conditions for the non-convex optimization problem. The approach in [220] checks whether the candidate solution also satisfies the KKT conditions for the Shor relaxation.

of the KKT conditions for the Shor relaxation is a sufficient (but not necessary) condition which certifies that the candidate solution is a global optimum. The required mathematical operations rely on sparse linear algebra computations that can be performed very quickly relative to directly solving the Shor relaxation.

4.1.2 Moment/Sum-of-Squares Relaxation Hierarchies

While the Shor relaxation in [164] is exact for certain power system optimization problems, there are also cases for which the relaxation fails to be exact. One approach for globally solving such cases is to use generalizations of the Shor relaxation that are developed using the Lasserre hierarchy for polynomial optimization problems [221, 222]. Relaxations from the Lasserre hierarchy are formulated as SDPs with matrices of increasing size. For polynomial optimization problems that satisfy certain technical conditions, including many problems relevant to power systems such as OPF, the relaxations’ solutions converge to the globally optimal objective value at a finite relaxation order in the Lasserre hierarchy [223, 224]. In addition to the Lasserre hierarchy, several other closely related moment/sum-of-squares relaxation hierarchies have also been developed with differing characteristics.

The moment/sum-of-squares relaxations have a deep theoretical grounding based on truncated moment series in the primal formulation and sum-of-squares polynomials of increasing degrees in the dual formulation [221, 222, 225]. The presentation in this section focuses on a conceptual understanding of the moment/sum-of-squares relaxations. Additional theoretical and technical details are provided in [222, 226]. With a focus on the moment (primal) formulation and for notational convenience, the term “moment” relaxations is hereafter used as a synonym for “moment/sum-of-squares” relaxations.

This section presents a mathematical overview of the moment relaxation hierarchies, discusses the exactness of the relaxations and the relationships among the relaxation hierarchies, and summarizes computational challenges and recent advances.

The Lasserre Hierarchy in Real Variables

The moment relaxations can be understood using the observation that constraints which are redundant in a non-convex optimization problem may serve to tighten a relaxation. Moment relaxation theory can thus be viewed as a systematic method for choosing appropriate constraints to enforce in the relaxation.

The Lasserre hierarchy [222] requires a polynomial optimization problem in terms of real variables. Thus, development of the moment relaxations proceeds from the power flow formulation (2.4) with real variables V_{di} and V_{qi} , $i = 1, \dots, n$. Define the vector of decision variables $\hat{x} \in \mathbb{R}^{2n}$ as

$$\hat{x} = \begin{bmatrix} V_{d1} & \dots & V_{dn} & V_{q1} & \dots & V_{qn} \end{bmatrix}^\top. \quad (4.11)$$

Using a vector of non-negative integers $\alpha \in \mathbb{N}^{2n}$, a monomial is

$$\hat{x}^\alpha = V_{d1}^{\alpha_1} V_{d2}^{\alpha_2} \cdots V_{qn}^{\alpha_{2n}}. \quad (4.12)$$

A polynomial $h(\hat{x})$ is

$$h(\hat{x}) = \sum_{\alpha \in \mathbb{N}^{2n}} h_\alpha \hat{x}^\alpha, \quad (4.13)$$

where h_α is the scalar multiplier of the monomial \hat{x}^α .

Define a linear functional $L_y \{\cdot\}$ which takes a polynomial argument. This functional replaces the monomials \hat{x}^α in a polynomial with “lifted” scalar variables y_α :

$$L_y \{h\} = \sum_{\alpha \in \mathbb{N}^{2n}} h_\alpha y_\alpha. \quad (4.14)$$

Thus, $L_y \{h\}$ converts a polynomial $h(\hat{x})$ to a linear combination of scalars y . For a matrix argument $\mathbf{H}(\hat{x})$, the functional $L_y \{\mathbf{H}\}$ is applied componentwise to each element.

Consider, for example, the polynomial $h(\hat{x}) = V_{d2}^2 + V_{q2}^2 - 0.81$. The constraint $h(\hat{x}) \geq 0$ enforces a lower limit of 0.9 per unit on the voltage magnitude at bus 2. Applying the linear functional yields $L_y(h) = y_{0200} + y_{0002} - 0.81y_{0000}$. The term y_{0000} corresponds to the fact that $\hat{x}^0 = 1$.

Let γ be an integer that denotes the order of the relaxation in the moment hierarchy. The relaxation order γ must generally be greater

than or equal to half of the largest degree of the polynomials in the constraints and the objective function. All polynomials in the power flow equations (2.4) are quadratic, and thus only require $\gamma \geq 1$. More generally, the expressions for other quantities may involve higher-degree polynomials in terms of the voltage components V_d and V_q .⁸ When these constraints are convex, they can often be represented using SOCP formulations as discussed in §3.2. Thus, first-order moment relaxations, i.e., $\gamma = 1$, are typically well-defined even if some polynomials have degree greater than two. Further details are provided in [122].

For the order- γ moment relaxation in the Lasserre hierarchy, define a vector x_γ consisting of all monomials of the voltage components V_d and V_q up to order γ :

$$x_\gamma = \begin{bmatrix} 1 & V_{d1} & \dots & V_{qn} & V_{d1}^2 & V_{d1}V_{d2} & \dots \\ & \dots & V_{qn}^2 & V_{d1}^3 & V_{d1}^2V_{d2} & \dots & V_{qn}^\gamma \end{bmatrix}^\top. \quad (4.15)$$

Note that x_γ is used to indicate the vector of monomials in (4.15) as opposed to the γ -th entry of the vector x .

The moment relaxations are formulated using positive semidefinite constraints on so-called *moment* and *localizing* matrices. The order- γ symmetric moment matrix \mathbf{M}_γ is composed of entries y_α corresponding to monomials with degree up to 2γ :

$$\mathbf{M}_\gamma \{y\} = L_y \left\{ x_\gamma x_\gamma^\top \right\}. \quad (4.16)$$

Symmetric localizing matrices are defined for each constraint $h(\hat{x}) \geq 0$ in the polynomial optimization problem. Consider a polynomial $h(\hat{x})$ with degree 2η . (For typical power system optimization problems, the constraint and cost-function polynomials have even degree.) The localizing matrix associated with $h(\hat{x}) \geq 0$ is

$$\mathbf{M}_{\gamma-\eta} \{h y\} = L_y \left\{ h x_{\gamma-\eta} x_{\gamma-\eta}^\top \right\}. \quad (4.17)$$

⁸For instance, apparent power line flows and quadratic costs of active power generation are quadratic expressions in terms of the active and reactive power flows and the active power injections, respectively, which are themselves quadratic in the voltage components. Thus, expressions for apparent power line flows and quadratic costs of power injections are quartic in the voltage components.

4.1. Semidefinite Programming Relaxations

57

$$x_2 = \begin{bmatrix} 1 & V_{d1} & V_{d2} & V_{q1} & V_{q2} & V_{d1}^2 & V_{d1}V_{q1} & V_{d1}V_{q2} & V_{d2}^2 & V_{d2}V_{q1} & V_{d2}V_{q2} & V_{q1}^2 & V_{q1}V_{q2} & V_{q2}^2 \end{bmatrix}^\top, \quad (4.18)$$

$$\mathbf{M}_2 \{y\} = L_y \left\{ x_2 x_2^\top \right\} =$$

$$\begin{bmatrix} y_{0000} & y_{0001} & y_{0100} & y_{0010} & y_{0001} & y_{2000} & y_{1100} & y_{1010} & y_{1001} & y_{0200} & y_{1110} & y_{1101} & y_{0110} & y_{0011} \\ y_{1000} & y_{2000} & y_{1100} & y_{1010} & y_{0101} & y_{3000} & y_{2100} & y_{2010} & y_{2001} & y_{1200} & y_{1110} & y_{1101} & y_{1010} & y_{1001} \\ y_{0100} & y_{1100} & y_{0200} & y_{0110} & y_{0101} & y_{2100} & y_{1200} & y_{1110} & y_{1101} & y_{0300} & y_{0210} & y_{0201} & y_{0120} & y_{0111} \\ y_{0010} & y_{1010} & y_{0110} & y_{0020} & y_{0011} & y_{2010} & y_{1110} & y_{1020} & y_{1011} & y_{0210} & y_{0120} & y_{0111} & y_{0030} & y_{0021} \\ y_{0001} & y_{1001} & y_{1011} & y_{0011} & y_{0002} & y_{2001} & y_{1101} & y_{1011} & y_{1002} & y_{0201} & y_{0111} & y_{0102} & y_{0021} & y_{0012} \\ y_{2000} & y_{3000} & y_{2100} & y_{2010} & y_{2001} & y_{4000} & y_{3100} & y_{3010} & y_{3001} & y_{2200} & y_{2110} & y_{2101} & y_{2110} & y_{2011} \\ y_{1100} & y_{2100} & y_{1200} & y_{1110} & y_{1101} & y_{3100} & y_{2200} & y_{2110} & y_{2101} & y_{1300} & y_{1210} & y_{1201} & y_{1120} & y_{1111} \\ y_{1010} & y_{2010} & y_{1110} & y_{1020} & y_{1011} & y_{3010} & y_{2110} & y_{2020} & y_{2011} & y_{1210} & y_{1120} & y_{1111} & y_{1030} & y_{1021} \\ y_{1001} & y_{2001} & y_{1101} & y_{1011} & y_{1002} & y_{3001} & y_{2101} & y_{2011} & y_{2002} & y_{1201} & y_{1111} & y_{1102} & y_{1021} & y_{1012} \\ y_{0200} & y_{1200} & y_{0300} & y_{0210} & y_{0201} & y_{2200} & y_{1300} & y_{1210} & y_{1201} & y_{0400} & y_{0310} & y_{0301} & y_{0220} & y_{0211} \\ y_{0110} & y_{1110} & y_{0210} & y_{0120} & y_{0111} & y_{2110} & y_{1210} & y_{1120} & y_{1111} & y_{0310} & y_{0220} & y_{0211} & y_{0130} & y_{0121} \\ y_{0101} & y_{1101} & y_{0201} & y_{0111} & y_{0102} & y_{2101} & y_{1201} & y_{1111} & y_{1102} & y_{0301} & y_{0211} & y_{0202} & y_{0121} & y_{0112} \\ y_{0020} & y_{1020} & y_{0120} & y_{0030} & y_{0021} & y_{2020} & y_{1120} & y_{1030} & y_{1021} & y_{0220} & y_{0130} & y_{0121} & y_{0040} & y_{0031} \\ y_{0011} & y_{1011} & y_{0111} & y_{0021} & y_{0012} & y_{2011} & y_{1111} & y_{1021} & y_{1012} & y_{0211} & y_{0121} & y_{0112} & y_{0031} & y_{0022} \\ y_{0002} & y_{1002} & y_{0102} & y_{0012} & y_{0003} & y_{2002} & y_{1102} & y_{1012} & y_{1003} & y_{0202} & y_{0112} & y_{0103} & y_{0022} & y_{0013} \\ y_{0000} & y_{1000} & y_{1000} & y_{0100} & y_{0001} & y_{1200} & y_{1002} & y_{081} y_{1000} & y_{0300} + y_{0102} - y_{081} y_{1000} & y_{0210} + y_{0012} - y_{081} y_{0010} & y_{0201} + y_{0003} - y_{081} y_{0001} \\ y_{1200} & y_{1002} & y_{081} y_{1000} & y_{2200} & y_{2002} & y_{081} y_{2000} & y_{1300} & y_{1102} - y_{081} y_{1100} & y_{1210} & y_{1012} - y_{081} y_{1010} & y_{1201} & y_{1003} - y_{081} y_{1001} \\ y_{0300} & y_{0102} & y_{081} y_{0100} & y_{1300} & y_{1102} - y_{081} y_{1100} & y_{0400} & y_{0202} & y_{081} y_{0200} & y_{0310} & y_{0112} - y_{081} y_{0110} & y_{0301} & y_{0103} - y_{081} y_{0101} \\ y_{0210} & y_{0012} & y_{081} y_{0010} & y_{1210} & y_{1012} - y_{081} y_{1010} & y_{0310} & y_{0112} - y_{081} y_{0110} & y_{0220} & y_{0022} - y_{081} y_{0020} & y_{0211} & y_{0013} - y_{081} y_{0011} \\ y_{0201} & y_{0003} & y_{081} y_{0001} & y_{1201} & y_{1003} - y_{081} y_{1001} & y_{0301} & y_{0103} - y_{081} y_{0101} & y_{0211} & y_{0013} - y_{081} y_{0011} & y_{0202} & y_{0004} - y_{081} y_{0002} \end{bmatrix}. \quad (4.19)$$

$$\mathbf{M}_1 \left\{ (V_{d2}^2 + V_{q2}^2 - 0.81) y \right\} = L_y \left\{ (V_{d2}^2 + V_{q2}^2 - 0.81) x_1 x_1^\top \right\} =$$

$$\begin{bmatrix} y_{0200} + y_{0002} - 0.81 y_{0000} & y_{1200} + y_{1002} - 0.81 y_{1000} & y_{0300} + y_{0102} - 0.81 y_{0100} & y_{0210} + y_{0012} - 0.81 y_{0010} & y_{0201} + y_{0003} - 0.81 y_{0001} \\ y_{1200} + y_{1002} - 0.81 y_{1000} & y_{2200} + y_{2002} - 0.81 y_{2000} & y_{1300} + y_{1102} - 0.81 y_{1100} & y_{1210} + y_{1012} - 0.81 y_{1010} & y_{1201} + y_{1003} - 0.81 y_{1001} \\ y_{0300} + y_{0102} - 0.81 y_{0100} & y_{1300} + y_{1102} - 0.81 y_{1100} & y_{0400} + y_{0202} - 0.81 y_{0200} & y_{0310} + y_{0112} - 0.81 y_{0110} & y_{0301} + y_{0103} - 0.81 y_{0101} \\ y_{0210} + y_{0012} - 0.81 y_{0010} & y_{1210} + y_{1012} - 0.81 y_{1010} & y_{0310} + y_{0112} - 0.81 y_{0110} & y_{0220} + y_{0022} - 0.81 y_{0020} & y_{0211} + y_{0013} - 0.81 y_{0011} \\ y_{0201} + y_{0003} - 0.81 y_{0001} & y_{1201} + y_{1003} - 0.81 y_{1001} & y_{0301} + y_{0103} - 0.81 y_{0101} & y_{0211} + y_{0013} - 0.81 y_{0011} & y_{0202} + y_{0004} - 0.81 y_{0002} \end{bmatrix}. \quad (4.20)$$

The vector x_2 and the moment matrix $\mathbf{M}_2\{y\}$ associated with a two-bus system are shown in (4.18) and (4.19), respectively, for the second-order moment relaxation. An example localizing matrix for the voltage magnitude constraint $h(\hat{x}) = V_{d2}^2 + V_{q2}^2 - 0.81$ is given in (4.20). Example moment and localizing matrices for a three-bus system are considered in [122].

While the moment relaxations can accommodate more general polynomial constraints on the power injections and voltage magnitudes, consider for illustrative purposes an optimization problem with box constraints on these quantities: $P_i^{min} \leq P_i \leq P_i^{max}$, $Q_i^{min} \leq Q_i \leq Q_i^{max}$, and $(V_i^{min})^2 \leq |V_i|^2 \leq (V_i^{max})^2$. Also consider an objective function that minimizes the generic polynomial $f_C(\hat{x})$. The order- γ moment relaxation is:

$$\min_y L_y \{f_C\} \quad (4.21a)$$

subject to

$$\mathbf{M}_{\gamma-1} \left\{ \left(f_{Pi} - P_i^{min} \right) y \right\} \succeq 0, \quad \forall k \in \mathcal{N}, \quad (4.21b)$$

$$\mathbf{M}_{\gamma-1} \left\{ \left(P_i^{max} - f_{Pi} \right) y \right\} \succeq 0, \quad \forall k \in \mathcal{N}, \quad (4.21c)$$

$$\mathbf{M}_{\gamma-1} \left\{ \left(f_{Qi} - Q_i^{min} \right) y \right\} \succeq 0, \quad \forall k \in \mathcal{N}, \quad (4.21d)$$

$$\mathbf{M}_{\gamma-1} \left\{ \left(Q_i^{max} - f_{Qi} \right) y \right\} \succeq 0, \quad \forall k \in \mathcal{N}, \quad (4.21e)$$

$$\mathbf{M}_{\gamma-1} \left\{ \left(f_{Vi} - (V_i^{min})^2 \right) y \right\} \succeq 0, \quad \forall k \in \mathcal{N}, \quad (4.21f)$$

$$\mathbf{M}_{\gamma-1} \left\{ \left((V_i^{max})^2 - f_{Vi} \right) y \right\} \succeq 0, \quad \forall k \in \mathcal{N}, \quad (4.21g)$$

$$\mathbf{M}_\gamma \{y\} \succeq 0, \quad (4.21h)$$

$$y_{00\dots 0} = 1, \quad (4.21i)$$

$$y_{\star \dots \star \rho \star \dots \star} = 0, \quad \rho = 1, \dots, 2\gamma, \quad (4.21j)$$

where f_{Pi} , f_{Qi} , and f_{Vi} are polynomial expressions in the voltage components V_d and V_q for active power injection, reactive power injection, and squared voltage magnitude, respectively, at bus i , i.e., the right-hand sides of (2.4). The positive semidefinite constraints (4.21b)–(4.21g) are applied to the localizing matrices, (4.21h) corresponds to the moment matrix, and (4.21i) results from the fact that $\hat{x}^0 = 1$.

In (4.21j), ρ is in the index $n + 1$ and \star is used to denote any integer. Thus, (4.21j) enforces the angle reference constraint by setting to zero all terms corresponding to monomials which contain V_{q1} . Alternatively, the angle reference can be enforced by eliminating all monomials containing the term V_{q1} from x_γ while also deleting the corresponding rows and columns from the moment and localizing matrices. Eliminating V_{q1} reduces the size of the semidefinite program, thus improving computational tractability.

Note that power system optimization problems often have several characteristics that can be exploited to improve the computational aspects of the moment relaxations (e.g., equality constraints and the lack of odd-order monomials). Further details and illustrative examples are provided in [122, 129, 227].

Observe that the moment relaxations form a hierarchy. The upper left submatrices in the moment and localizing matrices for the order- γ relaxation are equivalent to the matrices in the order- $(\gamma - 1)$ relaxation. Since a necessary condition for positive semidefiniteness of a matrix is positive semidefiniteness of its principal submatrices, the higher-order relaxations generalize the lower-order relaxations. In particular, note that the entries in the first five rows and columns of the second-order moment matrix in (4.19) and the $(1, 1)$ entry of the second-order localizing matrix in (4.20) correspond to the moment and localizing matrices for the first-order relaxation. Moreover, note that the first-order moment relaxation is equivalent to the Shor relaxation of [164] given in (4.2).

Conceptually, formulation of the higher-order relaxations can be viewed as the addition of constraints that are redundant in the non-convex problem but strengthen the moment relaxations. Consider a generic polynomial constraint $g(\hat{x}) \geq 0$ with degree 2η . The rank-one matrix $x_{\gamma-\eta} x_{\gamma-\eta}^\top$ is positive semidefinite by construction, and the scalar $g(\hat{x})$ is non-negative due to the constraint $g(\hat{x}) \geq 0$. Thus, their product $g(\hat{x}) x_{\gamma-\eta} x_{\gamma-\eta}^\top$ is a rank-one positive semidefinite matrix, and the constraint $g(\hat{x}) x_{\gamma-\eta} x_{\gamma-\eta}^\top \succeq 0$ is redundant with the constraint $g(\hat{x}) \geq 0$. Relaxing to $L_y \left\{ g(\hat{x}) x_{\gamma-\eta} x_{\gamma-\eta}^\top \right\} \succeq 0$ (i.e., formulating this constraint in terms of the “lifted” variables y_α and dropping the rank

constraint) results in the localizing matrix constraint $\mathbf{M}_{\gamma-\eta}\{g|y\} \succeq 0$, which can tighten the moment relaxation. Likewise, the constraint $x_\gamma x_\gamma^\top \succeq 0$ is always satisfied by construction, so adding a relaxed version of this constraint (i.e., the moment matrix constraint $\mathbf{M}_\gamma\{y\} \succeq 0$ in (4.21h)) is valid. Observe that the objective function (4.21a) is also relaxed, the constraint (4.21i) is a relaxation of $x^0 = 1$, and (4.21j) is implied by the angle reference constraint $V_{q1} = 0$. Thus, the moment hierarchy (4.21) provides relaxations of the original non-convex power system optimization problem.

A “flat extension condition” is sufficient to certify exactness of the order- γ moment relaxation [222, 228]. The order- γ relaxation satisfies the flat extension condition if the upper-left block of the moment matrix corresponding to the order- $(\gamma - 1)$ relaxation has the same rank as the full moment matrix:

$$\text{rank}(\mathbf{M}_\gamma\{y\}) = \text{rank}(\mathbf{M}_{\gamma-1}\{y\}). \quad (4.22)$$

Define $r = \text{rank}(\mathbf{M}_\gamma\{y\})$. References [222, 228] provide an algorithm for recovering r unique global optima from a solution satisfying (4.22). Thus, the Lasserre hierarchy is capable of providing multiple global optima. Even though typical power system optimization problems, such as OPF, may often yield multiple *local* optima [3], it is unusual to have multiple *global* optima. Atypical cases with multiple global optima are discussed in [227].

A more specific sufficient condition for exactness of the order- γ relaxation is provided by

$$\text{rank}(\mathbf{M}_\gamma\{y\}) = 1. \quad (4.23)$$

A solution that satisfies (4.23) provides a single global optimum which can be recovered in a similar manner as for the Shor relaxation of [164]. In this case, the global solution V^* is determined by a spectral decomposition of the diagonal block of the moment matrix corresponding to the second-order monomials (i.e., $|\alpha| = 2$, where $|\cdot|$ indicates the one-norm). Let ν be the unit-length eigenvector corresponding to the non-zero eigenvalue λ of $\mathbf{M}_\gamma\{y\}$. Denote ν_d and ν_q as the vectors consisting of the entries of ν from ν_2 to ν_{n+1} and from ν_{n+2} to ν_{2n+1} ,

respectively.⁹ Then the vector

$$V^* = \sqrt{\lambda} (\nu_d + j\nu_q) \quad (4.24)$$

gives the globally optimal voltage phasors.¹⁰

A Hierarchy in Complex Variables

A related relaxation hierarchy that employs SDP constraints in complex variables is proposed in [129]. (Alternative presentations of this complex moment hierarchy are given in [226, 229] and further mathematical details are available in [230].) As will be discussed in the following section, at a given relaxation order, the complex moment hierarchy in [129] produces relaxations that have computational advantages over the relaxations from the Lasserre hierarchy. These computational advantages come at the cost of tightness for some optimization problems.

In contrast to the real variables used in the Lasserre hierarchy (4.21), the complex moment relaxation hierarchy in [129] is constructed directly from polynomials in the voltage phasors V and their complex conjugates \bar{V} . Specifically, let \hat{z} be the vector of complex voltage phasors:

$$\hat{z} = [V_1 \ \cdots \ V_n]^\top. \quad (4.25)$$

Define a generic polynomial $h(\hat{z})$ as

$$h(\hat{z}) = \sum_{\alpha, \beta \in \mathbb{N}^n} h_{\alpha, \beta} \hat{z}^\alpha \bar{\hat{z}}^\beta, \quad (4.26)$$

where $h_{\alpha, \beta}$ is a complex scalar and the integer vectors α and β correspond to the exponents of the non-conjugated and conjugated voltage

⁹If the reference angle constraint $V_{q1} = 0$ is used to eliminate V_{q1} , the vector ν_q is redefined as $\nu_q = [0 \ \tilde{\nu}_q^\top]^\top$, where $\tilde{\nu}_q$ consists of the entries of ν from ν_{n+2} to ν_{2n} .

¹⁰One can attempt to recover a solution even if the rank condition (4.23) is not satisfied by applying (4.24) with ν as the eigenvalue corresponding to the *largest* (but not the only non-zero) eigenvalue of $\mathbf{M}_\gamma\{y\}$. A global solution is obtained if this yields a feasible voltage profile with a corresponding objective value that matches the bound from the solution to the moment relaxation. While there are no guarantees that the resulting voltage profile will be feasible (much less globally optimal), it may be sufficiently close to the global solution in order to be practically useful for some problems.

phasors, respectively. Note that the polynomials' outputs are real-valued quantities, i.e., $\bar{h}_{\alpha,\beta} = h_{\beta,\alpha}$.

Let γ denote the relaxation order, with the same requirements on the choice of γ as in the Lasserre hierarchy. Let z_γ denote the vector of monomials without complex conjugate terms (i.e., $\beta = 00 \cdots 0$) up to order γ :

$$z_\gamma := \begin{bmatrix} 1 & V_1 & \dots & V_n & V_1^2 & V_1 V_2 & \dots \\ & \dots & V_n^2 & V_1^3 & V_1^2 V_2 & \dots & V_n^\gamma \end{bmatrix}^\top. \quad (4.27)$$

As for x_γ in the Lasserre hierarchy, z_γ is used to indicate the vector of monomials in (4.27) as opposed to the γ -th entry of the vector z .

Define the linear functional $\hat{L}_{\hat{y}} \{\cdot\}$ which replaces the monomial $\hat{z}^\alpha \bar{\hat{z}}^\beta$ with the complex scalar variable $\hat{y}_{\alpha,\beta}$:

$$\hat{L}_{\hat{y}} \{h\} = \sum_{\alpha,\beta \in \mathbb{N}^n} h_{\alpha,\beta} \hat{y}_{\alpha,\beta}. \quad (4.28)$$

Analogous to (4.16), the Hermitian moment matrix for the order- γ relaxation in the complex moment hierarchy proposed in [129] is

$$\hat{\mathbf{M}}_\gamma \{\hat{y}\} = \hat{L}_{\hat{y}} \left\{ z_\gamma z_\gamma^H \right\}. \quad (4.29)$$

Let the generic polynomial constraint $h(\hat{z}) \geq 0$ have the largest degree $|\alpha + \beta|$ among all monomials equal to 2η . Analogous to (4.17), the Hermitian localizing matrix associated with this constraint is

$$\hat{\mathbf{M}}_{\gamma-\eta} \{h \hat{y}\} = \hat{L}_{\hat{y}} \left\{ h z_{\gamma-\eta} z_{\gamma-\eta}^H \right\}. \quad (4.30)$$

As an illustrative example for the second-order complex moment relaxation of a two-bus problem, (4.31), (4.32), and (4.33) provide z_2 , the moment matrix $\hat{\mathbf{M}}_2 \{\hat{y}\}$, and the example localizing matrix $\hat{\mathbf{M}}_1 \left\{ (V_2 \bar{V}_2 - 0.81) \hat{y} \right\}$ for the constraint $h(\hat{z}) = V_2 \bar{V}_2 - 0.81 \geq 0$:

$$z_2 = [1 \ V_1 \ V_2 \ V_1^2 \ V_1 V_2 \ V_2^2]^\top, \quad (4.31)$$

$$\hat{\mathbf{M}}_2 \{ \hat{y} \}$$

$$= \hat{L}_{\hat{y}} \{ z_2 z_2^H \} = \begin{bmatrix} \hat{y}_{00,00} & \hat{y}_{00,10} & \hat{y}_{00,01} & \hat{y}_{00,20} & \hat{y}_{00,11} & \hat{y}_{00,02} \\ \hat{y}_{10,00} & \hat{y}_{10,10} & \hat{y}_{10,01} & \hat{y}_{10,20} & \hat{y}_{10,11} & \hat{y}_{10,02} \\ \hat{y}_{01,00} & \hat{y}_{01,10} & \hat{y}_{01,01} & \hat{y}_{01,20} & \hat{y}_{01,11} & \hat{y}_{01,02} \\ \hat{y}_{20,00} & \hat{y}_{20,10} & \hat{y}_{20,01} & \hat{y}_{20,20} & \hat{y}_{20,11} & \hat{y}_{20,02} \\ \hat{y}_{11,00} & \hat{y}_{11,10} & \hat{y}_{11,01} & \hat{y}_{11,20} & \hat{y}_{11,11} & \hat{y}_{11,02} \\ \hat{y}_{02,00} & \hat{y}_{02,10} & \hat{y}_{02,01} & \hat{y}_{02,20} & \hat{y}_{02,11} & \hat{y}_{02,02} \end{bmatrix}, \quad (4.32)$$

$$\begin{aligned} \hat{\mathbf{M}}_1 \left\{ \left(V_2 \bar{V}_2 - 0.81 \right) \hat{y} \right\} &= \hat{L}_{\hat{y}} \left\{ \left(V_2 \bar{V}_2 - 0.81 \right) z_{\gamma-1} z_{\gamma-1}^H \right\} \\ &= \begin{bmatrix} \hat{y}_{01,01} - 0.81 \hat{y}_{00,00} & \hat{y}_{01,11} - 0.81 \hat{y}_{00,10} & \hat{y}_{01,02} - 0.81 \hat{y}_{00,01} \\ \hat{y}_{11,01} - 0.81 \hat{y}_{10,00} & \hat{y}_{11,11} - 0.81 \hat{y}_{10,10} & \hat{y}_{11,02} - 0.81 \hat{y}_{10,01} \\ \hat{y}_{02,01} - 0.81 \hat{y}_{01,00} & \hat{y}_{02,11} - 0.81 \hat{y}_{01,10} & \hat{y}_{02,02} - 0.81 \hat{y}_{01,01} \end{bmatrix}. \end{aligned} \quad (4.33)$$

For illustrative purposes, consider again the set of box constraints on the power injections and voltage magnitudes as well as a generic objective function $\hat{f}_C(\hat{z})$. The complex moment relaxation hierarchy proposed in [129] is formed using the constraints

$$\min_{\hat{y}} \hat{L}_{\hat{y}} \left\{ \hat{f}_C \right\} \quad (4.34a)$$

subject to

$$\hat{\mathbf{M}}_{\gamma-1} \left\{ \left(\hat{f}_{Pi} - P_i^{min} \right) \hat{y} \right\} \succeq 0, \quad \forall i \in \mathcal{N}, \quad (4.34b)$$

$$\hat{\mathbf{M}}_{\gamma-1} \left\{ \left(P_i^{max} - \hat{f}_{Pi} \right) \hat{y} \right\} \succeq 0, \quad \forall i \in \mathcal{N}, \quad (4.34c)$$

$$\hat{\mathbf{M}}_{\gamma-1} \left\{ \left(\hat{f}_{Qi} - Q_i^{min} \right) \hat{y} \right\} \succeq 0, \quad \forall i \in \mathcal{N}, \quad (4.34d)$$

$$\hat{\mathbf{M}}_{\gamma-1} \left\{ \left(Q_i^{max} - \hat{f}_{Qi} \right) \hat{y} \right\} \succeq 0, \quad \forall i \in \mathcal{N}, \quad (4.34e)$$

$$\hat{\mathbf{M}}_{\gamma-1} \left\{ \left(\hat{f}_{Vi} - (V_i^{min})^2 \right) \hat{y} \right\} \succeq 0, \quad \forall i \in \mathcal{N}, \quad (4.34f)$$

$$\hat{\mathbf{M}}_{\gamma-1} \left\{ \left((V_i^{max})^2 - \hat{f}_{Vi} \right) \hat{y} \right\} \succeq 0, \quad \forall i \in \mathcal{N}, \quad (4.34g)$$

$$\hat{\mathbf{M}}_\gamma \{ \hat{y} \} \succeq 0, \quad (4.34h)$$

$$\hat{y}_{0...0,0...0} = 1, \quad (4.34i)$$

where \hat{f}_{Pi} , \hat{f}_{Qi} , and \hat{f}_{Vi} are polynomial expressions in the complex voltage phasors V for active power injection, reactive power injection, and squared voltage magnitude, respectively, at bus i , i.e., the right-hand sides of (2.3). The positive semidefinite constraints (4.34b)–(4.34g) are applied to the localizing matrices, (4.34h) corresponds to the moment matrix, and (4.34i) results from the fact that $\hat{z}^0 \bar{\hat{z}}^0 = 1$.

Similar to the Lasserre hierarchy, characteristics of the power flow equations and typical power system optimization problems facilitate certain simplifications to the complex moment hierarchy. In particular, [129] describes how to exploit the presence of equality constraints and the fact that all monomials have a balanced number of conjugated and non-conjugated variables, i.e., $|\alpha| = |\beta|$ for all monomials $\hat{z}^\alpha \bar{\hat{z}}^\beta$ in the power flow equations.

Similar to the “flat extension condition” (4.22) for certifying exactness of the Lasserre hierarchy, [129] provides a sufficient condition for exactness of the order- γ relaxation in the complex moment hierarchy:

$$\text{rank}(\hat{\mathbf{M}}_\gamma \{\hat{y}\}) = \text{rank}(\hat{\mathbf{M}}_{\gamma-2} \{\hat{y}\}). \quad (4.35)$$

Both the flat extension condition (4.22) for the Lasserre hierarchy and condition (4.35) for the complex hierarchy compare the rank of the full moment matrix for the order- γ relaxation with the rank of a certain upper-left block of the moment matrix. Specifically, the flat extension condition (4.22) considers the block corresponding to the order- $(\gamma - 1)$ moment matrix, $\mathbf{M}_{\gamma-1} \{y\}$, while condition (4.35) for the complex hierarchy considers the smaller block corresponding to the order- $(\gamma - 2)$ moment matrix, $\hat{\mathbf{M}}_{\gamma-2} \{\hat{y}\}$. Define $\hat{r} = \text{rank}(\hat{\mathbf{M}}_\gamma \{\hat{y}\})$. An algorithm proposed in [231] enables the recovery of \hat{r} unique global optima from a solution satisfying (4.35), as is done in [232]. Thus, like the Lasserre hierarchy, the complex moment hierarchy is also capable of providing multiple global optima.

Furthermore, a global solution can be extracted from a solution to the order- γ relaxation in the complex moment hierarchy (4.34) which satisfies the condition

$$\text{rank}(\hat{\mathbf{M}}_\gamma \{\hat{y}\}) = 1. \quad (4.36)$$

Analogous to the Lasserre hierarchy, the global solution V^* is then determined by a spectral decomposition of the diagonal block of the moment matrix corresponding to the second-order monomials (i.e., $|\alpha + \beta| = 2$). Specifically, let ν denote a unit-length eigenvector corresponding to the non-zero eigenvalue λ of $\hat{\mathbf{M}}_\gamma\{\hat{y}\}$. Let $\tilde{\nu}$ denote the vector consisting of the entries of ν from ν_2 to ν_{n+1} . Then the globally optimal voltage phasors are

$$V^* = \sqrt{\lambda} \tilde{\nu}, \quad (4.37)$$

rotated such that $\angle \tilde{\nu}_1 = 0^\circ$.¹¹

Note that the complex hierarchy (4.34) does not enforce a constraint analogous to the angle reference constraint (4.21j) in the Lasserre hierarchy (4.21). To explain this, observe that the complex moment matrix $\hat{\mathbf{M}}_\gamma\{\hat{y}\}$ is invariant to rotations of its constituent eigenvectors. Specifically, consider the eigendecomposition $\hat{\mathbf{M}}_\gamma\{\hat{y}\} = \sum_{i=1}^r \lambda_i \nu_i \nu_i^H$. Observe that $\sum_{i=1}^r \lambda_i (\nu_i e^{j\phi_i}) (\nu_i e^{j\phi_i})^H = \lambda_i e^{j\phi_i} e^{-j\phi_i} \nu_i \nu_i^H = \sum_{i=1}^r \lambda_i \nu_i \nu_i^H = \hat{\mathbf{M}}_\gamma\{\hat{y}\}$, where scalars ϕ_i describe arbitrary rotations to the eigenvectors ν_i . In the context of power system optimization problems, this invariance implies that a moment matrix satisfying (4.36) is consistent with any uniform rotation of the angles for the voltage vector defined in (4.37). Hence, ν in (4.37) can be rotated to match the specified reference angle without explicitly enforcing an angle reference constraint analogous to (4.21j).

Alternatively, the angle reference could be enforced by including positive-semidefinite-constrained localizing matrices corresponding to the constraint $V_1 - \bar{V}_1 = 0$ in (4.34). However, the fact that the terms in this constraint are linear in the voltage phasors alters the otherwise purely quadratic dependence of the power flow equations on the voltage phasors. Thus, explicitly including an angle reference constraint would preclude the ability to exploit the structure related to odd-order monomials described in [129]. Since exploiting this structure is most relevant for larger problems, tightening the higher-order relaxations via the constraint $V_1 - \bar{V}_1 = 0$ may be advantageous for small problems where computational speed is less of a concern.

¹¹For cases where $\text{rank}(\hat{\mathbf{M}}_\gamma\{\hat{y}\}) > 1$, footnote 10 also applies for the complex moment hierarchy with (4.23) and (4.24) replaced by (4.36) and (4.37).

As will be further discussed in the following section, the complex moment hierarchy (4.34) has smaller matrices and is therefore more computationally tractable than the Lasserre hierarchy (4.21) of the same relaxation order when applied to complex polynomial optimization problems. For general polynomial optimization problems, this improved tractability comes at the cost of tightness: there exist general complex polynomial optimization problems for which the order- γ relaxation in the Lasserre hierarchy is strictly tighter than the order- γ relaxation in the complex moment hierarchy [129]. Regardless, the complex hierarchy often has superior performance compared to the Lasserre hierarchy for typical power system optimization problems [129]. Further computational improvements may potentially be realized by developing specialized SDP solvers that better exploit complex variable structures [130].

A Mixed SDP/SOCP Hierarchy

The “mixed SDP/SOCP” hierarchy proposed in [233] is formulated using a combination of SDP and SOCP constraints. This hierarchy is intended to be tighter than the first-order moment relaxation but more computationally tractable than the higher-order moment relaxations which use SDP constraints.

Necessary (but not sufficient) conditions for positive semidefiniteness of a matrix can be expressed as rotated SOCP constraints. For a generic symmetric matrix \mathbf{A} , the SOCP-based necessary conditions for $\mathbf{A} \succeq 0$ are

$$\mathbf{A}_{ii} \geq 0, \tag{4.38a}$$

$$\mathbf{A}_{ii}\mathbf{A}_{kk} \geq |\mathbf{A}_{ik}|^2, \quad \forall \{(i, k) \mid k > i\}. \tag{4.38b}$$

To form a relaxation that is at least as tight as the first-order moment relaxation, the mixed SDP/SOCP hierarchy applies a positive semidefinite constraint to the moment matrix $\mathbf{M}_1\{y\}$ in the first-order relaxation (4.21h). The higher-order moment and localizing constraints are relaxed using the SOCP condition in (4.38).

Specifically, the mixed SDP/SOCP hierarchy enforces a positive semidefinite constraint on the square submatrix of $\mathbf{M}_\gamma\{y\}$ consisting

of the rows and columns indexed 2 through $2n + 1$, with the SOCP constraints (4.38) applied to the remaining terms in the moment matrix $\mathbf{M}_\gamma\{y\}$. SOCP constraints (4.38) are formulated for all the localizing matrices (4.21b)–(4.21g). Note that network sparsity can be exploited to eliminate unnecessary SOCP constraints. See [122] for an illustrative example of the mixed SDP/SOCP hierarchy applied to a small test case. Also note that a similar mixed SDP/SOCP approach could also be applied to the complex moment hierarchy of [129] (i.e., relaxing (4.34) using the SOCP necessary condition for positive semidefiniteness (4.38)).

The SDSOS Relaxation Hierarchy

The approach in [234, 235] formulates a hierarchy of relaxations that are based on so-called Scaled Diagonally Dominant Sum-of-Squares (SDSOS) polynomials of increasing degree [236]. Relaxations in the SDSOS hierarchy take the form of SOCP problems.¹² While typically presented in a “sum-of-squares” representation that is the dual of the moment hierarchies discussed in this section, the SDSOS hierarchy used in [234, 235] is equivalent to relaxing the SDP constraints in the Lasserre hierarchy (4.21) to SOCP constraints using the necessary conditions for positive semidefiniteness of a matrix described in (4.38) [237]. The approach in [234, 235] is thus similar to the mixed SDP/SOCP hierarchy, with the difference being that the constraints associated with the first-order relaxation are also relaxed from an SDP to an SOCP formulation. In particular, the first-order relaxation in the SDSOS hierarchy is equivalent to the dual of the SOCP relaxation that will be discussed in §4.2.1 [235]. Thus, the mixed SDP/SOCP hierarchy is generally tighter than the SDSOS hierarchy, while the SDSOS hierarchy is computationally faster than the mixed SDP/SOCP hierarchy at the same relaxation order.

Note that a related Diagonally Dominant Sum-of-Squares (DSOS) hierarchy composed of linear programming relaxations is applied to the

¹²The SDSOS hierarchy does not include any SDP constraints and therefore only requires an SOCP solver. The SDSOS hierarchy is nevertheless discussed in this section due to its close relationship to the moment relaxation hierarchies.

OPF problem in [235]. The DSOS hierarchy is a further relaxation of the SDSOS hierarchy.

Also note that a related approach that constructs an alternative SDSOS hierarchy is proposed in [238] but has not yet been applied to power system optimization problems due to computational challenges related to an exponential number of SOCP constraints in its formulation. A recent approach proposed in [239, 240] iteratively generates these SOCP constraints, which may enable application of the hierarchy in [238] to power system optimization problems.

Exactness and Comparisons Among Relaxation Hierarchies

Applications of the moment relaxations to power system optimization have focused on the OPF problem [122, 129, 227, 233, 241–245], although recent developments include consideration of chance-constrained OPF problems [246], unit commitment problems [247], techniques for ensuring voltage constraint satisfaction [248], and transient stability analyses [249–251]. This section focuses on results for OPF problems. Application of the moment relaxations to other power system optimization problems is an open research area that would likely prove fruitful.

Observe that the first-order moment relaxation (i.e., $\gamma = 1$) is equivalent to the Shor relaxation. Thus, the higher-order moment relaxations inherit the sufficient conditions for exactness of the Shor relaxation described in §4.1.1 and the SOCP relaxations described later in §4.2.3.

For polynomial optimization problems that satisfy a certain technical condition, moment relaxations in the Lasserre hierarchy (4.21) converge to the global optima at a finite order [222].¹³ While the best known upper bound on this relaxation order is impractically large [222], low-order moment relaxations suffice for globally solving many power system optimization problems of practical interest.

Figure 4.3 uses the five-bus system “WB5” from [3] (with the modified objective function discussed in §2.3) to demonstrate the ability of relaxations from the Lasserre hierarchy to find the global optimum to a

¹³A compact feasible space is sufficient for satisfying this technical condition. Typical power system optimization problems include upper limits on voltage magnitudes, and thus power system optimization problems generally satisfy this condition.

challenging OPF problem. This problem has an objective that is a convex quadratic function of the active power generation. The unconstrained minimizer of this objective function is at an infeasible point inside the convex hull of the feasible space for the OPF problem's constraints. Focusing solely on tightening the constraints of a convex relaxation to more closely approximate the convex hull of the OPF problem's constraints is not sufficient to yield the globally optimal solution. Rather, the relaxations must address the objective function. In contrast to the other relaxations discussed in this monograph, the moment relaxations discussed in this section can obtain the global optima to such problems due to their treatment of the higher-order terms in the objective functions. Further discussion on this topic and another illustrative test case are provided in [245]. See also [241] and [122] for other illustrations that explore the ability of low-order moment relaxations to globally solve a variety of challenging power system optimization problems, including problems with multiple local optima and disconnected feasible spaces.

For problems that include a *sphere constraint*, relaxations in the complex moment hierarchy are guaranteed to converge to the global optima with increasing relaxation order [129].¹⁴ For a given relaxation order, the Lasserre hierarchy (4.21) is at least as tight as the complex moment hierarchy (4.34) [129], and there exist general complex polynomial optimization problems for which the Lasserre hierarchy is tighter. Nevertheless, numerical experiments suggest that the complex hierarchy is often exact at the same relaxation order as the Lasserre hierarchy for typical power system optimization problems [129].

For a given order, the mixed SDP/SOCP hierarchy proposed in [233] is a relaxation of the Lasserre hierarchy. Therefore, relaxations from the mixed SDP/SOCP hierarchy are generally weaker than those of the same order from the Lasserre hierarchy. (See [122] for example OPF problems where the mixed SDP/SOCP hierarchy is less tight than the

¹⁴A sphere constraint can be explicitly added to a power system optimization problem by summing the upper limits on voltage magnitudes at each bus and converting to an equality constraint: $|\psi|^2 + \sum_{i \in \mathcal{N}} V_i \bar{V}_i = \sum_{i \in \mathcal{N}} (V_i^{max})^2$, where ψ is a slack variable. Since typical power system optimization problems include upper limits on the voltage magnitudes, explicitly including this sphere constraint in the problem formulation generally does not restrict the applicability of the convergence theorem in [129].

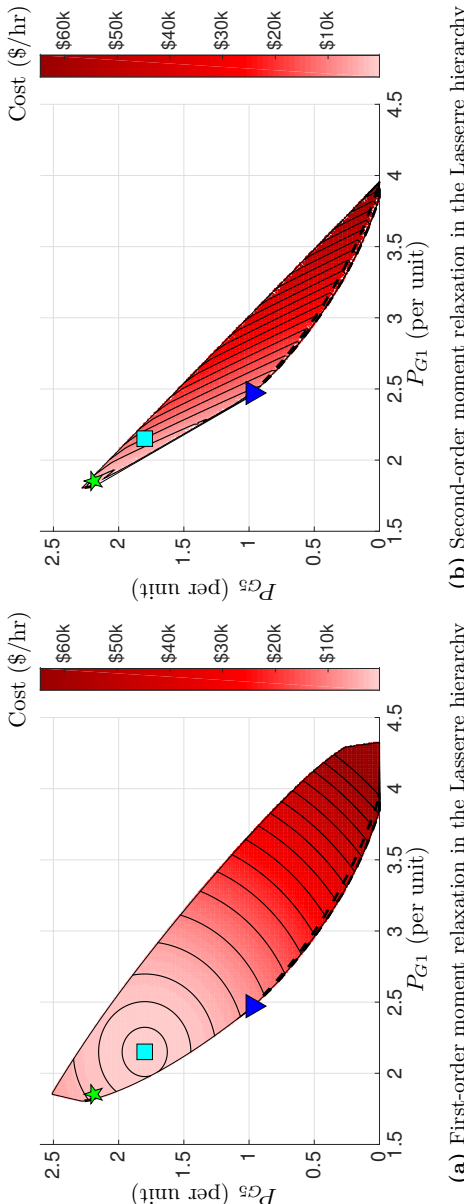


Figure 4.3: Projections of the feasible spaces of the OPF problem and the first- and second-order Lasserre relaxations for a modified version of the five-bus system “WB5” from [3]. Compared to the projection in Figure 2.6b, the projections shown here look down vertically. The feasible space for the OPF problem is denoted by the region inside the dashed black curves at the bottom-left and upper-left portions of the colored region. (The green star largely obscures the upper-left portion.) The feasible spaces for the relaxations are shown by the colored regions. The OPF problem’s objective function is modified to a convex quadratic function of active power generation with an unconstrained minimizer at the light blue square. The thin black lines are contours of the objective functions for the relaxations. The green star denotes the OPF problem’s global solution and the dark blue triangle is a local optimum of the OPF problem.

Observe the difference in the objective functions for the relaxations. The solution to the first-order relaxation is at the light blue square. The first-order relaxation therefore fails to be exact, yielding a strict lower bound on the optimal objective value.

The solution to the second-order relaxation is at the green star, which matches the OPF problem’s global optimum. Thus, the second-order relaxation is exact.

Lasserre hierarchy.) Likewise, since the SDSOS hierarchy in [234] is a further relaxation of the mixed SDP/SOCP hierarchy, it is generally not as tight at a given relaxation order as the other hierarchies discussed in this monograph. Note that neither solutions resulting from the mixed SDP/SOCP hierarchy nor those from the SDSOS hierarchy in [234] are guaranteed to converge to the globally optimal objective value of an optimization problem with increasing relaxation order [237], although other related SOCP and LP hierarchies may be constructed which do have such convergence guarantees [238, 252].

Computational Developments

The computational burden of the moment relaxations grows quickly with both increasing relaxation order and with system size. As one measure of the computational burden, the moment matrices for the Lasserre hierarchy (4.21) and the complex moment hierarchy (4.34) for the order- γ relaxation of an n -bus system have number of rows and columns equal to κ_R and κ_C , respectively:

$$\kappa_R = \frac{(2n - 1 + \gamma)!}{(2n - 1)! \gamma!}, \quad (4.39a)$$

$$\kappa_C = 2 \frac{(n + \gamma)!}{n! \gamma!}. \quad (4.39b)$$

The size of the moment matrix for the Lasserre hierarchy is based on elimination of V_{q1} using the angle reference constraint $V_{q1} = 0$. The size of the moment matrix for the complex moment hierarchy is based on a conversion to a real-valued representation using the approach in §3.3. This accounts for the factor of 2 in (4.39b).

Figure 4.4 illustrates the relative sizes of these matrices for a 10-bus system at various relaxation orders. Observe that the matrices for the complex moment hierarchy are significantly smaller than the matrices for the Lasserre hierarchy, which explains the complex moment hierarchy's advantage in computational tractability. For example, $n = 10$ and $\gamma = 3$ correspond to $\kappa_R = 1540$ and $\kappa_C = 572$.

The rapid growth in the size of the matrices limits the computational tractability of dense formulations of the second-order moment relaxations to systems with no more than approximately 10 buses. As

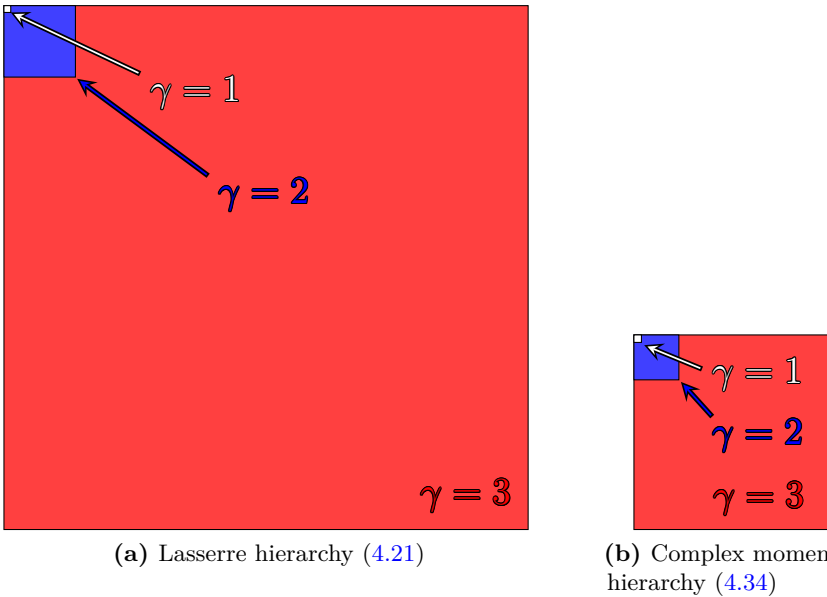


Figure 4.4: Relative sizes of the moment matrices for the order- γ relaxation of a 10-bus system for the Lasserre hierarchy (4.21h) and the complex moment hierarchy (4.34h) given by κ_R in (4.39a) and κ_C in (4.39b), respectively. The small white squares in the upper left corners correspond to $\gamma = 1$, the blue squares correspond to $\gamma = 2$, and the red squares correspond to $\gamma = 3$.

for the Shor relaxation discussed in §4.1.1, computational tractability of the moment relaxations depends on the ability to exploit the network's chordal sparsity. Similar to the approach used for the Shor relaxation discussed in §4.1.1, the positive semidefinite constraints on the moment and localizing matrices can be decomposed into constraints on smaller matrices corresponding to the maximal cliques of a certain chordal extension. This approach was first proposed for moment relaxations of general polynomial optimization problems in [253] and for OPF problems in [227]. The chordal sparsity exploiting approach is applicable to all the aforementioned moment hierarchies. Note that the SOCP constraints associated with the moment matrix for the mixed SDP/SOCP and the SDSOS hierarchies benefit from two sources of sparsity: 1) the chordal sparsity enables a decomposition that only considers certain submatrices, and 2) only terms in the moment matrix which appear in localizing matrices require SOCP constraints. Moreover,

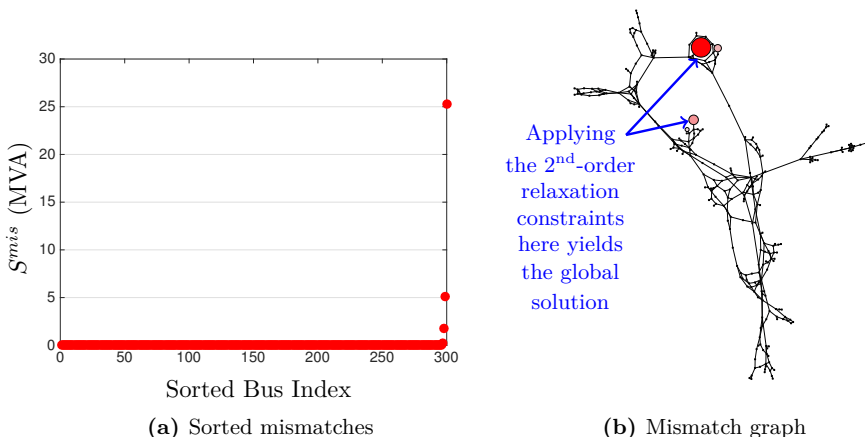


Figure 4.5: The power injection mismatches S_i^{mis} defined in (4.40) for the first-order Lasserre relaxation (4.21) applied to the IEEE 300-bus system. (Note that a minimum resistance of 1×10^{-4} per unit is enforced on all lines.) Figure 4.5a shows the power injection mismatches sorted in increasing order. Observe that most buses have small mismatch while a few buses have large mismatch. Figure 4.5b plots the mismatches on the network graph with the size of each bus i corresponding to S_i^{mis} . Applying the second-order constraints from the Lasserre relaxation to the two buses indicated by blue arrows, with the first-order relaxation's constraints elsewhere, yields the global solution to the OPF problem. (All mismatches for this solution are less than 0.002 MVA.)

recall that the SOCP constraints in the higher-order relaxations of the mixed SDP/SOCP hierarchy and in the SDSOS hierarchy are more computationally tractable than the SDP constraints in the Lasserre hierarchy of the same order.

While exploiting chordal sparsity does not affect the tightness of the first-order relaxation (or, equivalently, the Shor relaxation), higher-order moment relaxations that exploit chordal sparsity are generally not as tight as their dense counterparts. However, low-order moment relaxations are still capable of solving many relevant problems.

The tractability of the chordal-sparsity-exploiting moment relaxations depends on the network topology. The IEEE 39-bus system is the largest standard test case that is tractable for the sparse second-order moment relaxation in the Lasserre hierarchy. Extension to larger problems exploits the observation that the first-order relaxation is often sufficiently accurate for most constraints in large-scale problems [141].

By only enforcing the computationally expensive higher-order constraints associated with certain “problematic” buses, the *multi-ordered* relaxation approach in [129, 219, 227] is capable of globally solving problems with hundreds to thousands of buses. The problematic buses are iteratively identified using a heuristic based on *power injection mismatches* between the solution to the relaxation and the injections associated with the closest rank-one moment matrix. Specifically, the power injection mismatch vector $S^{mis} \in \mathbb{R}^n$ is

$$S_i^{mis} = |(L_y \{f_{Pi}\} - f_{Pi}(V^*)) + j(L_y \{f_{Qi}\} - f_{Qi}(V^*))|, \quad (4.40)$$

where V^* is defined in (4.24) with the eigenvector ν corresponding to the *largest* eigenvalue. If there is only one non-zero eigenvalue, the relaxation satisfies the rank condition (4.23) and therefore provides the globally optimal solution. Conversely, if there are multiple non-zero eigenvalues, the approach in [129, 227] effectively considers the mismatch computed using the power injections associated with the high-rank solution relative to the power injections associated with the closest rank-one moment matrix. Typically, the power injection mismatches are small at the majority of buses, with a few buses (i.e., the “problematic” buses) having large mismatches [129, 141, 227]. This suggests that there exists a non-convexity associated with some subregion of the network. To exploit this observation, an iterative algorithm in [129, 227] successively enforces higher-order constraints at buses where the power injection mismatches are high in order to progressively tighten the relaxation. The algorithm retains the aforementioned convergence guarantees provided by the hierarchies.

Figure 4.5 illustrates the application of this approach to the IEEE 300-bus system [227]. Also, [229] provides further analysis of the key parameter in this approach (i.e., the number of additional buses at which to apply the higher-order constraints at each iteration). Finally, note that an analogous approach is applicable to the other hierarchies. Reference [129] provides specific details regarding application to the complex moment hierarchy and to more general polynomial optimization problems.

Despite this progress, further work in improving the formulations and SDP solution algorithms is needed to achieve computational competitiveness with existing local solution algorithms. Note that the distributed computing algorithms and other proposed computational approaches for the Shor relaxation described in §4.1.1 are generally extendable to the moment relaxations.

4.2 Second-Order Cone Programming Relaxations of the Power Flow Equations

Convex relaxations of power system optimization problems using SOCP formulations were first proposed prior to the development of SDP-based relaxations. In 2006, Jabr formulated an SOCP relaxation and tested it using OPF problems for radial networks [194]. A variety of subsequent research has developed related SOCP relaxations and studied their characteristics. This section presents various SOCP relaxations, discusses their relative tightness and sufficient conditions which guarantee their exactness, and summarizes their computational characteristics.

4.2.1 Bus Injection Model Relaxations

The first group of SOCP relaxations are based on the bus injection model of the power flow equations discussed in §2.1.1. This section summarizes Jabr's relaxation [194] and the Quadratic Convex (QC) relaxation [143, 155, 176, 254]. Note that the “Strong SOCP” relaxation proposed in [255] (along with related work in [256]) strengthens Jabr's relaxation with a variety of linear constraints and is therefore discussed in conjunction with other tightening approaches in §4.4.2. Also note that despite being discussed in §4.1.2 with the other relaxation hierarchies, relaxations in the SDSOS hierarchy are formulated as SOCPs.

Jabr's Relaxation

Jabr's SOCP relaxation [194] is based on the bus injection model of the power flow equations (2.3). This relaxation defines new variables for the squared voltage magnitude at bus i , $c_{ii} = |V_i|^2 = V_{di}^2 + V_{qi}^2$, the real part of the product of the voltage phasors at buses i and k ,

$c_{ik} = |V_i| |V_k| \cos(\theta_i - \theta_k) = V_{di}V_{dk} + V_{qi}V_{qk}$, and the negative imaginary part of the product of the voltage phasors at buses i and k , $s_{ik} = -|V_i| |V_k| \sin(\theta_i - \theta_k) = V_{di}V_{qk} - V_{qi}V_{dk}$.¹⁵ This change of variables, which was first proposed in [257], results in the following representation of the power flow equations for a radial network:

$$P_i = \mathbf{G}_{ii}c_{ii} + \sum_{\substack{k=1,\dots,n \\ k \neq i}} \mathbf{G}_{ik}c_{ik} - \mathbf{B}_{ik}s_{ik}, \quad \forall i \in \mathcal{N}, \quad (4.41a)$$

$$Q_i = -\mathbf{B}_{ii}c_{ii} + \sum_{\substack{k=1,\dots,n \\ k \neq i}} -\mathbf{B}_{ik}c_{ik} - \mathbf{G}_{ik}s_{ik}, \quad \forall i \in \mathcal{N}, \quad (4.41b)$$

$$c_{ik} = c_{ki}, \quad \forall (i, k) \in \mathcal{L}, \quad (4.41c)$$

$$s_{ik} = -s_{ki}, \quad \forall (i, k) \in \mathcal{L}, \quad (4.41d)$$

$$c_{ik}^2 + s_{ik}^2 = c_{ii}c_{kk}, \quad \forall (i, k) \in \mathcal{L}. \quad (4.41e)$$

While an exact representation for radial networks, the formulation (4.41) is a relaxation for mesh networks due to the fact that it does not ensure the ability to recover a set of voltage angles that sum to zero (mod 2π radians) around each loop. Let θ_i denote the voltage angle associated with bus i . Augmenting (4.41) with the non-convex constraint $\tan(\theta_k - \theta_i) = \frac{s_{ik}}{c_{ik}}, \forall (i, k) \in \mathcal{L}$ results in a formulation that is equivalent to the power flow equations for mesh networks [255].

The formulation (4.41) is non-convex due to the equality constraint (4.41e). A convex relaxation is formed by replacing (4.41e) with a less-stringent inequality constraint:

$$c_{ik}^2 + s_{ik}^2 \leq c_{ii}c_{kk}, \quad \forall (i, k) \in \mathcal{L}. \quad (4.42)$$

Observe that (4.42) is a rotated SOCP of the form (3.8), so standard SOCP solution techniques can be applied to the resulting problem. The formulation defined by (4.41a)–(4.41d), (4.42) is hereafter denoted as “Jabr’s relaxation”.

The formulation (4.41) can also be derived by applying a necessary condition for positive semidefiniteness of a Hermitian matrix to the

¹⁵To better match the subsequent literature [143, 255], the formulation (4.41) is a slight modification of that used in [194]; the voltage magnitudes in (4.41) are not divided by a factor of $\sqrt{2}$ and the term s_{ij} is defined with the opposite sign.

4.2. Second-Order Cone Programming Relaxations

77

Shor relaxation in complex variables. Specifically, a necessary condition for $\mathbf{Z} \succeq 0$ in (4.8) takes the form of rotated SOCP constraints on the 2×2 submatrices associated with each line:

$$\mathbf{Z}_{ii} \geq 0, \quad i = 1, \dots, n, \quad (4.43a)$$

$$\mathbf{Z}_{ii}\mathbf{Z}_{kk} \geq |\mathbf{Z}_{ik}|^2, \quad \forall (i, k) \in \mathcal{L}. \quad (4.43b)$$

This necessary condition is implied by the non-negativity of the diagonal entries and all 2×2 determinants of positive semidefinite matrices.

Replacing the SDP constraint (4.8) in the complex Shor relaxation with the less stringent constraints (4.43) yields an SOCP formulation that is equivalent to Jabr's relaxation.¹⁶ Note that the relaxation formed by applying the necessary condition (4.43) directly to the real matrix \mathbf{W} in (4.3) is weaker and less computationally tractable than the SOCP relaxation (4.43) derived from the Hermitian matrix \mathbf{Z} [129, Appendix E].

The QC Relaxation

The “Quadratic Convex” (QC) relaxation, which was initially proposed in [258, 259] and studied for OPF applications in [143], augments Jabr's relaxation with new variables for the voltage angles θ_i and voltage magnitudes, $|V_i|$, $\forall i \in \mathcal{N}$. Using these additional variables, the QC relaxation formulates linear and SOCP constraints that relax the trigonometric terms in the polar representation of the power flow equations (2.5). The QC relaxation is particularly effective when applied to problems with small admissible ranges for both voltage magnitudes and angle differences between connected buses. Also, since the QC relaxation's constraints implicitly formulate a relaxation of the angle consistency condition around cycles, the QC relaxation is designed to be applicable to mesh networks.

¹⁶To see this equivalence, let $c_{ik} = \text{Re}(\mathbf{Z}_{ik})$ and $s_{ik} = \text{Im}(\mathbf{Z}_{ik})$. Observe that $\text{Re}(\mathbf{Z}_{ik}) = \text{Re}(\mathbf{Z}_{ki})$ and $\text{Im}(\mathbf{Z}_{ik}) = -\text{Im}(\mathbf{Z}_{ki})$ due to the fact that \mathbf{Z} is a Hermitian matrix. Thus, (4.41c) and (4.41d) are satisfied. Further observe that the diagonal entries \mathbf{Z}_{ii} of the Hermitian matrix \mathbf{Z} are real. Notice that (4.43b) is equivalent to $\mathbf{Z}_{ii}\mathbf{Z}_{kk} \geq \text{Re}(\mathbf{Z}_{ik})^2 + \text{Im}(\mathbf{Z}_{ik})^2$, and thus (4.42) is satisfied. Since $\text{tr}(\mathbf{H}_k \mathbf{Z})$ and $\text{tr}(\tilde{\mathbf{H}}_k \mathbf{Z})$ (where \mathbf{H}_k and $\tilde{\mathbf{H}}_k$ are defined in (4.6)) are equivalent to the right-hand sides of (4.41a) and (4.41b), the remaining constraints in Jabr's relaxation are satisfied. Hence, applying (4.43) yields an SOCP formulation equivalent to Jabr's relaxation.

The QC relaxation relies on convex envelopes around various non-convex functions. These envelopes are described in terms of a generic decision variable x , which is later replaced with variables representing the voltage magnitudes and the angle differences. Let x^{max} and x^{min} denote specified upper and lower limits, respectively, on a decision variable x . Also let $x^m = \max\{|x^{min}|, |x^{max}|\}$. Then define the set-valued functions.¹⁷

$$\langle x^2 \rangle^T = \left\{ t : \begin{cases} t \leq (x^{min} + x^{max})x - x^{min}x^{max} \\ t \geq x^2 \end{cases} \right\}, \quad (4.44a)$$

$$\langle \sin(x) \rangle^S = \left\{ t : \begin{cases} t \leq \cos\left(\frac{x^m}{2}\right)\left(x - \frac{x^m}{2}\right) + \sin\left(\frac{x^m}{2}\right) \\ t \geq \cos\left(\frac{x^m}{2}\right)\left(x + \frac{x^m}{2}\right) - \sin\left(\frac{x^m}{2}\right) \end{cases} \right\}, \quad (4.44b)$$

$$\begin{aligned} \langle \cos(x) \rangle^C &= \left\{ t : \begin{cases} t \leq 1 - \frac{1-\cos(x^m)}{(x^m)^2}x^2 \\ t \geq \frac{\cos(x^{min})-\cos(x^{max})}{x^{min}-x^{max}}(x - x^{min}) + \cos(x^{min}) \end{cases} \right\}. \end{aligned} \quad (4.44c)$$

The functions (4.44a)–(4.44c) are convex envelopes for:

- The square of a variable, $\langle x^2 \rangle^T$,
- The sine function, $\langle \sin(x) \rangle^S$, and
- The cosine function, $\langle \cos(x) \rangle^C$.

Figure 4.6 provides illustrations of these envelopes. The convex envelope in (4.44a) encloses the square function using a quadratic inequality constraint and a linear function that lies above the square function. The convex envelope in (4.44b) encloses the sine function in a polyhedral set. The convex envelope in (4.44c) uses quadratic and linear functions that lie above and below the cosine function. The QC relaxation also uses McCormick envelopes [125] denoted as $\langle xy \rangle^M$ for the bilinear product

¹⁷The definitions in (4.44) from [176, 254] allow for asymmetric upper and lower bounds on the angle differences, i.e., x^{min} is not necessarily equal to $-x^{max}$. These definitions thus generalize the QC formulation in [143], which requires that $x^{min} = -x^{max}$ when x represents an angle difference.

4.2. Second-Order Cone Programming Relaxations

79

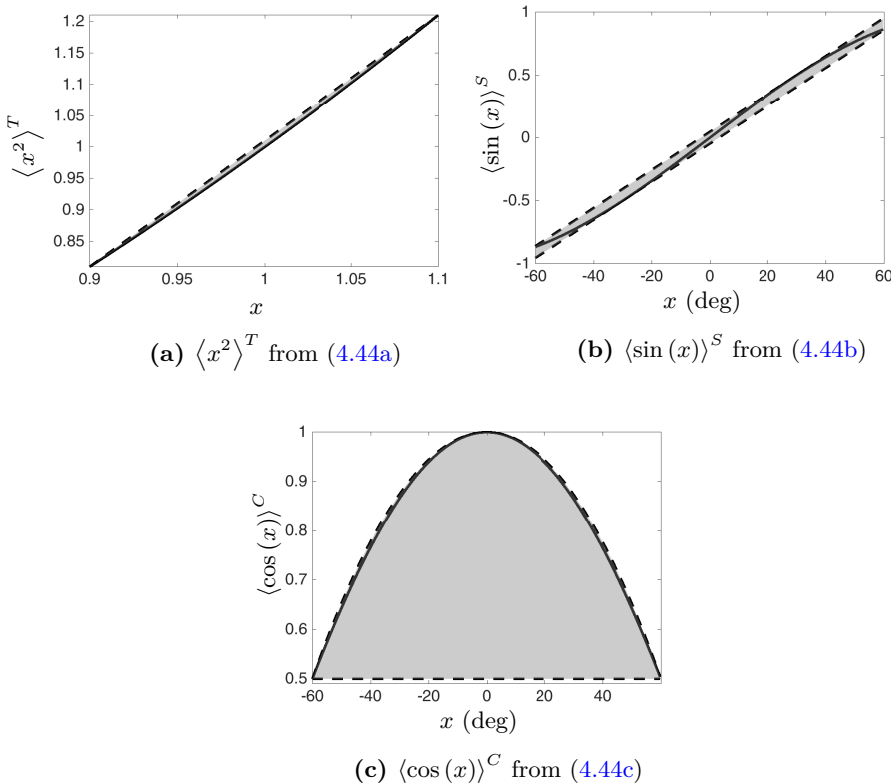


Figure 4.6: Convex envelopes defined in (4.44). In Figures 4.6a–4.6c, the solid lines represent the non-convex functions and the gray regions outlined by the dashed lines represent the convex envelopes.

xy , where x and y are generic variables. The McCormick envelopes are defined in (3.2).

The convex envelopes for sine and cosine presented in (4.44b) and (4.44c), i.e., $\langle \sin(x) \rangle^S$ and $\langle \cos(x) \rangle^C$, assume that the angle x has upper and lower bounds x^{min} and x^{max} that satisfy $-\frac{\pi}{2} \leq x^{min} \leq x^{max} \leq \frac{\pi}{2}$. Lower bounds x^{min} that are non-negative and upper bounds x^{max} that are non-positive can be further exploited to improve the convex envelopes for the trigonometric functions [176, 254]. (Such bounds can be obtained using *bound tightening* techniques, such as those that

will be discussed in §4.4.1.) Specifically, [176, 254] proposes the following tighter sine envelope $\langle \sin(x) \rangle^{S'}$:

$$\begin{aligned} \langle \sin(x) \rangle^{S'} &= \langle \sin(x) \rangle^S \\ &\cap \left\{ t : \begin{cases} t \geq \frac{\sin(x^{\min}) - \sin(x^{\max})}{x^{\min} - x^{\max}} (x - x^{\min}) + \sin(x^{\min}), & \text{if } x^{\max} \geq x^{\min} \geq 0 \\ t \leq \frac{\sin(x^{\min}) - \sin(x^{\max})}{x^{\min} - x^{\max}} (x - x^{\min}) + \sin(x^{\min}), & \text{if } x^{\min} \leq x^{\max} \leq 0 \end{cases} \right\}. \end{aligned} \quad (4.45)$$

Recent work in [155] extends [176, 254] to form tighter envelopes $\langle \sin(x) \rangle^{S''}$ and $\langle \cos(x) \rangle^{C''}$ by enclosing the trigonometric functions using convex quadratic constraints. Similar to (4.45), the tighter envelopes proposed in [155] are applicable to variables associated with lines for which $0 \leq x^{\min} \leq x^{\max} \leq \frac{\pi}{2}$ or $-\frac{\pi}{2} \leq x^{\min} \leq x^{\max} \leq 0$. For each such line $(i, k) \in \mathcal{L}$, define scalars α_{ik} , β_{ik} , and γ_{ik} that are functions of three parameters denoted as a , b , and c :

$$\alpha_{ik}(a, b, c) = \frac{(\sin(a + c) - \sin(a)) \cdot (a - b) - c \cdot (\sin(a) - \sin(b))}{c \cdot (a - b) \cdot (a - b + c)}, \quad (4.46a)$$

$$\beta_{ik}(a, b, c) = \frac{\sin(a) - \sin(b)}{a - b} - \alpha_{ik}(a, b, c) \cdot (a + b), \quad (4.46b)$$

$$\gamma_{ik}(a, b, c) = \alpha_{ik}(a, b, c) \cdot a \cdot b + \sin(a) - \frac{a \cdot (\sin(a) - \sin(b))}{a - b}. \quad (4.46c)$$

Let $0 < \epsilon < \frac{\pi}{2} - x^{\max}$ be a small positive constant. Using (4.46), define

$\alpha_{ik}^{(sp)}$, $\beta_{ik}^{(sp)}$, and $\gamma_{ik}^{(sp)}$ as α_{ik} , β_{ik} , and γ_{ik} evaluated at $(a, b, c) = (x^{\max}, x^{\min}, \epsilon)$;

$\alpha_{ik}^{(sn)}$, $\beta_{ik}^{(sn)}$, and $\gamma_{ik}^{(sn)}$ as α_{ik} , β_{ik} , and γ_{ik} evaluated at $(a, b, c) = (x^{\min}, x^{\max}, -\epsilon)$;

$\alpha_{ik}^{(cp)}$, $\beta_{ik}^{(cp)}$, and $\gamma_{ik}^{(cp)}$ as α_{ik} , β_{ik} , and γ_{ik} evaluated at $(a, b, c) = (\frac{\pi}{2} - x^{\min}, \frac{\pi}{2} - x^{\max}, \epsilon)$; and

4.2. Second-Order Cone Programming Relaxations

81

$\alpha_{ik}^{(cn)}$, $\beta_{ik}^{(cn)}$, and $\gamma_{ik}^{(cn)}$ as α_{ik} , β_{ik} , and γ_{ik} evaluated at $(a, b, c) = (\frac{\pi}{2} + x^{\max}, \frac{\pi}{2} + x^{\min}, \epsilon)$.

The tighter envelopes proposed in [155] are

$$\langle \sin(x) \rangle^{S''} = \langle \sin(x) \rangle^{S'} \cap \left\{ t : \begin{cases} t \leq \alpha_{ik}^{sp} x^2 + \beta_{ik}^{sp} x + \gamma_{ik}^{sp}, & \text{if } 0 \leq x^{\min} \leq x^{\max} \\ t \geq \alpha_{ik}^{sn} x^2 + \beta_{ik}^{sn} x + \gamma_{ik}^{sn}, & \text{if } x^{\min} \leq x^{\max} \leq 0 \end{cases} \right\}, \quad (4.47a)$$

$$\langle \cos(x) \rangle^{C''} = \langle \cos(x) \rangle^C \cap \left\{ t : \begin{cases} t \leq \alpha_{ik}^{cp} \left(\frac{\pi}{2} - x\right)^2 + \beta_{ik}^{cp} \left(\frac{\pi}{2} - x\right) + \gamma_{ik}^{cp}, & \text{if } 0 \leq x^{\min} \leq x^{\max} \\ t \leq \alpha_{ik}^{cn} \left(\frac{\pi}{2} + x\right)^2 + \beta_{ik}^{cn} \left(\frac{\pi}{2} + x\right) + \gamma_{ik}^{cn}, & \text{if } x^{\min} \leq x^{\max} \leq 0 \end{cases} \right\}. \quad (4.47b)$$

Figure 4.7 provides an illustrative example of the tighter envelope for the sine function, $\langle \sin(x) \rangle^{S''}$, when $0 \leq x^{\min} \leq x^{\max}$. Note that the convex quadratic expressions in (4.47) can be formulated as SOCP constraints using the conversion described in §3.2.

The QC relaxation uses the convex envelopes defined above to formulate a relaxation of the power flow equations:

$$c_{ii} \in \left\langle |V_i|^2 \right\rangle^T, \quad \forall i \in \mathcal{N}, \quad (4.48a)$$

$$c_{ik} \in \left\langle \langle |V_i| |V_k| \rangle^M \cdot \langle \cos(\theta_i - \theta_k) \rangle^{C''} \right\rangle^M, \quad \forall (i, k) \in \mathcal{L}, \quad (4.48b)$$

$$s_{ik} \in \left\langle \langle |V_i| |V_k| \rangle^M \cdot \langle \sin(\theta_i - \theta_k) \rangle^{S''} \right\rangle^M, \quad \forall (i, k) \in \mathcal{L}, \quad (4.48c)$$

$$\text{Equations (4.41a)–(4.41d), (4.42).} \quad (4.48d)$$

The angle θ_i at the reference bus is fixed to zero.

Note that forming the convex envelopes defined in (4.44) requires upper and lower bounds on voltage magnitudes, V_i^{\min} and V_i^{\max} , $\forall i \in \mathcal{N}$, and voltage angle differences θ_{ik}^{\min} and θ_{ik}^{\max} , $\forall (i, k) \in \mathcal{L}$, where $\theta_{ik} = \theta_i - \theta_k$. The voltage magnitude bounds are enforced using $(V_i^{\min})^2 \leq c_{ii} \leq (V_i^{\max})^2$, $\forall i \in \mathcal{N}$, and the angle difference bounds are enforced using $\tan(\theta_{ik}^{\min}) c_{ik} \leq s_{ik} \leq \tan(\theta_{ik}^{\max}) c_{ik}$, $\forall (i, k) \in \mathcal{L}$. Under typical operating conditions, the voltage angle differences between connected buses are small. Additionally, restrictions associated with system stability may also require enforcing explicit phase angle

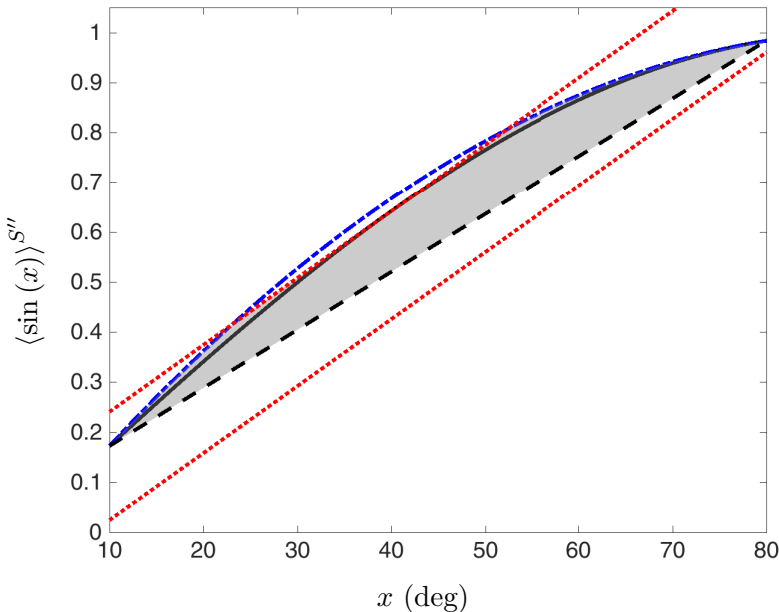


Figure 4.7: The tighter convex envelope for the sine function, $\langle \sin(x) \rangle^{S''}$, proposed in [155, 176, 254] that is applicable when $0 \leq x^{\min} \leq x^{\max}$. The solid black curve is the sine function. The dotted red lines correspond to the original envelope specified in [143] (i.e., the dashed black lines in Figure 4.6b), which does not exploit non-negativity of the bounds. The dashed black line in Figure 4.7 is the improved lower bound proposed in [176, 254]. The dash-dot blue curve in Figure 4.7 is the upper bound proposed in [155], which takes the form of an SOCP constraint. The gray region formed by their intersection is the resulting tighter convex envelope $\langle \sin(x) \rangle^{S''}$. See (4.45) and (4.47) for the mathematical descriptions of this envelope and similar envelopes for the sine function when $x^{\min} \leq x^{\max} \leq 0$ and the cosine function when $0 \leq x^{\min} \leq x^{\max}$ or $x^{\min} \leq x^{\max} \leq 0$.

difference constraints between certain buses. Thus, it is often reasonable to consider upper and lower bounds on voltage angle differences.

Using “nested-McCormick” envelopes, as in (4.48b) and (4.48c), generally does not yield the convex hull of a trilinear product. In contrast, Meyer and Floudas envelopes [260, 261] and extreme point envelopes [262] provide hyperplane and vertex forms, respectively, for

the convex hulls of trilinear products. References [263] and [264] demonstrate that applying these envelopes to the QC relaxation reduces the optimality gaps for a variety of OPF test cases. Further analysis in [265] shows that while the Meyer and Floudas envelopes and the extreme point envelopes yield equivalently tight relaxations, their distinct mathematical formulations lead to differing computational performance. Empirical results in [265] indicate that the extreme point envelopes often yield superior computational performance for OPF problems. Additional recent work in [266] further improves the extreme point envelopes by enforcing the consistency between the voltage magnitude products $V_i V_k$ that are shared in the terms $V_i V_k \cos(\theta_i - \theta_k)$ and $V_i V_k \sin(\theta_i - \theta_k)$.

The QC relaxation presented in (4.48) can also be strengthened using a variety of other convex constraints [176, 254, 263] as well as bound tightening techniques [267]. Similarly, the approaches in [255, 256] augment Jabr's relaxation with a variety of linear constraints that are implied by various non-linear relationships to form a "Strong SOCP" relaxation. Further details are provided in §4.4.2.

In an effort to improve computational tractability at the cost of decreased tightness, related research [268] uses weaker linear envelopes that enclose the second-order cone constraints to further relax a formulation that is similar to the QC relaxation (4.48). The resulting linear program provides reasonable accuracy relative to the original relaxation with comparable or superior computation times.

4.2.2 Branch Flow Model Relaxations

Other SOCP relaxations are based on the branch flow model of the power flow equations (2.7). This section summarizes the branch flow relaxation derived from the DistFlow equations [69] and the SOCP relaxation in [269, 270].

Relaxation of the DistFlow Equations

Similar to (4.41), the DistFlow equations (2.7) neglect the voltage phase angles and are thus an exact representation for radial networks but a relaxation of mesh networks. The DistFlow equations (2.7a)–(2.7c) are linear in the flows of squared current magnitude ℓ_{ik} , active power P_{ik} ,

and reactive power Q_{ik} on line $(i, k) \in \mathcal{L}$ as well as the squared voltage magnitude $|V_i|^2$ at each bus $i \in \mathcal{N}$. The *Branch Flow Relaxation* is formed by replacing (2.7d) with an inequality that takes the form of a rotated SOCP constraint:

$$\ell_{ik} |V_i|^2 \geq P_{ik}^2 + Q_{ik}^2, \quad \forall (i, k) \in \mathcal{L}. \quad (4.49)$$

Note that (4.49) is sometimes presented in the literature via introduction of new variables for the squared voltage magnitudes, i.e., $v_i = |V_i|^2$, in order to yield $\ell_{ik} v_i \geq P_{ik}^2 + Q_{ik}^2$.

As shown in [74, 271], the feasible space of the branch flow relaxation (2.7a)–(2.7c), (4.49) has a one-to-one mapping to the feasible space of Jabr's relaxation (4.41a)–(4.41d), (4.42), indicating an equivalence between these relaxations. This result is extended to more general line models in [71].

Note that both the bus injection and branch flow models can be extended to develop relaxations of the power flow equations for unbalanced three-phase networks, using both phase components [167–169] and symmetrical components [146]. Even for radial network topologies, the relaxations of the power flow equations for unbalanced three-phase network models require formulations with SDP constraints due to the coupling between the variables associated with different phases.

By avoiding the subtraction of variables with similar values, the branch flow relaxation has numerical convergence characteristics that are superior to those of the bus injection relaxation [143, 168]. The numerical superiority of the branch flow model is particularly evident for relaxations of three-phase power flow models [168] and large-scale single-phase systems [143].

SOCOP Formulation of Δ Inequalities, Loss Inequalities, and Circle Inequalities

Other SOCP constraints can be formulated from the branch flow model. These include the so-called “ Δ inequalities”, “loss inequalities”, and “circle inequalities” proposed in [269, 270]. Note that related derivations are presented in [71].

The Δ and loss inequalities in [270] are formulated with lifted variables representing the magnitudes of the differences in voltage components between connected buses. This section derives these inequalities for the active power flow equations with series admittance line models. (The derivation can be extended for reactive power flows and formulations with more general line models [269].)

The active power flow through a line with admittance $g_{ik} + jb_{ik}$ is

$$P_{ik} = (V_{di} - V_{dk})(g_{ik}V_{dk} + b_{ik}V_{qk}) + (V_{qi} - V_{qk})(-b_{ik}V_{dk} + g_{ik}V_{qk}). \quad (4.50)$$

Let μ_{ik} and ν_{ik} denote upper bounds on the quantities $(g_{ik}V_{dk} + b_{ik}V_{qk})$ and $(-b_{ik}V_{dk} + g_{ik}V_{qk})$, respectively. One possible upper bound for both μ_{ik} and ν_{ik} is $\sqrt{g_{ik}^2 + b_{ik}^2}V_i^{max}$. A valid inequality is

$$|P_{ik}| \leq \mu_{ik} |V_{di} - V_{dk}| + \nu_{ik} |V_{qi} - V_{qk}|. \quad (4.51)$$

Replacing the expressions $|V_{di} - V_{dk}|$ and $|V_{qi} - V_{qk}|$ with the “lifted” variables $d_{d,ik}$ and $d_{q,ik}$, respectively, yields the Δ inequalities

$$|P_{ik}| \leq \mu_{ik} d_{d,ik} + \nu_{ik} d_{q,ik}, \quad \forall (i, k) \in \mathcal{L}, \quad (4.52a)$$

$$d_{d,ik} \geq 0, \quad d_{q,ik} \geq 0, \quad \forall (i, k) \in \mathcal{L}. \quad (4.52b)$$

By themselves, the Δ inequalities are trivially satisfied with sufficiently large values for the lifted variables $d_{d,ik}$ and $d_{q,ik}$. The Δ inequalities are relevant when combined with the loss inequalities described next. The losses on the line (i, k) are

$$P_{ik} + P_{ki} = g_{ik} \left((V_{di} - V_{dk})^2 + (V_{qi} - V_{qk})^2 \right). \quad (4.53)$$

Relaxing the equality in (4.53) to an inequality and substituting the lifted variables $d_{d,ik}$ and $d_{q,ik}$ yields the loss inequality constraint

$$P_{ik} + P_{ki} \geq g_{ik} \left(d_{d,ik}^2 + d_{q,ik}^2 \right). \quad (4.54)$$

The loss inequality (4.54) is formulated as an SOCP constraint that effectively enforces upper bounds on the lifted variables $d_{d,ik}$ and $d_{q,ik}$.

The circle inequality constraints in [270] are related to the “sending” and “receiving” circles associated with the power flowing through a

line [272, p. 104]. The power flow through the line $(i, k) \in \mathcal{L}$ must satisfy the “circle constraint”

$$\left(P_{ik} - g_{ik} |V_i|^2 \right)^2 + \left(Q_{ik} + b_{ik} |V_i|^2 \right)^2 \leq |V_i|^2 |V_k|^2 \left(g_{ik}^2 + b_{ik}^2 \right). \quad (4.55)$$

Observe that (4.55) is a rotated SOCP constraint (cf (3.8)) in terms of the squared voltage magnitudes $|V_i|^2$ and $|V_k|^2$. The circle constraints can be extended to more general line models [269].

The SOCP relaxation in [269, 270] is formulated with most of the same variables as the branch flow relaxation (2.7a)–(2.7c), (4.49) (squared voltage magnitudes $|V_i|^2, \forall i \in \mathcal{N}$, and flows of active power P_{ik} and reactive power Q_{ik} on lines $(i, k) \in \mathcal{L}$) and the additional “lifted” variables $d_{d,ik}$ and $d_{q,ik}, \forall (i, k) \in \mathcal{L}$, as well as the Δ inequality, loss inequality, and circle inequality constraints (4.52), (4.54), and (4.55), respectively. The approach in [269] also leverages the flexibility provided by the choice of the reference bus to develop constraints that tighten the SOCP relaxations. Note that there is currently no known comparison of the tightness and computational characteristics of this relaxation relative to other relaxations.

4.2.3 Exactness

A variety of research efforts have developed a priori sufficient conditions which guarantee that Jabr’s SOCP relaxation (4.41a)–(4.41d), (4.42) and the branch flow relaxation (2.7a)–(2.7c), (4.49) are exact. Note that satisfaction of sufficient conditions for exactness of these SOCP relaxations also guarantees exactness for tighter relaxations (e.g., the Shor relaxation in §4.1.1, the moment relaxations in §4.1.2, the QC relaxation in §4.2.1, the SDSOS relaxations in §4.2.1, and the “Strong SOCP” relaxation in §4.3). This section summarizes the known sufficient conditions for exactness of these relaxations. Most of the literature has focused on characterizing the exactness of the SOCP relaxations with respect to OPF problems; less is known regarding exactness for other problems. Also note that no simple algorithm can solve all OPF problems since these problems are generally NP-Hard [1], even for radial networks [2].

Many of these sufficient conditions use a *load oversatisfaction* assumption that allows the active and reactive load demands to be arbitrarily increased or, equivalently, there is no lower limit on the power injections P_i and Q_i . The load oversatisfaction assumption provides attractive theoretical features which facilitate the development of many of the following sufficient conditions for exactness of the power flow relaxations. However, the load oversatisfaction assumption does not match the behavior of many realistic load models, which often consider demands that are constants or functions of the voltage magnitudes (e.g., ZIP models). Various problem formulations allow loads to be curtailed at a high cost or time-shifted to achieve some system objective [273]. Curtailment is the converse of the load oversatisfaction assumption. Time-shifting is loosely related to the load oversatisfaction assumption in the sense that loads increase their consumption at one time period. However, this increase is not arbitrary as modeled by the load oversatisfaction assumption but is rather matched by a decrease in some other time period, and there are typically limits on the quantity of time-shifted load demands. References [274] and [275] discuss other limits regarding the practical applicability of many existing sufficient conditions for exactness of various SOCP relaxation.

Known sufficient conditions for exactness of Jabr's SOCP relaxation (4.41a)–(4.41d), (4.42) and the branch flow relaxation (2.7a)–(2.7c), (4.49) take one of the following forms:

- Meshed networks with many controllable phase-shifting transformers and a load oversatisfaction assumption [276] or other non-trivial technical assumptions [277]. The controllable phase-shifting transformers must be located so that there exists a spanning tree of the power system network for which there is a phase-shifting transformer on every branch in the network that is not in the spanning tree. This is a significantly higher deployment than is present in typical power systems. Additionally, the sufficient conditions require an idealized model of phase-shifting transformers (continuously actuatable without limits on phase shifts).

- Radial networks that also satisfy at least one of a variety of non-trivial technical assumptions. One possible assumption is load oversatisfaction, but others are more general [75, 277].
- Radial networks for which there is either no reverse power flow or reverse power flow that consists only of reactive power or only of active power [278].
- Mesh networks that are purely resistive (i.e., zero reactances, zero susceptances, and no reactive injections) and either a load oversatisfaction assumption or other conditions on the voltage and power injection limits [279, 280].

Note that these sufficient conditions are only applicable to problems that use balanced single-phase equivalent network models, even for the conditions that rely on radial network topologies. A detailed survey of many of the known sufficient conditions is provided in [75].

4.2.4 Computational Developments

SOCP formulations often have significant computational advantages over the SDP formulations, due to both the inherently superior computational complexity of SOCP problems [126] and the relative maturity of SOCP solvers. In addition to a variety of academic solvers, SOCP problems can also be addressed using commercial solvers, such as CPLEX, Gurobi, and MOSEK. The computational advantages of SOCP solvers are evident in both run-times and numerical precision. Further, by leveraging the mixed-integer capabilities of the commercial solvers, SOCP representations of the power flow equations can be augmented with a moderate number of discrete variables for small- to moderate-size problems.

Similar to corresponding efforts for the Shor relaxation described in §4.1.1, distributed computation techniques are also applicable to the SOCP relaxations. For instance, [215] applies ADMM to the branch flow relaxation (2.7a)–(2.7c), (4.49). The subproblems in the ADMM formulation have closed-form solutions that can be quickly evaluated. For a realistic 2065-bus radial test case, the distributed solution algorithm

in [215] converges in 1114 iterations, which requires 1153 seconds when implemented on a single machine. With an average solution time per iteration of 0.56 seconds, a parallel implementation may significantly speed computation time given sufficient computing machinery with low-latency communications. Related work in [281, 282] analyzes the performance of an ADMM algorithm on OPF problems with various representations of the power flow equations, including the QC relaxation, Jabr’s relaxation, and the DistFlow relaxation as well as several approximations discussed in §5 (DC power flow and LPAC). Another decomposition technique proposed in [283] solves (in parallel) SOCP relaxations for certain segments of the network, with a modified Bender’s decomposition used to ensure consistency between the voltage phasors on the tie-lines between network segments. Additional recent work in [284] proposes an adaptive penalty scheme and other modifications to speed the execution of an ADMM algorithm for solving SOCP relaxations of OPF problems. Further work is needed to evaluate these and other distributed algorithms, particularly to analyze their practical performance after accounting for factors such as communication delay between the computation nodes.

4.3 Linear Relaxations of the Power Flow Equations

Although they often yield weaker objective value bounds, linear relaxations can have computational and theoretical advantages over SDP and SOCP relaxations. This section describes linear relaxations developed using constraints that are implied by the power flow equations with specified bounds on certain quantities. Note that the linear relaxations may be formulated as either linear programs or quadratic programs depending on the form of the objective function.

4.3.1 The Network Flow Relaxation

The power flow equations require that flows entering and leaving a node obey Ohm’s and Kirchhoff’s laws. In contrast, the *network flow* relaxation [285, 286] allows the flows entering a node to be arbitrarily distributed so long as the active and reactive power losses on each line

are non-negative. Let $g_{sh,i} + jb_{sh,i}$ denote the shunt admittance at bus i . Denote the total shunt susceptance associated with the Π -circuit model of the line (i, k) as $b_{c,ik}$. The network flow relaxation is formulated in terms of the active power flows P_{ik} and the reactive power flows Q_{ik} for each line $(i, k) \in \mathcal{L}$ and the squared voltage magnitudes $|V_i|^2$ at each bus $i \in \mathcal{N}$:

$$P_i = g_{sh,i} |V_i|^2 + \sum_{(i,k) \in \mathcal{L}} P_{ik} + \sum_{(k,i) \in \mathcal{L}} P_{ki}, \quad \forall i \in \mathcal{N}, \quad (4.56a)$$

$$Q_i = -b_{sh,i} |V_i|^2 + \sum_{(i,k) \in \mathcal{L}} Q_{ik} + \sum_{(k,i) \in \mathcal{L}} Q_{ki}, \quad \forall i \in \mathcal{N}, \quad (4.56b)$$

$$P_{ik} + P_{ki} \geq 0, \quad \forall (i, k) \in \mathcal{L}, \quad (4.56c)$$

$$Q_{ik} + Q_{ki} \geq -\frac{b_{c,ik}}{2} (|V_i|^2 + |V_k|^2), \quad \forall (i, k) \in \mathcal{L}. \quad (4.56d)$$

The network flow formulation in (4.56) is a valid relaxation for systems where all lines have series impedances with non-negative resistances and non-negative reactances [285, 286]. Negative resistances are not associated with any physical device. Negative reactances correspond to lines with capacitive series elements. While rare, such lines may be physically present in some systems. More commonly, power flow datasets may include lines with negative resistances and negative series reactances as mathematical artifacts of models arising from, for example, equivalenced regions of the network [287] and three-winding transformers. (The mutual coupling in three-winding transformers may result in models with negative resistances and reactances.) For systems where all lines have series impedances with non-negative resistances and reactances, the network flow relaxation (4.56) is a further relaxation of Jabr's SOCP formulation presented in §4.2 [285, 286].

4.3.2 The Copper Plate Relaxation

The “copper plate” model neglects the power flow equations entirely to yield a simple power balance constraint relating all power injections in the network. Using the same definitions as in §4.3.1, the copper plate

4.3. Linear Relaxations

91

model is

$$\sum_{i \in \mathcal{N}} P_i \geq \sum_{i \in \mathcal{N}} g_{sh,i} |V_i|^2, \quad (4.57a)$$

$$\sum_{i \in \mathcal{N}} Q_i \geq - \sum_{i \in \mathcal{N}} b_{sh,i} |V_i|^2 - \sum_{(i,k) \in \mathcal{L}} \frac{b_{c,ik}}{2} (|V_i|^2 + |V_k|^2). \quad (4.57b)$$

Similar to the network flow model, the copper plate model is a valid relaxation of the power flow equations for systems where all lines have series impedances with non-negative resistances and reactances. For such systems, the copper plate model further relaxes the network flow model [285, 286].

4.3.3 The Taylor-Hoover Relaxation

The linear relaxation proposed by Taylor and Hoover in [288] is formulated with variables $|V_i|^2$ for the squared voltage magnitude at bus $i \in \mathcal{N}$, P_{ik} and P_{ki} for the active power flows into each terminal of line $(i,k) \in \mathcal{L}$, and Q_{ik} and Q_{ki} for the reactive power flows into each terminal of line $(i,k) \in \mathcal{L}$. For a line modeled as a Π circuit with mutual admittance $g_{ik} + jb_{ik}$ and total shunt susceptance $b_{c,ik}$, the Taylor-Hoover relaxation [288] enforces the equalities

$$g_{ik} (P_{ik} - P_{ki}) - b_{ik} (Q_{ik} - Q_{ki}) = \left(g_{ik}^2 + b_{ik}^2 + b_{ik} \frac{b_{c,ik}}{2} \right) (|V_i|^2 - |V_k|^2), \quad (4.58a)$$

$$b_{ik} (P_{ik} + P_{ki}) + g_{ik} (Q_{ik} + Q_{ki}) = -g_{ik} \frac{b_{c,ik}}{2} (|V_i|^2 + |V_k|^2). \quad (4.58b)$$

The equalities in (4.58) result from the relaxation of linear combinations of the non-linear expressions for the active and reactive line flows. Note that non-physical negative line losses may result when using this relaxation [285].

4.3.4 McCormick Relaxations

With known bounds on each variable, standard optimization tools such as McCormick envelopes [125] can be employed to construct linear relaxations of the rectangular power flow equations (2.4). The

McCormick relaxation of a bilinear product is given in (3.2). The “Rectangular McCormick” relaxation in [255] applies (3.2) to the rectangular form of the power flow equations (2.4) using the bounds $V_{di}, V_{qi} \in [-V_i^{\max}, V_i^{\max}]$. Similar approaches are proposed in [289] and [290]. The loose bounds available for the voltage components make this relaxation relatively weak. Bound tightening techniques, discussed in §4.4.1, are therefore particularly important for the McCormick relaxation in rectangular coordinates. Note that the specification of a reference angle yields tighter bounds on the voltage components at the reference bus (e.g., selecting bus 1 as the reference implies $V_{q1} = 0$ and $V_{d1} \in [V_1^{\min}, V_1^{\max}]$). As shown in [291], these tighter constraints corresponding to the reference bus voltage are particularly important when applying bound tightening methods to the Rectangular McCormick relaxation.

A stronger linear relaxation is derived by applying McCormick envelopes to the formulation used in Jabr’s relaxation (4.41) [255]. The bounds available for the variables c_{ik} and s_{ik} facilitate a tighter linear relaxation when combined with “lifted” variables C_{ik} , S_{ik} , and D_{ik} , $\forall (i, k) \in \mathcal{L}$:

$$-V_i^{\max} V_k^{\max} \leq c_{ik}, s_{ik} \leq V_i^{\max} V_k^{\max}, \quad (4.59a)$$

$$(V_i^{\min})^2 \leq c_{ii} \leq (V_i^{\max})^2, \quad (4.59b)$$

$$C_{ik} + S_{ik} = D_{ik}, \quad (4.59c)$$

$$C_{ik} \geq 0, S_{ik} \geq 0, \quad (4.59d)$$

$$D_{ik} \in \langle c_{ii} c_{kk} \rangle^M, C_{ik} \in \langle c_{ik} c_{ik} \rangle^M, S_{ik} \in \langle s_{ik} s_{ik} \rangle^M, \quad (4.59e)$$

$$\text{Equations (4.41a)} - \text{(4.41d)}. \quad (4.59f)$$

In [255], the relaxation (4.59) is referred to as the McCormick relaxation of the “alternative” formulation.

4.3.5 Bienstock-Muñoz LP Relaxations

The approach in [292] develops a family of LPs that approximate (to arbitrary accuracy) the solutions of power system optimization problems that may include integer constraints. This approach is particularly useful for power system optimization problems with network topologies that

have small treewidth¹⁸ since the numbers of variables and constraints in the resulting LPs scale exponentially with the treewidth, linearly with the size of the network, and logarithmically with the desired accuracy. The approach in [292] has strong theoretical properties but its effectiveness remains to be demonstrated for practical test cases.

4.3.6 Mixed-Integer Linear Programming Relaxations

Several relaxations employ discrete variables to model the power flow non-linearities. A relaxation proposed in [269] uses a technique from [293] to discretize the voltage component variables using binary variables. Specifically, the discretization in [269] effectively represents each variable as a number in a binary format to a specified precision (i.e., a generic non-negative continuous variable u is written as $u = \sum_{k=1}^T 2^{-k} y_k + \delta$, where the precision is given by the integer parameter $T > 1$, $y \in \{0, 1\}^T$, and $0 \leq \delta \leq 2^{-T}$). With this discretization for each variable, the bilinear products in the power flow equations can be written as the sum of the products of continuous and binary variables. Since each term in these summations can be exactly linearized, the power flow equations can be represented to a specified precision as a MILP. Thus, the precision of the formulation can be precisely controlled.

A similar discretization approach is proposed in [294] for problems with radial network topologies. Formulated in the context of graphical models, this approach exploits radial network structures through the use of a dynamic programming algorithm. This algorithm has a running time that is linear in the network size and polynomial in the discretization precision. Future work proposed in [294] includes several directions for extension of this approach to more general network topologies.

The discretization approach proposed in [295] uses an eigenvector calculation to reformulate the power flow equations as symmetric paraboloids. Delaunay triangulation and binary variables are then used to develop piecewise-linear interpolations of the paraboloid functions. A further contribution of [295] is a disjunctive convex optimization

¹⁸The *treewidth* of a graph is defined as one less than the size of the largest maximum clique among all possible chordal extensions of the graph (see §4.1.1).

approach that constructs outer approximations of the paraboloids to obtain a relaxation.

4.4 Techniques for Tightening Relaxations

This section discusses several methods for tightening the relaxations so that they more accurately represent the original non-convex problem. These include *bound tightening*, enforcing *valid constraints* (i.e., augmenting with constraints that are redundant in the original problem but tighten the relaxation), and embedding in a *spatial branch-and-bound* algorithm. Future research on relaxations using alternative power flow representations may also yield tighter relaxations.

4.4.1 Bound Tightening

The characteristics of many of the relaxations presented in §4.1–§4.3 and the valid constraints to be discussed in §4.4.2 are strongly dependent on the tightness of bounds on voltage magnitudes, angle differences, line flows, and power injections. The bounds on these quantities specified in the power system data set may be significantly larger than the values that are actually achievable due to the limitations imposed by other constraints. In other words, certain bounds may never be binding. Many of the relaxations can *self-tighten*: given an initial set of (potentially unachievable) bounds, a relaxation is used to maximize (or minimize) the expression associated with each bound. If the maximum achievable value for an expression is less than the specified upper bound (or the minimum achievable value is greater than the specified lower bound), then the specified bound can never be binding. The specified bound is then replaced with the objective value for the solution to the associated relaxation. Specifying tighter bounds may improve the relaxation, which can lead to still tighter bounds. (For instance, the tightness of the QC relaxation’s convex envelopes in §4.2.1 depend strongly on the quality of the available bounds on voltage magnitudes and angles.) Thus, an iterative “bound tightening” algorithm can be used to improve the relaxations. The iterative algorithm terminates upon reaching a fixed

point where no bounds are tightened during some iteration. Related approaches are proposed in [255, 256, 264, 266, 267, 295–298].

One particularly notable variant called “optimality-based bound tightening” [264, 266, 297] incorporates information from some known feasible point, which can be computed using a local solution algorithm. (See §6.) An optimality-based bound tightening algorithm follows the iterative approach described above while enforcing an additional constraint that restricts the objective function to be superior to the objective value corresponding to a known feasible point. Restricting the bound tightening algorithm to consider only the subset of the feasible space that is superior to a high-quality feasible point (i.e., a feasible point whose objective value is close to the globally optimal objective value) can thus enable the computation of substantially tighter bounds.

To improve computational tractability, the relaxations associated with each bound can be computed in parallel within each iteration. Further, the bound tightening algorithm can use a more tractable relaxation than the relaxation that is finally applied to solve the actual problem of interest. For instance, the approaches employed in [255] and [256] only consider the constraints associated with a subset of the network near the bound under consideration when performing the bound tightening, but solve the final relaxation of the OPF problem using the full set of tightened constraints. As another way to improve computational tractability, the approaches in [296] and [298] derive closed form analytical expressions that bound the maximum and minimum achievable values of various quantities in order to enable fast bound tightening.

4.4.2 Enforcing Valid Constraints

Constraints that are *valid but redundant* in the non-convex problem (hereafter called *valid constraints*) can tighten the relaxations. This section describes several approaches for developing valid constraints.

Combining Relaxations

A *dominance relationship* between two relaxations exists when one relaxation is always at least as tight as the other and there are problems for which it is tighter. Combining relaxations which do not dominate one

another generally results in a tighter relaxation. For instance, [176, 254] presents a formulation which combines the QC relaxation (4.48) and the Shor relaxation (4.7a)–(4.7c), (4.8). Figure 4.8 indicates the known dominance relationships among some of the convex relaxations [74, 122, 129, 176, 254, 255, 285]. There are known test cases which demonstrate that the QC and Strong SOCP relaxations in [143] and [255], respectively, neither dominate nor are dominated by the Shor relaxation of [164]. Determining the dominance relationships (or lack thereof) among other relaxations is an open problem.

Cuts from Tighter Relaxations

Rather than tightening a relaxation by adding all constraints associated with a non-dominated relaxation, alternative approaches augment a relaxation with a more limited set of constraints (“cuts”) derived from a non-dominated relaxation. Such approaches can yield tighter relaxations at a modest computational cost.

One such approach proposed in [269] tightens a linear power flow relaxation via cuts generated from the Shor relaxation. As in the Shor relaxation, the approach in [269] uses lifted variables that correspond to the products of voltage components. However, rather than explicitly enforcing a positive semidefinite constraint on the matrix \mathbf{W} composed of these lifted variables as in (4.3), the iterative approach in [269] generates cuts that are derived from necessary conditions for the matrix to be positive semidefinite. Specifically, each iteration k augments the relaxation with the constraint $x_k^\top \mathbf{W} x_k \geq 0$, where x_k is a specified vector. This constraint is a necessary condition for $\mathbf{W} \succeq 0$ that is linear in the entries of \mathbf{W} . One choice of an appropriate vector x_k is an eigenvector corresponding to a negative eigenvalue of the matrix \mathbf{W} . Thus, each iteration of the approach in [269] yields a tighter linear relaxation of the constraint $\mathbf{W} \succeq 0$.

Similar to the approach in [269], an algorithm used in [255, 256] iteratively tightens Jabr’s SOCP relaxation with valid linear cuts that are based on necessary conditions derived from the Shor relaxation. At each iteration of this algorithm, the solution to the SOCP relaxation is checked for feasibility in the Shor relaxation. The algorithm terminates

4.4. Techniques for Tightening Relaxations

97

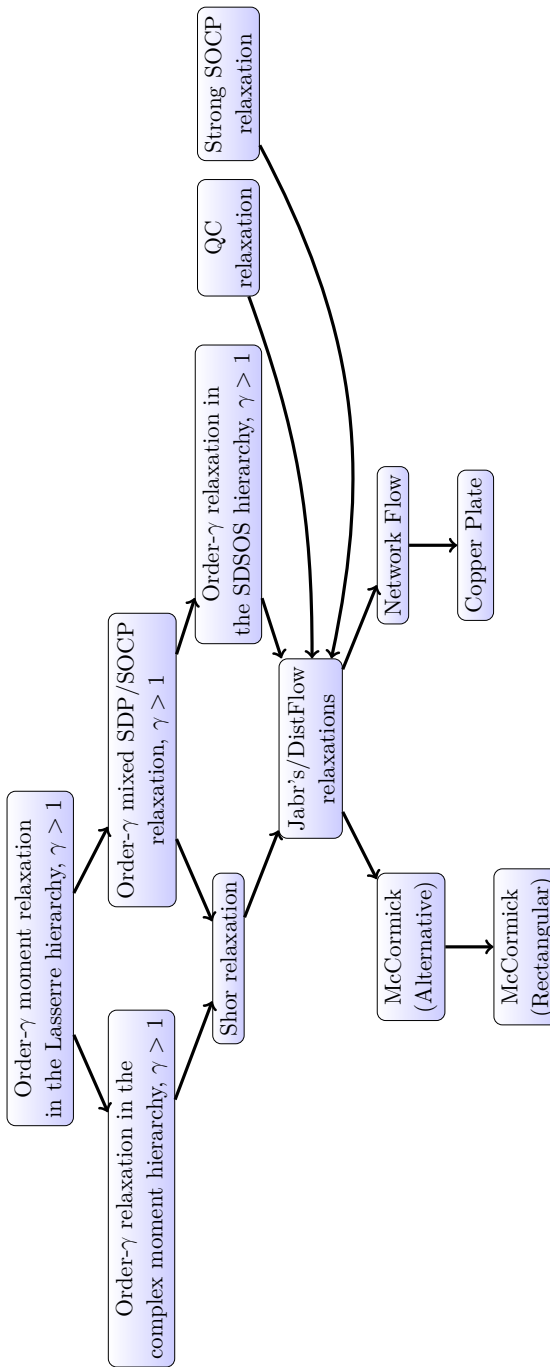


Figure 4.8: Proven dominance relationships among relaxations. The arrows point from the tighter relaxation to the dominated relaxation. Both the QC relaxation and the Strong SOCP relaxation neither dominate nor are dominated by the Shor relaxation [143, 255]. Note that combining relaxations which do not have a dominance relationship yields a generally tighter relaxation (e.g., the combination of the Shor and QC relaxations studied in [176] is generally tighter than Shor and QC relaxations individually). Also note that Figure 2 in [47] provides a similar illustration of relationships among various power flow relaxations and approximations.

if the resulting SOCP solution is feasible in the Shor relaxation or provides a sufficiently close bound on the globally optimal objective value. Otherwise, a *separation algorithm*, which is formulated as an SDP, computes a linear constraint that removes that iteration’s solution from the feasible space of the SOCP relaxation. To maintain computational tractability, the algorithm in [255, 256] solves a set of small SDP problems, each associated with a cycle in a cycle basis for the power system network [77]. Reference [299] provides a detailed explanation of this algorithm and proposes a related approach that uses a least-squares formulation.

Strong SOCP Relaxation

The “Strong SOCP” relaxation proposed in [255] and further advanced in [256] augments Jabr’s SOCP relaxation (4.41a)–(4.41d), (4.42) with valid constraints formed using conditions on matrix minors, constructing arctangent envelopes, and deriving cuts from the Shor relaxation as described above. This section reviews the matrix minor constraints and arctangent envelopes. See §4.4.1 for an overview of the iterative bound tightening technique that is also used to strengthen the Strong SOCP relaxation.

Matrix Minor Constraints Reference [256] develops valid constraints based on 2×2 minors (i.e., determinants of 2×2 submatrices) of the matrix \mathbf{Z} in (4.7d). The approach in [256] classifies the 2×2 minors into three categories:

$$\begin{vmatrix} \mathbf{Z}_{ii} & \mathbf{Z}_{ij} \\ \mathbf{Z}_{ji} & \mathbf{Z}_{jj} \end{vmatrix} = 0, \quad (\text{Edge Minor}), \quad (4.60\text{a})$$

$$\begin{vmatrix} \mathbf{Z}_{ii} & \mathbf{Z}_{ij} \\ \mathbf{Z}_{ki} & \mathbf{Z}_{kj} \end{vmatrix} = 0, \quad (\text{Three-Cycle Minor}), \quad (4.60\text{b})$$

$$\begin{vmatrix} \mathbf{Z}_{ij} & \mathbf{Z}_{ik} \\ \mathbf{Z}_{lj} & \mathbf{Z}_{lk} \end{vmatrix} = 0, \quad (\text{Four-Cycle Minor}), \quad (4.60\text{c})$$

where $|\cdot|$ denotes the determinant of a matrix argument. Figure 4.9 shows examples for each category of minor.

$\begin{bmatrix} \mathbf{Z}_{11} & \mathbf{Z}_{12} & \boxed{\mathbf{Z}_{13}} & \mathbf{Z}_{14} \\ \mathbf{Z}_{21} & \mathbf{Z}_{22} & \mathbf{Z}_{23} & \mathbf{Z}_{24} \\ \boxed{\mathbf{Z}_{31}} & \mathbf{Z}_{32} & \boxed{\mathbf{Z}_{33}} & \mathbf{Z}_{34} \\ \mathbf{Z}_{41} & \mathbf{Z}_{42} & \mathbf{Z}_{43} & \mathbf{Z}_{44} \end{bmatrix}$	$\begin{bmatrix} \mathbf{Z}_{11} & \mathbf{Z}_{12} & \boxed{\mathbf{Z}_{13}} & \mathbf{Z}_{14} \\ \boxed{\mathbf{Z}_{21}} & \mathbf{Z}_{22} & \boxed{\mathbf{Z}_{23}} & \mathbf{Z}_{24} \\ \mathbf{Z}_{31} & \mathbf{Z}_{32} & \mathbf{Z}_{33} & \mathbf{Z}_{34} \\ \mathbf{Z}_{41} & \mathbf{Z}_{42} & \mathbf{Z}_{43} & \mathbf{Z}_{44} \end{bmatrix}$	$\begin{bmatrix} \mathbf{Z}_{11} & \boxed{\mathbf{Z}_{12}} & \mathbf{Z}_{13} & \boxed{\mathbf{Z}_{14}} \\ \mathbf{Z}_{21} & \mathbf{Z}_{22} & \mathbf{Z}_{23} & \mathbf{Z}_{24} \\ \mathbf{Z}_{31} & \boxed{\mathbf{Z}_{32}} & \mathbf{Z}_{33} & \boxed{\mathbf{Z}_{34}} \\ \mathbf{Z}_{41} & \mathbf{Z}_{42} & \mathbf{Z}_{43} & \mathbf{Z}_{44} \end{bmatrix}$
(a) An edge minor	(b) A three-cycle minor	(c) A four-cycle minor

Figure 4.9: Example 2×2 submatrices for the matrix minors (i.e., the determinants of the submatrices) defined in [256] for the matrix \mathbf{Z} in (4.7d). The condition $\text{rank}(\mathbf{Z}) = 1$ implies that the minors are equal to zero. Convex envelopes based on certain choices of each type of minor are used in [256] to tighten Jabr’s SOCP relaxation.

Each category of minors has a corresponding set of valid constraints. The edge minors in (4.60a) are closely related to Jabr’s relaxation in §4.2.1, i.e., relaxing the non-convex set of constraints $\mathbf{Z}_{ii}\mathbf{Z}_{kk} = |\mathbf{Z}_{ik}|^2$, $\mathbf{Z}_{ii} \geq 0$, $\mathbf{Z}_{kk} \geq 0$ to the rotated SOCP constraints $\mathbf{Z}_{ii}\mathbf{Z}_{kk} \geq |\mathbf{Z}_{ik}|^2$, $\mathbf{Z}_{ii} \geq 0$, $\mathbf{Z}_{kk} \geq 0$. The approach in [256] additionally enforces outer polyhedral envelopes of the convex hull of the non-convex constraints $\mathbf{Z}_{ii}\mathbf{Z}_{kk} \leq |\mathbf{Z}_{ik}|^2$. These outer envelopes each consist of four linear inequalities. Using McCormick relaxations, similar approaches are applied to develop convex envelopes for the three-cycle and four-cycle minors in (4.60b) and (4.60c), respectively. The full mathematical descriptions of these envelopes are provided in [256].

Note that the matrix minor constraints in [256] can be interpreted in terms of the “cycle constraints” derived in [255]. Moreover, the Complex Valued Inequalities previously proposed in [300], which are discussed later in this section, are also derived based on similar matrix minor constraints. Finally, note that since formulating convex envelopes for all possible minors quickly becomes intractable with increasing system size, [256] uses a subset of the minors determined using a cycle decomposition approach and [300] proposes a spatial branch-and-cut algorithm that iteratively strengthens a relaxation by adding related constraints.

Arctangent Envelopes The trigonometric relationships underlying the definitions of the variables c_{ik} and s_{ik} in Jabr’s relaxation can be

expressed in terms of the arctangent function: $\theta_{ki} = \arctan\left(\frac{s_{ik}}{c_{ik}}\right)$, where $\theta_{ki} = \theta_k - \theta_i$.¹⁹ In order to enforce a relaxed version of this relationship, the Strong SOCP relaxation employs convex envelopes that enclose the arctangent functions. Consider the non-convex sets

$$\left\{ (c_{ik}, s_{ik}, \theta_{ki}) \mid \theta_{ki} = \arctan\left(\frac{s_{ik}}{c_{ik}}\right), c_{ik}^{\min} \leq c_{ik} \leq c_{ik}^{\max}, s_{ik}^{\min} \leq s_{ik} \leq s_{ik}^{\max}, \theta_{ki}^{\min} \leq \theta_{ki} \leq \theta_{ki}^{\max} \right\}, \quad \forall (i, k) \in \mathcal{L}. \quad (4.61)$$

For each line $(i, k) \in \mathcal{L}$, the arctangent envelopes construct a convex enclosure of (4.61) consisting of two linear inequalities that upper bound (4.61) and two linear inequalities that lower bound (4.61). Arctangent envelopes were first proposed in [255] and later improved in [256]. Also note that a related formulation proposed in [301] uses piecewise representations of similar arctangent envelopes within an iterative “outer approximation” algorithm. The following discussion considers the version of the arctangent envelopes presented in [256].

The arctangent envelopes use the following definitions. Define four points z_{ik}^1 , z_{ik}^2 , z_{ik}^3 , and z_{ik}^4 in the space $(c_{ik}, s_{ik}, \theta_{ki})$ as the corners of the box containing the arctangent function over the constraints $c_{ik}^{\min} \leq c_{ik} \leq c_{ik}^{\max}$ (where $c_{ik}^{\min} > 0$) and $s_{ik}^{\min} \leq s_{ik} \leq s_{ik}^{\max}$:

$$z_{ik}^1 = \left(c_{ik}^{\min}, s_{ik}^{\max}, \arctan\left(s_{ik}^{\max}/c_{ik}^{\min}\right) \right), \quad (4.62a)$$

$$z_{ik}^2 = \left(c_{ik}^{\max}, s_{ik}^{\max}, \arctan\left(s_{ik}^{\max}/c_{ik}^{\max}\right) \right), \quad (4.62b)$$

$$z_{ik}^3 = \left(c_{ik}^{\max}, s_{ik}^{\min}, \arctan\left(s_{ik}^{\min}/c_{ik}^{\max}\right) \right), \quad (4.62c)$$

$$z_{ik}^4 = \left(c_{ik}^{\min}, s_{ik}^{\min}, \arctan\left(s_{ik}^{\min}/c_{ik}^{\min}\right) \right). \quad (4.62d)$$

Define two planes in the space $(c_{ik}, s_{ik}, \theta_{ki})$. The first, denoted $\theta_{ki} = \gamma_{ik}^{(1)} + \alpha_{ik}^{(1)} c_{ik} + \beta_{ik}^{(1)} s_{ik}$, passes through the points $\{z_{ik}^1, z_{ik}^2, z_{ik}^3\}$ and the second, denoted $\theta_{ki} = \gamma_{ik}^{(2)} + \alpha_{ik}^{(2)} c_{ik} + \beta_{ik}^{(2)} s_{ik}$, passes through the

¹⁹Note that [255] and [256] use a definition for θ_{ik} that is the negative of the definition used in other papers. Matching the definition $\theta_{ik} = \theta_i - \theta_k$ used throughout the remainder of this monograph results in the use of θ_{ki} for the arctangent envelopes discussed in this section.

4.4. Techniques for Tightening Relaxations

101

points $\{z_{ik}^1, z_{ik}^3, z_{ik}^4\}$. For $m = 1, 2$, define $\Delta\gamma_{ik}^{(m)}$ as the globally optimal objective value of the following optimization problem:

$$\begin{aligned}\Delta\gamma_{ik}^{(m)} &= \max_{c_{ik}, s_{ik}} \arctan\left(\frac{s_{ik}}{c_{ik}}\right) - \left(\gamma_{ik}^{(m)} + \alpha_{ik}^{(m)} c_{ik} + \beta_{ik}^{(m)} s_{ik}\right) \\ \text{subject to } c_{ik}^{\min} &\leq c_{ik} \leq c_{ik}^{\max}, \quad s_{ik}^{\min} \leq s_{ik} \leq s_{ik}^{\max}, \\ c_{ik} \tan\left(\theta_{ki}^{\min}\right) &\leq s_{ik} \leq c_{ik} \tan(\theta_{ki}^{\max}).\end{aligned}\quad (4.63)$$

Although (4.63) is non-convex, its global solution can be computed analytically by enumerating all possible KKT points and selecting the maximum. As shown in [256, Appendix A], enumerating all KKT points of (4.63) is accomplished by solving four one-dimensional optimization problems. These one-dimensional optimization problems have explicit expressions for their solutions. Finally, define $\hat{\gamma}_{ik}^{(m)} = \gamma_{ik}^{(m)} + \Delta\gamma_{ik}^{(m)}$ for $m = 1, 2$. Using these definitions, the upper bounding inequalities are

$$\hat{\gamma}_{ik}^{(m)} + \alpha_{ik}^{(m)} c_{ik} + \beta_{ik}^{(m)} s_{ik} \geq \theta_{ki}, \quad m = 1, 2. \quad (4.64)$$

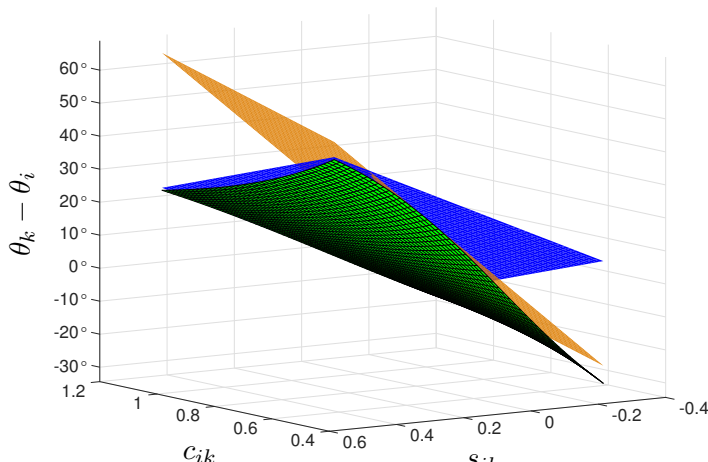
Lower bounding inequalities are defined similarly. Let $\theta_{ki} = \gamma_{ik}^{(3)} + \alpha_{ik}^{(3)} c_{ik} + \beta_{ik}^{(3)} s_{ik}$ and $\theta_{ki} = \gamma_{ik}^{(4)} + \alpha_{ik}^{(4)} c_{ik} + \beta_{ik}^{(4)} s_{ik}$ denote the planes passing through the points $\{z_{ik}^1, z_{ik}^2, z_{ik}^4\}$ and $\{z_{ik}^2, z_{ik}^3, z_{ik}^4\}$, respectively. For $m = 3, 4$, define $\Delta\gamma_{ik}^{(m)}$ as the global solution to (4.63), with the maximization instead changed to minimization. Let $\hat{\gamma}_{ik}^{(m)} = \gamma_{ik}^{(m)} - \Delta\gamma_{ik}^{(m)}$ for $m = 3, 4$. The lower bounding inequalities are

$$\hat{\gamma}_{ik}^{(m)} + \alpha_{ik}^{(m)} c_{ik} + \beta_{ik}^{(m)} s_{ik} \leq \theta_{ki}, \quad m = 3, 4. \quad (4.65)$$

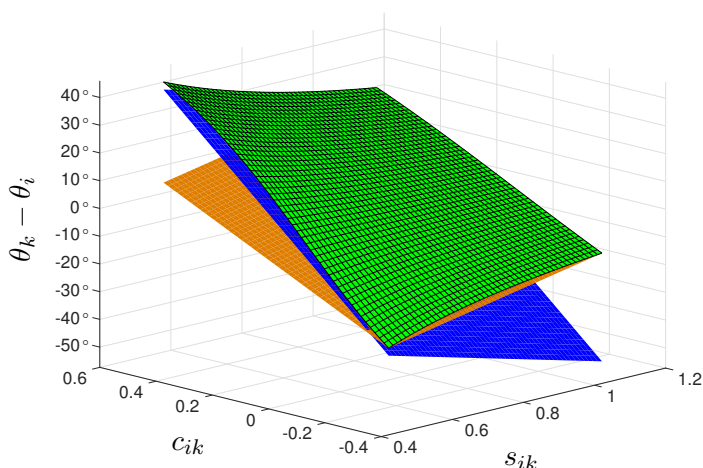
Figures 4.10a and 4.10b show an example of the upper and lower envelopes from (4.64) and (4.65), respectively.

Lifted Non-Linear Cuts / Complex Valued Inequalities

Two independent research efforts described in [176, 254] and [300] discovered a set of valid inequalities that are implied by phase angle difference constraints (i.e., $\theta_{ik}^{\min} \leq \theta_i - \theta_k \leq \theta_{ik}^{\max}, \forall (i, k) \in \mathcal{L}$, where $-\frac{\pi}{2} \leq \theta_{ik}^{\min} \leq \theta_{ik}^{\max} \leq \frac{\pi}{2}$) and the voltage magnitude limits (i.e., $V_i^{\min} \leq V_i \leq V_i^{\max}, \forall i \in \mathcal{N}$). These valid inequalities are termed



(a) Upper Envelope



(b) Lower Envelope

Figure 4.10: Illustrative examples of arctangent envelopes. The upper and lower envelopes from (4.64) and (4.65), respectively, are depicted using the blue and orange planes. The green surface is the arctangent function, $\theta_k - \theta_i = \arctan\left(\frac{s_{ik}}{c_{ik}}\right)$.

“Lifted Non-Linear Cuts” in [176, 254] and “Complex Valued Inequalities” in [300]. Consider the formulation in [176, 254], which uses the following definitions:

$$V_i^\sigma = V_i^{\min} + V_i^{\max}, \quad \forall i \in \mathcal{N}, \quad (4.66a)$$

$$\phi_{ik} = (\theta_{ik}^{\max} + \theta_{ik}^{\min}) / 2, \quad \forall (i, k) \in \mathcal{L}, \quad (4.66b)$$

$$\delta_{ik} = (\theta_{ik}^{\max} - \theta_{ik}^{\min}) / 2, \quad \forall (i, k) \in \mathcal{L}. \quad (4.66c)$$

The Lifted Non-Linear Cuts proposed in [176, 254] are

$$\begin{aligned} & V_i^\sigma V_k^\sigma (c_{ik} \cos(\phi_{ik}) + s_{ik} \sin(\phi_{ik})) - V_k^{\max} \cos(\delta_{ik}) V_k^\sigma c_{ii} \\ & - V_i^{\max} \cos(\delta_{ik}) V_i^\sigma c_{kk} \\ & \geq V_i^{\max} V_k^{\max} \cos(\delta_{ik}) (V_i^{\min} V_k^{\min} - V_i^{\max} V_k^{\max}), \end{aligned} \quad (4.67a)$$

$$\begin{aligned} & V_i^\sigma V_k^\sigma (c_{ik} \cos(\phi_{ik}) + s_{ik} \sin(\phi_{ik})) - V_k^{\min} \cos(\delta_{ik}) V_k^\sigma c_{ii} \\ & - V_i^{\min} \cos(\delta_{ik}) V_i^\sigma c_{kk} \\ & \geq -V_i^{\min} V_k^{\min} \cos(\delta_{ik}) (V_i^{\min} V_k^{\min} - V_i^{\max} V_k^{\max}). \end{aligned} \quad (4.67b)$$

Note that (4.67) is linear in the space of variables c_{ik} , s_{ik} , c_{ii} , and c_{kk} . A visualization of these constraints is provided in [302]. Using a different mathematical formulation resulting from an alternative parameterization of the variable bounds, the approach in [300] yields constraints that are equivalent to (4.67) [254]. Note that (4.67) generalizes other valid inequalities proposed in [98] and [171].

Second-Order Cone Surface Constraints

Many power flow formulations relax the equality constraint $c_{ik}^2 + s_{ik}^2 = c_{ii} c_{kk}$, $\forall (i, k) \in \mathcal{L}$, in (4.41e), to the inequality constraint $c_{ik}^2 + s_{ik}^2 \leq c_{ii} c_{kk}$ in (4.42), as proposed by Jabr [194]. The equality constraint has a geometric interpretation as a restriction of the c_{ik} and s_{ik} variables to the non-convex space represented by the surface of a second-order cone. The inequality constraint allows the c_{ik} and s_{ik} variables to be within the convex region formed by the union of the surface and the interior of the second-order cone. To better represent the equality constraint, [301] proposes a “surface constraint” formulation that introduces new variables \hat{l} and \hat{r} corresponding to the left- and right-hand sides, respectively,

of (4.41e) (i.e., \hat{l} represents $c_{ik}^2 + s_{ik}^2$ and \hat{r} represents $c_{ii} c_{kk}$). The surface constraint formulation proposed in [301] equates these variables and adds additional constraints derived using McCormick envelopes:

$$\hat{l} = \hat{r}, \quad (4.68a)$$

$$\hat{l} \leq \left(c_{ik}^{\min} + c_{ik}^{\max} \right) c_{ik} + \left(s_{ik}^{\min} + s_{ik}^{\max} \right) s_{ik} - c_{ik}^{\min} c_{ik}^{\max} - s_{ik}^{\min} s_{ik}^{\max}, \quad (4.68b)$$

$$\hat{r} \geq c_{kk}^{\max} c_{ii} + c_{ii}^{\max} c_{kk} - c_{ii}^{\max} c_{kk}^{\max}, \quad (4.68c)$$

$$\hat{r} \geq c_{kk}^{\min} c_{ii} + c_{ii}^{\min} c_{kk} - c_{ii}^{\min} c_{kk}^{\min}, \quad (4.68d)$$

where c_{ii}^{\min} , c_{ik}^{\min} , s_{ik}^{\min} , and c_{ii}^{\max} , c_{ik}^{\max} , s_{ik}^{\max} are lower and upper bounds, respectively, on the corresponding quantities. Reference [301] uses piecewise variants of these surface constraints within an iterative “outer approximation” algorithm that constructs successively tighter mixed-integer SOCP relaxations of optimal power flow problems.

Voltage Magnitude Difference Constraints

The bound tightening techniques discussed in §4.4.1 are typically applied to tighten the voltage magnitudes at each bus and the voltage angle differences between connected buses. For many problems, including typical OPF problems, the voltage magnitudes cannot be significantly tightened beyond the bounds specified by the test case. In contrast, limited reactive power injection capabilities often effectively constrain the voltage magnitude *differences* between connected buses to significantly more narrow ranges. Bounds on the voltage magnitude differences can be computed using bound tightening techniques that maximize and minimize the differences in voltage magnitudes. Figure 4.11 illustrates the effectiveness of applying bound tightening techniques to the voltage magnitude differences using the feasible space for a six-bus test system.

Reference [263] proposes a variety of constraints that exploit the potential availability of tight bounds on voltage magnitude differences. Define the voltage magnitude differences as $V_{ik}^{\Delta} = |V_i| - |V_k|$. Rewriting the voltage magnitude products $V_i V_k$ using V_{ik}^{Δ} yields

$$V_i V_k = \left(V_i^2 + V_k^2 - (V_{ik}^{\Delta})^2 \right) / 2, \quad \forall (i, k) \in \mathcal{L}. \quad (4.69)$$

4.4. Techniques for Tightening Relaxations

105

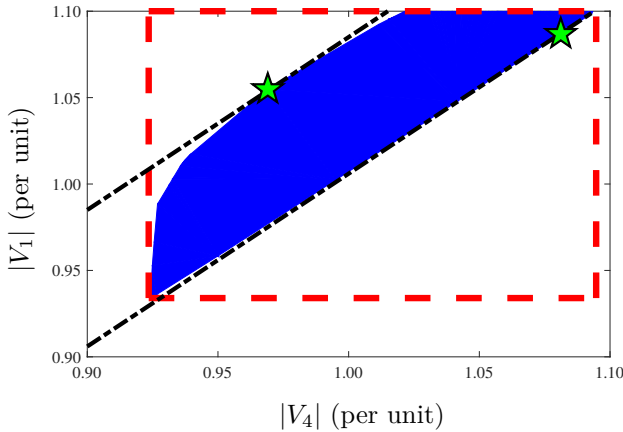


Figure 4.11: Bound tightening illustration for the “case6_c” test system from [178] showing a projection in terms of the voltage magnitudes $|V_1|$ and $|V_4|$. The blue region corresponds to the problem’s feasible space. The dashed red line indicates the best achievable tightening of the voltage magnitudes $|V_1|$ and $|V_4|$. The dot-dashed black lines correspond to $|V_1| - |V_4|$ and the largest and smallest achievable values of this difference occur at the green stars. The improvements in the bounds on $|V_1|$ and $|V_4|$ (reductions of 15.4% and 17.4%, respectively) are modest compared to the improvement in the bounds on the voltage magnitude difference $|V_1| - |V_4|$ of 77.5%.

Relaxing the left-hand side of (4.69) using a McCormick envelope (3.2), $\langle V_i V_k \rangle^M$, and the squared envelopes $\langle V_i^2 \rangle^T$ and $\langle V_k^2 \rangle^T$ defined in (4.44a) for all $(i, k) \in \mathcal{L}$ gives

$$w_{ik} = (c_{ii} + c_{kk} - U_{ik}) / 2, \quad (4.70a)$$

$$w_{ik} \in \langle V_i V_k \rangle^M, \quad (4.70b)$$

$$c_{ii} \in \langle V_i^2 \rangle^T, \quad c_{kk} \in \langle V_k^2 \rangle^T, \quad (4.70c)$$

$$U_{ik} \in \left\langle \left(V_{ik}^\Delta \right)^2 \right\rangle^T. \quad (4.70d)$$

Note that U_{ik} is a lifted variable representing the squared voltage magnitude differences, $(|V_i| - |V_k|)^2$.

A valid inequality is also formed by expanding $(V_i - V_k)^2$:

$$\left(V_{ik}^\Delta \right)^2 \leq V_i^2 - 2 V_i V_k + V_k^2. \quad (4.71)$$

Relaxing the right-hand side of (4.71) by applying McCormick (3.2) and squared (4.44a) envelopes yields the following SOCP constraint:

$$\left(V_{ik}^{\Delta} \right)^2 \leq c_{ii} - 2w_{ik} + c_{kk}. \quad (4.72)$$

Another constraint is constructed using McCormick envelopes (3.2) to relax the relationship $|V_i|^2 - |V_k|^2 = V_{ik}^{\Delta} (|V_i| + |V_k|)$, $\forall (i, k) \in \mathcal{L}$:

$$c_{ii} - c_{kk} = \hat{U}_{ik,i} + \hat{U}_{ik,k}, \quad (4.73a)$$

$$\hat{U}_{ik,i} \in \left\langle V_{ik}^{\Delta} \ V_i \right\rangle^M, \quad (4.73b)$$

$$\hat{U}_{ik,k} \in \left\langle V_{ik}^{\Delta} \ V_k \right\rangle^M. \quad (4.73c)$$

Note that $\hat{U}_{ik,i}$ is a lifted variable representing $(|V_i| - |V_k|) |V_i|$.

Finally, the approach in [263] also enforces constraints derived from the Taylor–Hoover relaxation [288] discussed in §4.3.3. Specifically, (4.58a) is relaxed using McCormick envelopes to obtain one additional constraint per line $(i, k) \in \mathcal{L}$:

$$c_{ii} - c_{kk} = \left(\frac{g_{ik} (P_{ik} - P_{ki}) - b_{ik} (Q_{ik} - Q_{ki})}{g_{ik}^2 + b_{ik}^2 + b_{ik} \frac{b_{c,ik}}{2}} \right). \quad (4.74)$$

In summary, the set of voltage difference constraints proposed in [263] consists of (4.70), (4.72)–(4.74). Note that initial bounds on V_{ik}^{Δ} can be computed as $V_i^{min} - V_k^{max} \leq V_{ik}^{\Delta} \leq V_i^{max} - V_k^{min}$. Bounds on the other added variables (U_{ik} , $\hat{U}_{ik,i}$, and $\hat{U}_{ik,k}$) are computed via straightforward manipulations of the bounds on the voltage magnitudes and voltage magnitude differences.

4.4.3 Spatial Branch-and-Bound Algorithms

Spatial branch-and-bound is a commonly used algorithm for addressing non-convex optimization problems. This iterative algorithm splits the feasible space into (typically disjoint) subsets. Consider a minimization problem. A local optimization algorithm or a heuristic is used to find a feasible point in each subset. These feasible points provide upper bounds on the objective values within each subset, and a relaxation is applied to obtain lower bounds in each subset. A subset is eliminated

from further consideration if it has a corresponding lower bound that is greater than the least upper bound among all subsets. (In other words, a subset cannot contain the global minimum if all feasible points within the subset have objective values that are greater than a feasible point in a different subset.) If an upper bound is sufficiently close to the least lower bound among all subsets (i.e., the *optimality gap* is sufficiently small), then the algorithm terminates. Otherwise, one of the subsets of the feasible space is split into more subsets (which is referred to as “branching”), and the algorithm continues. Closely related “spatial branch-and-cut” algorithms additionally generate and enforce valid constraints at various points throughout a branch-and-bound algorithm to tighten the relaxations.

The computational tractability of a spatial branch-and-bound algorithm depends on the specifics of how the subsets are constructed (i.e., the branching step). A good branching algorithm will quickly eliminate large regions of the feasible space from consideration. The speed and quality of the upper and lower bounding algorithms are also key to obtaining a computationally tractable spatial branch-and-bound algorithm. Applications of spatial branch-and-bound and spatial branch-and-cut algorithms to power system optimization problems include:

- Reference [303], which branches on either the active and reactive power injections or the voltage magnitudes and uses the Shor relaxation to obtain lower bounds.
- Reference [304], which branches on the active and reactive power injections (using either a rectangular or ellipsoidal bisection scheme) with the Lagrangian dual of the OPF problem used to compute lower bounds. Further related work in [305] applies decomposition approaches based on Bender’s Cut and Alternating Direction Method of Multipliers (ADMM) algorithms to speed convergence.
- Reference [181], which iteratively generates cuts relevant to the branch flow relaxations of optimization problems with balanced single-phase equivalent radial network models. The cuts in [181]

are based on the difference between the active power losses computed by $\sum_{(i,k) \in \mathcal{L}} R_{ik} \ell_{ik}$ and by $\sum_{(i,k) \in \mathcal{L}} R_{ik} \left(\frac{P_{ik}^2 + Q_{ik}^2}{|V_i|^2} \right)$ in the DistFlow equations (2.7). Reference [182] proposes related cuts that extend the applicability of this approach.

- Reference [171], which uses the McCormick relaxation techniques in the software BARON [306] augmented with certain valid constraints. The valid constraints in [171] are based on the intersection of the bounds on the variables c_{ik} and s_{ik} (see the definitions in §4.2.1) with the constraint $V_i^{min} V_k^{min} \leq c_{ik}^2 + s_{ik}^2 \leq V_i^{max} V_k^{max}$ implied by the voltage magnitude limits. Note that these valid constraints are dominated by the Lifted Non-Linear Cuts / Complex Valued Inequalities proposed in [176, 254, 300] (see §4.4.2).
- Reference [300], which proposes several branching strategies based on the violation of a determinant condition related to certain 2×2 submatrices.
- Reference [289], which branches on the voltage components V_d and V_q for the power flow equations in rectangular coordinates (2.4) using McCormick envelopes to convexify the bilinear terms.
- Reference [256], which branches on the variables c_{ik} or s_{ik} associated with the line $(i, k) \in \mathcal{L}$ that has the largest mismatch between the representation of the voltage angle difference $\theta_k - \theta_i$ defined by the arctangent envelope (see §4.4.2) and $\arctan\left(\frac{s_{ik}}{c_{ik}}\right)$.
- References [264, 307, 308], which apply bound tightening and McCormick relaxation techniques while adaptively partitioning the feasible space into differently sized subsets.
- Reference [301], which augments Jabr's SOCP relaxation discussed in §4.2.1 with piecewise versions of the second-order cone surface constraints and arctangent envelopes discussed in §4.4.2. The approach in [301] uses binary variables to iteratively partition the c_{ik} and s_{ik} variables, yielding a sequence of increasingly tighter mixed-integer SOCP relaxations of OPF problems. Similar techniques are applied to unit commitment problems in [309].

4.4.4 Relaxations Using Alternative Power Flow Representations

The relaxations presented in this monograph are often derived from the power flow equations with the voltages (in various representations) as the decision variables. The power flow equations represented with other choices of decision variables can yield relaxations with diverse characteristics. For instance, the power flow equations can be represented in terms of current injections:

$$P_i + jQ_i = \bar{I}_i \sum_{k=1}^n \mathbf{Z}_{ik} I_k, \quad \forall i \in \mathcal{N}, \quad (4.75)$$

where $I \in \mathbb{C}^n$ is the vector of current injections at each bus and \mathbf{Z} is the bus impedance matrix, which is the inverse of the admittance matrix \mathbf{Y} defined in (2.1) (i.e., $\mathbf{Z} = \mathbf{Y}^{-1}$). Since the bus impedance matrix \mathbf{Z} is generally dense, chordal sparsity cannot be exploited in this coordinate system, which results in the Shor relaxation being computationally inferior to the corresponding formulation based on voltages described in §4.1.1.

As another example, [255, §3.1.6] shows that a semidefinite relaxation of an alternative power flow representation gives weaker bounds than the Shor relaxation. It is also known that certain SOCP relaxations have equivalent tightness but different computational characteristics when derived from the bus injection model of the power flow equations versus the DistFlow equations [74, 168]. Moreover, the QC relaxation described in §4.2.1 relies on typical characteristics specific to the polar coordinate representation of the voltages (2.5) (i.e., small admissible ranges for voltage magnitudes and angle differences).

These results suggest the possibility that other coordinate transformations could yield superior performance for some problems. Related open questions include determining the impact of coordinate transformations on the relaxations and developing methods for selecting the best coordinate transformation for a given problem.

5

Power Flow Approximations

Power flow approximations use a variety of assumptions to simplify the power flow equations. Stronger assumptions typically facilitate the development of simpler formulations that are more computationally tractable. Conversely, more generally applicable assumptions often require more complicated formulations which can be less tractable.

In contrast to a power flow relaxation, an approximation does not provide a bound on the optimal objective value and cannot prove infeasibility (i.e., infeasibility of an approximation guarantees nothing about infeasibility of the original non-convex problem or vice-versa). This is due to the fact that the feasible space of an approximation generally does not enclose the feasible space of the original non-convex problem. Also, unlike relaxations (see §4.4.2), approximations generally cannot be combined with one another, although an approximation could be augmented with constraints from a relaxation.

This section overviews a variety of power flow approximations. The approximations are categorized based on their associated optimization formulation (SOCP or linear constraints). Unless otherwise stated, the approximations discussed in this section apply to the power flow equations for general meshed network topologies.

5.1 Second-Order Cone Programming Approximations of the Power Flow Equations

Most SOCP representations of the power flow equations are relaxations rather than approximations. (See §4.2.) Three exceptions are Jabr's SOCP approximation [72], the QPAC approximation [310], and the Baradar–Hesamzadeh SOCP approximation [311].

5.1.1 Jabr's Approximation

Derivation of Jabr's SOCP approximation [72] begins with the same treatment as his SOCP relaxation in §4.2.1: relaxation of the equality constraint (4.41e) to an inequality (4.42) in formulation (4.41). As noted in §4.2.1, the formulation (4.41) is exact for radial networks but is a relaxation for mesh networks due to the potential for angle inconsistencies around cycles. In other words, the formulation (4.41) does not enforce the non-convex constraint

$$\theta_k - \theta_i = \arctan\left(\frac{s_{ik}}{c_{ik}}\right), \quad \forall (i, k) \in \mathcal{L}, \quad (5.1)$$

where θ_i is the variable denoting the voltage angle at bus $i \in \mathcal{N}$. Note that the angle at the reference bus is equal to zero.

Several previously discussed approaches (i.e., the QC relaxation in §4.2.1 and the arctangent envelopes and cycle constraints in §4.4.2) form convex relaxations of the non-convex constraint (5.1) or other closely related constraints on the angle differences. In contrast, the approach in [72] linearizes (5.1) to form an *approximation* rather than a relaxation. This linearization is

$$\theta_k - \theta_i + \frac{s_{ik}^\bullet c_{ik} - c_{ik}^\bullet s_{ik}}{(s_{ik}^\bullet)^2 + (c_{ik}^\bullet)^2} = \arctan\left(\frac{s_{ik}^\bullet}{c_{ik}^\bullet}\right), \quad \forall (i, k) \in \mathcal{L}, \quad (5.2)$$

where s_{ik}^\bullet and c_{ik}^\bullet indicate assumed values for the variables c_{ik} and s_{ik} .

The formulation (4.41a)–(4.41d), (4.42) is augmented with (5.2) to form an SOCP approximation. Starting from an initialization of $c_{ik}^\bullet = 1$ and $s_{ik}^\bullet = 0$, the approach in [72] iteratively improves the linearization (5.2) through repeated solution of the SOCP approximation to refine c_{ik}^\bullet and s_{ik}^\bullet .

5.1.2 The QPAC Approximation

The “Quadratic Programming AC” (QPAC) approximation [310] is derived using the following simplifications, computed around the nominal values $\theta_i - \theta_k = 0$, $\forall(i, k) \in \mathcal{L}$, and $V_i = 1$, $\forall i \in \mathcal{N}$:

- Second-order Taylor expansions of the sine and cosine functions, i.e., $\cos(\theta_i - \theta_k) \approx 1 - \frac{(\theta_i - \theta_k)^2}{2}$ and $\sin(\theta_i - \theta_k) \approx \theta_i - \theta_k$, $\forall(i, k) \in \mathcal{L}$.
- Tangent line approximations of the squared voltage magnitudes i.e., $|V_i|^2 \approx 2|V_i| - 1$, $\forall i \in \mathcal{N}$.
- Simplifications of the voltage magnitude products to unity, i.e., $|V_i||V_k| \approx 1.0$, $\forall(i, k) \in \mathcal{L}$.
- Relaxations of all quadratic equalities to inequality constraints.

Let U_{ik} and T_{ik} represent the squared differences in the voltage magnitudes and angles between buses i and k , $\forall(i, k) \in \mathcal{L}$, relaxed using the following SOCP constraints:

$$U_{ik} \geq (|V_i| - |V_k|)^2, \quad (5.3a)$$

$$T_{ik} \geq (\theta_i - \theta_k)^2. \quad (5.3b)$$

Applying the above simplifications and definitions to the polar form of the AC power flow equations (2.5) yields the QPAC approximation:

$$P_{ik} = g_{ik} (T_{ik} + U_{ik} + |V_i| - |V_k|) - b_{ik} (\theta_i - \theta_k), \quad (5.4a)$$

$$Q_{ik} = -b_{ik} (T_{ik} + U_{ik} + |V_i| - |V_k|) - g_{ik} (\theta_i - \theta_k), \quad (5.4b)$$

$$\text{Equation (5.3).} \quad (5.4c)$$

The QPAC approximation is applied to OPF and optimal capacitor placement problems in [310]. Results using the IEEE test cases [166] and several of the Polish test cases in MATPOWER [50] empirically demonstrate the QPAC approximation’s superior accuracy while maintaining reasonable computational speed relative to the DC power flow and LPAC approximations discussed in §5.2.3 and §5.2.6, respectively.

5.1.3 The Baradar–Hesamzadeh Approximation

The SOCP approximation proposed in [311], which builds on previous work in [148], is derived from the DistFlow equations (2.7).¹ Similar to the SOCP relaxation of the DistFlow equations in §4.2.2, the equality constraint (2.7d) is relaxed to the inequality constraint (4.49).

The remaining non-convexity is represented as

$$|V_i| |V_k| \sin(\theta_i - \theta_k) = X_{ik} (P_{ik} - R_{ik} \ell_{ik}) - R_{ik} (Q_{ik} - X_{ik} \ell_{ik}), \\ \forall (i, k) \in \mathcal{L}. \quad (5.5)$$

Rather than using a linearization as in Jabr's approximation (5.2), the Baradar–Hesamzadeh approximation uses a small angle approximation $\sin(\theta_i - \theta_k) \approx \theta_i - \theta_k$ and a near-nominal voltage magnitude approximation $|V| \approx 1$. These approximations are only applied to the constraint containing the angles, (5.5). The voltage magnitudes in the remainder of the formulation are free to take non-unity values. Applying these approximations to (5.5) yields

$$\theta_i - \theta_k = X_{ik} (P_{ik} - R_{ik} \ell_{ik}) - R_{ik} (Q_{ik} - X_{ik} \ell_{ik}), \quad \forall (i, k) \in \mathcal{L}. \quad (5.6)$$

The Baradar–Hesamzadeh approximation is (2.7a)–(2.7c), (4.49), and (5.6) enforced for each cycle in a cycle basis of the network [77].

There are several variants of the Baradar–Hesamzadeh approximation. In order to obtain a linear formulation that is well-suited to transmission expansion problems, the approach in [312] modifies the Baradar–Hesamzadeh approximation using a piecewise linearization of the expressions for the squared active and reactive power flows. Other work in [313] uses two techniques to create another variant of the Baradar–Hesamzadeh approximation. Both techniques exploit the following equivalence:

$$x y = \frac{1}{4} \left((x + y)^2 - (x - y)^2 \right), \quad (5.7)$$

¹The formulation presented in [311] uses receiving-end power flows and the line losses as decision variables. To match the formulation of the DistFlow equations (2.7), the Baradar–Hesamzadeh approximation is instead presented here with the sending-end power flows and the squared magnitude of the current flows as decision variables.

where x and y denote generic variables. The first technique in [313] obtains a degree-five polynomial approximation of the function $\sin(\theta_i - \theta_k)$ using a fifth-order Taylor expansion. By iteratively applying (5.7), lifted variables are applied to represent the higher-order terms in this Taylor expansion. These lifted variables are constrained to convex envelopes that are constructed in a manner similar to those used in the QC relaxation discussed in §4.2.1. Let \hat{s}_{ik} denote the lifted variable corresponding to $\sin(\theta_i - \theta_k)$ that results from this technique. The second technique in [313] also recursively applies the equivalence (5.7) to rewrite the trilinear product $|V_i| |V_k| \hat{s}_{ik}$. The squared terms resulting from the application of (5.7) are again represented using lifted variables that are enclosed in convex envelopes. A lifted variable obtained from these techniques is used to replace the term $|V_i| |V_k| \sin(\theta_i - \theta_k)$ in (5.5). The resulting constraint replaces (5.6) in the Baradar–Hesamzadeh approximation.

5.2 Linear Approximations of the Power Flow Equations

The majority of power flow approximations, including those most used in practice, take the form of linear relationships that are implemented as either LPs or quadratic programs, depending on the choice of objective function. Linear approximations leverage the maturity of LP and MILP algorithms (and the corresponding algorithms for QPs) to quickly solve large-scale practical problems. This section reviews a variety of linear approximations of the power flow equations.

5.2.1 Linearization Around a Specified Operating Point

This section first considers linearization of the non-linear power flow equations near a specified operating point. Different linearizations are constructed using various voltage coordinates and different operating point assumptions. This section describes linearizations of the power flow equations using both polar and rectangular coordinates for the voltage phasors and discusses the implicit manifold framework from [314].

Note that other linearizations can be derived from alternative representations of the power flow equations. For instance, [59, 64, 65]

studies a linearization of an “IV” power flow formulation whose decision variables consist of both bus voltage and current injection phasors in rectangular coordinates. Additionally, the approaches in [60, 61] maintain both voltage and current variables in order to exploit linearizations developed using circuit theory. These circuit-theoretic approaches can improve robustness with respect to the initialization of various numerical methods and provide advantages in modeling flexibility. Extensions to unbalanced three-phase systems are presented in [62, 63].

Linearizations using Polar Coordinates

Linearizations using the polar representation (2.5) of the voltage phasors are commonly used since the voltage magnitudes and the angle differences typically vary over small ranges near known nominal values. Linearizing the power flow equations in polar voltage coordinates (2.5) via a first-order Taylor series expansion yields

$$\begin{bmatrix} P \\ Q \end{bmatrix} = \begin{bmatrix} P^\bullet \\ Q^\bullet \end{bmatrix} + \mathbf{J}_p|_{V=|V^\bullet|\angle\theta^\bullet} \left(\begin{bmatrix} \theta \\ |V| \end{bmatrix} - \begin{bmatrix} \theta^\bullet \\ |V^\bullet| \end{bmatrix} \right), \quad (5.8)$$

where $|V|$ and θ denote the vectors of voltage magnitudes and voltage angles and P and Q denote the vectors of active and reactive power injections. The notation $(\cdot)^\bullet$ denotes the value of the corresponding variable at a specified operating point. Let $S = P + jQ$ denote the vector of complex power injections. Using the representation in [97], the $2n \times 2n$ Jacobian matrix \mathbf{J}_p is

$$\mathbf{J}_p = \begin{bmatrix} \text{Re}\left(\frac{\partial S}{\partial \theta}\right) & \text{Re}\left(\frac{\partial S}{\partial |V|}\right) \\ \text{Im}\left(\frac{\partial S}{\partial \theta}\right) & \text{Im}\left(\frac{\partial S}{\partial |V|}\right) \end{bmatrix}, \quad (5.9)$$

with the submatrices defined using

$$\frac{\partial S}{\partial \theta} = j \text{diag}(V) \left(\text{diag}(\bar{\mathbf{Y}} \bar{V}) - \bar{\mathbf{Y}} \text{diag}(\bar{V}) \right), \quad (5.10a)$$

$$\frac{\partial S}{\partial |V|} = \text{diag}(V) \left(\text{diag}(\bar{\mathbf{Y}} \bar{V}) + \bar{\mathbf{Y}} \text{diag}(\bar{V}) \right) \text{diag}(|V|)^{-1}, \quad (5.10b)$$

where V is the vector of voltage phasors, $\text{diag}(\cdot)$ denotes the diagonal matrix with the vector argument on the diagonal, and $(\bar{\cdot})$ is the complex conjugate applied componentwise.

While a linearization can be formulated for any operating point $|V^\bullet| \angle \theta^\bullet$ in (5.9), specific choices of operating points yield particularly well-studied power flow approximations. One commonly chosen operating point is a “flat” voltage profile, i.e., $V_i = 1\angle 0^\circ, \forall i \in \mathcal{N}$. Reference [314] shows that choosing a flat voltage profile and neglecting all shunt admittances² yields the so-called “Linear Coupled Power Flow” approximation presented in [315]. Reference [316] also proposes a similar approach with extensions that consider transformers with non-zero phase shifts and non-unity tap ratios as well as a further simplification based on an approximation that either assumes that all lines have the same resistance-to-reactance ratios or that the network is radial.

A slight extension of the Linear Coupled Power Flow called the “Voltage Difference” approximation in [317–319] additionally considers the possibility of non-unity voltage magnitudes. One can quickly derive the voltage difference approximation beginning with the equations for the active and reactive power flows through the line $(i, k) \in \mathcal{L}$ modeled as a series admittance $g_{ik} + jb_{ik}$:

$$P_{ik} = g_{ik} |V_i| (|V_i| - |V_k| \cos(\theta_i - \theta_k)) - b_{ik} |V_i| |V_k| \sin(\theta_i - \theta_k), \quad (5.11a)$$

$$Q_{ik} = -b_{ik} |V_i| (|V_i| - |V_k| \cos(\theta_i - \theta_k)) - g_{ik} |V_i| |V_k| \sin(\theta_i - \theta_k). \quad (5.11b)$$

Using the small-angle expansions for the trigonometric terms (i.e., $\sin(\theta_i - \theta_k) \approx \theta_i - \theta_k$ and $\cos(\theta_i - \theta_k) \approx 1$) and a uniform voltage profile assumption (i.e., $|V_i| \approx V_0, \forall i \in \mathcal{N}$, where V_0 is a specified scalar constant) yields the voltage difference approximation:

$$P_{ik} = V_0 g_{ik} (|V_i| - |V_k|) - V_0^2 b_{ik} (\theta_i - \theta_k), \quad (5.12a)$$

$$Q_{ik} = -V_0 b_{ik} (|V_i| - |V_k|) - V_0^2 g_{ik} (\theta_i - \theta_k). \quad (5.12b)$$

Note that (5.12) does not model active or reactive power losses (i.e., $P_{ik} + P_{ki} = Q_{ik} + Q_{ki} = 0, \forall (i, k) \in \mathcal{L}$). A related approach in [320, 321] uses a power flow linearization similar to (5.12) augmented with the piecewise-linear loss approximation that is described in §5.2.9.

²Shunt admittances at all buses are negligible and the Π -models of lines have zero shunt susceptances.

Similar to [269], another related approach proposed in [322] uses the “binary expansion” procedure from [293] to approximate products of voltage magnitudes with angle differences and squared angle differences.

Reference [323] describes another linear approximation based on polar voltage coordinates. Similar to the voltage difference approximation (5.12), the approach in [323] uses the small angle approximation $\sin(\theta_i - \theta_k) \approx \theta_i - \theta_k$ and a near-nominal voltage magnitude assumption, $|V_i| \approx 1$ and $|V_k| \approx 1$. In the same way as the QPAC approximation [310] discussed in §5.1.2, the approach in [323] uses a second-order Taylor expansion of the cosine function, $\cos(\theta_i - \theta_k) \approx 1 - \frac{(\theta_i - \theta_k)^2}{2}$, rather than the approximation $\cos(\theta_i - \theta_k) \approx 1$ used in the voltage difference approximation (5.12). This yields the approximation

$$P_{ik} = g_{ik} \left(|V_i|^2 - |V_i| |V_k| \right) - b_{ik} (\theta_i - \theta_k) + \frac{g_{ik}}{2} (\theta_i - \theta_k)^2, \quad (5.13a)$$

$$Q_{ik} = -b_{ik} \left(|V_i|^2 - |V_i| |V_k| \right) - g_{ik} (\theta_i - \theta_k) - \frac{b_{ik}}{2} (\theta_i - \theta_k)^2. \quad (5.13b)$$

Applying the identity $|V_i|^2 - |V_i| |V_k| = \frac{1}{2} \left(|V_i|^2 - |V_k|^2 + (|V_i| - |V_k|)^2 \right)$ to (5.13) yields

$$P_{ik} = \frac{g_{ik}}{2} (|V_i|^2 - |V_k|^2) - b_{ik} (\theta_i - \theta_k) + P_{ik}^L, \quad (5.14a)$$

$$Q_{ik} = -\frac{b_{ik}}{2} (|V_i|^2 - |V_k|^2) - g_{ik} (\theta_i - \theta_k) + Q_{ik}^L, \quad (5.14b)$$

where P_{ik}^L and Q_{ik}^L are terms associated with line losses that are defined as

$$P_{ik}^L = \frac{g_{ik}}{2} \left((\theta_i - \theta_k)^2 + (|V_i| - |V_k|)^2 \right), \quad (5.15a)$$

$$Q_{ik}^L = -\frac{b_{ik}}{2} \left((\theta_i - \theta_k)^2 + (|V_i| - |V_k|)^2 \right). \quad (5.15b)$$

In order to obtain approximations for the active and reactive line flows that are linear in the phase angle differences and squared voltage magnitudes, the approach in [323] replaces P_{ik}^L and Q_{ik}^L in (5.14) with affine functions of the squared voltage magnitudes and angle differences based on a loss factor linearization method. Further details are provided in the appendix of [323]. A related approach using a different loss factor representation is proposed in [324]. The approach in [324] replaces P_{ik}^L

and Q_{ik}^L in (5.14) with convex relaxations or piecewise approximations of the terms \tilde{P}_{ik}^L and \tilde{Q}_{ik}^L , respectively, which are defined as

$$\tilde{P}_{ik}^L = \frac{g_{ik}}{2} \left((\theta_i - \theta_k)^2 + \frac{(|V_i|^2 - |V_k|^2)^2}{4} \right), \quad (5.16a)$$

$$\tilde{Q}_{ik}^L = -\frac{b_{ik}}{2} \left((\theta_i - \theta_k)^2 + \frac{(|V_i|^2 - |V_k|^2)^2}{4} \right). \quad (5.16b)$$

Similar approaches are employed in [325, 326] to develop related iteratively updated power flow approximations.

Other recent work in [327] proposes a linear approximation derived from the power flow representation (2.6) that uses polar coordinates for both the voltage phasors and the admittance matrix, i.e., $V_i = |V_i| \angle \theta_i$ and $\mathbf{Y}_{ik} = |Y_{ik}| \angle \psi_{ik}$. The trigonometric terms in (2.6) are approximated as linear expressions in the angle differences $\theta_i - \theta_k$:

$$\cos(\theta_i - \theta_k + \psi_{ik}) \approx 0.95 (\cos(\psi_{ik}) - \sin(\psi_{ik})(\theta_i - \theta_k)), \quad (5.17a)$$

$$\sin(\theta_i - \theta_k + \psi_{ik}) \approx 0.95 (\sin(\psi_{ik}) + \cos(\psi_{ik})(\theta_i - \theta_k)), \quad (5.17b)$$

where 0.95 is a heuristically determined coefficient. Using (5.17) and assuming that $|V_i| \approx |V_k|$, $(i, k) \in \mathcal{L}$, yields the approximation

$$P_{ik} = 0.95 g_{ik} |V_i|^2 + 0.95 b_{ik} (|V_i|^2 \theta_i - |V_k|^2 \theta_k), \quad (5.18a)$$

$$Q_{ik} = -0.95 b_{ik} |V_i|^2 + 0.95 g_{ik} (|V_i|^2 \theta_i - |V_k|^2 \theta_k). \quad (5.18b)$$

Recent research in [328] linearizes a power flow representation that is based on a logarithmic transformation of the voltage magnitudes, $u_i = \ln |V_i|$, $\forall i \in \mathcal{N}$, similar to the formulations used in [56, 57, 329]. The “Logarithmic Transform Voltage Magnitude” (LTVM) linearization in [328] is

$$P_{ik} = g_{ik} (u_i - u_k) - b_{ik} (\theta_i - \theta_k), \quad (5.19a)$$

$$Q_{ik} = -b_{ik} (u_i - u_k) - g_{ik} (\theta_i - \theta_k), \quad (5.19b)$$

where each line $(i, k) \in \mathcal{L}$ is modeled as a series admittance $g_{ik} + jb_{ik}$. LTVM formulations for more detailed line models and numerical comparisons to other approaches are provided in [328].

References [330] and [331] present analytical and empirical analyses for many of polar coordinate linearizations discussed in this section. Moreover, [331] proposes a linearization framework based on generic nonlinear coordinate transformations that is applicable to many of the aforementioned linearizations in this section. References [330] and [331] also provide:

- Mathematical justifications for certain physical intuitions regarding power flow characteristics.
- Analytical and empirical comparisons of formulations that use $|V_i|^2$ for the independent variables, as in (5.14), to formulations that use $|V_i|$ itself, as in (5.12), and higher powers of $|V_i|$.
- A procedure for adaptively choosing the degree of the independent variables used in the linearization (e.g., selecting k for the expression $|V_i|^k$ included in the linearization) based on historical operational data.

Linearization using Rectangular Coordinates

The linearization of the power flow equations in rectangular coordinates (2.4) is compactly represented using the matrices \mathbf{L}_{Pi} , \mathbf{L}_{Qi} , and \mathbf{M}_i defined for the Shor relaxation in (4.1) and the vector $x = [V_{d1} \dots V_{dn} \ V_{q1} \dots V_{qn}]^\top$:

$$\begin{bmatrix} P \\ Q \\ |V|^2 \end{bmatrix} = \begin{bmatrix} P^\bullet \\ Q^\bullet \\ |V^\bullet|^2 \end{bmatrix} + \mathbf{J}_r|_{x=x^\bullet} (x - x^\bullet), \quad (5.20)$$

where rows $i = 1, \dots, n$ of the $3n \times 2n$ Jacobian matrix \mathbf{J}_r are $(2\mathbf{L}_{Pi} x^\bullet)^\top$, rows $i = n+1, \dots, 2n$ are $(2\mathbf{L}_{Qi} x^\bullet)^\top$, and rows $i = 2n+1, \dots, 3n$ are $(2\mathbf{M}_i x^\bullet)^\top$. The Jacobian matrix \mathbf{J}_r is evaluated at a specified operating point x^\bullet .

As with linearizations developed using the polar coordinate representation of the power flow equations, certain operating points x^\bullet are particularly well-studied. The approaches in [332–334] consider two choices of operating points: a “flat” voltage profile $V_i = 1\angle 0^\circ, \forall i \in \mathcal{N}$,

and the so-called “no-load” voltage profile. Let $\tilde{\mathbf{Y}}$ denote the block of the admittance matrix \mathbf{Y} excluding the row and column corresponding to the reference bus. Let \tilde{y} denote the column of the admittance matrix corresponding to the reference bus, excluding the entry of this column corresponding to the reference bus itself. The no-load voltage profile is defined as the length- $(n - 1)$ vector $\tilde{V}_{nl} = (-\tilde{\mathbf{Y}}^{-1} \tilde{y})$. For systems without PV buses, the no-load voltage profile corresponds to the voltage phasors at the non-reference buses for the case of zero power injections at every non-reference bus.

Define $\tilde{\mathbf{B}}$ as the imaginary part of the admittance matrix, $\text{Im}(\tilde{\mathbf{Y}})$, with the shunt susceptances neglected. By choosing a flat voltage profile, $1\angle 0^\circ$, and neglecting the conductances (i.e., $\text{Re}(\mathbf{Y}) = \mathbf{G} = 0$), [33] derives the following linear approximation for the voltages at the non-reference buses:

$$V = \mathbf{1}_{n-1} - j \tilde{\mathbf{B}}^{-1} P, \quad (5.21)$$

where $\mathbf{1}_{n-1}$ is the $(n - 1)$ -length vector of all ones. Error bounds in [333] characterize the accuracy of the linearization (5.21).

For a network without PV buses and negligible shunt admittances,³ [332–334] uses a linearization around the no-load voltage profile, V_{nl} , to obtain an approximation for the voltage phasors at the non-reference buses. Define $\tilde{\mathbf{Y}}_{nl} = \text{diag}(\tilde{V}_{nl}) \tilde{\mathbf{Y}}$. The approximation is $V = \tilde{V}_{nl} + \Delta V_d + j \Delta V_q$, where ΔV_d and ΔV_q are

$$\Delta V_d = \text{Re}(\tilde{\mathbf{Y}}_{nl}^{-1}) P + \text{Im}(\tilde{\mathbf{Y}}_{nl}^{-1}) Q, \quad (5.22a)$$

$$\Delta V_q = \text{Im}(\tilde{\mathbf{Y}}_{nl}^{-1}) P - \text{Re}(\tilde{\mathbf{Y}}_{nl}^{-1}) Q. \quad (5.22b)$$

By additionally approximating the voltage magnitude differences across each line as much smaller than the nominal voltage magnitudes, [332] and [333] extend (5.22) to represent voltage magnitudes at the non-reference buses:

$$|V| = \tilde{V}_{nl} + \Delta V_d. \quad (5.23)$$

Both [332] and [333] provide error bounds and consider further implications and special cases. Fixed-point arguments are used in

³See footnote 2. A more general formulation that allows non-negligible shunt susceptances is provided in [332, 333].

[332] to develop theory related to power flow solution existence. Note that [333] considers the possibility of constant current load models in extended versions of both (5.21) and (5.22). A related approach in [335, 336] considers unbalanced three-phase network models and develops linear approximations of other quantities (e.g., the magnitudes of line current flows).

Implicit Power Flow Manifold

The linearizations (5.8) and (5.20) explicitly relate the power injections and voltages. A general framework for studying linear approximations that *implicitly* relates the power injections and voltages is presented in [314]. Collect the voltages and power injections in a vector:

$$x = \begin{bmatrix} |V|^T & \theta^T & P^T & Q^T \end{bmatrix}^T, \quad (5.24)$$

and define the *power flow solution manifold* \mathcal{M} :

$$\mathcal{M} = \left\{ x \mid F(x) = \begin{bmatrix} \operatorname{Re} \left(\operatorname{diag}(|V| \angle \theta) \cdot \bar{\mathbf{Y}} \cdot |V| \angle -\theta \right) - P \\ \operatorname{Im} \left(\operatorname{diag}(|V| \angle \theta) \cdot \bar{\mathbf{Y}} \cdot |V| \angle -\theta \right) - Q \end{bmatrix} = 0 \right\}. \quad (5.25)$$

Let $x^* = [|V^*|^T \quad (\theta^*)^T \quad (P^*)^T \quad (Q^*)^T]^T$ denote a point on the power flow solution manifold \mathcal{M} (i.e., $F(x^*) = 0$). Define the $2n \times 4n$ matrix:

$$\mathbf{A}_{x^*} = \begin{bmatrix} \operatorname{Re} \left(\frac{\partial S}{\partial |V|} \right) & \operatorname{Re} \left(\frac{\partial S}{\partial \theta} \right) & -\mathbf{I}_n & \mathbf{0}_n \\ \operatorname{Im} \left(\frac{\partial S}{\partial |V|} \right) & \operatorname{Im} \left(\frac{\partial S}{\partial \theta} \right) & \mathbf{0}_n & -\mathbf{I}_n \end{bmatrix}, \quad (5.26)$$

where \mathbf{I}_n and $\mathbf{0}_n$ are the $n \times n$ identity and all zero matrices, respectively, and the other components of \mathbf{A}_{x^*} are defined in (5.10). The linear manifold that is tangent to the power flow solution manifold \mathcal{M} at x^* is

$$\mathbf{A}_{x^*} (x - x^*) = 0. \quad (5.27)$$

As a measure of the approximation quality, [314] provides a bound on the worst-case error between the linear approximation (5.27) and the actual power flow solution manifold (5.25). Specifically, consider a ball $\mathcal{B}(x^*, \delta)$ of radius δ around a point x^* that satisfies $F(x^*) = 0$. For any point x such that $x \in \mathcal{B}$ and $\mathbf{A}_{x^*} (x - x^*) = 0$, the following bound

is valid:

$$|F_i(x)| \leq \frac{B_i}{2} \|x - x^*\|^2, \quad i = 1, \dots, 2n, \quad (5.28)$$

where $F_i(x)$ is the i^{th} entry of the vector function $F(x)$ defined in (5.25) and the scalar B_i satisfies

$$\left\| \frac{\partial^2 F_i}{\partial x^2} \right\| \leq B_i, \quad \forall x \in \mathcal{B}(x^*, \delta). \quad (5.29)$$

In other words, the maximum error in the active or reactive power balance equations at a point x on the linearization is bounded by the squared distance to the point x^* around which the linearization is constructed, multiplied by a constant which is bounded by the norm of the Hessian matrix $\frac{\partial^2 F_i}{\partial x^2}$. Note that convenient expressions for the terms in the Hessian matrix are available in [97].

Many of the linear approximations in this section can be formulated in the framework of [314] using a linearization about a specified operating point along with various assumptions on the network parameters.

5.2.2 The Decoupled Power Flow Approximation

Decoupled power flow approximations assume that terms in the off-diagonal blocks of the power flow Jacobian matrix in polar voltage coordinates (i.e., $\text{Re}\left(\frac{\partial S}{\partial |V|}\right)$ and $\text{Im}\left(\frac{\partial S}{\partial \theta}\right)$ in (5.9)) are small. This assumption is reasonably accurate for typical transmission systems where the high reactance-to-resistance ratios ($X_{ik}/R_{ik} \gg 1$) result in the P to θ and Q to $|V|$ couplings being much stronger than the Q to θ and P to $|V|$ couplings. Neglecting the off-diagonal blocks in (5.8) yields

$$P = P^\bullet + \left[\text{Re} \left(\frac{\partial S}{\partial \theta} \right) \Big|_{V=|V^\bullet| \angle \theta^\bullet} \right] (\theta - \theta^\bullet), \quad (5.30a)$$

$$Q = Q^\bullet + \left[\text{Im} \left(\frac{\partial S}{\partial |V|} \right) \Big|_{V=|V^\bullet| \angle \theta^\bullet} \right] (|V| - |V^\bullet|). \quad (5.30b)$$

The “Fast Decoupled Load Flow” in [337] is a common variation of the decoupled power flow model which uses the approximations $\cos(\theta_i - \theta_k) \approx 0$, $\mathbf{G}_{ik} \sin(\theta_i - \theta_k) \ll \mathbf{B}_{ik}$, and $Q_i \ll \mathbf{B}_{ii} |V_i|^2$ to define

two matrices denoted by \mathbf{B}' and \mathbf{B}'' . The Fast Decoupled Load Flow comes in two versions: “XB” and “BX” [338]. In the XB version, the matrix \mathbf{B}' is the negative of the imaginary part of the admittance matrix, $-\text{Im}(Y) = -\mathbf{B}$, for a modified network representation that neglects shunt reactances, line charging shunts in the Π -circuit model, off-nominal tap ratios, and line resistances. The matrix \mathbf{B}'' is the negative of the imaginary part of the admittance matrix for a modified network representation that neglects phase-shifting transformers. The BX version has the same construction of the \mathbf{B}' and \mathbf{B}'' matrices with the exception that the line resistances are neglected when constructing \mathbf{B}'' rather than \mathbf{B}' . For both versions, the derivation uses an assumption of near-nominal voltage magnitudes.

The Fast Decoupled Load Flow model is

$$P = P^\bullet + \text{diag}(|V^\bullet|) \mathbf{B}' (\theta - \theta^\bullet), \quad (5.31a)$$

$$Q = Q^\bullet + \text{diag}(|V^\bullet|) \mathbf{B}'' (|V| - |V^\bullet|). \quad (5.31b)$$

For the purpose of solving the power flow equations, the Fast Decoupled Load Flow iteratively updates $|V^\bullet|$ and θ^\bullet . If this process is convergent, it yields the true power flow solution, not an approximation. The matrices \mathbf{B}' and \mathbf{B}'' are constant and therefore only need to be factored once, which endows the Fast Decoupled Load Flow with computational advantages. Each iteration is much faster than a Newton iteration, but more iterations are required. Furthermore, because the (approximate) Jacobian is not updated, often the convergence tolerance cannot be set as tightly as for Newton methods that update the Jacobian at each iteration. References [339] and [340] provide detailed analytical and empirical analyses of the convergence behavior for the Fast Decoupled Load Flow approximation when applied to solve the power flow equations.

5.2.3 The DC Power Flow Approximation

The most widely used power flow approximation is the DC power flow, with applications ranging from long-term planning to the operation of wholesale electricity markets. The derivation of the DC power flow approximation is closely related to a Taylor expansion of the active power flow equation around the voltage profile $V_i = 1.0\angle 0^\circ$, for all

$i \in \mathcal{N}$. Specifically, the DC power flow approximation is derived from the power flow equations in polar voltage coordinates (2.5) by neglecting the line resistances R_{ik} , using the small angle difference approximation $\sin(\theta_i - \theta_k) \approx \theta_i - \theta_k$, assuming near-nominal voltage magnitudes $|V| \approx 1$, and ignoring reactive power.

Denote the line susceptances by $b_{ik} = \frac{1}{X_{ik}}$, $\forall (i, k) \in \mathcal{L}$. Let $\mathbf{A}_{inc} \in \mathbb{R}^{n \times n_l}$ denote the network incidence matrix, where n_l is the number of lines. The matrix \mathbf{A}_{inc} has columns corresponding to the lines, with each column having two non-zero entries: +1 in the i^{th} entry and -1 in the k^{th} entry for line $(i, k) \in \mathcal{L}$. The DC power flow approximation can then be written,

$$P = \mathbf{A}_{inc} \operatorname{diag}(b) \mathbf{A}_{inc}^T \theta, \quad (5.32)$$

where b is the vector of line susceptances b_{ik} in the same order as the columns of \mathbf{A}_{inc} and the reference angle is fixed to zero.⁴

Off-nominal voltage ratios can be handled via modifications to b_{ik} and non-zero phase shifts can be modeled using pairs of injections at the associated terminal buses. For instance, MATPOWER [341] considers a line model connecting buses i and k that is composed of an ideal transformer with a tap ratio of τ_{ik} and a phase shift (in radians) of $\theta_{shift,ik}$ in series with a Π circuit. (See Figure 2.1.) This line model is represented in MATPOWER's DC power flow by modifying the line susceptances to $b_{ik} = \frac{1}{X_{ik} \tau_{ik}}$ and withdrawing/injecting, respectively, a quantity of active power given by $\frac{\theta_{shift,ik}}{X_{ik} \tau_{ik}}$ at buses i and k .

Several studies have attempted error analyses of the DC power flow approximation. Many of these studies are based on empirical analyses [342–354]. Some studies suggest that ascertaining generally applicable conclusions regarding the DC power flow accuracy appears challenging. For instance, [350] states that “At no stage in the tests were we able to discern any statistical patterns in the dc-flow error scatters. This defeated all our attempts to find concise, meaningful indices with which to characterize and display dc-model accuracies.” Other empirical studies had more optimistic conclusions. For instance, [352] found that the DC power flow approximation is reasonably accurate for test systems

⁴The matrix $\mathbf{A}_{inc} \operatorname{diag}(b) \mathbf{A}_{inc}^T$ is the same as the matrix \mathbf{B}' in the XB version of the Fast Decoupled Load Flow (5.31).

in normal operation with typical transmission line parameters when the voltage magnitudes are within $\pm 10\%$ of their nominal values and the voltage angle differences are within $\pm 15^\circ$. Research efforts have also focused on theoretical error analyses [355–357]. In particular, [355] and [357] bound the worst-case error for the DC power flow relative to the AC power flow.

There are many variations of the DC power flow approximation. For instance, one variant uses the susceptance $b_{ik} = -\text{Im}\left(\frac{1}{R_{ik}+jX_{ik}}\right)$ rather than $\frac{1}{X_{ik}}$. Another variant is the “Power Transfer Distribution Factor” (PTDF) model, which relates the active power flows and active power injections using the DC power flow approximation. To derive the PTDF model, the line flows are written as a function of θ as $P_{flow} = \text{diag}(b) \mathbf{A}_{inc}^\top \theta$. Substituting for θ in this expression using (5.32) yields the PTDF formulation:

$$P_{flow} = \underbrace{\text{diag}(b) \mathbf{A}_{inc}^\top (\mathbf{A}_{inc} \text{diag}(b) \mathbf{A}_{inc}^\top)^{-1} P}_{\text{PTDF Matrix}}, \quad (5.33a)$$

$$\sum_{i \in \mathcal{N}} P_i = 0, \quad (5.33b)$$

where the power injection variable associated with the reference bus and the corresponding row of \mathbf{A}_{inc} are removed such that the matrix inverse is well defined. Total power balance is enforced using (5.33b). The PTDF formulation of the DC power flow approximation has computational advantages for problems that only enforce flow limits on a subset of the lines. For such problems, only a limited number of rows in the dense PTDF matrix in (5.33a) are computed. Note that a similar “AC-PTDF” matrix can be developed using a first-order Taylor expansion around a nominal operating point [7].

A review of other DC power flow variants is provided in [350]. Many variants incorporate information from an assumed operating point (so-called “Hot Start” DC models, as opposed to “Cold Start” DC models such as the formulation in (5.32)). Appropriately distributing the losses throughout the network is the goal of many DC power flow variants (see §5.2.9 for further details). Also, [358] discusses related linear approximations of line losses, phase angles, and apparent power flows suitable for incorporation into DC power flow approximations.

Recent work in [359] regarding lossless networks suggests that post-processing the angle differences improves the quality of a DC power flow solution. Specifically, for a solution θ^* to the DC power flow equations (5.32), [359] (and the foundational work in [360]) provides both analytical and empirical arguments that the actual angle differences in the AC model are better represented by the expression $\arcsin(\theta_i^* - \theta_k^*)$ rather than the DC power flow solution, $\theta_i^* - \theta_k^*$. This enables the construction of an “interval-valued” DC approximation that better represents the constraints on maximum angle differences across the lines.

Reference [361] proposes a variant of the approach in [359] that incorporates the effects of losses. Specifically, the approach in [361] uses a nonlinear expression to iteratively update auxiliary variables representing the sines of the angle differences across each line while allowing for non-zero resistances. This approach is particularly advantageous for stressed networks with high resistance-to-reactance ratios. Moreover, for radial networks that satisfy certain conditions, [361] provides theoretical results showing that the iterative approach monotonically converges at an exponential rate to the solution of the active power flow equations.

5.2.4 A Linear Approximation of the Reactive Power Flow Equations

The DC power flow and its modifications do not represent the reactive power equations. Recent work in [362, 363] builds a linear approximation relating reactive power and voltage magnitudes. This section denotes the matrix $\mathbf{B} = \mathbf{A}_{inc} \text{diag}(b) \mathbf{A}_{inc}^\top$, where b is the vector of line susceptances $b_{ik} = -\text{Im}\left(\frac{1}{R_{ik} + jX_{ik}}\right)$.⁵ Using the small angle difference approximation, the reactive power flow equations are formulated as a function of the voltage magnitudes:

$$Q = \text{diag}(|V|) \mathbf{B} |V|. \quad (5.34)$$

The buses are divided into the set of generators and the set of loads denoted with subscripts G and L , respectively. Define \mathbf{B}_{LL} , \mathbf{B}_{LG} , \mathbf{B}_{GL} ,

⁵As discussed in §5.2.3, this definition of the matrix \mathbf{B} is used in a common variant of the DC power flow approximation.

and \mathbf{B}_{GG} as the submatrices of \mathbf{B} with rows and columns associated with the corresponding bus indices. The generator buses have specified voltage magnitudes $|V_G|$ and the loads have specified reactive demands Q_L . Denote \mathcal{G} as the set of generator buses. Define the minimum voltage magnitude among all generator buses as $|V_G^\circ| = \min_{i \in \mathcal{G}} |V_i|$ and generator voltage spread as the vector η_G , where $|V_G| = |V_G^\circ| (\mathbf{1}_{n_G} + \eta_G)$, and n_G denotes the number of generator buses. The linearization in [362, 363] approximates the relationship between the load buses' voltage magnitudes $|V_L|$ and reactive power demands Q_L :

$$\begin{aligned} |V_L| &= |V_G^\circ| \left(\mathbf{1}_{n_L} - \mathbf{B}_{LL}^{-1} \mathbf{B}_{LG} \eta_G \right) \\ &\quad + \frac{1}{|V_G^\circ|} \left(\mathbf{B}_{LL}^{-1} \text{diag} \left(\left(\mathbf{1}_{n_L} - \mathbf{B}_{LL}^{-1} \mathbf{B}_{LG} \eta_G \right)^{-1} \right) Q_L \right), \end{aligned} \quad (5.35)$$

where n_L denotes the number of load buses. Theory developed in [362, 363] provides an upper bound on the maximum approximation error relative to (5.34).

5.2.5 The Linearized DistFlow Approximation

The DistFlow equations (2.7) are an exact representation of the AC power flow equations for radial systems. The SOCP relaxation and approximation approaches in §4.2.2 and §5.1 relax the equality constraint (2.7d) to a convex inequality (4.49). As an alternative approach, the *Linearized DistFlow* approximation⁶ [69] assumes that the active and reactive losses $R_{ik}\ell_{ik}$ and $X_{ik}\ell_{ik}$, respectively, are much smaller than the active and reactive power flows P_{ik} and Q_{ik} . Specifically, the Linearized DistFlow approximation neglects the loss terms associated with the squared current magnitudes ℓ_{ik} in order to obtain

$$P_{ik} = -P_k + \sum_{m:k \rightarrow m} P_{km}, \quad (5.36a)$$

$$Q_{ik} = -Q_k + \sum_{m:k \rightarrow m} Q_{km}, \quad (5.36b)$$

⁶This formulation is also referred to as the *Simplified DistFlow* approximation.

$$|V_k|^2 = |V_i|^2 - 2(R_{ik}P_{ik} + X_{ik}Q_{ik}), \quad (5.36c)$$

for each line $(i, k) \in \mathcal{L}$.

For radial systems where all lines have $R_{ik} \geq 0$ and $X_{ik} \geq 0$, the Linearized DistFlow equations underestimate the complex power required to supply the loads and overestimate the voltage magnitudes [74]. In other words, $P_{ik} \geq P_{ik}^{lin}$, $Q_{ik} \geq Q_{ik}^{lin}$, and $|V_i| \leq |V_i^{lin}|$, where the superscript “*lin*” denotes the solution to (5.36) while the variables without superscripts correspond to the true DistFlow equations (2.7). Generalization of the Linearized DistFlow approximation (5.36) to unbalanced three-phase networks is undertaken in [168, 364, 365].

In related work, the approaches in [366] and [367] formulate other power flow approximations by linearizing the DistFlow equations around a nominal operating point. Reference [366] also applies a piecewise linear approximation of the relationship between the active and reactive power flows, P_{ik} and Q_{ik} , on each line $(i, k) \in \mathcal{L}$ and their squares, P_{ik}^2 and Q_{ik}^2 . While the formulation in [367] solely considers balanced radial networks, the linearization proposed in [366] considers radial distribution systems with both balanced single-phase and unbalanced three-phase network models.

5.2.6 The LPAC Approximation

The approach in [368] presents three versions (hot start, warm start, and cold start) of a so-called “Linear Programming AC” (LPAC) approximation of the power flow equations. All three versions of the LPAC approximation represent line losses, active and reactive power flows, voltage magnitudes, and phase angles. Linear approximations for other relevant functions, such as apparent power line flows, are also provided in [368].

The LPAC approximation uses equally spaced tangential line segments to form a convex envelope of the cosine function as shown in Figure 5.1.⁷ Observe that this envelope is a polyhedral outer enclosure of the convex envelope $\langle \cos(\theta_i - \theta_k) \rangle^C$ used in the QC relaxation (4.44c).

⁷The numerical results in [368] use 20 such segments for the function $\cos(\theta_i - \theta_k)$ over the range $\theta_i - \theta_k \in [-60^\circ, 60^\circ]$.

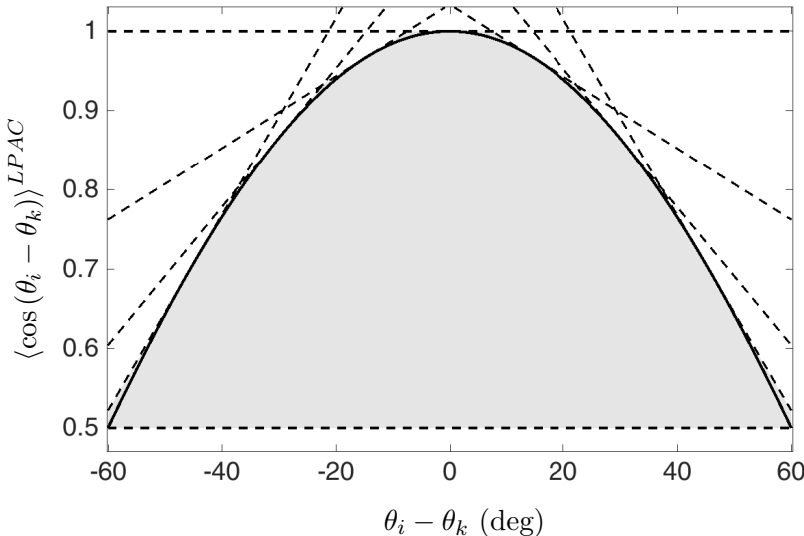


Figure 5.1: Cosine representation in the LPAC approximation. The black line is the cosine function. The dashed lines form the gray envelope, $\langle \cos(\theta_i - \theta_k) \rangle^{LPAC}$, for the function $\cos(\theta_i - \theta_k)$. Observe that this envelope is a polyhedral outer enclosure of the convex envelope $\langle \cos(\theta_i - \theta_k) \rangle^C$ used in the QC relaxation (4.44c). (See Figure 4.6c.)

(See Figure 4.6c.) Denote the variable associated with the convex relaxation of the cosine term for line $(i, k) \in \mathcal{L}$ as $\psi_{ik} \in [0, 1]$, i.e., $\psi_{ik} \in \langle \cos(\theta_i - \theta_k) \rangle^{LPAC}$, where $\langle \cos(\theta_i - \theta_k) \rangle^{LPAC}$ denotes the convex set associated with $\cos(\theta_i - \theta_k)$ shown in Figure 5.1. The objective function of the optimization problem has a term which maximizes ψ_{ik} to improve the quality of the cosine relaxation. The small angle approximation $\sin(\theta_i - \theta_k) \approx \theta_i - \theta_k$ is used for the sine function.

In the hot start version of the LPAC approximation, the voltage magnitudes $|V_i|$, $\forall i \in \mathcal{N}$, are assumed to take known values denoted $|V_i^h|$. Consider the line $(i, k) \in \mathcal{L}$ with admittance $g_{ik} + jb_{ik}$. The hot start LPAC approximation models active and reactive flows P_{ik} and Q_{ik} as

$$P_{ik} = \left| V_i^h \right|^2 g_{ik} - \left| V_i^h \right| \left| V_k^h \right| (g_{ik} \psi_{ik} + b_{ik} (\theta_i - \theta_k)), \quad (5.37a)$$

$$Q_{ik} = - \left| V_i^h \right|^2 b_{ik} - \left| V_i^h \right| \left| V_k^h \right| (g_{ik} (\theta_i - \theta_k) - b_{ik} \psi_{ik}), \quad (5.37b)$$

$$\psi_{ik} \in \langle \cos(\theta_i - \theta_k) \rangle^{LPAC}. \quad (5.37c)$$

The warm start version of the LPAC approximation assumes target values for the voltage magnitudes, $|V_i^t|$, $\forall i \in \mathcal{N}$, such that $|V_i| = |V_i^t| + \phi_i$ where ϕ_i is a scalar decision variable. The active power flow approximation (5.38a) solely uses the target voltage magnitudes $|V_i^t|$, while the reactive power approximation (5.38b) uses $|V_i^t| + \phi_i$:

$$P_{ik} = \left| V_i^t \right|^2 g_{ik} - \left| V_i^t \right| \left| V_k^t \right| (g_{ik} \psi_{ik} + b_{ik} (\theta_i - \theta_k)), \quad (5.38a)$$

$$\begin{aligned} Q_{ik} = & - \left| V_i^t \right|^2 b_{ik} - \left| V_i^t \right| \left| V_k^t \right| (g_{ik} (\theta_i - \theta_k) - b_{ik} \psi_{ik}) \\ & - \left| V_i^t \right| b_{ik} (\phi_i - \phi_k) - b_{ik} \phi_i \left(\left| V_i^t \right| - \left| V_k^t \right| \right), \end{aligned} \quad (5.38b)$$

$$\psi_{ik} \in \langle \cos(\theta_i - \theta_k) \rangle^{LPAC}. \quad (5.38c)$$

The reactive power approximation (5.38b) is derived using a first-order Taylor series expansion about the values $\phi_i = 0$, $\forall i \in \mathcal{N}$, and $\theta_i - \theta_k = 0$, $\forall (i, k) \in \mathcal{L}$.

The cold start version of the LPAC approximation sets the target voltage magnitudes at the load buses to $|V_i^t| = 1$ per unit. Voltage magnitudes at generator buses are fixed to values that are assumed to be known. The cold start version is otherwise identical to the warm start version (5.38).

5.2.7 Current Injection Linearization

The relaxations and approximations discussed thus far focus on the non-linearities in the power flow equations (2.3) or (2.7). In contrast, the approach in [369, 370] exploits the linear relationship between voltages and current injections ($\mathbf{YV} = I$, where $V \in \mathbb{C}^n$ is the vector of voltage phasors and $I \in \mathbb{C}^n$ is the vector of current injections) to locate all the non-linearities in the load models at each bus. Linearization of the bus power injection equations yields the so-called “Current Injection Linearization” in [369, 370].

Following the approach in [370], expanding the expression $\mathbf{Y}V = I$ in rectangular coordinates yields

$$\begin{bmatrix} \mathbf{G} & -\mathbf{B} \\ \mathbf{B} & \mathbf{G} \end{bmatrix} \begin{bmatrix} V_d \\ V_q \end{bmatrix} = \begin{bmatrix} I_d \\ I_q \end{bmatrix}, \quad (5.39)$$

where $\mathbf{Y} = \mathbf{G} + j\mathbf{B}$, $V = V_d + jV_q$, and $I = I_d + jI_q$. The current injections are non-linear functions of the voltages. These functions are dependent on the load model. The approach in [370] considers a “ZIP” load model that consists of constant-impedance, constant-current, and constant-power components at each bus $i \in \mathcal{N}$:

$$P_i = c_i^Z |V_i|^2 + c_i^I |V_i| + c_i^P, \quad (5.40a)$$

$$Q_i = \tilde{c}_i^Z |V_i|^2 + \tilde{c}_i^I |V_i| + \tilde{c}_i^P, \quad (5.40b)$$

where c_i^Z , c_i^I , and c_i^P are the specified coefficients associated with the constant-impedance, constant-current, and constant-power components of the ZIP model, respectively, for active power injections at bus $i \in \mathcal{N}$. Likewise, \tilde{c}_i^Z , \tilde{c}_i^I , and \tilde{c}_i^P are the specified coefficients of the corresponding quantities for reactive power injections at bus $i \in \mathcal{N}$.

Note that generators modeled as PV buses do not fit the form of (5.39) and (5.40) and are therefore not incorporated in the current injection linearization approach proposed in [369, 370]. Incorporating an approximate form for voltage magnitude constraints in the current injection linearization can be accomplished by linearizing the expression $|V_i| = \sqrt{|V_{di}|^2 + |V_{qi}|^2}$.

Expanding (5.40) into real and imaginary parts and using the power injection equation $P_i + jQ_i = (V_{di} + jV_{qi})(I_{di} - jI_{qi})$ yields expressions relating the voltage components and the current injection components:

$$I_{di} = c_i^Z V_{di} + c_i^I f_i^{(3)} + c_i^P f_i^{(1)} + \tilde{c}_i^Z V_{qi} + \tilde{c}_i^I f_i^{(4)} + \tilde{c}_i^P f_i^{(2)}, \quad (5.41a)$$

$$I_{qi} = c_i^Z V_{qi} + c_i^I f_i^{(4)} + c_i^P f_i^{(2)} - \tilde{c}_i^Z V_{di} - \tilde{c}_i^I f_i^{(3)} - \tilde{c}_i^P f_i^{(1)}, \quad (5.41b)$$

where, for all $i \in \mathcal{N}$, the non-linear functions $f_i^{(1)}, \dots, f_i^{(4)}$ are

$$\begin{aligned} f_i^{(1)} &= \frac{V_{di}}{|V_{di}|^2 + |V_{qi}|^2}, & f_i^{(2)} &= \frac{V_{qi}}{|V_{di}|^2 + |V_{qi}|^2}, \\ f_i^{(3)} &= \frac{V_{di}}{\sqrt{|V_{di}|^2 + |V_{qi}|^2}}, & f_i^{(4)} &= \frac{V_{qi}}{\sqrt{|V_{di}|^2 + |V_{qi}|^2}}. \end{aligned} \quad (5.42)$$

Thus, the non-linearities are isolated to the functions in (5.42).

Rather than linearizing the functions in (5.42) at a single point, [370] uses a curve fitting approach to model the non-linearities in a specified region. Specifically, [370] chooses coefficients $\alpha_i^{(k)}$, $\beta_i^{(k)}$, and $\gamma_i^{(k)}$ for each function $k = 1, \dots, 4$ at each bus $i \in \mathcal{N}$ that minimize the least-square error between the linear functions

$$\hat{f}_i^{(k)} = \alpha_i^{(k)} V_{di} + \beta_i^{(k)} V_{qi} + \gamma_i^{(k)}, \quad k = 1, \dots, 4, \forall i \in \mathcal{N}, \quad (5.43)$$

and the non-linear functions $f_i^{(k)}$, $k = 1, \dots, 4$, at an evenly distributed set of points. The current injection linearization is (5.39) with I_d and I_q defined by (5.41) where the functions $f_i^{(1)}, \dots, f_i^{(4)}$ are replaced by the linearizations $\hat{f}_i^{(1)}, \dots, \hat{f}_i^{(4)}$ in (5.43). An alternative approach in [371] represents the functions $f_i^{(1)}, \dots, f_i^{(4)}$ (as well as other nonlinear expressions involved in modeling limits on line flows and voltage magnitudes) using piecewise-linear approximations formulated with binary variables.

Note that the current injection linearization is applicable to unbalanced three-phase network models [370]. Also note that [59, 64] embed a similar “IV” formulation in an iterative linearization framework to locally solve the non-convex OPF problem. Other related circuit-theoretic approaches employed in [60–63] linearize formulations that include both voltage and current variables.

5.2.8 Optimal Adaptive Linearizations

As opposed to many previously described general approximation techniques, the approaches in [372] and [373] develop linearizations that are tailored to a *specific system* and *operating range of interest*. Both of these approaches find linearizations that minimize certain error metrics, but have differences in the metrics themselves as well as the quantities that are approximated. This section describes each of these approaches in turn.

Minimizing Worst-Case Error over a Specified Operating Range

The approach proposed in [372] computes a linearization for a given system that minimizes the worst-case error between the linearization and the AC power flow equations over a specific operating range.

Consider, for instance, a linearization that approximates the active power flows for a certain line $(l, m) \in \mathcal{L}$, P_{lm} , as a function of the active and reactive power injections at every bus:

$$P_{lm} = \ell_0 + \sum_{i \in \mathcal{N}} \ell_{P,i} P_i + \sum_{i \in \mathcal{N}} \ell_{Q,i} Q_i, \quad (5.44)$$

where $\ell_0 \in \mathbb{R}$, $\ell_P \in \mathbb{R}^n$, and $\ell_Q \in \mathbb{R}^n$ are the linearization's coefficients. Observe that the form of this linearization is similar to the Power Transfer Distribution Factor (PTDF) representation discussed in §5.2.3. In fact, the linearizations in [372] can be viewed as generalizations of AC-PTDF representations that consider a range of operating conditions rather than a single point.

Let \mathcal{O} denote a specified operating range that is dictated by bounds on the active and reactive power injections, voltage magnitudes, and angle differences:

$$\begin{aligned} \mathcal{O} = \{(P, Q, |V|, \theta) \mid & \forall i \in \mathcal{N}, P_i^{min} \leq P_i \leq P_i^{max}, \\ & Q_i^{min} \leq Q_i \leq Q_i^{max}, \\ & V_i^{min} \leq |V_i| \leq V_i^{max}, \\ & \forall (l, m) \in \mathcal{L}, \theta_{lm}^{min} \leq \theta_l - \theta_m \leq \theta_{lm}^{max}, \\ & \text{Power flow equations (2.5)}\}. \end{aligned} \quad (5.45)$$

Reference [372] formulates the bi-level optimization problem (5.46) whose solution provides the values for the coefficients ℓ_0 , ℓ_P , and ℓ_Q that minimize the worst-case linearization error for the active power flow on a certain line $(l, m) \in \mathcal{L}$:

$$\min_{\ell_0, \ell_P, \ell_Q} \max_{P, Q, |V|, \theta} \eta \quad (5.46a)$$

subject to

$$(P, Q, |V|, \theta) \in \mathcal{O} \quad (5.46b)$$

$$P_{lm} = g_{lm} |V_l|^2 - |V_l| |V_m| (g_{lm} \cos(\theta_l - \theta_m) + b_{lm} \sin(\theta_l - \theta_m)), \quad (5.46c)$$

$$\eta \geq \left(\ell_0 + \sum_{i \in \mathcal{N}} \ell_{P,i} P_i + \sum_{i \in \mathcal{N}} \ell_{Q,i} Q_i \right) - P_{lm}, \quad (5.46d)$$

$$\eta \geq P_{lm} - \left(\ell_0 + \sum_{i \in \mathcal{N}} \ell_{P,i} P_i + \sum_{i \in \mathcal{N}} \ell_{Q,i} Q_i \right). \quad (5.46e)$$

Constraint (5.46b) specifies the considered range of operation and the power flow equations. Constraints (5.46d) and (5.46e) in combination with the auxiliary variable η represent the absolute value of the linearization error. Approximations that relate a variety of other quantities, such as reactive power flows and voltage magnitudes, are computed using problems that are analogous to (5.46). Different linearization parameters ℓ_0 , ℓ_P , and ℓ_Q are determined for each quantity of interest.

Reference [372] solves (5.46) using a constraint generation algorithm that iterates between 1) a nonlinear optimization step that identifies a point $(P^*, Q^*, |V^*|, \theta^*) \in \mathcal{O}$ which yields the worst linearization error for given values of ℓ_0 , ℓ_P , ℓ_Q and 2) a linear program that finds the values for ℓ_0 , ℓ_P , ℓ_Q which minimize the worst-case error among all previously identified points. Empirical experiments with a variety of typical test cases found that the resulting “optimal linearizations” have up to a factor-of-four improvement in the worst-case linearization errors compared to using a Taylor series expansion around a nominal operating point as described in §5.2.1. Note that [372] also discusses a variety of possible extensions, such as weighted error metrics that more heavily penalize overestimating or underestimating the quantity of interest.

Minimizing Expected Error for a Specified Optimization Problem

The approach proposed in [373] also computes optimal linearizations, but has several distinctions from the aforementioned approach in [372]. In particular, the linearizations in [373] consider the *expected* error rather than the worst-case error. Additionally, [373] treats the problem of computing a linearization that minimizes the error for the solution to a specified OPF problem (parameterized by uncertain quantities such as renewable power injections) rather than the error over the entire operating range.

To compute the linearization that minimizes this error metric, [373] formulates a hierarchy of increasingly large semidefinite programs. This hierarchy is closely related to the moment/ sum-of-squares relaxation hierarchies discussed in §4.1.2. Solving a semidefinite program in this hierarchy yields an operating point. The linearization provided by the first-order Taylor expansion around this operating point is an estimate

of the optimal linearization. As the order in the hierarchy increases, the obtained linearizations approach the linearization that minimizes the error metric. For the test cases considered in [373], semidefinite programs corresponding to low orders in the hierarchy provide linearizations with small errors relative to other approaches for constructing linearizations. Note that while a sparse formulation is proposed to address computational challenges, further improvements to computational tractability may be needed to address large-scale systems with many sources of uncertainty.

5.2.9 Loss Approximations

Many power system optimization and control problems employ approximate representations of the active and reactive power losses. This section details two of the many existing variants of line-loss approximations. Alternative variants are provided in the references throughout this section.

For a line $(i, k) \in \mathcal{L}$ with admittance $g_{ik} + jb_{ik}$ and assuming near-unity voltage magnitudes, an approximation of the active and reactive power losses for each line can be formulated as a function of the squared phase angle difference, $(\theta_i - \theta_k)^2$ [320, 321, 358, 374–376]:

$$P_{loss,ik} \approx g_{ik} (\theta_i - \theta_k)^2, \quad (5.47a)$$

$$Q_{loss,ik} \approx -b_{ik} (\theta_i - \theta_k)^2. \quad (5.47b)$$

The quadratic constraints in (5.47) can be relaxed to a piecewise linear formulation [320, 321, 358, 375, 376]. As illustrated in Figure 5.2, the losses on each line $(i, k) \in \mathcal{L}$ are modeled with the constraints

$$P_{loss,ik} = g_{ik} \sum_{l=1}^L m_{ik,l} \Delta\theta_{ik,l}, \quad (5.48a)$$

$$Q_{loss,ik} = -b_{ik} \sum_{l=1}^L m_{ik,l} \Delta\theta_{ik,l}, \quad (5.48b)$$

$$\theta_i - \theta_k = \theta_{ik}^+ - \theta_{ik}^-, \quad (5.48c)$$

$$\theta_{ik}^+ \geq 0, \quad (5.48d)$$

$$\theta_{ik}^- \geq 0, \quad (5.48e)$$

$$\theta_{ik}^+ \leq \psi_{ik} \theta_{ik}^{max}, \quad (5.48f)$$

$$\theta_{ik}^- \leq (1 - \psi_{ik}) \theta_{ik}^{max}, \quad (5.48g)$$

$$\psi_{ik} \in \{0, 1\}, \quad (5.48h)$$

$$\theta_{ik}^+ + \theta_{ik}^- = \sum_{l=1}^L \Delta\theta_{ik,l}, \quad (5.48i)$$

$$\Delta\theta_{ik,l} \geq 0, \quad l = 1, \dots, L, \quad (5.48j)$$

$$\Delta\theta_{ik,l} \leq \theta_{ik}^{max}/L, \quad l = 1, \dots, L, \quad (5.48k)$$

$$\Delta\theta_{ik,l} \leq \Delta\theta_{ik,l-1}, \quad l = 2, \dots, L, \quad (5.48l)$$

$$\theta_{ik}^{max}/L - \Delta\theta_{ik,l-1} \leq \phi_{ik,l-1} \theta_{ik}^{max}/L, \quad l = 2, \dots, L, \quad (5.48m)$$

$$\Delta\theta_{ik,l} \leq (1 - \phi_{ik,l-1}) \theta_{ik}^{max}/L, \quad l = 2, \dots, L, \quad (5.48n)$$

$$\phi_{ik,l} \in \{0, 1\}, \quad l = 1, \dots, L - 1, \quad (5.48o)$$

where θ_{ik}^{max} is the maximum angle difference, L is the number of segments in the piecewise linear representation, and $m_{ik,l}$ is the slope of the linear representation for the l^{th} segment. For evenly spaced line segments, $m_{ik,l} = (2l - 1) \theta_{ik}^{max}/L$.

Constraints (5.48a)–(5.48c) model the relationship between the variables associated with the piecewise linearization (i.e., $\Delta\theta_{ik,l}$, $l = 1, \dots, L$, θ_{ik}^+ , and θ_{ik}^-) and those associated with the remainder of the optimization problem (i.e., $P_{loss,ik}$, $Q_{loss,ik}$, θ_i , and θ_k). An absolute value formulation $|\theta_i - \theta_k|$ exploits the even symmetry of the quadratic function, thereby halving the number of segments required for a given level of accuracy in the piecewise linear representation. Constraints (5.48d)–(5.48h) use the binary variable ψ_{ik} to model the complementarity condition ($\theta_{ik}^+ \theta_{ik}^- = 0$, $\theta_{ik}^+ \geq 0$, and $\theta_{ik}^- \geq 0$) that represents the absolute value formulation $|\theta_i - \theta_k| = \theta_{ik}^+ + \theta_{ik}^-$. Constraints (5.48j)–(5.48o) model the piecewise linear representation of $(\theta_{ik}^+ + \theta_{ik}^-)^2$. The binary variables $\phi_{ik,l}$, $l = 1, \dots, L - 1$, are used to maintain adjacency of the segments. Note that [377] proposes a related loss approximation based on the absolute values of the voltage magnitude differences and voltage angle differences.

The binary variables ψ_{ik} and $\phi_{ik,l}$ result in an MILP formulation. Theory developed in [320, 376] shows that the linear relaxation of the binary constraints (i.e., replacing the binary constraints $\psi_{ik} \in$

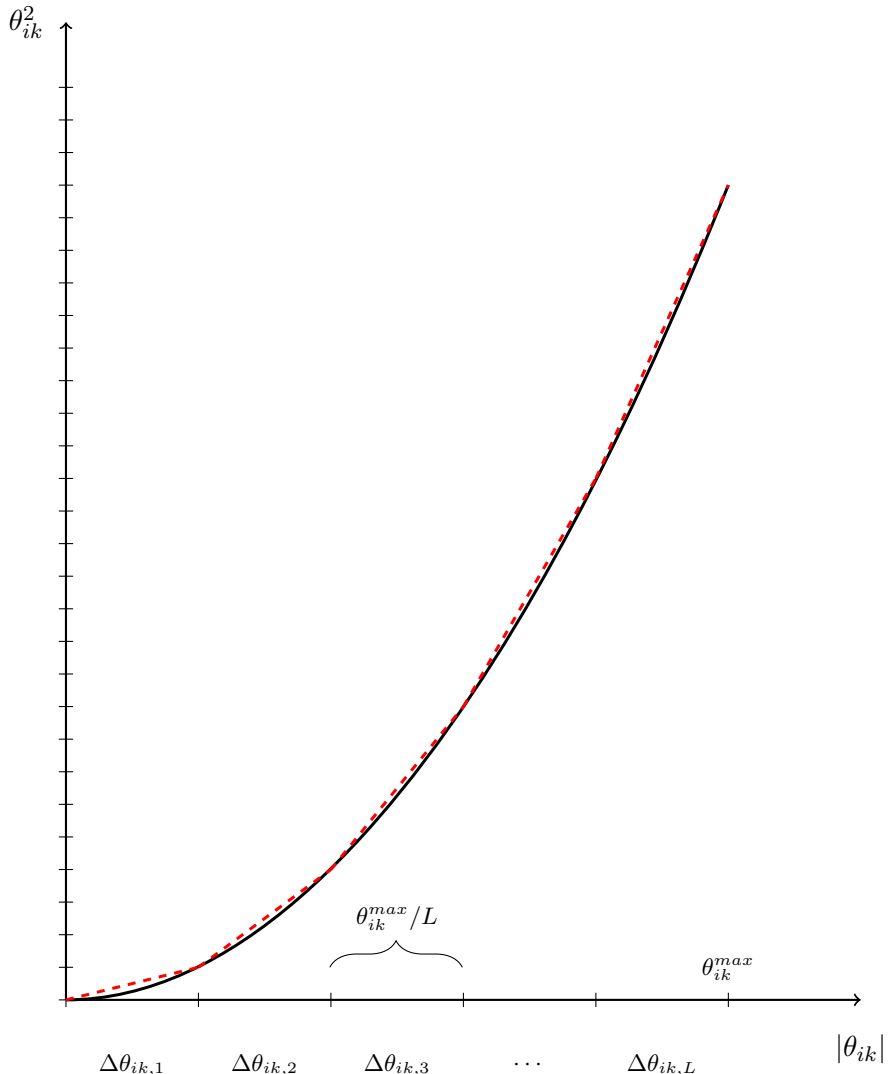


Figure 5.2: Piecewise-linear approximation (dashed red lines) of the squared angle difference function (black curve) used to approximate line losses.

$\{0, 1\}$ in (5.48h) and $\phi_{ik,l} \in \{0, 1\}$ in (5.48o) with the continuous constraints $0 \leq \psi_{ik} \leq 1$ and $0 \leq \phi_{ik,l} \leq 1$, respectively) is exact under certain conditions that depend on the solution's dual variables. In the

simplified case where reactive power is neglected, these conditions are equivalent to non-negativity of the dual variables associated with the active power balance constraints (i.e., non-negative Locational Marginal Prices (LMPs) for active power).

Other work in [378] constructs linear loss functions that do not assume fixed voltage magnitudes as in (5.47). In this case, line losses are approximated by a set of linear inequalities that are chosen to minimize the effect of the nonconvexity inherent in the loss function,

$$P_{loss,ik}(|V_i|, |V_k|, \theta_{ik}) = g_{ik} \left(|V_i|^2 + |V_k|^2 - 2|V_i||V_k| \cos(\theta_{ik}) \right), \quad (5.49)$$

where $\theta_{ik} = \theta_i - \theta_k$. The (local) convexity/concavity of (5.49) in terms of changes in bus voltage magnitude and angle variables about a specified base voltage condition is given by the eigenvalues of the Hessian matrix, $\nabla^2 P_{loss,ik}(|V_i|, |V_k|, \theta_{ik})$, which is shown in (5.50):

$$\begin{aligned} & \nabla^2 P_{loss,ik}(|V_i|, |V_k|, \theta_{ik}) \\ &= 2g_{ik} \begin{bmatrix} 1 & -\cos(\theta_{ik}) & |V_k| \sin(\theta_{ik}) \\ -\cos(\theta_{ik}) & 1 & |V_i| \sin(\theta_{ik}) \\ |V_k| \sin(\theta_{ik}) & |V_i| \sin(\theta_{ik}) & |V_i||V_k| \cos(\theta_{ik}) \end{bmatrix}. \end{aligned} \quad (5.50)$$

It is demonstrated in [378] that (5.50) has exactly two positive eigenvalues for all realistic operating conditions. The loss function is therefore a saddle, exhibiting convexity in two directions and concavity in the other. This motivates a loss model which comprises the loss linearization at the base voltage condition together with a set of loss linearizations formed by selecting appropriate neighboring voltage realizations. These neighboring points lie on the plane defined by the eigenvectors associated with the two positive eigenvalues. This enables the model to capture the local convex nonlinearity of losses while largely eliminating the influence from the concave direction.

Furthermore, it is shown in [378] that if at least one of the voltage magnitudes in (5.49) is fixed, then the Hessian is positive definite under realistic operating conditions. In this case the loss function is locally convex and can be approximated in the usual way by a set of linear inequality constraints.

6

Obtaining a Feasible Point

In comparison to the AC power flow equations summarized in §2, the relaxations and approximations discussed in §4 and §5 have various advantages in their computational tractability and theoretical characteristics (e.g., the convexity of the power flow relaxations and approximations is often useful for proving convergence of certain algorithms, the objective value bounds provided by relaxations as well as the ability to prove infeasibility are useful for a variety of purposes). Moreover, the approximate solutions obtained using the power flow relaxations and approximations are sufficient for some applications. However, other applications require a solution that is feasible for the AC power flow equations. For many of these applications, feasible points that only have local optimality guarantees are often acceptable, particularly when certified to be at least near global optimality via comparison with the bounds provided by convex relaxations.

The power system literature describes a wide variety of techniques for finding feasible AC power flow solutions for many optimization and control problems. A detailed survey of all such techniques is beyond the scope of this monograph, and the interested reader is directed to the reviews in, e.g., [8–17, 22, 24, 25]. Rather than attempt to

survey all the literature on this topic, this chapter first briefly reviews typical techniques and then focuses on recent developments that directly result from the power flow representations previously discussed in this monograph.

Note that the capabilities of various power flow relaxations and approximations are, in many ways, complementary to those of the local solution techniques summarized in this chapter. The discussion in §1 provides examples of such complementary capabilities.

6.1 Summary of Traditional Techniques

Many algorithms for finding feasible points to power system problems iteratively update some representation of the power flow equations. Despite challenging worst-case complexity [1, 2], knowledge of appropriate initializations often results in convergence to feasible points for certain practical problems (e.g., many instances of power flow and optimal power flow problems). Appropriate initializations may be available from knowledge of a previous or anticipated operating point, the solution to a relaxed or approximated problem formulation, or assumed operating point characteristics (e.g., a flat start initialization of $|V| \angle \theta = 1\angle 0^\circ$).

This section summarizes traditional algorithms for computing solutions to the power flow equations and locally solving optimal power flow problems. Other surveys discuss many variants of power flow [8, 9] and optimal power flow algorithms [10–17, 22–25] as well as algorithms for addressing other problems, such as unit commitment [28–31], state estimation [32–35], and transmission switching [36], to name just a few. (See §1 for references to additional surveys.)

6.1.1 Power Flow Solution Algorithms

As discussed in §2.2.1, the power flow equations have variables consisting of either the voltage phasors (for bus injection models) or the squared voltage magnitudes at the buses and the active power, reactive power, and squared magnitudes of the current flows on the lines (for the branch flow model). Specifying two constant parameter values per bus

(typically the active and reactive power injections at PQ buses, the active power injections and voltage magnitudes at PV buses, and the voltage magnitude and angle at a single slack bus) results in a square system of equalities. Solving the power flow equations means determining values for the associated variables that are consistent with these parameter values, without considering inequality constraints such as limits on voltage magnitudes and line flows.

A wide variety of power flow solution algorithms have been proposed [8, 9]. This section summarizes Newton-based, backward/forward sweep, and continuation algorithms. These algorithms have found widespread applications in power systems analyses.

Newton-Based Power Flow Algorithms

Typical Newton-based iterative algorithms for solving the power flow equations leverage the linear approximations developed around a specified operating point that are discussed in §5.2.1. Newton-based methods were first applied to modest-size power flow problems in the late 1950s [91] and later refined for application to larger problems using sparsity-exploiting numerical techniques for solving linear systems of equations [92, 93].

Let superscript (k) denote the value of the associated variable at the k -th iteration of the algorithm. Choose an initialization for the voltage phasors $|V^{(0)}|\angle\theta^{(0)}$ (e.g., a flat start initialization of $|V^{(0)}|\angle\theta^{(0)} = 1\angle 0^\circ$). Newton-based algorithms alternate between computing power injection “mismatches”, denoted by ΔP and ΔQ , and updating the voltage phasors by solving a linear system of equations. The mismatch corresponds to the difference between the power injections implied by the voltage phasors at the current iterate, $P^{(k)}$ and $Q^{(k)}$, and the specified power injections, P^\bullet and Q^\bullet :

$$\begin{aligned} \Delta P^{(k)} \\ = |V_i^{(k)}| \sum_{k=1}^n |V_k^{(k)}| \left(\mathbf{G}_{ik} \cos(\theta_i^{(k)} - \theta_k^{(k)}) + \mathbf{B}_{ik} \sin(\theta_i^{(k)} - \theta_k^{(k)}) \right) - P^\bullet, \end{aligned} \quad (6.1a)$$

$$\begin{aligned} \Delta Q^{(k)} \\ = |V_i^{(k)}| \sum_{k=1}^n |V_k^{(k)}| \left(\mathbf{G}_{ik} \sin(\theta_i^{(k)} - \theta_k^{(k)}) - \mathbf{B}_{ik} \cos(\theta_i^{(k)} - \theta_k^{(k)}) \right) - Q^\bullet. \end{aligned} \quad (6.1b)$$

The first-order Taylor expansion of (6.1) yields

$$\begin{bmatrix} \Delta P^{(k+1)} \\ \Delta Q^{(k+1)} \end{bmatrix} = \begin{bmatrix} \Delta P^{(k)} \\ \Delta Q^{(k)} \end{bmatrix} + \mathbf{J}_p|_{V=|V^{(k)}|\angle\theta^{(k)}} \left(\begin{bmatrix} \theta^{(k+1)} \\ |V^{(k+1)}| \end{bmatrix} - \begin{bmatrix} \theta^{(k)} \\ |V^{(k)}| \end{bmatrix} \right). \quad (6.2)$$

The desired voltage phasors $|V^{(k+1)}|\angle\theta^{(k+1)}$ should (ideally) drive the power injection mismatches $\Delta P^{(k+1)}$ and $\Delta Q^{(k+1)}$ toward zero. Therefore, after computing the power injection mismatches $\Delta P^{(k)}$ and $\Delta Q^{(k)}$, the following linear system is solved to compute the updated voltage phasors $|V^{(k+1)}|\angle\theta^{(k+1)}$:

$$\begin{bmatrix} \Delta P^{(k)} \\ \Delta Q^{(k)} \end{bmatrix} = -\mathbf{J}_p|_{V=|V^{(k)}|\angle\theta^{(k)}} \left(\begin{bmatrix} \theta^{(k+1)} \\ |V^{(k+1)}| \end{bmatrix} - \begin{bmatrix} \theta^{(k)} \\ |V^{(k)}| \end{bmatrix} \right). \quad (6.3)$$

Newton-based algorithms repeat this process until all of the power injection mismatches are less than a specified tolerance ϵ , i.e.,

$$\left\| \begin{bmatrix} |\Delta P^{(k)}| \\ |\Delta Q^{(k)}| \end{bmatrix} \right\|_\infty < \epsilon,$$

indicating that a solution of acceptable accuracy has been obtained. For a sufficiently close initialization, Newton-based methods converge quadratically to a power flow solution. Note that the regions of attraction within which an initialization will converge to a power flow solution are fractal in nature, exemplifying the complicated behavior exhibited by Newton-based methods when the initialization is not near a power flow solution [379–381]. Also note that step-size control via “optimal multipliers” precludes divergence of Newton-based algorithms [382].

Since the voltage magnitude and angle at the slack bus and the voltage magnitudes at PV buses are specified, these variables are fixed to their corresponding values in (6.3). Moreover, since the reactive power injections at PV buses and the active and reactive power injections at the slack bus do not have specified values, the equations corresponding

to these quantities are eliminated from (6.3). Values for these quantities can be explicitly computed after solving for the voltage magnitudes and angles.

Note that Newton-based methods can be applied using any of the Taylor expansion linearizations discussed in §5.2.1. Various power flow linearizations have different computational characteristics [383]. For instance, the Fast Decoupled Power Flow linearization [337] discussed in §5.2.2 only factors the matrices \mathbf{B}' and \mathbf{B}'' once, resulting in significant computational speed improvements for many power flow problems. [339] and [340] provide detailed analytical and empirical analyses of the convergence behavior for the Fast Decoupled Power Flow. Typical power system software packages such as MATPOWER [50] implement Newton methods that are based on a variety of power flow representations.

Backward/Forward Sweep Algorithm for the DistFlow Equations

Newton's method can be used to solve the DistFlow equations (2.7). However, the recursive structure of these equations lends itself to a more intuitive backward/forward sweep algorithm [384–386]. Number the source bus (substation) as bus 0. Denote the voltage set-point at this bus by V_{set} , and assume for simplicity that there are no other voltage-regulated buses in the network. Let V_{tol} and S_{tol} be tolerance parameters for mismatches in the source bus voltage magnitude and the power flows of the end buses. Referring to the network model of Figure 2.2, the algorithm can be expressed as follows:

Step 0: Initialize the squared voltage magnitude at the end buses of the feeder to $|V_k|^2 = 1.0$ per unit.

Step 1: At the end buses, $P_{km} + jQ_{km} = 0$ and $|V_k|^2$ is given (either by Step 0 or Step 4). Solve the DistFlow equations (2.7) to obtain P_{ik} , Q_{ik} , ℓ_{ik} , and $|V_i|^2$.

Step 2: Work backwards from the ends of the feeder to the source bus, computing P_{ik} , Q_{ik} , ℓ_{ik} , and $|V_i|^2$ at each bus.

Step 3: Calculate the voltage mismatch at the source bus, $V_{mis} = |V_{set}^2 - |V_0|^2|$, where $|V_0|^2$ is computed at Step 2.

Step 4: Set $|V_0|^2 = V_{set}^2$. Using the values of P_{0k} and Q_{0k} from Step 2, work forwards from the source bus calculating $\sum P_{km}$, $\sum Q_{km}$, ℓ_{ik} , and $|V_k|^2$ using the values of P_{ik} , Q_{ik} , and $|V_i|^2$ computed for the previous bus. If there are multiple lines emanating from bus k , then distribute these new values for $\sum P_{km}$ and $\sum Q_{km}$ to the lines in proportion to the flows computed at Step 2.

Step 5: Calculate the power mismatches at all of the end buses, $S_{mis} = |P_{km}| + |Q_{km}|$.

Step 6: Check the convergence criteria, $S_{mis} \leq S_{tol}$ for all of the end buses and $V_{mis} \leq V_{tol}$. If these criteria are satisfied, terminate the algorithm. Otherwise, go to Step 1.

This algorithm can be readily extended to three-phase unbalanced radial networks [386]. Additionally, a related forward-backward sweep technique for solving optimization problems is proposed in [387]. Applications of the technique in [387] include solving multiperiod OPF problems and optimizing the placement of energy storage devices.

Continuation Algorithms

It is often desirable to move from a known feasible point to a new solution corresponding to different parameter values, a process known as numerical continuation [388]. Such situations may arise when a power flow solution is easily obtained for particular parameter values λ_1 but the desired solution corresponds to different parameter values λ_2 (e.g., a much higher loading level). For notational convenience, consider the power flow equations in the general form,

$$\phi(x, \lambda) = 0, \quad (6.4)$$

where $x \in \mathbb{R}^{2n}$ are the voltage variables (magnitudes and angles, $|V_i|$ and θ_i , or the rectangular components, V_{di} and V_{qi} , for each bus $i \in \mathcal{N}$), $\lambda \in \mathbb{R}^p$ are parameters, and $\phi : \mathbb{R}^{2n+p} \rightarrow \mathbb{R}^{2n}$ denotes the power flow equations. A path between the solutions corresponding to λ_1 and λ_2 is given by

$$\phi(x, (1 - \gamma)\lambda_1 + \gamma\lambda_2) = 0,$$

where the scalar γ varies from 0 to 1. A closely related formulation arises when the parameters have a single degree of freedom, effectively $\lambda \in \mathbb{R}^1$, and the corresponding 1-manifold (or curve) defined by (6.4) is desired. For simplicity of notation, the following discussion of the continuation process will consider this latter case, where (6.4) is under-determined by dimension one and hence defines a 1-manifold. Continuation problems of this form have been explored extensively in the context of power systems [100, 389–391]. A variety of algorithms have been exploited, with the most versatile being a predictor-corrector Euler homotopy approach [388, 389].

To describe this predictor-corrector algorithm, it is convenient to rewrite (6.4) as

$$\phi(z) = 0, \quad (6.5)$$

where $z \equiv [\begin{smallmatrix} x \\ \lambda \end{smallmatrix}] \in \mathbb{R}^{2n+1}$ and $\phi : \mathbb{R}^{2n+1} \rightarrow \mathbb{R}^{2n}$. Assume that a point z_1 which satisfies (6.5) is known and another point on the curve described by (6.5) is desired.

The first step of the algorithm is to predict the next point on the curve. This is achieved by finding the vector that is tangent to the curve at z_1 and moving along that vector a predefined distance τ . This τ is a (scalar) control parameter that effectively determines the distance between successive points along the curve. The unit vector $v \in \mathbb{R}^{2n+1}$ that is tangent to the curve (6.5) at z_1 is given by

$$\left. \frac{\partial \phi}{\partial z} \right|_{z=z_1} v = 0, \quad (6.6a)$$

$$\|v\| = 1, \quad (6.6b)$$

where the Jacobian $\frac{\partial \phi}{\partial z}$ has dimension $2n \times (2n + 1)$. The prediction of the next point on the curve is

$$z_p = z_1 + \tau v.$$

The next step is to correct to a point z on the curve. This is done by solving for the point of intersection of the curve and a hyperplane that both passes through z_p and is orthogonal to v . Points z on this hyperplane are given by

$$(z - z_p)^\top v = 0, \quad (6.7)$$

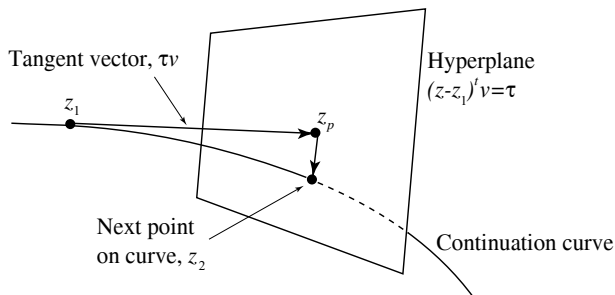


Figure 6.1: Predictor-corrector process for the Euler homotopy.

or, alternatively,

$$(z - z_1)^\top v = \tau. \quad (6.8)$$

Either (6.7) or (6.8) can be used. The point of intersection of the curve and the hyperplane is then given by

$$\phi(z) = 0, \quad (6.9a)$$

$$(z - z_1)^\top v = \tau. \quad (6.9b)$$

Note that z_1 , v , and τ are fixed in (6.9b), with z being the only unknown. The first $2n$ equations, which follow from (6.5), ensure the point is on the desired curve. The last equation, from (6.8), ensures the point is on the hyperplane. Together, (6.9) forms a set of $2n + 1$ equations in $2n + 1$ unknowns which can be solved using a standard Newton-based technique, as described in §6.1.1. The predictor-corrector process is illustrated in Figure 6.1.

After the second point z_2 on the curve has been determined, an approximate tangent vector can generally be used for obtaining successive points. The approximate tangent vector at the k -th point, which is used to calculate the $(k + 1)$ -th point, is given by

$$v_i = \frac{z_k - z_{k-1}}{\|z_k - z_{k-1}\|}.$$

This approximate tangent vector involves much less computation than finding the exact tangent vector using (6.6). However, the approximation may lose accuracy in regions of high curvature.

6.1.2 Algorithms for Locally Solving Optimal Power Flow Problems

A wide variety of local solution techniques have been applied to OPF problems [10–17, 22–25]. This section reviews two particularly successful classes of traditional techniques called Interior Point algorithms and Sequential Quadratic Programming algorithms. Further details on these and other local solution techniques are provided in [124, 392]. Power system software packages such as MATPOWER [50] and PowerModels.jl [51] provide interfaces to solvers that implement these and other optimization algorithms.

For notational convenience, the OPF problem (2.8) is rewritten as

$$\min f(x) \quad (6.10a)$$

subject to

$$g_i(x) \leq 0, \quad i = 1, \dots, m_{ineq}, \quad (6.10b)$$

$$h_j(x) = 0, \quad j = 1, \dots, m_{eq}. \quad (6.10c)$$

In (6.10), the vector x denotes the decision variables consisting of the voltage phasors. The inequality constraints $g_i(x) \leq 0$ denote the limits on line flows, power injections, phase angle differences, and voltage magnitudes. The equality constraints $h(x) = 0$ correspond to some representation of the power flow equations. The scalars m_{ineq} and m_{eq} denote the number of inequality and equality constraints, respectively. The objective, denoted $f(x)$, is chosen to optimize a specified quantity of interest, such as minimization of generation cost.

Interior Point Algorithms

Interior point algorithms are formulated by first introducing non-negative slack variables $s_i \geq 0$, $\forall i = 1, \dots, m_{ineq}$, in order to rewrite the inequality constraints $g_i(x) \leq 0$ with the equivalent formulation $g_i(x) + s_i = 0$. The inequality constraints $s_i \geq 0$ are then replaced with a so-called “barrier” term in the objective function that goes to infinity as the inequality becomes binding. This barrier term is weighted by a positive “barrier parameter” μ that is iteratively decreased towards zero as the algorithm converges. Interior point algorithms are formulated using a “log barrier” defined as the sum of the logarithms of the slack

variables s_i . The log-barrier formulation is

$$\min f(x) - \mu \sum_{i=1}^{m_{ineq}} \log s_i \quad (6.11a)$$

subject to

$$g_i(x) + s_i = 0, \quad i = 1, \dots, m_{ineq}, \quad (6.11b)$$

$$h_j(x) = 0, \quad j = 1, \dots, m_{eq}. \quad (6.11c)$$

Under mild conditions [393], a solution to (6.11) approaches a solution to (6.10) as the barrier parameter μ goes to zero. The KKT conditions for (6.11) are

$$\frac{\partial f(x)}{\partial x} + \gamma^\top \left(\frac{\partial g(x)}{\partial x} \right) + \lambda^\top \left(\frac{\partial h(x)}{\partial x} \right) = 0, \quad (6.12a)$$

$$g(x) + s = 0, \quad (6.12b)$$

$$h(x) = 0, \quad (6.12c)$$

$$\text{diag}(s) \gamma - \mu \mathbb{1}_{m_{ineq}} = 0, \quad (6.12d)$$

where γ and λ are vectors of Lagrange multipliers for (6.11b) and (6.11c), respectively; $\text{diag}(\cdot)$ denotes the diagonal matrix with the vector argument on the diagonal; and $\mathbb{1}$ is the vector of ones with length given by the associated subscript.

Each iteration of an interior point algorithm computes a Newton update step for the KKT conditions (6.12). The variables x , λ , γ , and s are updated according to rules which ensure that the non-negative variables γ and s do not approach zero too quickly. The barrier parameter μ is also updated at each iteration such that it approaches zero.

Typical variants of interior point algorithms use line-search methods, trust-region constraints, techniques for handling non-convexity via merit functions, and other modifications to guarantee convergence. More details regarding interior point algorithms and various extensions are available in [124, 392–394]. Software packages that implement interior point algorithms include Ipopt [395], Knitro [396], and LOQO [397]. The first applications of interior point algorithms in power systems include state estimation [398] and hydro scheduling problems [399] during the early 1990s. Subsequent work demonstrated that interior point

algorithms are capable of locally solving large-scale OPF problems [24, 400, 401]. Note that it is generally difficult to leverage information from a nearby solution, i.e., interior point algorithms are typically difficult to “warm start” because they require a sufficiently interior starting point [402].

Sequential Quadratic Programming Algorithms

Sequential quadratic programming (SQP) algorithms seek local solutions to nonlinear optimization problems by repeatedly solving specially constructed quadratic programs. For the generic OPF problem (6.10), each iteration k of an SQP algorithm solves the following quadratic program to obtain a search direction $d^{(k)}$:

$$\begin{aligned} d^{(k)} = & \\ \arg \min_d \quad & f(x^{(k)}) + \left(\nabla f(x^{(k)}) \right)^T d + \frac{1}{2} d^T \left(\nabla_{xx}^2 \mathcal{L}(x^{(k)}, \gamma^{(k)}, \lambda^{(k)}) \right) d \\ \text{subject to} & \end{aligned} \quad (6.13a)$$

$$g_i(x^{(k)}) + \left(\nabla g_i(x^{(k)}) \right)^T d \leq 0, \quad i = 1, \dots, m_{ineq}, \quad (6.13b)$$

$$h_j(x^{(k)}) + \left(\nabla h_j(x^{(k)}) \right)^T d = 0, \quad j = 1, \dots, m_{eq}, \quad (6.13c)$$

where γ and λ are vectors of Lagrange multipliers for (6.10b) and (6.10c), respectively; $x^{(k)}$ is the value of the decision variables at the current iterate; $\mathcal{L} = f(x) + \gamma^T g(x) + \lambda^T h(x)$ is the Lagrangian of (6.10); and ∇ and ∇_{xx}^2 denote the gradient and Hessian, respectively, with respect to x .

Each iteration of an SQP algorithm updates the primal decision variables by adding the step $d^{(k)}$ computed by solving (6.13), i.e., $x^{(k+1)} = x^{(k)} + d^{(k)}$. The values for the Lagrange multipliers at the next iteration, $\gamma^{(k+1)}$ and $\lambda^{(k+1)}$, are given by the dual variables for the constraints (6.13b) and (6.13c), respectively, computed at the current iteration.

The optimization problem (6.13) is a (potentially non-convex) quadratic program which can be solved using a variety of algorithms. When the Hessian is difficult to compute, SQP algorithms often employ so-called “quasi-Newton” techniques that construct modified matrices used

in place of $\nabla_{xx}^2 \mathcal{L}(x^{(k)}, \gamma^{(k)}, \lambda^{(k)})$ [124, 392]. Other SQP variants employ various line-search techniques, trust-region methods, merit functions, etc. [124, 392].

Once an SQP method finds the “active set”, i.e., the set of inequality constraints that are binding at the solution to (6.10), the iterates converge superlinearly or quadratically towards the solution, depending on the specific SQP variant. SQP methods can thus greatly benefit from being initialized at a point near the solution.

While predicated by various related applications of quadratic and linear programming techniques to OPF problems [13, 14], SQP methods of the form described in this section were first applied to OPF problems in the mid-1980s [403], where a sparse implementation demonstrated scalability to systems with thousands of buses. As reviewed in [16], subsequent work on OPF problems has refined SQP techniques via a variety of modifications. Typical variants of SQP methods are surveyed from a general optimization perspective in [124, 392]. SQP implementations include Knitro [396], SNOPT [404], and FilterSQP [405].

6.2 SDP-Based Techniques for Obtaining Feasible Points

Having briefly reviewed several important traditional techniques, this section returns to the main focus of this monograph regarding recent developments in power flow representations. In particular, this section discusses how SDP formulations of the power flow equations can be used to find feasible points for power flow and optimal power flow problems.

The Shor relaxation described in §4.1.1 finds the global solutions to some power system optimization problems. However, there are practical problems for which the solution to the Shor relaxation fails to satisfy the rank condition (4.4) [3, 103, 107, 121, 170–175]. Although the power injections associated with the solution to the Shor relaxation may be close to those of the global optimum, no physically meaningful voltage phasors can be directly recovered for such cases.

In other fields (e.g., compressed sensing) which employ Shor relaxation techniques to solve non-convex optimization problems, “penalization” approaches are often able to find feasible solutions that have objective values near the global optimum. A penalization approach

augments the objective function with a “penalty” term that promotes the satisfaction of the rank condition (4.4). Let $f(x)$ denote the cost function for the non-convex optimization problem. A penalization approach applies the Shor relaxation to a related optimization problem with the objective function $f_\lambda(x) = f(x) + \lambda\psi(x)$, where λ is a specified penalty parameter and $\psi(x)$ is a chosen penalty function. Since the constraints are left unchanged, any solution to a relaxation of a penalized problem that satisfies the rank condition (4.4) is *feasible* for the original non-convex optimization problem. Note that penalization approaches do not provide relaxations of the original non-convex problem because they do not yield bounds on the optimal objective values. Also note that an appropriate penalization may not exist. Furthermore, if an appropriate penalization does exist, the difficulty of finding it has the same worst-case complexity as solving the original optimization problem. Thus, the problem of choosing an appropriate penalty for OPF problems is generally NP-Hard [1, 2].

A successful penalization approach requires 1) the selection of a penalty function $\psi(x)$ that promotes exactness of the relaxation and 2) a means for choosing an appropriate penalty parameter λ . A common penalty function that has been shown to be valuable in other fields is the *nuclear norm* (i.e., the sum of the singular values of the matrix \mathbf{W} in the Shor relaxation (4.3)). The nuclear norm penalty is implemented using the matrix trace operator $\psi(x) = \text{tr}(\mathbf{W})$ in the Shor relaxation. The nuclear norm has desirable theoretical properties relevant to penalization approaches [406, 407]. However, choosing $\psi(x) = \text{tr}(\mathbf{W})$ generally results in poor performance for power system optimization problems. For the power flow equations, $\text{tr}(\mathbf{W})$ is equal to the sum of the squared voltage magnitudes. Since the voltage magnitudes are often constrained to be near nominal values, all feasible points have similar values of $\text{tr}(\mathbf{W})$.

While the nuclear norm is generally not appropriate, other penalty functions can work well for power system problems. Selection of objective functions for the Shor relaxation that yield physically meaningful solutions to the power flow equations is studied in [170] and [408]. To solve the power flow equations, [170] and [408] consider optimization problems with fixed active power injections and voltage magnitudes at

non-slack generator buses, fixed active and reactive power injections at the load buses, and a fixed voltage magnitude and angle at a single slack bus (i.e., the feasible spaces of the optimization problems consist solely of the (multiple) point solutions to the power flow equations). The approach in [170] uses objective functions that are linear combinations of squared voltage magnitudes to recover multiple solutions to the power flow equations. The approach in [408] uses the solution to a convex optimization problem to determine an appropriate objective function for obtaining a high-voltage power flow solution.

Penalty functions that are specific to OPF problems are explored in [98, 187]. The proposed approaches penalize the total reactive power injection, $\sum_{i=1}^n Q_i$, and the apparent power losses on certain “problematic” lines, $\sum_{(i,k) \in \mathcal{L}^*} |S_{ik} + S_{ki}|$ where $\mathcal{L}^* \subset \mathcal{L}$. The set of problematic lines \mathcal{L}^* corresponds to the lines associated with high-rank submatrices in the chordal-sparsity-exploiting formulation (see §4.1.1). Reference [409] applies a similar penalty approach to the state estimation problem.

There often exist penalizations of the total reactive power injection along with the apparent power losses on certain lines that result in feasible solutions with objective values that are near the global optimum (within 1% for a variety of test cases) [98, 187]. However, this is not always the case. Figure 6.2 provides an example of an OPF problem where the penalization approach in [98, 187] yields either infeasible points or feasible points that are far from the global optimum.

In related work, the approach in [219] uses a reactive power penalty along with selective application of the higher-order moment constraints (see §4.1.2). The resulting “penalized moment” relaxations find feasible solutions to a broader class of problems than either method individually.

While [98] and [187] show that a range of values for the penalty parameters results in feasible solutions for a variety of test cases, there is no guidance for choosing an appropriate value for the penalty parameter. Appropriate values can range over several orders of magnitude for realistic test cases. An alternative approach in [188] provides an algorithm for computing the penalty function. Specifically, this approach first solves the Shor relaxation. The generation cost function is constrained

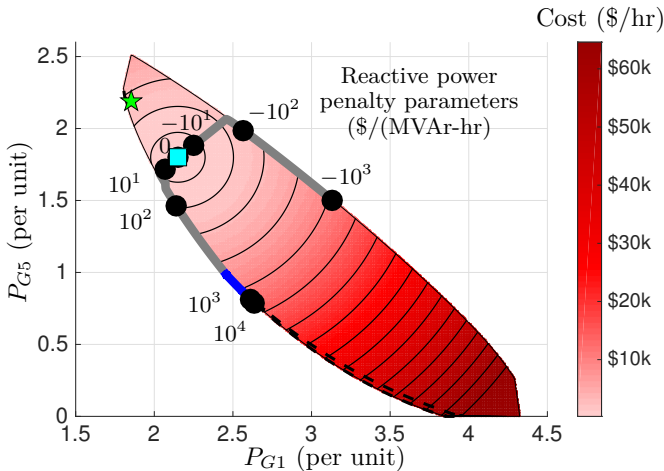


Figure 6.2: Projections of the feasible spaces of the OPF problem and the Shor relaxation for the five-bus system “WB5” from [3]. Compared to the projection in Figure 2.6b, the projection shown here looks down vertically. The disconnected feasible space for the OPF problem is denoted by the thin region inside the dashed black curves at the bottom-left and upper-left portions of the colored region. The feasible space for the relaxation is shown by the colored region. The OPF problem’s objective function is modified to a convex quadratic function of active power generation with an unconstrained minimizer at the light blue square. The thin black lines are contours of the objective function for the non-penalized relaxation. The green star denotes the OPF problem’s global solution. The colored region, OPF feasible space, cost contours, and local and global solutions are the same as in Figure 4.3a.

The thick gray and blue line denotes the solutions obtained with varying parameter values for a penalty function of total reactive power generation as proposed in [98, 187]. (Related penalties that include apparent power losses have similar behavior.) Specific penalty parameters in $\$/(\text{MVar-hr})$ are explicitly shown by the black dots along the thick line. The gray portion of the thick line corresponds to solutions of the penalized formulation that are not feasible for the OPF problem (i.e., do not satisfy the rank condition (4.4)). The blue portion of the thick line corresponds to solutions of the penalized formulation that are feasible for the OPF problem (i.e., satisfy the rank condition (4.4)).

The solution to the non-penalized relaxation is at the light blue square. Increasing the penalty parameter results in the solution to the penalized formulation moving away from the global optimum. A feasible point is first reached at a penalty parameter value of approximately $\$467/(\text{MVar-hr})$. With an objective value that is 198% greater than that of the global optimum, this feasible point is far from the global solution to the OPF problem at the green star. Negative values of the penalty parameter result in the solution to the penalized formulation being infeasible for the OPF problem. Thus, the penalization approach in [98, 187] fails to yield a near-globally-optimal solution for this problem.

to be close to the bound from the Shor relaxation in order to free the choice of the objective function in the relaxation. This facilitates the choice of a weighted Laplacian objective function. An iterative algorithm selects the weights for the weighted Laplacian matrix in terms of the “mismatches” in the apparent power line flows between the solution to the relaxation and the closest rank-one matrix. (The approach in [188] is similar to that described in §4.1.2 for determining where to apply the higher-order constraints in the moment relaxation hierarchies.) For many cases where the optimal solution has a generation cost that is indeed close to the value from the Shor relaxation, the Laplacian objective function generated with the algorithm in [188] is capable of finding a near-globally-optimal feasible solution without the need to externally specify a penalty parameter value.

Another approach for algorithmically selecting an appropriate penalty function is proposed in [410]. Specifically, this approach uses an ADMM formulation to iterate between solving a penalized Shor relaxation and an update of the penalty via a projection onto the space of rank-one matrices.

Other recent research in [173, 411, 412] leverages the Shor relaxation in attempts to obtain locally optimal solutions. Reference [411] augments the objective function in the Shor relaxation with a parameterized surrogate of the rank function. Using a majorization-minimization method that successively adjusts the relevant parameter in the rank surrogate function, the approach in [411] solves a series of semidefinite programs whose solutions converge to a rank-one matrix that corresponds to a stationary point of the original non-convex optimization problem.¹

Reference [412] also solves a series of semidefinite programs that converge to a stationary point of the non-convex optimization problem. To summarize the approach in [412], first observe that the rank-one condition (4.4) for the Shor relaxation is equivalent to the spectral condition $\text{tr}(\mathbf{W}) - \lambda_{\max}(\mathbf{W}) = 0$, where $\lambda_{\max}(\mathbf{W})$ denotes the maximum

¹A “stationary point” refers to a point that is either a local minimum, a local maximum, or a saddle point.

eigenvalue of the positive-semidefinite-constrained matrix \mathbf{W} .² Also observe that the expression $u^\top \mathbf{W} u$ is a lower bound on $\lambda_{max}(\mathbf{W})$ for any unit-length vector u . The approach in [412] aims to penalize the objective function by the expression $\text{tr}(\mathbf{W}) - \lambda_{max}(\mathbf{W})$. To accomplish this, the above observations are exploited by iteratively solving a sequence of semidefinite programs where the objective function at iteration $k + 1$ is penalized by the expression $\mu \left(\text{tr}(\mathbf{W}) - (x^{(k)})^\top \mathbf{W} x^{(k)} \right)$, where μ is a penalty parameter and $x^{(k)}$ denotes a unit-length eigenvector associated with the largest eigenvalue of the matrix \mathbf{W} from the previous iteration's solution. This approach is extended to unbalanced three-phase network models in [413], and a decomposed formulation appropriate for large-scale problems is presented in [414].

In related work, [173] also proposes an iterative penalization approach that seeks to satisfy the condition $\text{tr}(\mathbf{W}) - \lambda_{max}(\mathbf{W}) = 0$. Each iteration of the approach in [173] solves a penalized Shor relaxation with a penalty function constructed using an eigendecomposition. Let $\mathbf{W}^{(k)}$ denote the solution to the penalized Shor relaxation for iteration k , with the solution to the non-penalized Shor relaxation providing an initialization for the first iteration. Define the eigendecomposition $\mathbf{W}^{(k)} = \mathbf{U}^{(k)} \boldsymbol{\Lambda}^{(k)} (\mathbf{U}^{(k)})^\top$, where the diagonal matrix $\boldsymbol{\Lambda}$ contains the eigenvalues of $\mathbf{W}^{(k)}$ in decreasing order, with corresponding unit-length eigenvectors in the columns of the matrix $\mathbf{U}^{(k)}$. Define the matrix $\hat{\mathbf{U}}^{(k)}$ containing the columns of $\mathbf{U}^{(k)}$ corresponding to the second-largest eigenvalue through the smallest eigenvalue. Iteration $k + 1$ solves the Shor relaxation with the penalization term $\mu \cdot \text{tr}(\hat{\mathbf{U}}^{(k)} (\hat{\mathbf{U}}^{(k)})^\top \mathbf{W})$, where μ is a scalar penalty parameter. This iterative approach yields a globally optimal solution for the original non-convex optimization problem if the iterations converge to a point for which the corresponding penalization term, $\text{tr}(\hat{\mathbf{U}}^{(k)} (\hat{\mathbf{U}}^{(k)})^\top \mathbf{W})$, has value equal to zero. Note that while the iterations are not guaranteed to converge to such a point, the approach has promising empirical performance for a variety of distribution system test cases. The formulation in [173] considers

²Recall that the trace of a matrix is equal to the sum of its eigenvalues and that all eigenvalues of a positive semidefinite matrix are non-negative. Thus, for a positive semidefinite matrix, the maximum eigenvalue equaling the sum of the eigenvalues implies that at most one eigenvalue is non-zero.

an unbalanced three-phase network model and employs techniques for exploiting chordal sparsity and merging cliques in a manner similar to that discussed in §4.1.1 in order to improve computational tractability.

For some problems, an approximate solution can also be obtained via modification of the network parameters. As shown in [164], modifying the network by enforcing a small minimum resistance (e.g., 1×10^{-4} per unit) on all lines results in satisfaction of the rank condition (4.4) for some OPF problems that minimize increasing functions of active power generation. Additionally, as shown in [276] and discussed in §4.2.3, modifying the network with a sufficient number of controllable phase shifting transformers along with a load oversatisfaction assumption ensures that Jabr's SOCP relaxation and the branch flow relaxation are exact. Determining other modifications that tend to promote exactness of various relaxations is an open problem.

6.3 SOCP-Based Techniques for Obtaining Feasible Points

Similar to the traditional techniques discussed in §6.1 that iteratively update linearizations of the power flow equations, recently proposed approaches [415–417] successively solve SOCP problems. Reference [415] proposes an algorithm called “Feasible Point Pursuit–Successive Convex Approximation” to find an OPF solution that is at least locally optimal. This algorithm is applicable to problems with both balanced single-phase equivalent network models and unbalanced three-phase network models, including multiphase networks with both Wye and Delta connected devices [418]. Consider a generic power flow constraint of the form

$$x^\top \mathbf{A} x \geq b, \quad (6.14)$$

where \mathbf{A} is an indefinite matrix that represents one of the matrices in (4.1). The matrix \mathbf{A} can be separated into positive semidefinite and negative semidefinite components $\mathbf{A}^{(+)}$ and $\mathbf{A}^{(-)}$, respectively, with the constraint (6.14) rewritten as

$$x^\top \mathbf{A}^{(+)} x + x^\top \mathbf{A}^{(-)} x \geq b. \quad (6.15)$$

Analytical expressions for $\mathbf{A}^{(+)}$ and $\mathbf{A}^{(-)}$ are derived in [295, §5.3].

Since $\mathbf{A}^{(-)}$ is negative semidefinite, the following condition holds for any vectors x and z :

$$(x - z)^\top \mathbf{A}^{(-)} (x - z) \leq 0. \quad (6.16)$$

Expanding this expression and rearranging gives

$$x^\top \mathbf{A}^{(-)} x \leq 2z^\top \mathbf{A}^{(-)} x - z^\top \mathbf{A}^{(-)} z. \quad (6.17)$$

Substituting (6.17) into (6.15) yields

$$x^\top \mathbf{A}^{(+)} x + 2z^\top \mathbf{A}^{(-)} x \geq b + z^\top \mathbf{A}^{(-)} z. \quad (6.18)$$

For any specified vector z , enforcing the SOCP constraint (6.18) ensures satisfaction of (6.14). The iterative approach in [415] solves the SOCP problem corresponding to (6.18), with the solution used to update the value of z for the next iteration. The iterates converge to a KKT point of the associated optimization problem. Since the constraint (6.18) may result in infeasibility, the algorithm in [415] begins with a “feasible point pursuit” stage designed to achieve feasibility. Each subsequent step maintains feasibility.

References [240] and [419] provide further discussion of similar “Difference of Convex Programming” approaches which leverage sum-of-squares ideas that are closely related to the moment hierarchies described in §4.1.2. A similar successive convex approximation approach is presented in [416] for solving two-stage stochastic OPF problems with robust constraints. Likewise, [417] uses a closely related successive convex approximation approach to solve maximum loadability problems and bi-objective OPF problems. Other recent work in [420] applies a successive convex approximation approach to a formulation that is similar to the QC relaxation discussed in §4.2.1.

6.4 Convex Restrictions

When the power injection and voltage magnitude parameters P_i , Q_i , and $|V_i|$ are allowed to vary, the power flow equations generally have an associated nonzero-dimensional, non-convex feasible space. Relaxations of the power flow equations form convex spaces that completely enclose this non-convex feasible space. A converse idea is to construct “convex

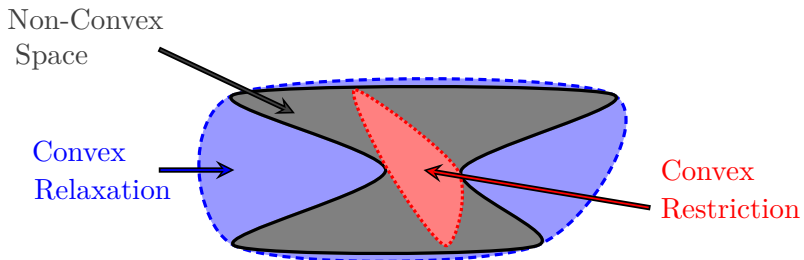


Figure 6.3: An illustration comparing a convex relaxation and a convex restriction. The gray region represents a non-convex feasible space. The blue region bounded by the dashed line represents the feasible space of a convex relaxation, which completely encloses the non-convex space. The red region bounded by the dotted line represents a convex restriction, which is completely enclosed within the non-convex space.

restrictions” that are completely *enclosed within* the non-convex feasible space.³ Whereas convex relaxations of minimization problems provide *lower bounds* on the optimal objective value and sufficient conditions to certify problem *infeasibility*, convex restrictions provide *upper bounds* on the optimal objective value and sufficient conditions to certify problem *feasibility*. Figure 6.3 provides an illustration comparing a convex restriction and a convex relaxation of a non-convex space.

A variety of approaches for constructing convex restrictions have been proposed. This section reviews recent work. A summary of older literature on this topic is provided in [421, Section II].

The approach in [422] starts from a feasible point with a non-singular power flow Jacobian. An SDP formulation that exploits the moment relaxation theory described in §4.1.2 is used to identify a region around this point within which the power flow Jacobian is non-singular and certain operational constraints are satisfied. The power flow equations are guaranteed to be feasible within this region and the region is convex by construction. Thus, this region provides a convex restriction.

Recent work in [65] constructs convex restrictions based on a current-voltage formulation of the power flow equations. Both currents and voltages are represented in rectangular coordinates. The formulation

³This monograph uses “convex restriction” instead of the alternative phrase “inner approximation” to avoid confusion with the power flow approximations discussed in §5.

in [65] is used to find conservative solutions to robust optimization problems relevant to emergency control situations where computational speed is particularly important.

Other recent work in [275] focuses on convex restrictions for radial networks. While there exist sufficient conditions for exactness of the SOCP relaxation, as discussed in §4.2.3, these conditions are not satisfied by all problems and there are radial test cases for which the SOCP relaxation is not exact. To address a broader class of optimization problems for radial networks, the approach in [275] augments an extended formulation of the DistFlow equations (2.7) with additional variables and constraints. These additional variables and constraints contract the feasible space of the augmented non-convex optimization problem. The approach in [275] relaxes this augmented non-convex problem using the same SOCP relaxation technique employed in (4.49). If the network topology and electrical parameters satisfy certain conditions, every feasible point (including the optimum) of this “augmented relaxed” SOCP formulation is guaranteed to have a corresponding physically meaningful power flow solution, which can be recovered using an iterative algorithm. Empirical experiments demonstrate that the contraction resulting from the augmented variables and constraints is not too severe for practical distribution systems, such that the augmented problem maintains a large quantity of the original problem’s feasible space.

Another research thrust relevant to developing convex restrictions exploits fixed-point theorems [332, 421, 423–430]. References [332, 421, 423, 425] apply the Banach fixed-point theorem [431] to construct conditions for power flow solvability in systems where only a single bus has a fixed voltage magnitude (i.e., systems with only slack and PQ buses). This approach was first proposed in [332] and then extended in [423] to reduce conservativeness and improve computational tractability. Reference [421] (with an extension to three-phase network models presented in [425]) generalizes the approaches in [332] and [423] using an implicit Z_{bus} formulation [432]. Using theory related to saddle-node bifurcations, recent work in [433] also presents a necessary condition for power flow solvability that generalizes the condition in [332]. The condition in [433] is applicable to systems with both constant-power and constant-current injections and can be used to construct real-time

voltage stability indices. In other recent work, [426] proposes conditions for power flow solvability using Brouwer's fixed-point theorem [434]. Under certain conditions, the approach in [426] generalizes the approaches in [332, 421, 423]. Moreover, the approach in [426] is applicable to a more general class of systems which can have multiple buses with fixed voltage magnitudes (i.e., systems with slack, PQ, and PV buses) as well as variation in other system parameters, such as network impedances. A similar approach based on Brouwer's theorem is proposed in [427] for systems without PV buses, and subsequent developments that are particularly relevant to OPF problem formulations are presented in [428]. Further advances in [430] generalize the work in [427, 428] using a lifted variable formulation that significantly reduces the conservativeness of the resulting convex restrictions. For lossless radial systems, other recent work in [424] leverages a fixed-point reformulation based on Brouwer's theorem as proposed in [435] to develop sufficient conditions that guarantee the existence and uniqueness of a high-voltage power flow solution. The conditions in [332, 421, 423–427] are used to construct convex restrictions for certain classes of systems. Note that the approach in [426] comes with tightness guarantees that bound a measure of the distance between the convex restriction and the non-convex feasible space.

Recent work in [329] provides theory related to power flow solution existence in systems with balanced radial networks where all lines have the same resistance-to-reactance ratios and all buses, except for a single slack bus, have fixed active and reactive power injections. For these systems, [329] derives necessary and sufficient conditions for the existence and uniqueness of a high-voltage power flow solution. Additionally, [329] shows that three solution methods (a fixed-point iteration proposed in [329], a variant of Jabr's SOCP relaxation [194] (see §4.2.1), and an energy function approach from [436]) all successfully find the high-voltage power flow solution for this class of systems, if the high-voltage solution exists. Finally, for this class of systems, [329] shows that:

- At the high-voltage solution, the voltage magnitudes are increasing functions of the reactive power injections.

- The high-voltage solution is a continuous function of the power injections.
- The high-voltage solution is the last to vanish as the system is loaded past the power flow solvability boundary.

Reference [113] also considers systems with balanced radial networks where every line has a uniform resistance-to-reactance ratio and all buses, with the exception of a single slack bus, have fixed active and reactive power injections. For such systems, [113] proves that the feasible spaces are convex. Moreover, [113] shows that arbitrarily small non-uniformities in the resistance-to-reactance ratios can result in non-convex feasible spaces for some problems. However, the active power feasible space (i.e., the set of active power injections for which there exists some feasible choice of reactive power injections) is convex for non-uniform resistance-to-reactance ratios. Additionally, [113] shows that the active power feasible space is convex for purely resistive networks regardless of their topology. Since the convex hull of any set of points in a convex feasible space is a convex restriction, it is straightforward to extend the convexity results in [113] to obtain convex restrictions.

Other recent work in [429] considers regions called “domains of \mathcal{V} -control” for three-phase unbalanced systems without PV buses. These regions are sets of power injections \mathcal{S} and voltage phasors \mathcal{V} (that satisfy specified voltage magnitude limits) for which 1) every choice of power injections in \mathcal{S} has exactly one corresponding power flow solution in \mathcal{V} and 2) any continuous trajectory of voltage phasors that starts in \mathcal{V} stays in \mathcal{V} as long as the corresponding power injection trajectory stays in \mathcal{S} . Reference [429] provides sufficient conditions for a region to be a domain of \mathcal{V} -control and a heuristic method for constructing these regions. Reference [429] also proves that local uniqueness of a power flow solution guarantees non-singularity of the power flow Jacobian matrix. Subsequent work in [437] proposes sufficient conditions for existence and uniqueness of power flow solutions and describes a polynomial-time algorithm for constructing domains of \mathcal{V} control that is an alternative to the heuristic method in [429].

Note that convex restrictions can also be established for individual inequality constraints in power system optimization problems. For

instance, the approach in [438, 439] constructs linear constraints which guarantee satisfaction of limits on the magnitudes of branch current flows, which are themselves given by non-linear expressions of the voltage phasors. The numerical analyses in [438, 439] demonstrate that replacing current flow constraints with these convex restrictions (while maintaining a non-convex power flow representation) improves computational tractability of the resulting optimization problem.

Reference [440] also focuses on the inequality constraints, seeking to certify that no choice of power injections within a specified uncertainty set has a corresponding power flow solution that violates limits on, e.g., voltage magnitudes and line flows. Convex relaxations and bound tightening techniques (see §4.4.1) are used to obtain conservative bounds the worst-case impacts of any possible uncertainty realization. If bounds on the most extreme achievable voltage magnitudes and line flows are within their specified limits, no uncertainty realization can cause inequality constraint violations. Certificates ensuring satisfaction of the inequality constraints are valuable for facilitating the use of “grid-agnostic” distributed energy resource controllers that do not model the distribution network. Moreover, [441] applies a related approach to solve robust OPF problems, which seek minimum-cost operating points that are secure with respect to all power injection fluctuations within a specified uncertainty set. Note that the algorithms in [440, 441] do not guarantee power flow solvability for all uncertainty realizations, only that any existing power flow solutions will satisfy the inequality constraints corresponding to the engineering limits. Also note that the algorithms in [440, 441] are applicable to systems with both PV and PQ buses as well as both radial and mesh network topologies. Finally, note that [442] also uses convex restriction techniques to solve certain robust AC OPF problems. Specifically, the approach in [442] is applicable to problems where all buses have generation or controllable loads such that all nodal power balance constraints can be modeled with inequalities.

7

Conclusion

This monograph has surveyed the literature of power flow representations, including both relaxations and approximations. Relaxations enclose the feasible space of the original non-convex problem in a convex space, thus providing bounds on the optimal objective value, the potential to certify problem infeasibility, and, for some problems, the global optimum. Approximations simplify the power flow equations using a variety of assumptions regarding both operating conditions (e.g., near nominal voltage magnitudes) and mathematical expressions (e.g., small angle approximations).

This concluding chapter provides a tabular summary of the surveyed power flow representations and a discussion regarding several open questions and future research directions.

7.1 Summary of the Power Flow Representations

The power flow representations reviewed in this paper are summarized in Table 7.1. The first column provides the name of the relaxation or approximation. The second column shows the type of optimization tool (SDP, SOCP, or LP) used to solve the corresponding representation. Depending on the form of the objective function, note that both linear

programming and quadratic programming solvers can be applied to the representations which have “LP” listed in the second column. The third column indicates whether a three-phase formulation is currently available and provides associated references. The fourth column provides brief notes on the power flow representation, such as theoretical guarantees and assumptions used in the representation’s derivation. The fifth column provides selected references for each power flow representation and the corresponding section of the monograph.

7.1. Summary of the Power Flow Representations

Table 7.1: Summary of power flow representations.

Name	Optim. Tool	Three-Phase	Notes	Selected References
RELAXATIONS				
Shor Relaxation	SDP	[159, 167–169]	Sufficient conditions for exactness (certain network topologies and technical conditions).	[141, 162–164, 197, 203], §4.1.1
Lasserre Moment Hierarchy	SDP	No	Guaranteed to converge to the global optimum with increasing relaxation order.	[219, 222, 227, 241–245], §4.1.2
Complex Moment Hierarchy	SDP	No	Guaranteed to converge to the global optimum with increasing relaxation order.	[129, 229], §4.1.2
Mixed SDP/SOCP Hierarchy	SDP & SOCP	No		[233], §4.1.2
SDSOS, DSOS Hierarchies	SOCP	No		[234–238], §4.1.2
Jabr’s Relaxation	SOCP*	[168]	Sufficient conditions for exactness (radial networks and satisfaction of technical conditions, etc.). Equivalent tightness as the DistFlow relaxation.	[194, 257], §4.2.1
QC Relaxation	SOCP	No		[143, 155, 176, 254, 258, 259], §4.2.1
Strong SOCP Relaxation	SOCP	No		[255, 256], §4.4.2
DistFlow Relaxation	SOCP*	[146, 167–169]	Sufficient conditions for exactness (radial networks and satisfaction of technical conditions, etc.). Equivalent tightness as Jabr’s relaxation.	[74, 75, 271], §4.2.2

* Three-phase formulations are semidefinite programs.

Table 7.1 – *Continued*

Name	Optim. Tool	Three-Phase	Notes	Selected References
Δ , Loss, Circle Inequalities	SOCP	No		[269, 270], §4.2.2
Network Flow	LP	No	Requires all lines to have series impedances with non-negative resistances and non-negative reactances.	[285], §4.3.1
Copper Plate	LP	No	Requires all lines to have series impedances with non-negative resistances and non-negative reactances.	[285], §4.3.2
Taylor-Hoover	LP	No		[288], §4.3.3
McCormick	LP	No		[125, 255, 307, 308], §4.3.4
Bienstock-Muñoz LP Relaxations	LP	No	Arbitrarily accurate solutions for sufficiently large LPs.	[292], §4.3.5
MILP Discretizations	MILP	No	Arbitrarily accurate solutions for sufficiently fine discretization tolerances.	[269, 295, 443], §4.3.6
APPROXIMATIONS				
Jabr's Approximation	SOCP	No	Linearization of the arctangent function and iteratively refined estimate of the voltage angles.	[72], §5.1.1
QPAC	SOCP	No	Second-order Taylor expansions of the sine and cosine functions, tangent approximations of the squared voltage magnitude functions, unity voltage magnitude products between connected buses, quadratic inequalities relaxed to equalities.	[310], §5.1.2
Baradar–Hesamzadeh	SOCP	No	Applies the small angle and nominal voltage magnitude approximations to an angle consistency constraint.	[148, 311–313], §5.1.3

7.1. Summary of the Power Flow Representations

167

Table 7.1 – *Continued*

Name	Optim. Tool	Three-Phase	Notes	Selected References
Linearization around an operating point	LP	[335, 336]	Can compute worst-case error bounds. Based on the choice of a nearby operating point. Certain specific operating points are particularly well-studied, providing theory related to solution existence in radial networks and error bounds.	[59–64, 97, 314, 315, 317–320, 322–325, 328, 330–333, 335, 336, 367], §5.2.1
Decoupled Power Flow	LP	No	Assumes near nominal voltage magnitudes, small angle differences, and high reactance-to-resistance ratios.	[337, 338], §5.2.2
DC Power Flow	LP	No	Small angle approximation, near-nominal voltage magnitudes, negligible losses, and ignores reactive power. Various attempts to generalize these assumptions.	[327, 342–350, 350, 351, 355–357, 359], §5.2.3
Linear Reactive Power Flow	LP	No	Assumptions based on small angle approximation, decoupled power flow, and lossless network.	[362, 363], §5.2.4
Linearized DistFlow	LP	[168, 364–366]	Underestimates active and reactive power flows and overestimates voltage magnitudes. Requires a radial network topology and assumes small active and reactive losses.	[69, 74, 168, 364–366], §5.2.5
LPAC	LP	No	Linear relaxation of the cosine function, linearization of the sine function, and near nominal voltage magnitudes.	[368], §5.2.6

Table 7.1 – *Continued*

Name	Optim. Tool	Three-Phase	Notes	Selected References
Current Injection Linearization	LP	[62, 63, 370]	Linear relationship between current injections and voltages implied by the network equations in combination with a linearization of the non-linear voltage and current relationships implied by the ZIP load model.	[59–64, 369–371], §5.2.7
Optimal Adaptive Linearizations	LP	No	Computes the linearization that minimizes a selected error metric for a specific system and operational range.	[372, 373], §5.2.8
Loss Approximations	MILP, LP	No	Losses approximated using the squared differences in angles. Alternative approach incorporates voltage magnitude effects. Possible relaxation of binary-constrained variables.	[320, 358, 375, 378], §5.2.9
TECHNIQUES FOR FINDING FEASIBLE POINTS				
Newton-based Algorithms	–	–	Reduce mismatches in the power flow equations by iteratively updating a linearization.	[91–93], §6.1.1
Backward/Forward Sweep Algorithms	–	–	By iterating backward and forward along a radial network, reduce mismatches in the power flow equations by updating values for active and reactive power flows, squared current flows, and squared voltage magnitudes.	[384–386], §6.1.1
Continuation Algorithms	–	–	Use a predictor–corrector homotopy to solve the power flow equations starting from a solution corresponding to different parameter values.	[100, 389–391], §6.1.1

7.1. Summary of the Power Flow Representations

Table 7.1 – *Continued*

Name	Optim. Tool	Three-Phase	Notes	Selected References
Interior Point Algorithms	–		Apply a Newton-based iteration to solve the KKT conditions of an optimization formulation that models inequality constraints via a log-barrier term in the objective function.	[24, 124, 392–394, 398–401], §6.1.2
Sequential Quadratic Programming	–		Iteratively solve particularly constructed quadratic programs based on first-order Taylor linearizations of the constraints and a second-order Taylor approximation of the Lagrangian function.	[16, 124, 392, 403], §6.1.2
Penalized SDP	SDP	No	With appropriate choice of penalty, the solution to the penalized problem is often close to the global solution of the original problem.	[98, 173, 187, 188, 219, 366, 410–413], §6.2
Successive Convex Approximations	SOCP	No	Converge to a KKT point of the non-convex optimization problem.	[240, 415–417, 419, 420], §5.1
Convex Restrictions	SDP, SOCP	No	Provide upper bounds on optimal objective value, sufficient conditions to certify feasibility.	[65, 113, 275, 329, 332, 415, 416, 421–426, 429], §6.4

- Many of the power flow representations can be strengthened using the approaches in §4.4.
 - A relaxation which dominates another (see Figure 4.8) inherits the guarantees of the dominated relaxation.
- See §4.1.1, §4.1.2, and §4.2.3 for discussions of the sufficient conditions for exactness for various relaxations.

7.2 Future Research Directions

Significant progress has been made in developing power flow formulations that are useful in a variety of contexts. However, there remain open questions that are deserving of further investigation. This section provides a non-exhaustive overview of open questions and future research directions.

- *Extension to unbalanced three-phase network models.* Many of the power flow representations considered in this survey have already been extended to consider unbalanced three-phase network models. Such extensions are potentially possible for other power flow representations, which would generalize their applicability to include typical models of distribution networks.
- *Further development of tightening approaches.* Tightening approaches such as those described in §4.4 are a subject of significant recent interest. In addition to creating new techniques, the existing approaches would benefit from further development. Possible topics include formulating higher-order versions of the valid constraints described in §4.4.2 for the moment/sum-of-squares hierarchies in §4.1.2, tightening the arctangent envelopes described in §4.4.2 to more closely enclose the convex hull of the arctangent function, and advancing bound tightening techniques in order to further tighten the relaxations. Improving the computational tractability of the various tightening approaches is another topic that could benefit from additional work.
- *Further characterization of dominance relationships among relaxations.* The relative tightness of a variety of power flow relaxations has been characterized in [74, 122, 129, 176, 254, 255, 285]. (See Figure 4.8.) Determining other dominance relationships (or proving the lack thereof using counterexamples) is a topic worthy of future research.
- *Ascertaining best practices for combining various power flow relaxations and tightening procedures.* As discussed in §4.4.2, combining

non-dominated relaxations and applying the other approaches discussed in §4.4 results in tighter relaxations. However, improved tightness may come at the cost of increased computational burden. Identifying best practices for balancing this trade-off is an important research objective.

- *Empirical error analyses.* All of the relaxations and approximations described in this survey introduce the possibility of errors relative to the non-linear power flow equations. These errors can be characterized using empirical approaches. For instance, [129, 171, 176, 233, 254, 255, 328, 330, 331, 352, 353, 358, 368, 444, 445] provide empirical comparisons among subsets of the power flow representations regarding characteristics that include the tightness of the objective value bounds, constraint violations, and computational speeds. Researchers and practitioners would benefit from further empirical analyses in order to remain up-to-date with this rapidly advancing research area. Analyses that consider specific problem settings would be particularly valuable (e.g., various network topologies and parameter ranges, applications requiring discrete variables [152, 353], and inclusion of methods for considering uncertainty such as chance constraints [446–451] or scenario-based approaches [416, 452–455]).
- *Analytical error analyses.* Errors in the power flow representations can also be characterized using analytical methods. For instance, [357] uses convex relaxation techniques to bound the worst-case error in the DC power flow approximation (see §5.2.3) over a specified range of operating conditions. (Other analytical error bounding methods are discussed in [314] and [332].) Similar approaches could be applied to develop worst-case error bounds for other power flow representations. Future work can also build upon the analytical techniques for power flow error analyses in [330] and [331].
- *Study of challenging test cases.* While existing power flow representations show promise for certain test cases and applications (e.g., OPF problems for many of the IEEE test cases), there

remain challenging problems deserving of further study. For instance, the PGLib archive has a variety of OPF test cases that exhibit non-negligible optimality gaps [179]. Closing these gaps is a topic of ongoing research, and further analyses will be needed to study the wide variety of test cases that are currently under development [180]. Other relevant work includes studying the feasible spaces of power system optimization problems and their relaxations to characterize both challenging and straightforward cases [3, 98, 100–114].

- *Exploration of synergies between local solution algorithms and various power flow representations.* There exist many mature local solution algorithms applicable to the non-convex optimization problems that result from the non-linear power flow equations, with the surveys [13–15] providing a comprehensive overview. Many of the power flow representations reviewed in this monograph have capabilities that are synergistic with local solution techniques. For instance, the bounds available from convex relaxations provide measures of the potential suboptimality of solutions from local solvers. Additionally, the solutions to the power flow representations considered in this monograph can serve as initializations for some local solvers, which can speed computations and encourage convergence to a better solution [450, 456, 457]. Additionally, by leveraging the KKT conditions for the Shor relaxation, the primal and dual variables from a local solution can be used to quickly compute a sufficient condition for global optimality [220]. Dual variables from a local solution can also be used to speed the computation of objective value bounds provided by the Shor relaxation [206]. Further development of these and other such synergies is an important direction for future research.
- *Exploitation of alternative convex optimization tools.* While LP, SOCP, and SDP formulations of the power flow equations have been applied to a variety of problems, there are several other convex programming tools that have not yet found widespread applications in power systems. Some of these tools have been applied to other network optimization problems. For instance,

geometric programming [458] has been used to represent natural gas flows [459]. Future work may discover applications of such tools to power system optimization problems.

- *Consideration of different coordinate systems.* Expressing the power flow variables in different coordinate systems may result in power flow representations with differing characteristics. For instance, the DistFlow model (2.7) yields the SOCP relaxations discussed in §4.2.2, while the bus injection model (2.3) yields quadratically constrained quadratic programs that can be addressed using polynomial optimization tools such as the Shor relaxation and the moment relaxation hierarchies described in §4.1. The power flow equations can be formulated in other coordinate systems, which may yield representations with desirable properties. The study of alternative coordinate systems is deserving of further work. Further discussion is provided in §4.4.4.
- *Derivation of sufficient conditions for exactness of various convex relaxations.* As summarized in §4.1.1, §4.1.2, and §4.2.3, there exists a substantial body of work regarding sufficient conditions under which several relaxations are guaranteed to be exact. However, empirical results show that many relaxations are exact for a much broader class of problems than guaranteed by existing sufficient conditions. Derivations of more general sufficient conditions would therefore be welcome contributions.
- *Identifying problem modifications that tend to result in exactness of a relaxation.* For cases where a relaxation fails to be exact, a perturbation to the problem may result in exactness of the relaxation in some instances. For example, enforcing a small minimum resistance on all lines results in exactness of the Shor relaxation for the IEEE 118-bus system with the nominal loading scenario and an objective function that minimizes generation cost [164]. Additionally, the penalization approaches discussed in §6.2 perturb the objective function with a penalty term in an attempt to obtain an exact relaxation to the penalized problem. The perturbations employed in such approaches must be chosen appropriately since

not all perturbations result in exactness of a relaxation. Moreover, even if a perturbation results in an exact relaxation, the corresponding solution may be far from the global optimum of the original non-convex problem. Future research directions include the development of more systematic approaches for identifying appropriate perturbations and better characterizations of their effectiveness.

- *Development of distributed algorithms.* Distributed algorithms that reduce or eliminate the need for centralized calculations are of increasing interest due to their potential advantages in sharing the computational tasks and communication burdens while maintaining privacy. As discussed in §4.1.1 and §4.2.4, distributed algorithms have been developed using several power flow representations. See [42–45] for detailed surveys of distributed optimization and control algorithms in a power systems context. Extension of these and other distributed algorithms using the power flow representations discussed in this monograph may prove advantageous for addressing operational challenges in future power systems.
- *Use of the power flow representations in a variety of applications.* The power flow equations are at the heart of many power system optimization and control problems. The recent advances in power flow representations detailed in this survey are thus applicable to a wide variety of problems. While existing work has largely focused on OPF problems, other research considers, e.g., state estimation [175, 409, 456, 460, 461], transmission switching and distribution network reconfiguration [152, 154–156, 462–467], multiperiod optimization with storage [457, 468], multi-objective problems [469], infrastructure planning [19, 69, 312, 445, 470–472], stochastic optimization [151, 416, 441, 450–455, 473], contingency analysis [183, 187, 352, 474–476], unit commitment [247, 309, 477–481], system restoration [353, 482], online (real-time) OPF [45, 483–486], electricity pricing [487], voltage stability margins [433, 488–491], and voltage constraint satisfaction [248, 440]. Much research is still required to further extend many of the power flow representations to these and other applications. Developing new power flow

7.2. Future Research Directions

175

representations that are specialized for particular applications is another important direction for future work.

Acknowledgements

The authors gratefully acknowledge discussions with Cédric Josz regarding the semidefinite programming relaxations, Mohammad Rasoul Narimani regarding the formulation of the QC relaxation, Bissan Ghaddar regarding the SDSOS hierarchies, and Andreas Wächter regarding local solution algorithms. The authors also greatly appreciate the valuable feedback and suggestions in the reviews from Carleton Coffrin and another anonymous reviewer.

The work by Daniel Molzahn was supported by the U.S. Department of Energy, Office of Electricity Delivery and Energy Reliability under contract DE-AC-02-06CH11357.

The work by Ian Hiskens was supported by the U.S. National Science Foundation through the grant CNS-1238962, “Foundations of Resilient Cyber-Physical Systems”.

Figures 2.3, 2.4, 2.5, 2.6, 2.7, 4.5, 4.11, and 6.1 are modified versions of figures originally presented in [100], [122], [103], [107], [107], [227], [263], and [100], respectively. These figures are reprinted with permission from IEEE.

References

- [1] D. Bienstock and A. Verma, “Strong NP-hardness of AC Power Flows Feasibility,” *arXiv:1512.07315*, December 2015.
- [2] K. Lehmann, A. Grastien, and P. Van Hentenryck, “AC-Feasibility on Tree Networks is NP-Hard,” *IEEE Transactions on Power Systems*, vol. 31, no. 1, pp. 798–801, January 2016.
- [3] W. A. Bukhsh, A. Grothey, K. I. M. McKinnon, and P. A. Trodden, “Local Solutions of the Optimal Power Flow Problem,” *IEEE Transactions on Power Systems*, vol. 28, no. 4, pp. 4780–4788, 2013.
- [4] A. M. Sasson and H. M. Merrill, “Some Applications of Optimization Techniques to Power Systems Problems,” *Proceedings of the IEEE*, vol. 62, no. 7, pp. 959–972, July 1974.
- [5] J. A. Momoh, *Electric Power System Applications of Optimization*. CRC Press, 2008.
- [6] P. W. Sauer and M. A. Pai, *Power System Dynamics and Stability*. Prentice Hall, 1998.
- [7] A. J. Wood, B. F. Wollenberg, and G. B. Sheble, *Power Generation, Operation and Control*. John Wiley and Sons, Inc., third ed., 2013.
- [8] B. Stott, “Review of Load-Flow Calculation Methods,” *Proceedings of the IEEE*, vol. 62, no. 7, pp. 916–929, July 1974.
- [9] D. Mehta, D. K. Molzahn, and K. Turitsyn, “Recent Advances in Computational Methods for the Power Flow Equations,” in *American Control Conference (ACC)*, (Boston, MA, USA), pp. 1753–1765, July 2016.

- [10] H. H. Happ, "Optimal Power Dispatch – A Comprehensive Survey," *IEEE Transactions on Power Apparatus and Systems*, vol. 96, no. 3, pp. 841–854, 1977.
- [11] S. N. Talukdar and F. F. Wu, "Computer-Aided Dispatch for Electric Power Systems," *Proceedings of the IEEE*, vol. 69, no. 10, pp. 1212–1231, October 1981.
- [12] J. L. Carpentier, "Optimal Power Flows: Uses, Methods and Developments," in *IFAC Symposium on Planning and Operation of Electric Energy Systems*, vol. 18, (Rio de Janeiro, Brazil), pp. 11–21, July 1985.
- [13] M. Huneault and F. D. Galiana, "A Survey of the Optimal Power Flow Literature," *IEEE Transactions on Power Systems*, vol. 6, no. 2, pp. 762–770, May 1991.
- [14] J. A. Momoh, R. Adapa, and M. E. El-Hawary, "A Review of Selected Optimal Power Flow Literature to 1993. Parts I and II," *IEEE Transactions on Power Systems*, vol. 14, no. 1, pp. 96–111, February 1999.
- [15] Z. Qiu, G. Deconinck, and R. Belmans, "A Literature Survey of Optimal Power Flow Problems in the Electricity Market Context," in *IEEE Power Systems Conference and Exposition (PSCE)*, (Seattle, WA, USA), pp. 1–6, March 2009.
- [16] S. Frank, I. Steponavice, and S. Rebennack, "Optimal Power Flow: A Bibliographic Survey, Parts I and II," *Energy Systems*, vol. 3, no. 3, pp. 221–289, 2012.
- [17] A. Castillo and R. P. O'Neill, "Survey of Approaches to Solving the ACOPF (OPF Paper 4)," tech. rep., US Federal Energy Regulatory Commission, March 2013.
- [18] P. Panciatici, M. C. Campi, S. Garatti, S. H. Low, D. K. Molzahn, X. A. Sun, and L. Wehenkel, "Advanced Optimization Methods for Power Systems," in *18th Power Systems Computation Conference (PSCC)*, (Wroclaw, Poland), pp. 1–18, August 2014.
- [19] J. A. Taylor, *Convex Optimization of Power Systems*. Cambridge University Press, April 2015.
- [20] S. Frank and S. Rebennack, "An Introduction to Optimal Power Flow: Theory, Formulation, and Examples," *IIE Transactions*, vol. 48, no. 12, pp. 1172–1197, 2016.
- [21] H. Abdi, S. D. Beigvand, and M. L. Scala, "A Review of Optimal Power Flow Studies applied to Smart Grids and Microgrids," *Renewable and Sustainable Energy Reviews*, vol. 71, pp. 742–766, May 2017.

- [22] B. Stott, O. Alsaç, and A. J. Monticelli, "Security Analysis and Optimization," *Proceedings of the IEEE*, vol. 75, no. 12, pp. 1623–1644, December 1987.
- [23] B. Stott and O. Alsaç, "Optimal Power Flow—Basic Requirements for Real-Life Problems and their Solutions," in *12th Symposium of Specialists in Electric Operational and Expansion Planning (SEPOPE)*, (Rio de Janeiro, Brazil), May 2012.
- [24] F. Capitanescu, J. L. M. Ramos, P. Panciatici, D. Kirschen, A. M. Marcolini, L. Platbrood, and L. Wehenkel, "State-of-the-Art, Challenges, and Future Trends in Security Constrained Optimal Power Flow," *Electric Power Systems Research*, vol. 81, no. 8, pp. 1731–1741, 2011.
- [25] F. Capitanescu, "Critical Review of Recent Advances and Further Developments Needed in AC Optimal Power Flow," *Electric Power Systems Research*, vol. 136, pp. 57–68, 2016.
- [26] S. Abhyankar, G. Geng, M. Anitescu, X. Wang, and V. Dinavahi, "Solution Techniques for Transient Stability-Constrained Optimal Power Flow – Part I," *IET Generation, Transmission & Distribution*, vol. 11, pp. 3177–3185, August 2017.
- [27] G. Geng, S. Abhyankar, X. Wang, and V. Dinavahi, "Solution Techniques for Transient Stability-Constrained Optimal Power Flow – Part II," *IET Generation, Transmission & Distribution*, vol. 11, pp. 3186–3193, August 2017.
- [28] S. Sen and D. P. Kothari, "Optimal Thermal Generating Unit Commitment: A Review," *International Journal of Electrical Power & Energy Systems*, vol. 20, no. 7, pp. 443–451, 1998.
- [29] N. P. Padhy, "Unit Commitment—A Bibliographical Survey," *IEEE Transactions on Power Systems*, vol. 19, no. 2, pp. 1196–1205, May 2004.
- [30] M. Tahanan, W. Van Ackooij, A. Frangioni, and F. Lacalandra, "Large-Scale Unit Commitment Under Uncertainty," *4OR*, vol. 13, no. 2, pp. 115–171, 2015.
- [31] W. van Ackooij, I. Danti Lopez, A. Frangioni, F. Lacalandra, and M. Tahanan, "Large-Scale Unit Commitment Under Uncertainty: An Updated Literature Survey," *Annals of Operations Research*, vol. 271, no. 1, pp. 11–85, December 2018.
- [32] F. F. Wu, "Power System State Estimation: A Survey," *International Journal of Electrical Power & Energy Systems*, vol. 12, no. 2, pp. 80–87, 1990.

- [33] A. Monticelli, *State Estimation in Electric Power Systems*. Kluwer Academic Publishers, 1999.
- [34] A. Abur and A. Gómez Expósito, *Power System State Estimation: Theory and Implementation*. Marcel Dekker, 2004.
- [35] V. Kekatos, G. Wang, H. Zhu, and G. B. Giannakis, “PSSE Redux: Convex Relaxation, Decentralized, Robust, and Dynamic Approaches,” *arXiv:1708.03981*, August 2017.
- [36] K. W. Hedman, S. S. Oren, and R. P. O’Neill, “A Review of Transmission Switching and Network Topology Optimization,” in *IEEE Power & Energy Society General Meeting*, pp. 1–7, July 2011.
- [37] C. W. Taylor, “Modeling of Voltage Collapse Including Dynamic Phenomena.” CIGRE Task Force 38-02-10 Report, 1993.
- [38] N. D. Hatziargyriou, J. van Hecke, and T. van Cutsem, “Indices Predicting Voltage Collapse Including Dynamic Phenomena.” CIGRE Task Force 38.02.11 Report, 1994.
- [39] I. Dobson, T. Van Cutsem, C. Vournas, C. L. DeMarco, M. Venkatasubramanian, T. Overbye, and C. A. Canizares, “Voltage Stability Assessment: Concepts, Practices and Tools.” IEEE Power Engineering Society, Power System Stability Subcommittee Special Publication SP101PSS, August 2002.
- [40] C. W. Taylor, *Power System Voltage Stability*. McGraw-Hill, 1994.
- [41] M. Vaiman, K. Bell, Y. Chen, B. Chowdhury, I. A. Dobson, P. Hines, M. Papic, S. Miller, and P. Zhang, “Risk Assessment of Cascading Outages: Methodologies and Challenges,” *IEEE Transactions on Power Systems*, vol. 27, no. 2, pp. 631–641, May 2012.
- [42] M. Yazdanian and A. Mehrizi-Sani, “Distributed Control Techniques in Microgrids,” *IEEE Transactions on Smart Grid*, vol. 5, no. 6, pp. 2901–2909, November 2014.
- [43] H. Han, X. Hou, J. Yang, J. Wu, M. Su, and J. M. Guerrero, “Review of Power Sharing Control Strategies for Islanding Operation of AC Microgrids,” *IEEE Transactions on Smart Grid*, vol. 7, no. 1, pp. 200–215, January 2016.
- [44] A. Kargarian, J. Mohammadi, J. Guo, S. Chakrabarti, M. Barati, G. Hug, S. Kar, and R. Baldick, “Toward Distributed/Decentralized DC Optimal Power Flow Implementation in Future Electric Power Systems,” *IEEE Transactions on Smart Grid*, vol. 9, no. 4, pp. 2574–2594, July 2018.

- [45] D. K. Molzahn, F. Dörfler, H. Sandberg, S. H. Low, S. Chakrabarti, R. Baldick, and J. Lavaei, “A Survey of Distributed Optimization and Control Algorithms for Electric Power Systems,” *IEEE Transactions on Smart Grid*, vol. 8, no. 6, pp. 2939–2940, November 2017.
- [46] G. A. Pagani and M. Aiello, “The Power Grid as a Complex Network: A Survey,” *Physica A: Statistical Mechanics and its Applications*, vol. 392, no. 11, pp. 2688–2700, 2013.
- [47] F. Geth, R. D’Hulst, and D. Van Hertem, “Convex Power Flow Models for Scalable Electricity Market Modelling,” in *24th International Conference & Exhibition on Electricity Distribution (CIRED)*, no. 1, (Glasgow, Scotland, UK), pp. 989–993, June 2017.
- [48] G. Wang and H. Hijazi, “Mathematical Programming Methods for Microgrid Design and Operations: A Survey on Deterministic and Stochastic Approaches,” *Computational Optimization and Applications*, June 2018.
- [49] C. Coffrin and L. A. Roald, “Convex Relaxations in Power System Optimization: A Brief Introduction,” *arXiv:1807.07227*, July 2018. videos available at https://www.youtube.com/watch?v=gB43Tmc0UpA&list=PLeuOzWTGxj2ZZ_XUutDwNFvNfSWwWCgR5.
- [50] R. D. Zimmerman, C. E. Murillo-Sánchez, and R. J. Thomas, “MATPOWER: Steady-State Operations, Planning, and Analysis Tools for Power Systems Research and Education,” *IEEE Transactions on Power Systems*, vol. 26, no. 1, pp. 12–19, 2011.
- [51] C. Coffrin, R. Bent, K. Sundar, Y. Ng, and M. Lubin, “PowerModels.jl: An Open-Source Framework for Exploring Power Flow Formulations,” in *20th Power Systems Computation Conference (PSCC)*, (Dublin, Ireland), June 2018.
- [52] B. C. Lesieutre and D. Wu, “An Efficient Method to Locate All the Load Flow Solutions – Revisited,” in *53rd Annual Allerton Conference on Communication, Control, and Computing (Allerton)*, (Monticello, IL, USA), pp. 381–388, September 2015.
- [53] D. Wu, D. K. Molzahn, B. C. Lesieutre, and K. Dvijotham, “A Deterministic Method to Identify Multiple Local Extrema for the AC Optimal Power Flow Problem,” *IEEE Transactions on Power Systems*, vol. 33, no. 1, pp. 654–668, January 2018.
- [54] Y. C. Chen and S. V. Dhople, “Power Divider,” *IEEE Transactions on Power Systems*, vol. 31, no. 6, pp. 5135–5143, 2016.

- [55] Y. C. Chen, A. Al-Digs, and S. V. Dhople, "Mapping Nodal Power Injections to Branch Flows in Connected LTI Electrical Networks," in *IEEE International Symposium on Circuits and Systems (ISCAS)*, pp. 2146–2149, May 2016.
- [56] D. Chéverez-González and C. L. DeMarco, "Characterization of Feasible LMPs: Inclusion of Losses and Reactive Power," in *39th North American Power Symposium*, (Las Cruces, NM, USA), pp. 440–447, September 2007.
- [57] J. Lin and D. Chéverez-González, "Network-Driven Dynamic Congestion based on Mutually Orthogonal LMP Decomposition," in *8th IREP Symposium on Bulk Power System Dynamics and Control*, (Rio de Janeiro, Brazil), pp. 1–8, August 2010.
- [58] B. Park, J. Netha, M. C. Ferris, and C. L. DeMarco, "Sparse Tableau Formulation for Optimal Power Flow Applications," *arXiv:1706.01372*, June 2017.
- [59] R. P. O'Neill, A. Castillo, and M. B. Cain, "The IV Formulation and Linear Approximations of the AC Optimal Power Flow Problem (OPF Paper 2)," tech. rep., US Federal Energy Regulatory Commission, December 2012.
- [60] D. M. Bromberg, M. Jereminov, X. Li, G. Hug, and L. Pileggi, "An Equivalent Circuit Formulation of the Power Flow Problem with Current and Voltage State Variables," in *IEEE Eindhoven PowerTech*, (Eindhoven, Netherlands), pp. 1–6, June 2015.
- [61] M. Jereminov, D. M. Bromberg, X. Li, G. Hug, and L. Pileggi, "Improving Robustness and Modeling Generality for Power Flow Analysis," in *IEEE PES Transmission and Distribution Conference and Exposition (PES T&D)*, (Dallas, TX, USA), pp. 1–5, May 2016.
- [62] M. Jereminov, D. M. Bromberg, A. Pandey, X. Li, G. Hug, and L. Pileggi, "An Equivalent Circuit Formulation for Three-Phase Power Flow Analysis of Distribution Systems," in *IEEE Power & Energy Society Transmission and Distribution Conference and Exposition (PES T&D)*, (Dallas, TX, USA), pp. 1–5, May 2016.
- [63] A. Pandey, M. Jereminov, X. Li, G. Hug, and L. Pileggi, "Unified Power System Analyses and Models using Equivalent Circuit Formulation," in *IEEE PES Conference on Innovative Smart Grid Technologies (ISGT)*, (Minneapolis, MN, USA), pp. 1–5, September 2016.

- [64] A. Castillo, P. Lipka, J. Watson, S. S. Oren, and R. P. O'Neill, "A Successive Linear Programming Approach to Solving the IV-ACOPF," *IEEE Transactions on Power Systems*, vol. 31, no. 4, pp. 2752–2763, July 2016.
- [65] S. Misra, L. A. Roald, M. Vuffray, and M. Chertkov, "Fast and Robust Determination of Power System Emergency Control Actions," in *10th IREP Symposium on Bulk Power System Dynamics and Control*, (Espinho, Portugal), August 2017.
- [66] A. Trias, "HELM: The Holomorphic Embedding Load-Flow Method. Foundations and Implementations," *Foundations and Trends in Electric Energy Systems*, vol. 3, no. 3–4, pp. 140–370, December 2018.
- [67] T. Chen and D. Mehta, "On the Network Topology Dependent Solution Count of the Algebraic Load Flow Equations," *IEEE Transactions on Power Systems*, vol. 33, no. 2, pp. 1451–1460, March 2018.
- [68] Y. V. Makarov, D. J. Hill, and I. A. Hiskens, "Properties of Quadratic Equations and their Application to Power System Analysis," *International Journal of Electrical Power & Energy Systems*, vol. 22, pp. 313–323, 2000.
- [69] M. E. Baran and F. F. Wu, "Optimal Capacitor Placement on Radial Distribution Systems," *IEEE Transactions on Power Delivery*, vol. 4, no. 1, pp. 725–734, January 1989.
- [70] M. Baran and F. F. Wu, "Optimal Sizing of Capacitors Placed on a Radial Distribution System," *IEEE Transactions on Power Delivery*, vol. 4, no. 1, pp. 735–743, January 1989.
- [71] C. Coffrin, H. L. Hijazi, and P. Van Hentenryck, "DistFlow Extensions for AC Transmission Systems," *arXiv:1506.04773*, June 2014.
- [72] R. A. Jabr, "A Conic Quadratic Format for the Load Flow Equations of Meshed Networks," *IEEE Transactions on Power Systems*, vol. 22, no. 4, pp. 2285–2286, November 2007.
- [73] S. Bose, S. H. Low, T. Teeraratkul, and B. Hassibi, "Equivalent Relaxations of Optimal Power Flow," *IEEE Transactions on Automatic Control*, vol. 60, no. 3, pp. 729–742, 2015.
- [74] S. H. Low, "Convex Relaxation of Optimal Power Flow—Part I: Formulations and Equivalence," *IEEE Transactions on Control of Network Systems*, vol. 1, no. 1, pp. 15–27, March 2014.
- [75] S. H. Low, "Convex Relaxation of Optimal Power Flow—Part II: Exactness," *IEEE Transactions on Control of Network Systems*, vol. 1, no. 2, pp. 177–189, June 2014.

- [76] N. Biggs, *Algebraic Graph Theory*. Cambridge University Press, 1993.
- [77] T. Kavitha, C. Liebchen, K. Mehlhorn, D. Michail, R. Rizzi, T. Ueckerdt, and K. A. Zweig, “Cycle Bases in Graphs Characterization, Algorithms, Complexity, and Applications,” *Computer Science Review*, vol. 3, no. 4, pp. 199–243, 2009.
- [78] J. Baillieul and C. Byrnes, “Geometric Critical Point Analysis of Lossless Power System Models,” *IEEE Transactions on Circuits and Systems*, vol. 29, no. 11, pp. 724–737, 1982.
- [79] D. K. Molzahn, D. Mehta, and M. Niemerg, “Toward Topologically Based Upper Bounds on the Number of Power Flow Solutions,” in *American Control Conference (ACC)*, (Boston, MA, USA), pp. 5927–5932, July 2016.
- [80] O. Coss, J. D. Hauenstein, H. Hoon, and D. K. Molzahn, “Locating and Counting Equilibria of the Kuramoto Model with Rank One Coupling,” *SIAM Journal on Applied Algebra and Geometry*, vol. 2, no. 1, pp. 45–71, 2018.
- [81] W. Ma and S. Thorp, “An Efficient Algorithm to Locate All the Load Flow Solutions,” *IEEE Transactions on Power Systems*, vol. 8, no. 3, pp. 1077–1083, 1993.
- [82] D. Mehta, H. D. Nguyen, and K. Turitsyn, “Numerical Polynomial Homotopy Continuation Method to Locate all the Power Flow Solutions,” *IET Generation, Transmission & Distribution*, vol. 10, no. 12, pp. 2972–2980, 2016.
- [83] A. Zacariah, Z. Charles, N. Boston, and B. C. Lesieutre, “Distributions of the Number of Solutions to the Network Power Flow Equations,” in *International Symposium on Circuits and Systems (ISCAS)*, (Florence, Italy), May 2018.
- [84] J. Y. Jackson, “Interpretation and Use of Generator Reactive Capability Diagrams,” *IEEE Transactions on Industry and General Applications*, no. 6, pp. 729–732, 1971.
- [85] P. Kundur, N. J. Balu, and M. G. Lauby, *Power System Stability and Control*. McGraw-hill New York, 1994.
- [86] D. Kosterev, A. Meklin, J. Undrill, B. Lesieutre, W. Price, D. Chassin, R. Bravo, and S. Yang, “Load Modeling in Power System Studies: WECC Progress Update,” in *IEEE Power & Energy Society General Meeting*, (Pittsburgh, PA, USA), pp. 1–8, 2008.
- [87] E. C. M. Stahl, “Economic Loading of Generating Stations,” *Electrical Engineering*, vol. 50, no. 9, pp. 722–727, September 1931.

- [88] M. J. Steinberg and T. H. Smith, *Economy Loading of Power Plants and Electric Systems*. Wiley, 1943.
- [89] L. K. Kirchmeyer, *Economic Operation of Power Systems*. Wiley New York, 1958.
- [90] J. B. Ward and H. W. Hale, “Digital Computer Solution of Power-Flow Problems,” *Transactions of the American Institute of Electrical Engineers. Part III: Power Apparatus and Systems*, vol. 75, no. 3, pp. 398–404, January 1956.
- [91] J. E. Van Ness, “Iteration Methods for Digital Load Flow Studies,” *Transactions of the American Institute of Electrical Engineers. Part III: Power Apparatus and Systems*, vol. 78, no. 3, pp. 583–586, April 1959.
- [92] N. Sato and W. F. Tinney, “Techniques for Exploiting the Sparsity or the Network Admittance Matrix,” *IEEE Transactions on Power Apparatus and Systems*, vol. 82, no. 69, pp. 944–950, December 1963.
- [93] W. F. Tinney and C. E. Hart, “Power Flow Solution by Newton’s Method,” *IEEE Transactions on Power Apparatus and Systems*, vol. PAS-86, no. 11, pp. 1449–1460, November 1967.
- [94] H. H. Spencer and H. L. Hazen, “Artificial Representation of Power Systems,” *Transactions of the American Institute of Electrical Engineers*, vol. XLIV, pp. 72–79, January 1925.
- [95] R. B. Squires, “Economic Dispatch of Generation Directly From Power System Voltages and Admittances,” *Transactions of the American Institute of Electrical Engineers. Part III: Power Apparatus and Systems*, vol. 79, no. 3, pp. 1235–1244, April 1960.
- [96] J. L. Carpentier, “Contribution a l’Etude du Dispatching Economique,” *Bulletin de la Societe Francaise des Electriques*, vol. 8, no. 3, pp. 431–447, 1962.
- [97] R. D. Zimmerman, “AC Power Flows, Generalized OPF Costs and their Derivatives using Complex Matrix Notation,” tech. rep., MATPOWER Technical Note 2, February 2010.
- [98] R. Madani, S. Sojoudi, and J. Lavaei, “Convex Relaxation for Optimal Power Flow Problem: Mesh Networks,” *IEEE Transactions on Power Systems*, vol. 30, no. 1, pp. 199–211, January 2015.
- [99] B. Park, L. Tang, M. C. Ferris, and C. L. DeMarco, “Examination of Three Different ACOPF Formulations With Generator Capability Curves,” *IEEE Transactions on Power Systems*, vol. 32, no. 4, pp. 2913–2923, July 2017.

- [100] I. A. Hiskens and R. J. Davy, "Exploring the Power Flow Solution Space Boundary," *IEEE Transactions on Power Systems*, vol. 16, no. 3, pp. 389–395, August 2001.
- [101] B. C. Lesieutre and I. A. Hiskens, "Convexity of the Set of Feasible Injections and Revenue Adequacy in FTR Markets," *IEEE Transactions on Power Systems*, vol. 20, no. 4, pp. 1790–1798, November 2005.
- [102] Y. V. Makarov, Z. Y. Dong, and D. J. Hill, "On Convexity of Power Flow Feasibility Boundary," *IEEE Transactions on Power Systems*, vol. 23, no. 2, pp. 811–813, May 2008.
- [103] D. K. Molzahn, B. C. Lesieutre, and C. L. DeMarco, "Investigation of Non-Zero Duality Gap Solutions to a Semidefinite Relaxation of the Power Flow Equations," in *47th Hawaii International Conference on Systems Sciences (HICSS)*, (Waikoloa, HI, USA), pp. 2325–2334, January 2014.
- [104] J. Lavaei, D. Tse, and B. Zhang, "Geometry of Power Flows and Optimization in Distribution Networks," *IEEE Transactions on Power Systems*, vol. 29, no. 2, pp. 572–583, March 2014.
- [105] S. Chandra, D. Mehta, and A. Chakrabortty, "Equilibria Analysis of Power Systems Using a Numerical Homotopy Method," in *IEEE Power & Energy Society General Meeting*, (Denver, CO, USA), pp. 1–5, July 2015.
- [106] B. Polyak and E. Gryazina, "Convexity/Nonconvexity Certificates for Power Flow Analysis," in *Proceedings of the First International Symposium on Energy System Optimization (ISESO)*, (Heidelberg, Germany), pp. 221–230, November 2015.
- [107] D. K. Molzahn, "Computing the Feasible Spaces of Optimal Power Flow Problems," *IEEE Transactionson Power Systems*, vol. 32, no. 6, pp. 4752–4763, November 2017.
- [108] H. D. Chiang and C. Y. Jiang, "Feasible Region of Optimal Power Flow: Characterization and Applications," *IEEE Transactions on Power Systems*, vol. 33, no. 1, pp. 236–244, January 2018.
- [109] M. R. Narimani, D. K. Molzahn, D. Wu, and M. L. Crow, "Empirical Investigation of Non-Convexities in Optimal Power Flow Problems," in *American Control Conference (ACC)*, (Milwaukee, WI, USA), June 2018.
- [110] D. K. Molzahn, "Identifying and Characterizing Non-Convexities in Feasible Spaces of Optimal Power Flow Problems," *IEEE Transactions on Circuits and Systems II: Express Briefs*, vol. 65, no. 5, pp. 672–676, May 2018.

- [111] K. Bestuzheva and H. Hijazi, “Invex Optimization Revisited,” *Journal of Global Optimization*, April 2018.
- [112] F. Thams, A. Venzke, R. Eriksson, and S. Chatzivasileiadis, “Efficient Database Generation for Data-driven Security Assessment of Power Systems,” *arXiv:1806.01074*, June 2018.
- [113] A. Dymarsky and K. Turitsyn, “Convexity of Solvability Set of Power Distribution Networks,” *arXiv:1803.11197*, March 2018.
- [114] A. Dymarsky, E. Gryazina, S. Volodin, and B. Polyak, “Geometry of Quadratic Maps via Convex Relaxation,” *arXiv:1810.00896*, October 2018.
- [115] M. Slater, “Lagrange Multipliers Revisited,” *Cowles Commission Discussion Paper No. 403*, November 1950.
- [116] X. Cao, J. Wang, and B. Zeng, “A Study on the Strong Duality of Conic Relaxation of AC Optimal Power Flow in Radial Networks,” *arXiv:1807.08785*, July 2018.
- [117] A. Hauswirth, S. Bolognani, G. Hug, and F. Dörfler, “Generic Existence of Unique Lagrange Multipliers in AC Optimal Power Flow,” *arXiv:1806.06615*, June 2018.
- [118] D. Peterson, “A Review of Constraint Qualifications in Finite-Dimensional Spaces,” *SIAM Review*, vol. 15, no. 3, pp. 639–654, 1973.
- [119] K. C. Almeida and F. D. Galiana, “Critical Cases in the Optimal Power Flow,” *IEEE Transactions on Power Systems*, vol. 11, no. 3, pp. 1509–1518, August 1996.
- [120] C. Coffrin, “Visualizations of AC Power Flow over a Line.” <https://github.com/ccoffrin/ac-powerflow-vis>, February 2017.
- [121] D. K. Molzahn, S. S. Baghsorkhi, and I. A. Hiskens, “Semidefinite Relaxations of Equivalent Optimal Power Flow Problems: An Illustrative Example,” in *IEEE International Symposium on Circuits and Systems (ISCAS)*, (Lisbon, Portugal), pp. 1887–1890, May 2015.
- [122] D. K. Molzahn and I. A. Hiskens, “Convex Relaxations of Optimal Power Flow Problems: An Illustrative Example,” *IEEE Transactions on Circuits and Systems I: Regular Papers*, vol. 63, no. 5, pp. 650–660, May 2016.
- [123] S. Boyd and L. Vandenberghe, *Convex Optimization*. Cambridge University Press, 2009.
- [124] J. Nocedal and S. Wright, *Numerical Optimization*. Springer-Verlag New York, 2nd ed., 2006.

- [125] G. P. McCormick, “Computability of Global Solutions to Factorable Nonconvex Programs: Part I—Convex Underestimating Problems,” *Mathematical Programming*, vol. 10, no. 1, pp. 147–175, December 1976.
- [126] M. S. Lobo, L. Vandenberghe, S. Boyd, and H. Lebret, “Applications of Second-Order Cone Programming,” *Linear Algebra and its Applications*, vol. 284, no. 1-3, pp. 193–228, 1998.
- [127] MOSEK ApS, “Modeling Cookbook.” <http://docs.mosek.com/MOSEKModelingCookbook-letter.pdf>.
- [128] G. Strang, *Linear Algebra and its Applications*. Orlando, FL: Harcourt Brace Jovanovich, 3rd ed., 1988.
- [129] C. Josz and D. K. Molzahn, “Lasserre Hierarchy for Large Scale Polynomial Optimization in Real and Complex Variables,” *SIAM Journal on Optimization*, vol. 28, no. 2, pp. 1017–1048, 2018.
- [130] J. C. Gilbert and C. Josz, “Plea for a Semidefinite Optimization Solver in Complex Numbers,” tech. rep., LAAS–Laboratoire d’analyse et d’architecture des systèmes (Toulouse, France), Mach 2017.
- [131] J. Löfberg, “YALMIP: A Toolbox for Modeling and Optimization in MATLAB,” in *IEEE International Symposium on Computer Aided Control Systems Design (CACSD)*, (New Orleans, LA, USA), pp. 284–289, September 2004.
- [132] M. Grant and S. Boyd, “CVX: Matlab Software for Disciplined Convex Programming, version 2.1.” <http://cvxr.com/cvx>, March 2017.
- [133] MOSEK ApS, “The MOSEK Optimization Toolbox.” <https://www.mosek.com/documentation/>.
- [134] M. Kočvara and M. Stingl, “PENSDP User’s Guide (Version 2.2).” <http://www.penopt.com/pensdp.html>.
- [135] J. F. Sturm, “Using SeDuMi 1.02, A MATLAB Toolbox for Optimization Over Symmetric Cones,” *Optimization Methods and Software*, vol. 11, no. 1, pp. 625–653, 1999.
- [136] R. H. Tütüncü, K. C. Toh, and M. J. Todd, “Solving Semidefinite-Quadratic-Linear Programs using SDPT3,” *Mathematical Programming*, vol. 95, no. 2, pp. 189–217, 2003.
- [137] M. Yamashita, K. Fujisawa, M. Fukuda, K. Kobayashi, K. Nakata, and M. Nakata, “Latest Developments in the SDPA Family for Solving Large-Scale SDPs,” in *Handbook on Semidefinite, Conic and Polynomial Optimization* (M. F. Anjos and J. B. Lasserre, eds.), (Boston, MA), pp. 687–713. Boston, MA: Springer US, 2012.

- [138] B. Borchers, "CSDP, A C Library for Semidefinite Programming," *Optimization Methods and Software*, vol. 11, no. 1-4, pp. 613–623, 1999.
- [139] T. Gally, M. E. Pfetsch, and S. Ulbrich, "A Framework for Solving Mixed-Integer Semidefinite Programs," *Optimization Methods and Software*, vol. 33, no. 3, pp. 594–632, 2018.
- [140] M. Lubin, E. Yamangil, R. Bent, and J. P. Vielma, "Extended Formulations in Mixed-Integer Convex Programming," in *18th International Conference on Integer Programming and Combinatorial Optimization (IPCO)*, (Liège, Belgium), pp. 102–113, June 2016.
- [141] D. K. Molzahn, J. T. Holzer, B. C. Lesieutre, and C. L. DeMarco, "Implementation of a Large-Scale Optimal Power Flow Solver Based on Semidefinite Programming," *IEEE Transactions on Power Systems*, vol. 28, no. 4, pp. 3987–3998, November 2013.
- [142] M. Andersen, A. Hansson, and L. Vandenberghe, "Reduced-Complexity Semidefinite Relaxations of Optimal Power Flow Problems," *IEEE Transactions on Power Systems*, vol. 29, no. 4, pp. 1855–1863, July 2014.
- [143] C. Coffrin, H. L. Hijazi, and P. Van Hentenryck, "The QC Relaxation: A Theoretical and Computational Study on Optimal Power Flow," *IEEE Transactions on Power Systems*, vol. 31, no. 4, pp. 3008–3018, July 2016.
- [144] D. K. Molzahn, "Incorporating Squirrel-Cage Induction Machine Models in Convex Relaxations of Optimal Power Flow Problems," *IEEE Transactions on Power Systems*, vol. 32, no. 6, pp. 4972–4974, November 2017.
- [145] D. K. Molzahn, B. C. Lesieutre, and C. L. DeMarco, "Approximate Representation of ZIP Loads in a Semidefinite Relaxation of the OPF Problem," *IEEE Transactions on Power Systems*, vol. 29, no. 4, pp. 1864–1865, July 2014.
- [146] Z. Wang, D. S. Kirschen, and B. Zhang, "Accurate Semidefinite Programming Models for Optimal Power Flow in Distribution Systems," *arXiv:1711.07853*, December 2017.
- [147] R. A. Jabr, "Optimal Power Flow Using an Extended Conic Quadratic Formulation," *IEEE Transactions on Power Systems*, vol. 23, no. 3, pp. 1000–1008, August 2008.
- [148] M. Baradar, M. R. Hesamzadeh, and M. Ghandhari, "Second-Order Cone Programming for Optimal Power Flow in VSC-Type AC-DC Grids," *IEEE Transactions on Power Systems*, vol. 28, no. 4, pp. 4282–4291, November 2013.

- [149] S. Bahrami, F. Therrien, V. W. S. Wong, and J. Jatskevich, “Semidefinite Relaxation of Optimal Power Flow for AC–DC Grids,” *IEEE Transactions on Power Systems*, vol. 32, no. 1, pp. 289–304, January 2017.
- [150] L. Cupelli, J. T. Ruiz, and A. Monti, “Optimal Voltage Control in Power Systems: Inclusion of Discrete Decision Variables,” in *19th IEEE Mediterranean Electrotechnical Conference (MELECON)*, (Marrakech, Morocco), pp. 138–143, May 2018.
- [151] A. Venzke and S. Chatzivasileiadis, “Convex Relaxations of Probabilistic AC Optimal Power Flow for Interconnected AC and HVDC Grids,” *arXiv:1804.00035*, April 2018.
- [152] E. Bruglia, S. Alaggia, and F. Paganini, “Distribution Network Management based on Optimal Power Flow: Integration of Discrete Decision Variables,” in *51st Annual Conference on Information Sciences and Systems (CISS)*, (Baltimore, MD, USA), pp. 1–6, March 2017.
- [153] C.-Y. Chang, S. Martinez, and J. Cortes, “Virtual-Voltage Partition-Based Approach to Mixed-Integer Optimal Power Flow Problems,” in *55th Annual Allerton Conference on Communication, Control, and Computing (Allerton)*, (Monticello, IL, USA), pp. 307–314, September 2017.
- [154] B. Kocuk, S. S. Dey, and X. A. Sun, “New Formulation and Strong MISOCP Relaxations for AC Optimal Transmission Switching Problem,” *IEEE Transactions on Power Systems*, vol. 32, no. 6, pp. 4161–4170, November 2017.
- [155] K. Bestuzheva, H. L. Hijazi, and C. Coffrin, “Convex Relaxations for Quadratic On/Off Constraints and Applications to Optimal Transmission Switching,” Preprint: http://www.optimization-online.org/DB_FILE/2016/07/5565.pdf, 2016.
- [156] Y. Liu, J. Li, and L. Wu, “Coordinated Optimal Network Reconfiguration and Voltage Regulator/DER Control for Unbalanced Distribution Systems,” to appear in *IEEE Transactions on Smart Grid*, 2019.
- [157] B. A. Robbins, H. Zhu, and A. Domínguez-García, “Optimal Tap Setting of Voltage Regulation Transformers in Unbalanced Distribution Systems,” *IEEE Transactions on Power Systems*, vol. 31, no. 1, pp. 256–267, January 2016.
- [158] W. Wu, Z. Tian, and B. Zhang, “An Exact Linearization Method for OLTC of Transformer in Branch Flow Model,” *IEEE Transactions on Power Systems*, vol. 32, no. 3, pp. 2475–2476, May 2017.

- [159] Y. Liu, J. Li, L. Wu, and T. Ortmeyer, "Chordal Relaxation Based ACOPF for Unbalanced Distribution Systems with DERs and Voltage Regulation Devices," *IEEE Transactions on Power Systems*, vol. 33, no. 1, pp. 970–984, 2018.
- [160] M. Bazrafshan, N. Gatsis, and H. Zhu, "Optimal Tap Selection of Step-Voltage Regulators in Multi-Phase Distribution Networks," in *20th Power Systems Computation Conference (PSCC)*, (Dublin, Ireland), June 2018.
- [161] M. Bazrafshan, N. Gatsis, and H. Zhu, "Optimal Power Flow with Step-Voltage Regulators in Multi-Phase Distribution Networks," *arXiv:1901.04566*, January 2019.
- [162] N. Z. Shor, "Quadratic Optimization Problems," *Soviet Journal of Computer and Systems Sciences*, vol. 25, pp. 1–11, 1987.
- [163] X. Bai, H. Wei, K. Fujisawa, and Y. Wang, "Semidefinite Programming for Optimal Power Flow Problems," *International Journal of Electrical Power & Energy Systems*, vol. 30, no. 6-7, pp. 383–392, 2008.
- [164] J. Lavaei and S. H. Low, "Zero Duality Gap in Optimal Power Flow Problem," *IEEE Transactions on Power Systems*, vol. 27, no. 1, pp. 92–107, February 2012.
- [165] J. Lavaei and S. H. Low, "Convexification of Optimal Power Flow Problem," in *48th Annual Allerton Conference on Communication, Control, and Computing (Allerton)*, (Monticello, IL, USA), pp. 223–232, September 2010.
- [166] University of Washington Department of Electrical Engineering, "Power Systems Test Case Archive." <http://www.ee.washington.edu/research/pstca/>.
- [167] E. Dall'Anese, H. Zhu, and G. B. Giannakis, "Distributed Optimal Power Flow for Smart Microgrids," *IEEE Transactions on Smart Grid*, vol. 4, no. 3, pp. 1464–1475, September 2013.
- [168] L. Gan and S. H. Low, "Convex Relaxations and Linear Approximation for Optimal Power Flow in Multiphase Radial Networks," in *18th Power Systems Computation Conference (PSCC)*, (Wroclaw, Poland), pp. 1–9, August 2014.
- [169] C. Zhao, E. Dall'Anese, and S. H. Low, "Convex Relaxation of OPF in Multiphase Radial Networks with Delta Connections," in *10th IREP Symposium on Bulk Power System Dynamics and Control*, (Espinho, Portugal), August 2017.

- [170] B. C. Lesieutre, D. K. Molzahn, A. R. Borden, and C. L. DeMarco, “Examining the Limits of the Application of Semidefinite Programming to Power Flow Problems,” in *49th Annual Allerton Conference on Communication, Control, and Computing (Allerton)*, (Monticello, IL, USA), September 2011.
- [171] B. Kocuk, S. S. Dey, and X. A. Sun, “Inexactness of SDP Relaxation and Valid Inequalities for Optimal Power Flow,” *IEEE Transactions on Power Systems*, vol. 31, no. 1, pp. 642–651, January 2016.
- [172] I. Zorin, S. Vasilyev, and E. Gryazina, “Fragility of the Semidefinite Relaxation for the Optimal Power Flow Problem,” in *IEEE International Conference on the Science of Electrical Engineering (ICSEE)*, (Eilat, Israel), pp. 1–5, November 2016.
- [173] W. Wang and N. Yu, “Chordal Conversion based Convex Iteration Algorithm for Three-phase Optimal Power Flow Problems,” *IEEE Transactions on Power Systems*, vol. 33, no. 2, pp. 1603–1613, March 2018.
- [174] T. W. K. Mak, L. Shi, and P. Van Hentenryck, “Phase Transitions for Optimality Gaps in Optimal Power Flows: A Study on the French Transmission Network,” *arXiv:1807.05460*, July 2018.
- [175] B. Park, “Examining the rank of Semi-definite Programming for Power System State Estimation,” *arXiv:1802.06094*, February 2018.
- [176] C. Coffrin, H. L. Hijazi, and P. Van Hentenryck, “Strengthening the SDP Relaxation of AC Power Flows with Convex Envelopes, Bound Tightening, and Valid Inequalities,” *IEEE Transactions on Power Systems*, vol. 32, no. 5, pp. 3549–3558, September 2017.
- [177] A. Eltved, J. Dahl, and M. S. Andersen, “On the Robustness and Scalability of Semidefinite Relaxation for Optimal Power Flow Problems,” *arXiv:1806.08620*, June 2018.
- [178] C. Coffrin, D. Gordon, and P. Scott, “NESTA, The NICTA Energy System Test Case Archive,” *arXiv:1411.0359*, August 2016.
- [179] IEEE PES Task Force on Benchmarks for Validation of Emerging Power System Algorithms, “Power Grid Lib – Optimal Power Flow.” <https://github.com/power-grid-lib/pglib-opf>.
- [180] ARPA-E, “Generating Realistic Information for Development of Distribution and Transmission Algorithms (GRID DATA).” <https://arpa-e.energy.gov/?q=pdfs/grid-data-de-foa-0001357>, June 2015. Funding Opportunity Announcement Number DE-FOA-0001357.

- [181] S. Y. Abdelouadoud, R. Girard, F. P. Neirac, and T. Guiot, “Optimal Power Flow of a Distribution System based on Increasingly Tight Cutting Planes Added to a Second Order Cone Relaxation,” *International Journal of Electrical Power & Energy Systems*, vol. 69, pp. 9–17, July 2015.
- [182] H. Gao, J. Liu, L. Wang, and Y. Liu, “Cutting Planes based Relaxed Optimal Power Flow in Active Distribution Systems,” *Electric Power Systems Research*, vol. 143, pp. 272–280, 2017.
- [183] C. Coffrin, R. Bent, B. Tasseeff, K. Sundar, and S. Backhaus, “Relaxations of AC Maximal Load Delivery for Severe Contingency Analysis,” to appear in *IEEE Transactions on Power Systems*, 2019.
- [184] B. Zhang and D. Tse, “Geometry of Injection Regions of Power Networks,” *IEEE Transactions on Power Systems*, vol. 28, no. 2, pp. 788–797, May 2013.
- [185] H. Mahboubi and J. Lavaei, “Analysis of Semidefinite Programming Relaxation of Optimal Power Flow for Cyclic Networks,” in *IEEE 57th Annual Conference on Decision and Control (CDC)*, (Miami Beach, FL, USA), December 2018.
- [186] R. Madani, S. Sojoudi, G. Fazelnia, and J. Lavaei, “Finding Low-Rank Solutions of Sparse Linear Matrix Inequalities using Convex Optimization,” *SIAM Journal on Optimization*, vol. 27, no. 2, pp. 725–758, 2017.
- [187] R. Madani, M. Ashraphijuo, and J. Lavaei, “Promises of Conic Relaxation for Contingency-Constrained Optimal Power Flow Problem,” *IEEE Transactions on Power Systems*, vol. 31, no. 2, pp. 1297–1307, March 2016.
- [188] D. K. Molzahn, C. Josz, I. A. Hiskens, and P. Panciatici, “A Laplacian-Based Approach for Finding Near Globally Optimal Solutions to OPF Problems,” *IEEE Transactions on Power Systems*, vol. 32, no. 1, pp. 305–315, 2017.
- [189] R. Louca, P. Seiler, and E. Bitar, “A Rank Minimization Algorithm to Enhance Semidefinite Relaxations of Optimal Power Flow,” in *51st Annual Allerton Conference on Communication, Control, and Computing (Allerton)*, (Monticello, IL, USA), pp. 1010–1020, October 2013.
- [190] R. Gron, C. R. Johnson, E. M. Sá, and H. Wolkowicz, “Positive Definite Completions of Partial Hermitian Matrices,” *Linear Algebra and its Applications*, vol. 58, pp. 109–124, 1984.
- [191] L. Vandenberghe and M. S. Andersen, “Chordal Graphs and Semidefinite Optimization,” *Foundations and Trends in Optimization*, vol. 1, no. 4, pp. 241–433, 2015.

- [192] T. A. Davis, J. R. Gilbert, S. Larimore, and E. Ng, "Algorithm 836: COLAMD, a Column Approximate Minimum Degree Ordering Algorithm," *ACM Transactions on Mathematical Software*, vol. 30, no. 3, pp. 377–380, September 2004.
- [193] R. E. Tarjan and M. Yannakakis, "Simple Linear-Time Algorithms to Test Chordality of Graphs, Test Acyclicity of Hypergraphs, and Selectively Reduce Acyclic Hypergraphs," *SIAM Journal on Computing*, vol. 13, pp. 566–579, 1984.
- [194] R. A. Jabr, "Radial Distribution Load Flow using Conic Programming," *IEEE Transactions on Power Systems*, vol. 21, no. 3, pp. 1458–1459, August 2006.
- [195] J. Dancis, "Positive Semidefinite Completions of Partial Hermitian Matrices," *Linear Algebra and its Applications*, vol. 175, pp. 97–114, 1992.
- [196] M. Fukuda, M. Kojima, K. Murota, and K. Nakata, "Exploiting Sparsity in Semidefinite Programming via Matrix Completion I: General Framework," *SIAM Journal on Optimization*, vol. 11, no. 3, pp. 647–674, 2001.
- [197] R. A. Jabr, "Exploiting Sparsity in SDP Relaxations of the OPF Problem," *IEEE Transactions on Power Systems*, vol. 27, no. 2, pp. 1138–1139, May 2012.
- [198] J. A. Kersulis, I. A. Hiskens, C. Coffrin, and D. K. Molzahn, "Topological Graph Metrics for Detecting Grid Anomalies and Improving Algorithms," in *20th Power Systems Computation Conference (PSCC)*, (Dublin, Ireland), June 2018.
- [199] R. Y. Zhang and J. Lavaei, "Sparse Semidefinite Programs with Guaranteed Near-Linear Time Complexity via Dualized Clique Tree Conversion," *arXiv:1710.03475*, August 2018.
- [200] J. Löfberg, "Dualize It: Software for Automatic Primal and Dual Conversions of Conic Programs," *Optimization Methods and Software*, vol. 24, no. 3, pp. 313–325, 2009.
- [201] S. Sojoudi and J. Lavaei, "Physics of Power Networks Makes Hard Optimization Problems Easy to Solve," in *IEEE Power & Energy Society General Meeting*, (San Diego, CA, USA), pp. 1–8, July 2012.
- [202] C. Bingane, M. F. Anjos, and S. Le Digabel, "Tight-and-Cheap Conic Relaxation for the AC Optimal Power Flow Problem," *IEEE Transactions on Power Systems*, vol. 33, no. 6, pp. 7181–7188, 2018.

- [203] H. L. Hijazi, C. Coffrin, and P. Van Hentenryck, “Polynomial SDP Cuts for Optimal Power Flow,” in *19th Power Systems Computation Conference (PSCC)*, (Genoa, Italy), pp. 1–7, June 2016.
- [204] J. B. Lasserre, “On Representations of the Feasible Set in Convex Optimization,” *Optimization Letters*, vol. 4, no. 1, pp. 1–5, 2010.
- [205] J. B. Lasserre, “On Convex Optimization without Convex Representation,” *Optimization Letters*, vol. 5, no. 4, pp. 549–556, 2011.
- [206] A. Barzegar, D. K. Molzahn, and R. Su, “A Method for Quickly Bounding the Optimal Objective Value of an OPF Problem Using a Semidefinite Relaxation and a Local Solution,” *arXiv:1808.04557*, August 2018.
- [207] M. Yamashita, K. Fujisawa, M. Fukuda, K. Nakata, and M. Nakata, “Algorithm 925: Parallel Solver for Semidefinite Programming Problem Having Sparse Schur Complement Matrix,” *ACM Transactions on Mathematical Software*, vol. 39, no. 1, November 2012.
- [208] J. Mareček and M. Takáč, “A Low-Rank Coordinate-Descent Algorithm for Semidefinite Programming Relaxations of Optimal Power Flow,” *Optimization Methods and Software*, vol. 32, no. 4, pp. 849–871, 2017.
- [209] J. Liu, A. C. Liddell, J. Mareček, and M. Takáč, “Hybrid Methods in Solving Alternating-Current Optimal Power Flows,” *IEEE Transactions on Smart Grid*, vol. 8, no. 6, pp. 2988–2998, November 2017.
- [210] A. Lam, B. Zhang, and D. N. Tse, “Distributed Algorithms for Optimal Power Flow Problem,” in *IEEE 51st Annual Conference on Decision and Control (CDC)*, (Maui, HI, USA), pp. 430–437, December 2012.
- [211] A. Y.S. Lam, B. Zhang, A. Domínguez-García, and D. Tse, “An Optimal and Distributed Method for Voltage Regulation in Power Distribution Systems,” *IEEE Transactions on Power Systems*, vol. 30, no. 4, pp. 1714–17726, July 2015.
- [212] R. Madani, A. Kalbat, and J. Lavaei, “ADMM for Sparse Semidefinite Programming with Applications to Optimal Power Flow,” in *IEEE 54th Annual Conference on Decision and Control (CDC)*, (Osaka, Japan), pp. 5932–5939, December 2015.
- [213] R. Madani, A. Kalbat, and J. Lavaei, “A Low-Complexity Parallelizable Numerical Algorithm for Sparse Semidefinite Programming,” *IEEE Transactions on Control of Network Systems*, vol. 5, no. 4, pp. 1898–1909, December 2018.

- [214] Q. Peng and S. H. Low, "Distributed Algorithm for Optimal Power Flow on an Unbalanced Radial Network," in *IEEE 54th Annual Conference on Decision and Control (CDC)*, (Osaka, Japan), pp. 6915–6920, December 2015.
- [215] Q. Peng and S. H. Low, "Distributed Optimal Power Flow Algorithm for Radial Networks, I: Balanced Single Phase Case," *IEEE Transactions on Smart Grid*, vol. 9, no. 1, pp. 111–121, 2018.
- [216] C. Josz, S. Fliscounakis, J. Maeght, and P. Panciatici, "AC Power Flow Data in MATPOWER and QCQP Format: iTesla, RTE Snapshots, and PEGASE," *arXiv:1603:01533*, March 2016.
- [217] A. Raghunathan and A. Knyazev, "Degeneracy in Maximal Clique Decomposition for Semidefinite Programs," in *American Control Conference (ACC)*, (Boston, MA, USA), pp. 5605–5611, July 2016.
- [218] V. Kungurtsev and J. Marecek, "A Two-Step Pre-Processing for Semidefinite Programming," *arXiv:1806.10868*, June 2018.
- [219] D. K. Molzahn, C. Josz, I. A. Hiskens, and P. Panciatici, "Solution of Optimal Power Flow Problems using Moment Relaxations Augmented with Objective Function Penalization," in *IEEE 54th Annual Conference on Decision and Control (CDC)*, (Osaka, Japan), pp. 31–38, December 2015.
- [220] D. K. Molzahn, B. C. Lesieutre, and C. L. DeMarco, "A Sufficient Condition for Global Optimality of Solutions to the Optimal Power Flow Problem," *IEEE Transactions on Power Systems*, vol. 29, no. 2, pp. 978–979, March 2014.
- [221] J. B. Lasserre, "Global Optimization with Polynomials and the Problem of Moments," *SIAM Journal on Optimization*, vol. 11, no. 3, pp. 796–817, 2001.
- [222] J. B. Lasserre, *Moments, Positive Polynomials and Their Applications*, vol. 1. Imperial College Press, 2010.
- [223] C. Josz and D. Henrion, "Strong Duality in Lasserre's Hierarchy for Polynomial Optimization," *Optimization Letters*, vol. 10, no. 1, pp. 3–10, January 2016.
- [224] J. Nie, "Optimality Conditions and Finite Convergence of Lasserre's Hierarchy," *Mathematical Programming*, vol. 146, no. 1-2, pp. 97–121, August 2014.
- [225] P. A. Parrilo, "Semidefinite Programming Relaxations for Semialgebraic Problems," *Mathematical Programming*, vol. 96, pp. 293–320, 2003.

- [226] R. Y. Zhang, C. Josz, and S. Sojoudi, “Conic Optimization Theory: Convexification Techniques and Numerical Algorithms,” in *American Control Conference (ACC)*, (Milwaukee, WI, USA), June 2018.
- [227] D. K. Molzahn and I. A. Hiskens, “Sparsity-Exploiting Moment-Based Relaxations of the Optimal Power Flow Problem,” *IEEE Transactions on Power Systems*, vol. 30, no. 6, pp. 3168–3180, November 2015.
- [228] D. Henrion and J. B. Lasserre, “Detecting Global Optimality and Extracting Solutions in GloptiPoly,” in *Positive Polynomials in Control* (D. Henrion and A. Garulli, eds.), pp. 293–310, Springer Berlin Heidelberg, 2005.
- [229] D. K. Molzahn, C. Josz, I. A. Hiskens, and P. Panciatici, “Computational Analysis of Sparsity-Exploiting Moment Relaxations of the OPF Problem,” in *19th Power Systems Computation Conference (PSCC)*, (Genoa, Italy), pp. 1–7, June 2016.
- [230] C. Josz and D. K. Molzahn, “Moment/Sums-of-Squares Hierarchy for Complex Polynomial Optimization,” *arXiv:1508.02068*, August 2015.
- [231] J. Harmouch, H. Khalil, and B. Mourrain, “Structured Low Rank Decomposition of Multivariate Hankel Matrices,” *Linear Algebra and its Applications*, vol. 542, pp. 162–185, 2018.
- [232] C. Josz, J. B. Lasserre, and B. Mourrain, “Sparse Polynomial Interpolation: Compressed Sensing, Super Resolution, or Prony?,” *arXiv:1708.06187*, August 2017.
- [233] D. K. Molzahn and I. A. Hiskens, “Mixed SDP/SOCP Moment Relaxations of the Optimal Power Flow Problem,” in *IEEE Eindhoven PowerTech*, (Eindhoven, Netherlands), pp. 1–6, June 2015.
- [234] X. Kuang, L. Zuluaga, B. Ghaddar, and J. Naoum-Sawaya, “Approximating the ACOPF Problem with a Hierarchy of SOCP Problems,” in *IEEE Power & Energy Society General Meeting*, (Denver, CO, USA), pp. 1–5, July 2015.
- [235] X. Kuang, B. Ghaddar, J. Naoum-Sawaya, and L. F. Zuluaga, “Alternative LP and SOCP Hierarchies for ACOPF Problems,” *IEEE Transactions on Power Systems*, vol. 32, no. 4, pp. 2828–2836, July 2017.
- [236] A. A. Ahmadi and A. Majumdar, “DSOS and SDSOS Optimization: LP and SOCP-based Alternatives to Sum of Squares Optimization,” in *48th Annual Conference on Information Sciences and Systems (CISS)*, (Princeton, NJ, USA), pp. 1–5, 2014.

- [237] C. Josz, “Counterexample to Global Convergence of DSOS and SDSOS Hierarchies,” *arXiv:1707.02964*, July 2017.
- [238] X. Kuang, B. Ghaddar, J. Naoum-Sawaya, and L. F. Zuluaga, “Alternative SDP and SOCP Approximations for Polynomial Optimization,” *EURO Journal on Computational Optimization*, pp. 1–23, August 2018.
- [239] A. A. Ahmadi, S. Dash, and G. Hall, “Optimization over Structured Subsets of Positive Semidefinite Matrices via Column Generation,” *Discrete Optimization*, vol. 24, pp. 129–151, 2017.
- [240] G. Hall, *Optimization over Nonnegative and Convex Polynomials With and Without Semidefinite Programming*. dissertation, Princeton University, June 2018.
- [241] D. K. Molzahn and I. A. Hiskens, “Moment-Based Relaxation of the Optimal Power Flow Problem,” in *18th Power Systems Computation Conference (PSCC)*, (Wroclaw, Poland), pp. 1–7, August 2014.
- [242] C. Josz, J. Maeght, P. Panciatici, and J. C. Gilbert, “Application of the Moment-SOS Approach to Global Optimization of the OPF Problem,” *IEEE Transactions on Power Systems*, vol. 30, no. 1, pp. 463–470, January 2015.
- [243] B. Ghaddar, J. Marecek, and M. Mevissen, “Optimal Power Flow as a Polynomial Optimization Problem,” *IEEE Transactions on Power Systems*, vol. 31, no. 1, pp. 539–546, January 2016.
- [244] J. Tian and H. Wei, “Global Optimization for the OPF Problem via Two-Degree SDP Method,” *IEEJ Transactions on Electrical and Electronic Engineering*, vol. 10, no. 1, pp. 109–111, January 2015.
- [245] D. K. Molzahn and I. A. Hiskens, “Moment Relaxations of Optimal Power Flow Problems: Beyond the Convex Hull,” in *IEEE Global Conference on Signal and Information Processing (GlobalSIP)*, (Washington, DC, USA), pp. 856–860, December 2016.
- [246] T. Weisser, L. A. Roald, and S. Misra, “Chance-Constrained Optimization for Non-Linear Network Flow Problems,” *arXiv:1803.02696*, March 2018.
- [247] E. Dumon, M. Ruiz, H. Godard, and J. Maeght, “SDP Resolution Techniques for the Optimal Power Flow with Unit Commitment,” in *IEEE Manchester PowerTech*, (Manchester, England, UK), pp. 1–6, June 2017.

- [248] R. Pedersen, C. Sloth, and R. Wisniewski, "Verification of Power Grid Voltage Constraint Satisfaction – A Barrier Certificate Approach," in *European Control Conference (ECC)*, (Aalborg, Denmark), pp. 447–452, June 2016.
- [249] M. Anghel, F. Milano, and A. Papachristodoulou, "Algorithmic Construction of Lyapunov Functions for Power Grid Stability Analysis," *IEEE Transactions on Circuits and Systems I: Regular Papers*, vol. 60, pp. 2533–2546, 2013.
- [250] C. Josz, D. K. Molzahn, M. Tacchi, and S. Sojoudi, "Transient Stability Analysis of Power Systems via Occupation Measures," *arXiv:1811.01372*, November 2018.
- [251] M. Tacchi, B. Marinescu, M. Anghel, S. Kundu, S. Benahmed, and C. Cardozo, "Power System Transient Stability Analysis Using Sum Of Squares Programming," in *20th Power Systems Computation Conference (PSCC)*, (Dublin, Ireland), June 2018.
- [252] A. A. Ahmadi and A. Majumdar, "Response to "Counterexample to Global Convergence of DSOS and SDSOS Hierarchies"," *arXiv:1710.02901*, October 2017.
- [253] H. Waki, S. Kim, M. Kojima, and M. Muramatsu, "Sums of Squares and Semidefinite Program Relaxations for Polynomial Optimization Problems with Structured Sparsity," *SIAM Journal on Optimization*, vol. 17, no. 1, pp. 218–242, 2006.
- [254] C. Coffrin, H. L. Hijazi, and P. Van Hentenryck, "Strengthening the SDP Relaxation of AC Power Flows with Convex Envelopes, Bound Tightening, and Lifted Nonlinear Cuts," *arXiv:1512.04644*, January 2016.
- [255] B. Kocuk, S. S. Dey, and X. A. Sun, "Strong SOCP Relaxations of the Optimal Power Flow Problem," *Operations Research*, vol. 64, no. 6, pp. 1177–1196, 2016.
- [256] B. Kocuk, S. S. Dey, and X. A. Sun, "Matrix Minor Reformulation and SOCP-based Spatial Branch-and-Cut Method for the AC Optimal Power Flow Problem," *Mathematical Programming C*, vol. 10, no. 4, pp. 557–596, December 2018.
- [257] A. Gómez Expósito and E. Romero Ramos, "Reliable Load Flow Technique for Radial Distribution Networks," *IEEE Transactions on Power Systems*, vol. 14, no. 3, pp. 1063–1069, August 1999.

- [258] H. Hijazi, C. Coffrin, and P. Van Hentenryck, "Convex Quadratic Relaxations for Mixed-Integer Nonlinear Programs in Power Systems," Preprint: http://www.optimization-online.org/DB_HTML/2013/09/4057.html, September 2013.
- [259] H. Hijazi, C. Coffrin, and P. Van Hentenryck, "Convex Quadratic Relaxations for Mixed-Integer Nonlinear Programs in Power Systems," *Mathematical Programming Computation*, vol. 9, no. 3, pp. 321–367, September 2017.
- [260] C. A. Meyer and C. A. Floudas, *Trilinear Monomials with Positive or Negative Domains: Facets of the Convex and Concave Envelopes*, pp. 327–352. Boston, MA: Springer US, 2004.
- [261] C. A. Meyer and C. A. Floudas, "Trilinear Monomials with Mixed Sign Domains: Facets of the Convex and Concave Envelopes," *Journal of Global Optimization*, vol. 29, no. 2, pp. 125–155, 2004.
- [262] A. D. Rikun, "A Convex Envelope Formula for Multilinear Functions," *Journal of Global Optimization*, vol. 10, no. 4, pp. 425–437, 1997.
- [263] M. R. Narimani, D. K. Molzahn, and M. L. Crow, "Improving QC Relaxations of OPF Problems via Voltage Magnitude Difference Constraints and Envelopes for Trilinear Monomials," in *20th Power Systems Computation Conference (PSCC)*, (Dublin, Ireland), June 2018.
- [264] M. Lu, H. Nagarajan, R. Bent, S. D. Eksioglu, and S. J. Mason, "Tight Piecewise Convex Relaxations for Global Optimization of Optimal Power Flow," in *20th Power Systems Computation Conference (PSCC)*, (Dublin, Ireland), June 2018.
- [265] M. R. Narimani, D. K. Molzahn, H. Nagarajan, and M. L. Crow, "Comparison of Various Trilinear Monomial Envelopes for Convex Relaxations of Optimal Power Flow Problems," in *IEEE Global Conference on Signal and Information Processing (GlobalSIP)*, (Anaheim, CA, USA), November 2018.
- [266] K. Sundar, H. Nagarajan, S. Misra, M. Lu, C. Coffrin, and R. Bent, "Optimization-Based Bound Tightening using a Strengthened QC-Relaxation of the Optimal Power Flow Problem," *arXiv:1809.04565*, September 2018.
- [267] C. Coffrin, H. L. Hijazi, and P. Van Hentenryck, "Strengthening Convex Relaxations with Bound Tightening for Power Network Optimization," in *21st International Conference on Principles and Practice of Constraint Programming (CP)* (G. Pesant, ed.), pp. 39–57, Cork, Ireland: Springer International Publishing, August 2015. Lecture Notes in Computer Science 9255.

- [268] S. Mhanna, G. Verbič, and A. C. Chapman, “Tight LP Approximations for the Optimal Power Flow Problem,” in *19th Power Systems Computation Conference (PSCC)*, (Genoa, Italy), pp. 1–7, June 2016.
- [269] D. Bienstock and G. Muñoz, “On Linear Relaxations of OPF Problems,” *arXiv:1411.1120*, November 2014.
- [270] D. Bienstock and G. Muñoz, “Approximate Method for AC Transmission Switching Based on a Simple Relaxation for ACOPF Problems,” in *IEEE Power & Energy Society General Meeting*, (Denver, CO, USA), pp. 1–5, July 2015.
- [271] B. Subhommesh, S. H. Low, and K. M. Chandy, “Equivalence of Branch Flow and Bus Injection Models,” in *50th Annual Allerton Conference on Communication, Control, and Computing (Allerton)*, (Monticello, IL, USA), pp. 1893–1899, October 2012.
- [272] A. R. Bergen and V. Vittal, *Power Systems Analysis*. Prentice-Hall, 1999.
- [273] D. S. Callaway and I. A. Hiskens, “Achieving Controllability of Electric Loads,” *Proceedings of the IEEE*, vol. 99, no. 1, pp. 184–199, November 2011.
- [274] K. Christakou, D.-C. Tomozei, J.-Y. Le Boudec, and M. Paolone, “AC OPF in Radial Distribution Networks – Part I: On the Limits of the Branch Flow Convexification and the Alternating Direction Method of Multipliers,” *Electric Power Systems Research*, vol. 143, pp. 438–450, February 2017.
- [275] M. Nick, R. Cherkaoui, J. Y. LeBoudec, and M. Paolone, “An Exact Convex Formulation of the Optimal Power Flow in Radial Distribution Networks Including Transverse Components,” *IEEE Transactions on Automatic Control*, vol. 63, no. 3, pp. 682–697, March 2018.
- [276] S. Sojoudi and J. Lavaei, “Convexification of Optimal Power Flow Problem by Means of Phase Shifters,” in *IEEE International Conference on Smart Grid Communications (SmartGridComm)*, (Vancouver, BC, Canada), pp. 756–761, October 2013.
- [277] S. Sojoudi, S. Fattah, and J. Lavaei, “Convexification of Generalized Network Flow Problem,” to appear in *Mathematical Programming Series A*, 2019.
- [278] S. Huang, Q. Wu, J. Wang, and H. Zhao, “A Sufficient Condition on Convex Relaxation of AC Optimal Power Flow in Distribution Networks,” *IEEE Transactions on Power Systems*, vol. 32, no. 2, pp. 1359–1368, 2016.

- [279] L. Gan and S. H. Low, "Optimal Power Flow in Direct Current Networks," *IEEE Transactions on Power Systems*, vol. 29, no. 6, pp. 2892–2904, November 2014.
- [280] C. W. Tan, D. W. H. Cai, and X. Lou, "Resistive Network Optimal Power Flow: Uniqueness and Algorithms," *IEEE Transactions on Power Systems*, vol. 30, no. 1, pp. 263–273, January 2015.
- [281] P. Scott and S. Thiébaut, "Dynamic Optimal Power Flow in Microgrids using the Alternating Direction Method of Multipliers," *arXiv:1410.7868*, October 2014.
- [282] P. Scott and S. Thiébaut, "Distributed Multi-Period Optimal Power Flow for Demand Response in Microgrids," in *ACM Sixth International Conference on Future Energy Systems (e-Energy)*, pp. 17–26, July 2015.
- [283] Z. Yuan and M. R. Hesamzadeh, "A Modified Benders Decomposition Algorithm to Solve Second-Order Cone AC Optimal Power Flow," to appear in *IEEE Transactions on Smart Grid*, 2019.
- [284] S. Mhanna, A. Chapman, and G. Verbic, "Accelerated Methods for the SOCP-relaxed Component-based Distributed Optimal Power Flow," in *20th Power Systems Computation Conference (PSCC)*, (Dublin, Ireland), June 2018.
- [285] C. Coffrin, H. L. Hijazi, and P. Van Hentenryck, "Network Flow and Copper Plate Relaxations for AC Transmission Systems," in *19th Power Systems Computation Conference (PSCC)*, (Genoa, Italy), pp. 1–8, June 2016.
- [286] C. Coffrin, H. L. Hijazi, and P. Van Hentenryck, "Network Flow and Copper Plate Relaxations for AC Transmission Systems," *arXiv:1506.05202*, November 2015.
- [287] S. Deckmann, A. Pizzolante, A. Monticelli, B. Stott, and O. Alsaç, "Studies on Power System Load Flow Equivalencing," *IEEE Transactions on Power Apparatus and Systems*, no. 6, pp. 2301–2310, 1980.
- [288] J. A. Taylor and F. S. Hover, "Linear Relaxations for Transmission System Planning," *IEEE Transactions on Power Systems*, vol. 26, no. 4, pp. 2533–2538, November 2011.
- [289] Z. Qin, Y. Hou, and Y. Chen, "Convex Envelopes of Optimal Power Flow with Branch Flow Model in Rectangular Form," in *IEEE Power & Energy Society General Meeting*, (Denver, CO, USA), pp. 1–5, July 2015.

- [290] Q. Gemine, D. Ernst, Q. Louveaux, and B. Cornélusse, “Relaxations for Multi-Period Optimal Power Flow Problems with Discrete Decision Variables,” in *18th Power Systems Computation Conference (PSCC)*, (Wroclaw, Poland), pp. 1–7, August 2014.
- [291] M. Bynum, A. Castillo, J.-P. Watson, and C. D. Laird, “Strengthened SOCP Relaxations for ACOPF with McCormick Envelopes and Bounds Tightening,” in *13th International Symposium on Process Systems Engineering (PSE 2018)*, vol. 44, (San Diego. CA, USA), pp. 1555–1560, July 2018.
- [292] D. Bienstock and G. Muñoz, “LP Formulations for Polynomial Optimization Problems,” *SIAM Journal on Optimization*, vol. 28, no. 2, pp. 1121–1150, 2018.
- [293] F. Glover, “Improved Linear Integer Programming Formulations of Nonlinear Integer Problems,” *Management Science*, vol. 22, no. 4, pp. 455–460, December 1975.
- [294] K. Dvijotham, M. Chertkov, P. Van Hentenryck, M. Vuffray, and S. Misra, “Graphical Models for Optimal Power Flow,” *Constraints*, vol. 22, no. 1, pp. 24–49, 2017.
- [295] J. D. Foster, *Mixed-Integer Quadratically-Constrained Programming, Piecewise-Linear Approximation and Error Analysis with Applications in Power Flow*. dissertation, The University of Newcastle, Australia, School of Mathematical and Physical Sciences, November 2013.
- [296] C. Chen, A. Atamtürk, and S. S. Oren, “Bound Tightening for the Alternating Current Optimal Power Flow Problem,” *IEEE Transactions on Power Systems*, vol. 31, no. 5, pp. 3729–3736, September 2016.
- [297] M. Bynum, A. Castillo, J.-P. Watson, and C. Laird, “Tightening McCormick Relaxations Toward Global Solution of the ACOPF Problem,” *IEEE Transactions on Power Systems*, vol. 34, no. 1, pp. 814–817, January 2019.
- [298] D. Shchetinin, “Efficient Bound Tightening Techniques for Convex Relaxations of AC Optimal Power Flow,” submitted to *IEEE Transactions on Power Systems*, 2018.
- [299] Z. Miao, L. Fan, H. G. Aghamolki, and B. Zeng, “Least Square Estimation-Based SDP Cuts for SOCP Relaxation of AC OPF,” *IEEE Transactions on Automatic Control*, vol. 63, no. 1, pp. 241–248, January 2018.

- [300] C. Chen, A. Atamtürk, and S. S. Oren, “A Spatial Branch-and-Cut Method for Nonconvex QCQP with Bounded Complex Variables,” *Mathematical Programming, Series A*, vol. 165, no. 2, pp. 549–577, October 2017.
- [301] J. Liu, M. Bynum, A. Castillo, J.-P. Watson, and C. D. Laird, “A Multitree Approach for Global Solution of ACOPF Problems using Piecewise Outer Approximations,” *Computers & Chemical Engineering*, vol. 114, pp. 145–157, 2018.
- [302] C. Coffrin, “Lifted Nonlinear Cuts Animation.” source code available at <https://github.com/ccoffrin/lnc-animation>, animation available at <https://imgur.com/gallery/7JjPfy6>, April 2016.
- [303] A. Gopalakrishnan, A. Raghunathan, D. Nikovski, and L. T. Biegler, “Global Optimization of Optimal Power Flow using a Branch & Bound Algorithm,” in *50th Annual Allerton Conference on Communication, Control, and Computing (Allerton)*, (Monticello, IL, USA), pp. 609–616, October 2012.
- [304] D. Phan, “Lagrangian Duality and Branch-and-Bound Algorithms for Optimal Power Flow,” *Operations Research*, vol. 60, no. 2, pp. 275–285, 2012.
- [305] D. Phan and J. Kalagnanam, “Some Efficient Optimization Methods for Solving the Security-Constrained Optimal Power Flow Problem,” *IEEE Transactions on Power Systems*, vol. 29, no. 2, pp. 863–872, March 2014.
- [306] M. Tawarmalani and N. V. Sahinidis, *Convexification and Global Optimization in Continuous and Mixed-Integer Nonlinear Programming: Theory, Algorithms, Software, and Applications*, vol. 65. Springer Science & Business Media, 2002.
- [307] H. Nagarajan, M. Lu, E. Yamangil, and R. Bent, “Tightening McCormick Relaxations for Nonlinear Programs via Dynamic Multivariate Partitioning,” in *22nd International Conference on Principles and Practice of Constraint Programming (CP)* (M. Rueher, ed.), pp. 369–387, Toulouse, France: Springer International Publishing, September 2016. Lecture Notes in Computer Science 9892.
- [308] H. Nagarajan, M. Lu, S. Wang, R. Bent, and K. Sundar, “An Adaptive, Multivariate Partitioning Algorithm for Global Optimization of Nonconvex Programs,” *arXiv:1707.02514*, July 2017.
- [309] J. Liu, A. Castillo, J.-P. Watson, and C. D. Laird, “Global Solution Strategies for the Network-Constrained Unit Commitment Problem with AC Transmission Constraints,” to appear in *IEEE Transactions on Power Systems*, 2019.

- [310] C. Coffrin, H. L. Hijazi, and P. Van Hentenryck, “Alternating Current (AC) Power Flow Analysis in an Electrical Power Network,” 2012-05-23. Patent US20150088439A1.
- [311] M. Baradar and M. R. Hesamzadeh, “AC Power Flow Representation in Conic Format,” *IEEE Transactions on Power Systems*, vol. 30, no. 1, pp. 546–547, January 2015.
- [312] L. H. Macedo, C. V. Montes, J. F. Franco, M. J. Rider, and R. Romero, “MILP Branch Flow Model for Concurrent AC Multistage Transmission Expansion and Reactive Power Planning with Security Constraints,” *IET Generation, Transmission & Distribution*, vol. 10, pp. 3023–3032, September 2016.
- [313] Z. Yuan and M. R. Hesamzadeh, “Improving the Accuracy of Second-Order Cone AC Optimal Power Flow by Convex Approximations,” in *IEEE Innovative Smart Grid Technologies–Asia (ISGT Asia)*, (Singapore), pp. 172–177, May 2018.
- [314] S. Bolognani and F. Dörfler, “Fast Power System Analysis via Implicit Linearization of the Power Flow Manifold,” in *53rd Annual Allerton Conference on Communication, Control, and Computing (Allerton)*, (Monticello, IL, USA), pp. 402–409, September 2015.
- [315] D. Deka, S. Backhaus, and M. Chertkov, “Structure Learning and Statistical Estimation in Distribution Networks – Part I,” *arXiv:1501.04131*, February 2015.
- [316] J. Yang, N. Zhang, C. Kang, and Q. Xia, “A State-Independent Linear Power Flow Model With Accurate Estimation of Voltage Magnitude,” *IEEE Transactions on Power Systems*, vol. 32, no. 5, pp. 3607–3617, September 2017.
- [317] A. Moser, *Langfristig optimale Struktur und Betriebsmittelwahl für 110-kV-Überlandnetze*. dissertation, RWTH Aachen University, 1995.
- [318] A. Braun, *Anlagen- und Strukturoptimierung von 110-kV-Netzen*. dissertation, RWTH Aachen University, 2001.
- [319] A. M. C. A. Koster and S. Lemkens, *Designing AC Power Grids Using Integer Linear Programming*, pp. 478–483. Hamburg, Germany: Springer Berlin Heidelberg, 2011.
- [320] H. Zhang, V. Vittal, G. T. Heydt, and J. Quintero, “A Relaxed AC Optimal Power Flow Model based on a Taylor Series,” in *IEEE Innovative Smart Grid Technologies–Asia (ISGT Asia)*, (Bangalore, India), pp. 1–5, November 2013.

- [321] H. Zhang, G. T. Heydt, V. Vittal, and J. Quintero, "An Improved Network Model for Transmission Expansion Planning Considering Reactive Power and Network Losses," *IEEE Transactions on Power Systems*, vol. 28, no. 3, pp. 3471–3479, August 2013.
- [322] T. Akbari and M. T. Bina, "Linear Approximated Formulation of AC Optimal Power Flow using Binary Discretisation," *IET Generation, Transmission & Distribution*, vol. 10, pp. 1117–1123, April 2016.
- [323] Z. Yang, H. Zhong, A. Bose, T. Zheng, Q. Xia, and C. Kang, "A Linearized OPF Model with Reactive Power and Voltage Magnitude: A Pathway to Improve the MW-Only DC OPF," *IEEE Transactions on Power Systems*, vol. 33, no. 2, pp. 1734–1745, March 2018.
- [324] Z. Yang, H. Zhong, Q. Xia, and C. Kang, "A Novel Network Model for Optimal Power Flow with Reactive Power and Network Losses," *Electric Power Systems Research*, vol. 144, pp. 63–71, 2017.
- [325] Z. Yang, H. Zhong, Q. Xia, A. Bose, and C. Kang, "Optimal Power Flow based on Successive Linear Approximation of Power Flow Equations," *IET Generation, Transmission & Distribution*, vol. 10, no. 14, pp. 3654–3662, 2016.
- [326] Z. Yang, A. Bose, H. Zhong, N. Zhang, Q. Xia, and C. Kang, "Optimal Reactive Power Dispatch With Accurately Modeled Discrete Control Devices: A Successive Linear Approximation Approach," *IEEE Transactions on Power Systems*, vol. 32, no. 3, pp. 2435–2444, May 2017.
- [327] S. M. Fatemi, S. Abedi, G. B. Gharehpetian, S. H. Hosseiniyan, and M. Abedi, "Introducing a Novel DC Power Flow Method With Reactive Power Considerations," *IEEE Transactions on Power Systems*, vol. 30, no. 6, pp. 3012–3023, November 2015.
- [328] Z. Li, J. Yu, and Q. H. Wu, "Approximate Linear Power Flow Using Logarithmic Transform of Voltage Magnitudes With Reactive Power and Transmission Loss Consideration," *IEEE Transactions on Power Systems*, vol. 33, no. 4, pp. 4593–4603, July 2018.
- [329] K. Dvijotham, E. Mallada, and J. W. Simpson-Porco, "High-Voltage Solution in Radial Power Networks: Existence, Properties, and Equivalent Algorithms," *IEEE Control Systems Letters*, vol. 1, no. 2, pp. 322–327, October 2017.
- [330] Z. Yang, H. Zhong, Q. Xia, and C. Kang, "Solving OPF using Linear Approximations: Fundamental Analysis and Numerical Demonstration," *IET Generation, Transmission & Distribution*, vol. 11, pp. 4115–4125, November 2017.

- [331] Z. Yang, K. Xie, J. Yu, H. Zhong, N. Zhang, and Q. Xia, "A General Formulation of Linear Power Flow Models: Basic Theory and Error Analysis," to appear in *IEEE Transactions on Power Systems*, 2019.
- [332] S. Bolognani and S. Zampieri, "On the Existence and Linear Approximation of the Power Flow Solution in Power Distribution Networks," *IEEE Transactions on Power Systems*, vol. 31, no. 1, pp. 163–172, January 2016.
- [333] S. V. Dhople, S. S. Guggilam, and Y. C. Chen, "Linear Approximations to AC Power Flow in Rectangular Coordinates," in *53rd Annual Allerton Conference on Communication, Control, and Computing (Allerton)*, (Monticello, IL, USA), pp. 211–217, September 2015.
- [334] S. S. Guggilam, E. Dall'Anese, Y. C. Chen, S. V. Dhople, and G. B. Giannakis, "Scalable Optimization Methods for Distribution Networks With High PV Integration," *IEEE Transactions on Smart Grid*, vol. 7, no. 4, pp. 2061–2070, July 2016.
- [335] A. Bernstein, C. Wang, E. Dall'Anese, J.-Y. Le Boudec, and C. Zhao, "Load-Flow in Multiphase Distribution Networks: Existence, Uniqueness, and Linear Models," *IEEE Transactions on Power Systems*, vol. 33, no. 6, pp. 5832–5843, November 2018.
- [336] A. Bernstein and E. Dall'Anese, "Linear Power-Flow Models in Multiphase Distribution Networks," in *7th IEEE International Conference on Innovative Smart Grid Technologies (ISGT Europe)*, (Torino, Italy), pp. 1–6, September 2017.
- [337] B. Stott and O. Alsaç, "Fast Decoupled Load Flow," *IEEE Transactions on Power Apparatus and Systems*, vol. PAS-93, no. 3, pp. 859–869, May 1974.
- [338] R. A. M. van Amerongen, "A General-Purpose Version of the Fast Decoupled Load Flow," *IEEE Transactions on Power Systems*, vol. 4, no. 2, pp. 760–770, May 1989.
- [339] F. F. Wu, "Theoretical Study of the Convergence of the Fast Decoupled Load Flow," *IEEE Transactions on Power Apparatus and Systems*, vol. 96, no. 1, pp. 268–275, January 1977.
- [340] J. Nanda, D. P. Kothari, and S. C. Srivastava, "Some Important Observations on Fast Decoupled Load Flow Algorithm," *Proceedings of the IEEE*, vol. 75, no. 5, pp. 732–733, May 1987.
- [341] R. D. Zimmerman and C. E. Murillo-Sánchez, "MATPOWER 6.0 User's Manual," tech. rep., Power Systems Engineering Research Center, December 2016.

- [342] P. Yan and A. Sekar, "Study of Linear Models in Steady State Load Flow Analysis of Power Systems," in *IEEE Power & Energy Society Winter Meeting*, vol. 1, (New York, NY, USA), pp. 666–671, 2002.
- [343] M. Liu and G. Gross, "Effectiveness of the Distribution Factor Approximations Used in Congestion Modeling," in *14th Power Systems Computation Conference (PSCC)*, (Seville, Spain), June 2002.
- [344] T. J. Overbye, X. Cheng, and Y. Sun, "A Comparison of the AC and DC Power Flow Models for LMP Calculations," in *37th Hawaii International Conference on System Sciences (HICSS)*, (Big Island, HI, USA), pp. 1–9, January 2004.
- [345] R. Baldick, K. Dixit, and T. J. Overbye, "Empirical Analysis of the Variation of Distribution Factors with Loading," in *IEEE Power & Energy Society General Meeting*, (San Francisco, CA, USA), pp. 221–229, June 2005.
- [346] K. Purchala, L. Meeus, D. Van Dommelen, and R. Belmans, "Usefulness of DC Power Flow for Active Power Flow Analysis," in *IEEE Power & Energy Society General Meeting*, (San Francisco, CA, USA), pp. 454–459, June 2005.
- [347] D. Van Hertem, J. Verboomen, K. Purchala, R. Belmans, and W. L. Kling, "Usefulness of DC Power Flow for Active Power Flow Analysis with Flow Controlling Devices," in *8th IEE International Conference on AC and DC Power Transmission (ACDC)*, (London, England, UK), pp. 58–62, March 2006.
- [348] F. Li and R. Bo, "DCOPF-Based LMP Simulation: Algorithm, Comparison With ACOPF, and Sensitivity," *IEEE Transactions on Power Systems*, vol. 22, no. 4, pp. 1475–1485, November 2007.
- [349] C. Duthaler, M. Emery, G. Andersson, and M. Kurzidem, "Analysis of the Use of Power Transfer Distribution Factors (PTDF) in the UCTE Transmission Grid," in *16th Power Systems Computation Conference (PSCC)*, (Glasgow, Scotland, UK), July 2008.
- [350] B. Stott, J. Jardim, and O. Alsaç, "DC Power Flow Revisited," *IEEE Transactions on Power Systems*, vol. 24, no. 3, pp. 1290–1300, August 2009.
- [351] Y. Qi, D. Shi, and D. Tylavsky, "Impact of Assumptions on DC Power Flow Model Accuracy," in *North American Power Symposium (NAPS)*, (Champaign, IL, USA), pp. 1–6, September 2012.

- [352] C. Coffrin, P. Van Hentenryck, and R. Bent, “Accurate Load and Generation Scheduling for Linearized DC Models with Contingencies,” in *IEEE Power & Energy Society General Meeting*, (San Diego, CA, USA), pp. 1–8, July 2012.
- [353] C. Coffrin and P. Van Hentenryck, “Transmission System Restoration with Co-Optimization of Repairs, Load Pickups, and Generation Dispatch,” *International Journal of Electrical Power & Energy Systems*, vol. 72, pp. 144–154, 2015. Special Issue for the 18th Power Systems Computation Conference (PSCC).
- [354] H. Cetinay, S. Soltan, F. A. Kuipers, G. Zussman, and P. Van Mieghem, “Comparing the Effects of Failures in Power Grids under the AC and DC Power Flow Models,” *IEEE Transactions on Network Science and Engineering*, vol. 5, no. 4, pp. 301–312, October 2018.
- [355] R. Kaye and F. F. Wu, “Analysis of Linearized Decoupled Power Flow Approximations for Steady-State Security Assessment,” *IEEE Transactions on Circuits and Systems*, vol. 31, no. 7, pp. 623–636, July 1984.
- [356] R. Baldick, “Variation of Distribution Factors with Loading,” *IEEE Transactions on Power Systems*, vol. 18, no. 4, pp. 1316–1323, November 2003.
- [357] K. Dvijotham and D. K. Molzahn, “Error Bounds on Linear Power Flow Approximations: A Convex Relaxation Approach,” in *IEEE 55th Annual Conference on Decision and Control (CDC)*, (Las Vegas, NV, USA), pp. 2411–2418, December 2016.
- [358] C. Coffrin, P. Van Hentenryck, and R. Bent, “Approximating Line Losses and Apparent Power in AC Power Flow Linearizations,” in *IEEE Power & Energy Society General Meeting*, (San Diego, CA, USA), pp. 1–8, July 2012.
- [359] F. Dörfler and F. Bullo, “Novel Insights into Lossless AC and DC Power Flow,” in *IEEE Power & Energy Society General Meeting*, (Vancouver, BC, Canada), pp. 1–5, July 2013.
- [360] F. Dörfler, M. Chertkov, and F. Bullo, “Synchronization in Complex Oscillator Networks and Smart Grids,” *Proceedings of the National Academy of Sciences of the United States of America*, vol. 110, no. 6, pp. 2005–2010, 2013.
- [361] J. W. Simpson-Porco, “Lossy DC Power Flow,” *IEEE Transactions on Power Systems*, vol. 33, no. 3, pp. 2477–2485, May 2018.

- [362] B. Gentile, J. W. Simpson-Porco, F. Dörfler, S. Zampieri, and F. Bullo, “On Reactive Power Flow and Voltage Stability in Microgrids,” in *American Control Conference (ACC)*, (Portland, OR, USA), pp. 759–764, June 2014.
- [363] J. W. Simpson-Porco, F. Dörfler, and F. Bullo, “Voltage Collapse in Complex Power Grids,” *Nature Communications*, vol. 7, no. 10790, February 2016.
- [364] D. B. Arnold, M. D. Sankur, R. Dobbe, K. Brady, D. S. Callaway, and A. Von Meier, “Optimal Dispatch of Reactive Power for Voltage Regulation and Balancing in Unbalanced Distribution Systems,” in *IEEE Power & Energy Society General Meeting*, (Boston, MA, USA), pp. 1–5, 2016.
- [365] M. D. Sankur, R. Dobbe, E. Stewart, D. S. Callaway, and D. B. Arnold, “A Linearized Power Flow Model for Optimization in Unbalanced Distribution Systems,” *arXiv:1606.04492*, November 2016.
- [366] J. Franco, L. Ochoa, and R. Romero, “AC OPF for Smart Distribution Networks: An Efficient and Robust Quadratic Approach,” *IEEE Transactions on Smart Grid*, vol. 9, no. 5, pp. 4613–4623, September 2018.
- [367] A. R. D. Fazio, M. Russo, S. Valeri, and M. D. Santis, “Linear Method for Steady-State Analysis of Radial Distribution Systems,” *International Journal of Electrical Power & Energy Systems*, vol. 99, pp. 744–755, 2018.
- [368] C. Coffrin and P. Van Hentenryck, “A Linear-Programming Approximation of AC Power Flows,” *INFORMS Journal on Computing*, vol. 26, no. 4, pp. 718–734, 2014.
- [369] J. R. Martí, H. Ahmadi, and L. Bashualdo, “Linear Power-Flow Formulation Based on a Voltage-Dependent Load Model,” *IEEE Transactions on Power Delivery*, vol. 28, no. 3, pp. 1682–1690, July 2013.
- [370] H. Ahmadi, J. R. Martí, and A. von Meier, “A Linear Power Flow Formulation for Three-Phase Distribution Systems,” *IEEE Transactions on Power Systems*, vol. 31, no. 6, pp. 5012–5021, November 2016.
- [371] R. S. Ferreira, C. L. T. Borges, and M. V. F. Pereira, “A Flexible Mixed-Integer Linear Programming Approach to the AC Optimal Power Flow in Distribution Systems,” *IEEE Transactions on Power Systems*, vol. 29, no. 5, pp. 2447–2459, September 2014.
- [372] S. Misra, D. K. Molzahn, and K. Dvijotham, “Optimal Adaptive Linearizations of the AC Power Flow Equations,” in *20th Power Systems Computation Conference (PSCC)*, (Dublin, Ireland), June 2018.

- [373] M. Hohmann, J. Warrington, and J. Lygeros, “Optimal Linearizations of Power Systems with Uncertain Supply and Demand,” to appear in *IEEE Transactions on Power Systems*, 2019.
- [374] P. S. Martin, *Mejoras en la Eficacia Computacional de Modelos Probabilistas de Explotación Generación/Red a Medio Plazo*. dissertation, University Pontifica de Comillas, Madrid, Spain, 1998.
- [375] A. L. Motto, F. D. Galiana, A. J. Conejo, and J. M. Arroyo, “Network-Constrained Multiperiod Auction for a Pool-Based Electricity Market,” *IEEE Transactions on Power Systems*, vol. 17, no. 3, pp. 646–653, August 2002.
- [376] M. R. Almassalkhi and I. A. Hiskens, “Model-Predictive Cascade Mitigation in Electric Power Systems With Storage and Renewables—Part I: Theory and Implementation,” *IEEE Transactions on Power Systems*, vol. 30, no. 1, pp. 67–77, January 2015.
- [377] P. Fortenbacher and T. Demiray, “Linear/Quadratic Programming-Based Optimal Power Flow using Linear Power Flow and Absolute Loss Approximations,” *arXiv:1711.00317*, December 2017.
- [378] J. A. Martin and I. A. Hiskens, “Generalized Line Loss Relaxation in Polar Voltage Coordinates,” *IEEE Transactions on Power Systems*, vol. 32, no. 3, pp. 1980–1189, 2017.
- [379] J. S. Thorp and S. A. Naqavi, “Load Flow Fractals,” in *28th IEEE Conference on Decision and Control*, (Tampa, FL, USA), pp. 1822–1827, December 1989.
- [380] J. S. Thorp, S. A. Naqavi, and H. Chiang, “More Load Flow Fractals,” in *29th IEEE Conference on Decision and Control*, (Honolulu, HI, USA), pp. 3028–3030, December 1990.
- [381] J.-J. Deng and H.-D. Chiang, “Convergence Region of Newton Iterative Power Flow Method: Numerical Studies,” *Journal of Applied Mathematics*, October 2013.
- [382] J. E. Tate and T. J. Overbye, “A Comparison of the Optimal Multiplier in Polar and Rectangular Coordinates,” *IEEE Transactions on Power Systems*, vol. 20, no. 4, pp. 1667–1674, November 2005.
- [383] V. H. Quintana and N. Müller, “Studies of Load Flow Methods in Polar and Rectangular Coordinates,” *Electric Power Systems Research*, vol. 20, no. 3, pp. 225–235, 1991.

- [384] D. Shirmohammadi, H. W. Hong, A. Semlyen, and G. X. Luo, "A Compensation-based Power Flow Method for Weakly Meshed Distribution and Transmission Networks," *IEEE Transactions on Power Systems*, vol. 3, no. 2, pp. 753–762, May 1988.
- [385] E. Bompard, E. Carpaneto, G. Chicco, and R. Napoli, "Convergence of the Backward-Forward Sweep Method for the Load Flow Analysis of Radial Distribution Systems," *International Journal of Electrical Power & Energy Systems*, vol. 22, no. 7, pp. 521–530, October 2000.
- [386] W. H. Kersting, *Distribution System Modeling and Analysis, Third Edition*. Boca Raton, FL: CRC Press, 2012.
- [387] P. Fortenbacher, M. Zellner, and G. Andersson, "Optimal Sizing and Placement of Distributed Storage in Low Voltage Networks," in *19th Power Systems Computation Conference (PSCC)*, (Genoa, Italy), pp. 1–7, June 2016.
- [388] C. B. Garcia and W. I. Zangwill, *Pathways to Solutions, Fixed Points and Equilibria*. Englewood Cliffs, NJ: Prentice Hall, 1981.
- [389] G. B. Price, "A Generalized Circle Diagram Approach for Global Analysis of Transmission System Performance," *IEEE Transactions on Power Apparatus and Systems*, vol. PAS-103, no. 10, pp. 2881–2890, October 1984.
- [390] V. Ajjarapu and C. Christy, "The Continuation Power Flow: A Tool for Steady State Voltage Stability Analysis," *IEEE Transactions on Power Systems*, vol. 7, no. 1, pp. 416–423, February 1992.
- [391] C. A. Cañizares and F. L. Alvarado, "Point of Collapse and Continuation Methods for Large AC/DC Systems," *IEEE Transactions on Power Systems*, vol. 8, no. 1, pp. 1–8, February 1993.
- [392] A. Wächter, "Nonlinear Optimization Algorithms," in *Advances and Trends in Optimization with Engineering Applications* (T. Terlaky, M. F. Anjos, and S. Ahmed, eds.), ch. 17, pp. 221–235, SIAM, 2017.
- [393] A. Forsgren, P. E. Gill, and M. H. Wright, "Interior Methods for Nonlinear Optimization," *SIAM Review*, vol. 44, no. 4, pp. 525–597, 2002.
- [394] N. Gould, D. Orban, and P. Toint, "Numerical Methods for Large-Scale Nonlinear Optimization," *Acta Numerica*, vol. 14, pp. 299–361, 2005.
- [395] A. Wächter and L. T. Biegler, "On the Implementation of a Primal-Dual Interior Point Filter Line Search Algorithm for Large-Scale Nonlinear Programming," *Mathematical Programming*, vol. 106, no. 1, pp. 25–57, 2006.

- [396] R. H. Byrd, J. Nocedal, and R. A. Waltz, "Knitro: An Integrated Package for Nonlinear Optimization," in *Large-Scale Nonlinear Optimization*, pp. 35–59, Springer, 2006.
- [397] R. J. Vanderbei, "LOQO: An Interior Point Code for Quadratic Programming," *Optimization Methods and Software*, vol. 11, no. 1-4, pp. 451–484, 1999.
- [398] K. A. Clements, P. W. Davis, and K. D. Frey, "An Interior Point Algorithm for Weighted Least Absolute Value Power System State Estimation," in *IEEE Power & Energy Society Winter Meeting*, (New York, NY, USA), February 1991.
- [399] K. Ponnambalam, V. H. Quintana, and A. Vannelli, "A Fast Algorithm for Power System Optimization Problems using an Interior Point Method," *IEEE Transactions on Power Systems*, vol. 7, no. 2, pp. 892–899, May 1992.
- [400] H. Wang, C. E. Murillo-Sanchez, R. D. Zimmerman, and R. J. Thomas, "On Computational Issues of Market-Based Optimal Power Flow," *IEEE Transactions on Power Systems*, vol. 22, no. 3, pp. 1185–1193, August 2007.
- [401] F. Capitanescu and L. Wehenkel, "Experiments with the Interior-Point Method for Solving Large Scale Optimal Power Flow Problems," *Electric Power Systems Research*, vol. 95, pp. 276–283, 2013.
- [402] A. Forsgren, "On Warm Starts for Interior Methods," in *22nd IFIP TC7 Conference on System Modeling and Optimization* (F. Ceragioli, A. Dontchev, H. Futura, K. Marti, and L. Pandolfi, eds.), (Torino, Italy), pp. 51–66, July 2005.
- [403] R. C. Burchett, H. H. Happ, and D. R. Vierath, "Quadratically Convergent Optimal Power Flow," *IEEE Transactions on Power Apparatus and Systems*, vol. PAS-103, no. 11, pp. 3267–3275, November 1984.
- [404] P. Gill, W. Murray, and M. Saunders, "SNOPT: An SQP Algorithm for Large-Scale Constrained Optimization," *SIAM Review*, vol. 47, no. 1, pp. 99–131, 2005.
- [405] R. Fletcher and S. Leyffer, "Nonlinear Programming without a Penalty Function," *Mathematical Programming*, vol. 91, no. 2, pp. 239–269, January 2002.
- [406] M. Fazel, *Matrix Rank Minimization with Applications*. dissertation, Stanford University, March 2002.

- [407] B. Recht, M. Fazel, and P. A. Parrilo, "Guaranteed Minimum Rank Solutions to Linear Matrix Equations via Nuclear Norm Minimization," *SIAM Review*, vol. 52, pp. 471–501, 2010.
- [408] R. Madani, J. Lavaei, and R. Baldick, "Convexification of Power Flow Problem over Arbitrary Networks," in *IEEE 54th Annual Conference on Decision and Control (CDC)*, (Osaka, Japan), pp. 1–8, December 2015.
- [409] Y. Zhang, R. Madani, and J. Lavaei, "Conic Relaxations for Power System State Estimation with Line Measurements," *IEEE Transactions on Control of Network Systems*, vol. 5, no. 3, pp. 1193–1205, September 2018.
- [410] S. You and Q. Peng, "A Non-Convex Alternating Direction Method of Multipliers Heuristic for Optimal Power Flow," in *IEEE International Conference on Smart Grid Communications (SmartGridComm)*, (Venice, Italy), pp. 788–793, November 2014.
- [411] T. Liu, B. Sun, and D. H. K. Tsang, "Rank-one Solutions for SDP Relaxation of QCQPs in Power Systems," to appear in *IEEE Transactions on Smart Grid*, 2019.
- [412] Y. Shi, H. D. Tuan, H. Tuy, and S. Su, "Global Optimization for Optimal Power Flow over Transmission Networks," *Journal of Global Optimization*, vol. 69, no. 3, pp. 745–760, November 2017.
- [413] Y. Shi, H. D. Tuan, and A. V. Savkin, "Three-Phase Optimal Power Flow for Smart Grids by Iterative Nonsmooth Optimization," in *6th International Conference on Smart Cities and Green ICT Systems – Volume 1: SMARTGREENS*, (Porto, Portugal), pp. 323–328, April 2017.
- [414] Y. Shi, H. D. Tuan, P. Apkarian, and A. V. Savkin, "Global Optimal Power Flow over Large-Scale Power Transmission Network," *Systems & Control Letters*, vol. 118, pp. 16–21, August 2018.
- [415] A. S. Zamzam, N. D. Sidiropoulos, and E. Dall'Anese, "Beyond Relaxations and Newton-Raphson: Solving AC OPF for Multi-Phase Systems with Renewables," *IEEE Transactions on Smart Grid*, vol. 9, no. 5, pp. 3966–3975, September 2018.
- [416] R. Louca and E. Bitar, "Stochastic AC Optimal Power Flow with Affine Recourse," in *IEEE 55th Annual Conference on Decision and Control (CDC)*, (Las Vegas, NV, USA), pp. 2431–2436, December 2016.
- [417] W. Wei, J. Wang, N. Li, and S. Mei, "Optimal Power Flow of Radial Networks and Its Variations: A Sequential Convex Optimization Approach," *IEEE Transactions on Smart Grid*, vol. 8, no. 6, pp. 2974–2987, November 2017.

- [418] A. S. Zamzam, C. Zhao, E. Dall'Anese, and N. D. Sidiropoulos, "A QCQP Approach for OPF In Multiphase Radial Networks with Wye and Delta Connections," in *10th IREP Symposium on Bulk Power System Dynamics and Control*, (Espinho, Portugal), August 2017.
- [419] A. A. Ahmadi and G. Hall, "DC Decomposition of Nonconvex Polynomials with Algebraic Techniques," *Mathematical Programming*, April 2017.
- [420] Z. Tian and W. Wu, "Recover Feasible Solutions for SOCP Relaxation of Optimal Power Flow Problems in Mesh Networks," *arXiv:1708.06504*, August 2017.
- [421] C. Wang, A. Bernstein, J.-Y. Le Boudec, and M. Paolone, "Explicit Conditions on Existence and Uniqueness of Load-Flow Solutions in Distribution Networks," *IEEE Transactions on Smart Grid*, vol. 9, no. 2, pp. 953–962, March 2018.
- [422] K. Dvijotham and K. Turitsyn, "Construction of Power Flow Feasibility Sets," *arXiv:1506.07191*, July 2015.
- [423] S. Yu, H. D. Nguyen, and K. Turitsyn, "Simple Certificate of Solvability of Power Flow Equations for Distribution Systems," in *IEEE Power & Energy Society General Meeting*, (Denver, CO, USA), pp. 1–5, July 2015.
- [424] J. W. Simpson-Porco, "A Theory of Solvability for Lossless Power Flow Equations – Part II: Conditions for Radial Networks," *IEEE Transactions on Control of Network Systems*, vol. 5, no. 3, pp. 1373–1385, September 2018.
- [425] C. Wang, A. Bernstein, J.-Y. Le Boudec, and M. Paolone, "Existence and Uniqueness of Load-Flow Solutions in Three-Phase Distribution Networks," *IEEE Transactions on Power Systems*, vol. 32, no. 4, pp. 3319–3320, 2017.
- [426] K. Dvijotham, H. D. Nguyen, and K. Turitsyn, "Solvability Regions of Affinely Parameterized Quadratic Equations," *IEEE Control Systems Letters*, vol. 2, no. 1, pp. 25–30, January 2018.
- [427] H. D. Nguyen, K. Dvijotham, S. Yu, and K. Turitsyn, "A Framework for Robust Steady-State Voltage Stability of Distribution Systems," *arXiv:1705.05774*, May 2017.
- [428] H. D. Nguyen, K. Dvijotham, and K. Turitsyn, "Constructing Convex Inner Approximations of Steady-State Security Regions," *IEEE Transactions on Power Systems*, vol. 34, no. 1, pp. 257–267, January 2019.

- [429] C. Wang, J.-Y. Le Boudec, and M. Paolone, "Controlling the Electrical State via Uncertain Power Injections in Three-Phase Distribution Networks," to appear in *IEEE Transactions on Smart Grid*, 2019.
- [430] D. Lee, H. D. Nguyen, K. Dvijotham, and K. Turitsyn, "Convex Restriction of Power Flow Feasibility Set," *arXiv:1803.00818*, March 2018.
- [431] L. Debnath and P. Mikusiński, *Hilbert Spaces with Applications*. Academic Press, 2005.
- [432] T. H. Chen, M. S. Chen, K. J. Hwang, P. Kotas, and E. A. Chebli, "Distribution System Power Flow Analysis—A Rigid Approach," *IEEE Transactions on Power Delivery*, vol. 6, no. 3, pp. 1146–1152, July 1991.
- [433] Z. Wang, B. Cui, and J. Wang, "A Necessary Condition for Power Flow Insolvability in Power Distribution Systems With Distributed Generators," *IEEE Transactions on Power Systems*, vol. 32, no. 2, pp. 1440–1450, March 2017.
- [434] G. Teschl, "Topics in Real and Functional Analysis." <http://www.mat.univie.ac.at/~gerald/ftp/book-fa/fa.pdf>, April 2017.
- [435] J. W. Simpson-Porco, "A Theory of Solvability for Lossless Power Flow Equations – Part I: Fixed-Point Power Flow," *IEEE Transactions on Control of Network Systems*, vol. 5, no. 3, pp. 1361–1372, September 2018.
- [436] K. Dvijotham, S. H. Low, and M. Chertkov, "Convexity of Energy-Like Functions: Theoretical Results and Applications to Power System Operations," *arXiv:1501.04052*, February 2015.
- [437] C. Wang, E. Stai, and J.-Y. Le Boudec, "A Polynomial-Time Method for Testing Admissibility of Uncertain Power Injections in Microgrids," *arXiv:1810.06256*, October 2018.
- [438] D. Shchetinin, T. T. De Rubira, and G. Hug, "Conservative Linear Line Flow Constraints for AC Optimal Power Flow," in *IEEE Manchester PowerTech*, (Manchester, England, UK), pp. 1–6, June 2017.
- [439] D. Shchetinin, T. T. De Rubira, and G. Hug, "On the Construction of Linear Approximations of Line Flow Constraints for AC Optimal Power Flow," to appear in *IEEE Transactions on Power Systems*, 2019.
- [440] D. K. Molzahn and L. A. Roald, "Grid-Aware versus Grid-Agnostic Distribution System Control: A Method for Certifying Engineering Constraint Satisfaction," in *52nd Hawaii International Conference on Systems Sciences (HICSS)*, (Wailea, Hawaii, USA), January 2019.

- [441] D. K. Molzahn and L. A. Roald, "Towards an AC Optimal Power Flow Algorithm with Robust Feasibility Guarantees," in *20th Power Systems Computation Conference (PSCC)*, (Dublin, Ireland), June 2018.
- [442] R. Louca and E. Bitar, "Robust AC Optimal Power Flow," to appear in *IEEE Transactions on Power Systems*, 2019.
- [443] N. A. Ruhi, K. Dvijotham, N. Chen, and A. Wierman, "Opportunities for Price Manipulation by Aggregators in Electricity Markets," *IEEE Transactions on Smart Grid*, vol. 9, no. 6, pp. 5687–5698, November 2018.
- [444] S. Emiroglu, G. Ozdemir, and M. Baran, "Assessment of Linear Distribution Feeder Models used in Optimization Methods," in *IEEE Power Energy Society Innovative Smart Grid Technologies Conference (ISGT)*, (Minneapolis, MN, USA), pp. 1–5, September 2016.
- [445] H. Nagarajan, R. Bent, P. Van Hentenryck, S. Backhaus, and E. Yamangil, "Resilient Transmission Grid Design: AC Relaxation vs. DC Approximation," *arXiv:1703.05893*, March 2017.
- [446] D. Bienstock, M. Chertkov, and S. Harnett, "Chance-Constrained Optimal Power Flow: Risk-Aware Network Control Under Uncertainty," *SIAM Review*, vol. 56, no. 3, pp. 461–495, 2014.
- [447] J. Schmidli, L. A. Roald, S. Chatzivasileiadis, and G. Andersson, "Stochastic AC Optimal Power Flow with Approximate Chance-Constraints," in *IEEE Power & Energy Society General Meeting*, (Boston, MA, USA), pp. 1–5, July 2016.
- [448] L. A. Roald, D. K. Molzahn, and A. F. Tobler, "Power System Optimization with Uncertainty and AC Power Flow: Analysis of an Iterative Algorithm," in *10th IREP Symposium on Bulk Power System Dynamics and Control*, (Espinho, Portugal), August 2017.
- [449] L. A. Roald and G. Andersson, "Chance-Constrained AC Optimal Power Flow: Reformulations and Efficient Algorithms," *IEEE Transactions on Power Systems*, vol. 33, no. 3, pp. 2906–2918, May 2018.
- [450] L. Halilbasic, P. Pinson, and S. Chatzivasileiadis, "Convex Relaxations and Approximations of Chance-Constrained AC-OPF Problems," to appear in *IEEE Transactions on Power Systems*, 2019.
- [451] B. Li, M. Vrakopoulou, and J. L. Mathieu, "Chance Constrained Reserve Scheduling Using Uncertain Controllable Loads—Part II: Analytical Reformulation," to appear in *IEEE Transactions on Smart Grid*, 2019.

- [452] M. Vrakopoulou, M. Katsampani, K. Margellos, J. Lygeros, and G. Andersson, "Probabilistic Security-Constrained AC Optimal Power Flow," in *IEEE Grenoble PowerTech*, (Grenoble, France), pp. 1–6, June 2013.
- [453] A. Venzke, L. Halilbasic, U. Markovic, G. Hug, and S. Chatzivasileiadis, "Convex Relaxations of Chance Constrained AC Optimal Power Flow," *IEEE Transactions on Power Systems*, vol. 33, no. 3, pp. 2829–2841, May 2018.
- [454] J. F. Marley, M. Vrakopoulou, and I. A. Hiskens, "Towards the Maximization of Renewable Energy Integration Using a Stochastic AC-QP Optimal Power Flow Algorithm," in *10th IREP Symposium on Bulk Power System Dynamics and Control*, (Espinho, Portugal), August 2017.
- [455] M. Vrakopoulou, B. Li, and J. L. Mathieu, "Chance Constrained Reserve Scheduling Using Uncertain Controllable Loads—Part I: Formulation and Scenario-based Analysis," to appear in *IEEE Transactions on Smart Grid*, 2019.
- [456] Y. Weng, Q. Li, R. Negi, and M. Ilic, "Semidefinite Programming for Power System State Estimation," in *IEEE Power & Energy Society General Meeting*, (San Diego, CA, USA), pp. 1–8, July 2012.
- [457] J. F. Marley, D. K. Molzahn, and I. A. Hiskens, "Solving Multiperiod OPF Problems using an AC-QP Algorithm Initialized with an SOCP Relaxation," *IEEE Transactions on Power Systems*, vol. 32, no. 5, pp. 3538–3548, September 2017.
- [458] S. Boyd, S.-J. Kim, L. Vandenberghe, and A. Hassibi, "A Tutorial on Geometric Programming," *Optimization and Engineering*, vol. 8, no. 1, p. 67, 2007.
- [459] S. Misra, M. W. Fisher, S. Backhaus, R. Bent, M. Chertkov, and F. Pan, "Optimal Compression in Natural Gas Networks: A Geometric Programming Approach," *IEEE Transactions on Control of Network Systems*, vol. 2, no. 1, pp. 47–56, March 2015.
- [460] H. Zhu and G. B. Giannakis, "Power System Nonlinear State Estimation Using Distributed Semidefinite Programming," *IEEE Journal of Selected Topics in Signal Processing*, vol. 8, no. 6, pp. 1039–1050, December 2014.
- [461] H. G. Aghamolki, Z. Miao, and L. Fan, "SOCP Convex Relaxation-Based Simultaneous State Estimation and Bad Data Identification," *arXiv:1804.05130*, April 2018.
- [462] M. E. Baran and F. F. Wu, "Network Reconfiguration in Distribution Systems for Loss Reduction and Load Balancing," *IEEE Transactions on Power Delivery*, vol. 4, no. 2, pp. 1401–1407, April 1989.

- [463] R. A. Jabr, R. Singh, and B. C. Pal, "Minimum Loss Network Reconfiguration Using Mixed-Integer Convex Programming," *IEEE Transactions on Power Systems*, vol. 27, no. 2, pp. 1106–1115, May 2012.
- [464] J. A. Taylor and F. S. Hover, "Convex Models of Distribution System Reconfiguration," *IEEE Transactions on Power Systems*, vol. 27, no. 3, pp. 1407–1413, August 2012.
- [465] C. Coffrin, H. L. Hijazi, K. Lehmann, and P. Van Hentenryck, "Primal and Dual Bounds for Optimal Transmission Switching," in *18th Power Systems Computation Conference (PSCC)*, (Wroclaw, Poland), pp. 1–8, August 2014.
- [466] H. L. Hijazi and S. Thiébaut, "Optimal AC Distribution Systems Reconfiguration," in *18th Power Systems Computation Conference (PSCC)*, (Wroclaw, Poland), August 2014.
- [467] M. Lu, H. Nagarajan, E. Yamangil, R. Bent, S. Backhaus, and A. Barnes, "Optimal Transmission Line Switching under Geomagnetic Disturbances," *IEEE Transactions on Power Systems*, vol. 33, no. 3, pp. 2539–2550, May 2018.
- [468] D. Gayme and U. Topcu, "Optimal Power Flow with Large-Scale Storage Integration," *IEEE Transactions on Power Systems*, vol. 28, no. 2, pp. 709–717, May 2013.
- [469] E. Davoodi, E. Babaei, and B. Mohammadi-ivatloo, "An Efficient Covexified SDP Model for Multi-Objective Optimal Power Flow," *International Journal of Electrical Power & Energy Systems*, vol. 102, pp. 254–264, 2018.
- [470] R. Bent, C. Coffrin, R. R. E. Gumucio, and P. Van Hentenryck, "Transmission Network Expansion Planning: Bridging the Gap between AC Heuristics and DC Approximations," in *18th Power Systems Computation Conference (PSCC)*, (Wroclaw, Poland), pp. 1–8, August 2014.
- [471] S. Merkli, A. Domahidi, J. Jerez, and R. S. Smith, "Globally Optimal AC Power System Upgrade Planning under Operational Policy Constraints," in *European Control Conference (ECC)*, (Limassol, Cyprus), June 2018.
- [472] B. Ghaddar and R. A. Jabr, "Power Transmission Network Expansion Planning: A Semidefinite Programming Branch-and-Bound Approach," to appear in *European Journal of Operational Research*, 2019.
- [473] A. Lorca and X. A. Sun, "The Adaptive Robust Multi-Period Alternating Current Optimal Power Flow Problem," *IEEE Transactions on Power Systems*, vol. 33, no. 2, pp. 1993–2003, March 2018.

- [474] Y. Liu and M. Ferris, "Security-Constrained Economic Dispatch using Semidefinite Programming," in *IEEE Power & Energy Society General Meeting*, (Denver, CO, USA), pp. 1–5, July 2015.
- [475] K. Sundar, C. Coffrin, H. Nagarajan, and R. Bent, "Probabilistic N-k Failure-Identification for Power Systems," *arXiv:1704.05391*, July 2018.
- [476] X. Wu, A. J. Conejo, and N. Amjady, "Robust Security Constrained ACOPF via Conic Programming: Identifying the Worst Contingencies," *IEEE Transactions on Power Systems*, vol. 33, no. 6, pp. 5884–5891, November 2018.
- [477] A. Lorca and X. A. Sun, "Multistage Robust Unit Commitment with Dynamic Uncertainty Sets and Energy Storage," *IEEE Transactions on Power Systems*, vol. 32, no. 3, pp. 1678–1688, May 2017.
- [478] A. Nasri, S. J. Kazempour, A. J. Conejo, and M. Ghandhari, "Network-Constrained AC Unit Commitment Under Uncertainty: A Benders' Decomposition Approach," *IEEE Transactions on Power Systems*, vol. 31, no. 1, pp. 412–422, January 2016.
- [479] C. Gambella, J. Marecek, M. Mevissen, J. M. F. Ortega, S. P. Djukic, and M. Pezic, "Transmission-Constrained Unit Commitment," *arXiv:1806.09408*, June 2018.
- [480] R. Madani, A. Atamtürk, and A. Davoudi, "A Scalable Semidefinite Relaxation Approach to Grid Scheduling," tech. rep., Industrial Engineering & Operations Research, University of California, Berkeley, July 2017. BCOL Research Report 17.03, *arXiv:1707:03541*.
- [481] E. Salgado, A. Scozzari, F. Tardella, and L. Liberti, "Alternating Current Optimal Power Flow with Generator Selection," in *International Symposium on Combinatorial Optimization (ISCO)*, (Marrakesh, Morocco), April 2018.
- [482] N. C. Koutsoukis, P. A. Karafotis, P. S. Georgilakis, and N. D. Hatziairgyriou, "Optimal Service Restoration of Power Distribution Networks Considering Voltage Regulation," in *IEEE Manchester PowerTech*, (Manchester, England, UK), pp. 1–6, June 2017.
- [483] L. Gan and S. H. Low, "An Online Gradient Algorithm for Optimal Power Flow on Radial Networks," *IEEE Journal on Selected Areas in Communication*, vol. 34, no. 3, pp. 625–638, March 2016.
- [484] E. Dall'Anese, S. V. Dhople, and G. B. Giannakis, "Photovoltaic Inverter Controllers Seeking AC Optimal Power Flow Solutions," *IEEE Transactions on Power Systems*, vol. 31, no. 4, pp. 2809–2823, 2016.

- [485] E. Dall'Anese and A. Simonetto, "Optimal Power Flow Pursuit," *IEEE Transactions on Smart Grid*, vol. 9, no. 2, pp. 942–952, March 2018.
- [486] G. Wang, V. Kekatos, A. J. Conejo, and G. B. Giannakis, "Ergodic Energy Management Leveraging Resource Variability in Distribution Grids," *IEEE Transactions on Power Systems*, vol. 31, no. 6, pp. 4765–4775, 2016.
- [487] Z. Yuan, M. R. Hesamzadeh, and D. R. Biggar, "Distribution Locational Marginal Pricing by Convexified ACOPF and Hierarchical Dispatch," *IEEE Transactions on Smart Grid*, vol. 9, no. 4, pp. 3133–3142, July 2018.
- [488] D. K. Molzahn, B. C. Lesieutre, and C. L. DeMarco, "A Sufficient Condition for Power Flow Insolvability With Applications to Voltage Stability Margins," *IEEE Transactions on Power Systems*, vol. 28, no. 3, pp. 2592–2601, August 2013.
- [489] D. K. Molzahn, V. Dawar, B. C. Lesieutre, and C. L. DeMarco, "Sufficient Conditions for Power Flow Insolvability Considering Reactive Power Limited Generators with Applications to Voltage Stability Margins," in *9th IREP Symposium on Bulk Power System Dynamics and Control*, (Rethymno, Greece), August 2013.
- [490] D. K. Molzahn, I. A. Hiskens, and B. C. Lesieutre, "Calculation of Voltage Stability Margins and Certification of Power Flow Insolvability using Second-Order Cone Programming," in *49th Hawaii International Conference on Systems Sciences (HICSS)*, (Koloa, HI, USA), pp. 2307–2316, January 2016.
- [491] B. Cui and X. A. Sun, "A New Voltage Stability-Constrained Optimal Power Flow Model: Sufficient Condition, SOCP Representation, and Relaxation," *IEEE Transactions on Power Systems*, vol. 33, no. 5, pp. 5092–5102, September 2018.